Robust Flight-to-Gate Assignment Planning with Airside and Landside Constraints

J. L'Ortye

TU Delft

Robust Flight-to-Gate Assignment Planning with Airside and Landside Constraints

by

Jules L'Ortye
4091604

to obtain the degree of Master of Science at Delft University of Technology and to be defended publicly on Friday April 26, 2019 at 2:30pm.

Thesis committee:

Dr. M.A. Mitici	Delft University of Technology	Daily supervisor
Dr. ir. H.G. Visser	Delft University of Technology	External supervisor
Prof. dr. R. Curran	Delft University of Technology	Section chair
Dr. ir. E.J. van Kampen	Delft University of Technology	External committee member

This thesis is confidential and cannot be made public until April 26, 2019.

An electronic version of this thesis is available at `http://repository.tudelft.nl/`.

Rotterdam
April 15, 2019

Acknowledgements

This report is the final deliverable to obtain the Master's degree in Aerospace Engineering at Delft University of Technology. Working on this report wouldn't have nearly been as fun if it weren't for Anne-Marleen Beets. Though I am thrilled to deliver the final report, I will miss the days we spent together on the 3rd floor. I would like to thank Oscar Da Costa Gomez for his ongoing support and strategic advice during the times I needed it, and for those times when I thought I didn't need it. Not only during the time I worked on this report, but also the many years prior to that, my parents, Han L'Ortye and Anita L'Ortye-Dijkmans, have been incredible in helping me move forward. I cannot thank you enough for your unconditional support. Finally, I would like to extend a special thanks to my supervisor Mihaela Mitici. Throughout the entire process of writing this thesis, you have gone to great lengths to help me complete the project, and together we made something I am proud of.

Jules L'Ortye
Rotterdam, April 2019

Executive Summary

The Flight-to-Gate Assignment Problem (FGAP) covers the optimal assignment of flights, or rather the aircraft serving these flights, to the available aircraft stands, known as gates. Existing models in literature do not consider implement airside and landside constraints simultaneously. Research on improving the robustness of the solution to the FGAP is still ongoing. Therefore, the objective of this study is to develop a FGAP model that includes both landside and airside constraints in addition to implementing an predefined level of robustness. The contributions of this paper to existing literature are threefold: a FGAP model is proposed that considers airside and landside constraints, flight splitting options are implemented in the FGAP model, and a novel optimisation algorithm is described to implement a threshold for passenger waiting time at an airport.

This report describes a FGAP model with airside and landside constraints where overlap probability is used as a proxy for robustness. This model extends the FGAP model developed by Schaijk & Visser (2017). Three distinct specifications of the FGAP model with airside and landside constraints are proposed: The A-FGAP model has active airside constraints and inactive landside constraints. The DC-FGAP model has active airside and landside constraints and enforces upper bounds on passenger demand per time step at landside passenger facilities. This upper bound is determined using the declared capacity. The WT-FGAP model has active airside and landside constraints and ensures a gate assignment plan is constructed such that the expected maximum waiting for passengers does not exceed a predefined threshold.

A case study of Amsterdam Airport Schiphol using the flight schedule of July 4, 2018, with a planning horizon between 00:00 and 23:59 is used as support for the analysis of the FGAP models. The A-FGAP model provides the most cost-efficient approach by at the expense of passenger comfort. The DC-FGAP model ensures a high level of passenger comfort by ensuring waiting times of less than one minute for airport passengers. However, this comes at an increased cost for the airport operator due to flight segment reallocation. Finally, the WT-FGAP model provides an intermediate approach, where the expected maximum waiting time of passengers is ensured to be below a user-defined threshold with a 95% probability. The DC-FGAP model creates a gate assignment at an increased cost compared to the WT-FGAP model, but does offer a superior passenger experience since waiting times are non-existent.

The solution to the A-FGAP model does not depend on the declared capacity. The objective function value the WT-FGAP model decreases as the scaling factor increases. However, these values deviate no more than 1% from the objective function value of the A-FGAP model. For scaling factors larger or equal to 0.95, the objective function value of the DC-FGAP model decreases as the scaling factor increases. For smaller scaling factors, no feasible solutions to the DC-FGAP model exist. If the maximum waiting time threshold is varied, the objective function value of the WT-FGAP model is bounded; the lower bound and the upper bound are

the objective function values of the A-FGAP model and DC-FGAP model respectively. Build times increase exponentially as the compression factor of the data decreases. Solving times vary between the FGAP models considered and, in general, increase exponentially as the compression factor of the data decreases.

Future work includes the implementation of flight-specific input, methods to decrease build and solving times, and probability modelling. Flight-specific input, including flight-specific presence probabilities, check-in rates, transfer-rates and load factor, allows for a more realistic representation of flights in the flight-to-gate assignment problem. A decrease in build and solving times allows for larger data sets to be analysed, possibly leading to an analysis of the flight-to-gate assignment problem covering all gates and flight in the planning horizon at AMS. As a result of flight splitting, presence probability curves of flight segments are non-continuous. Extending the analysis to produce continuous flight presence probabilities for flight segment will reduce the number of violations of the maximum overlap probability constraint.

Contents

List of Figures

List of Tables

List of Abbreviations

A-FGAP	FGAP model with Airside constraints only
AMS	Amsterdam Airport Schiphol
AO	Airport-Oriented
API	Application Programming Interface
ATA	Actual Time of Arrival
ATD	Actual Time of Departure
AX	Aircaft eXcel file
A1	Immigration facilities
A2	Baggage claim facilities
CDF	Cumulative Density Function
CPLEX	C-programming simPLEX method
D1	Check-in and bag drop facilities
D2	Departing security and border control facilities
DC-FGAP	FGAP model with airside and landside constraints, where passenger demand cannot exceed the Declared Capacity
ETD	Expected Total semi-Deviation
EVI	Expected Variance of Idle times
FGAP	Flight-to-Gate Assignment Problem
FL	Flight List
FS	Flight-Specific
GAP	Gate Assignment Plan
JSON	JavaScript Object Notation
KLM	Koninklijke Luchtvaart Maatschappij
LHR	London Heathrow (airport)
LP	Linear Programming (problem)
N/A	Not Applicable
O&D	Origin and Destination (passengers)
OT	Other Terminal
PO	Passenger-Oriented
RX	Region eXcel file
STA	Scheduled Time of Arrival
STD	Scheduled Time of Departure
T1	Transfer security facilities

WT:FGAP	FGAP model with airside and landside constraints, where expected maximum passenger Waiting Times cannot exceed a user-defined threshold

List of Symbols

The list of symbols includes an overview of the decision variables, functions, Greek parameters, indices, Roman parameters and sets.

Decision Variables

$x_{i,j,t}$: Binary variable; indicates whether flight segment $i \in N$ is assigned to gate $j \in G_i^1$ at time step $t \in K$;

$y_{p,q,t}$: Integer variable; indicates the passenger demand at facility p in terminal $q \in T$ from $t \in K$ until $t + \delta_t$;

$z_{i,j,q}$: Binary variable; indicates whether flight segment $i \in N_a \cup N_d$ is assigned to gate $j \in G_i^1$ and its departing passenger streams are handled by terminal $q \in T$;

Functions

$f(p_{i,t}, r)$: Scaling function used in maximum overlap probability constraint;

Greek Parameters

α: Scaling factor used in sensitivity analysis of declared capacity;

$\beta_{a,arr}$: Scaling coefficient for arriving leg of airline flight presence probability;

$\beta_{a,dep}$: Scaling coefficient for departing leg of airline flight presence probability;

$\beta_{r,arr}$: Scaling coefficient for arriving leg of region flight presence probability;

$\beta_{r,dep}$: Scaling coefficient for departing leg of region flight presence probability;

$\gamma_{i,p,q,t}$: The fraction of all passengers boarding or disembarking flight segment $i \in N_a \cup N_d$ that use facility $p \in H$ in terminal $q \in T$ during time step $t \in K$;

Δ_s: Sensitivity parameter that indicates the decrease of $b_{p,q,t}$ in the WT-FGAP model if a waiting time criterion violation occurs;

δ_t: Spacing between discrete time steps $t \in K$ in minutes;

η_i: Number of seats in the aircraft serving flight segment $i \in N$;

$\lambda_{i,p,q,t}$: Unscaled elliptical distribution of passengers boarding or disembarking flight segment $i \in N_a \cup N_d$ that use facility $p \; inH$ in terminal $q \in T$ during time step $t \in K$;

$\rho_{i,p,q}$: The total number of passengers from flight segment $i \in N_a \cup N_d$ that will use facility $p \in H$ in terminal $q \in T$;

Indices

i: Index of a flight segment to the sets of N, N_a, N_d, E_v^1 and E_w^2;

j: Index of a gate to the sets M, G_i^1, G_o^2 and G_q^3;

l: Index of flight to the set F;

o: Index of pairing of gates in the set O;

n: Index to the set of peak demand periods at facility $p \in H$ in terminal $q \in T$, denoted by $U_{p,q}$;

p: Index of a facility to the set H;

q: Index of a terminal to the set T;

t: Index of a time step to the set K;

v: Index of unrealistic flight assignment in the set V;

w: Index of maximum overlap probability criterion violation in the set W;

Roman Parameters and Variables

A_{eq}: Equality matrix of a linear programming problem;

A_{ineq}: Inequality matrix of a linear programming problem;

$a_{p,q,n}$: Scaling coefficient for parabolic peak demand approximation for peak demand n at facility p in terminal $q \in T$;

$\mathbf{b}_{eq}$: Equality vector of a linear programming problem;

$\mathbf{b}_{ineq}$: Inequality vector of a linear programming problem;

$b_{p,q,t}$: Maximum number of passengers at facility $p \in H$ in terminal $q \in T$ between time step $t \in K$ and $t + \delta_t$;

$c_{i,j}^{\text{Customs}}$: The cost of assigning flight segment $i \in N$ to gate $j \in G_i^1$ for a single time step from a customs perspective;

$c_{i,j}^{\text{Size}}$: The cost of assigning flight segment $i \in N$ to gate $j \in G_i^1$ for a single time step from a size perspective;

$c_{i,j}^{\text{Type}}$: The cost of assigning flight segment $i \in N$ to gate $j \in G_i^1$ for a single time step from a flight segment type perspective;

$c_{i,j}^{a}$: The cost of assigning flight segment $i \in N$ to gate $j \in G_i^1$ for a single time step;

$c_{i,j,q}^{l}$: The cost of assigning flight segment $i \in N_a \cup N_d$ to gate $j \in G_i^1$ and terminal $q \in T$;

$C_{p,q}$: The declared capacity of facility $p \in H$ in terminal $q \in T$ per time step of length δ_t;

$C_{p,q}^{\text{scaled}}$: Scaled declared capacity used in sensitivity analysis, equal to $\alpha \cdot C_{p,q}$;

$D_{i,p,q,t}$: The number of passengers of flight segment $i \in N_a \cup N_d$ that use facility $p \in H$ in terminal $q \in T$ during time step t;

$\mathbf{f}$: Vector of cost coefficients of a linear programming problem;

F_{CI}: Fraction of all departing passengers that use facility D1;

F_{TF}: Fraction of all arriving passengers on SkyTeam flights that transfer at AMS;

F_{LF}: Average load factor over all flights at AMS;

$fp_{a,t,arr}$: Airline identity arrival flight presence probability of the option a corresponding to flight $l \in F$ and time step $t \in K$;

$fp_{a,t,dep}$: Airline identity departing flight presence probability of the option a corresponding to flight $l \in F$ and time step $t \in K$;

$fp_{l,t}$: Flight presence probability of flight $l \in F$ at time step $t \in K$;

$fp_{l,t,arr}$: Flight presence probability of the arriving leg of flight $l \in F$ at time step $t \in K$;

$fp_{l,t,dep}$: Flight presence probability of the departing leg of flight $l \in F$ at time step $t \in K$;

$fp_{r,t,arr}$: Origin region arrival flight presence probability of the option r corresponding to flight $l \in F$ at time step $t \in K$;

$fp_{r,t,dep}$: Destination region arrival flight presence probability of the option r corresponding to flight $l \in F$ at time step $t \in K$;

F_V: Binary flag taking a value of 1 if a solution to a FGAP model is altered to remove one or more maximum overlap probability criterion violation;

F_{WT}: Binary flag taking a value of 1 if FGAP model is altered to remove one or more maximum waiting time criterion violation;

$h^u_{p,q}$: the number of passengers handled in iteration cycle u as a percentage of the the number of passengers handled in iteration cycle 1 for facility $p \in H$ in terminal $q \in T$

I_V: Indicator variable taking a value of 1 if a solution to a FGAP model is not valid because of a violation of the maximum overlap probability constraint in equation (5.4.11);

I_{WT}: Indicator variable taking a value of 1 if a solution to a FGAP model is not valid because the expected maximum waiting time ($T^{\max}_{p,q}$) at atleast one facility $p \in H$ in terminal $q \in T$ exceeds W^T;

$L_{p,q,n}$: Queue length for facility $p \in H$ in terminal $q \in T$ during peak period n, measured in number of passengers;

$L^{\max}_{p,q,n}$: Maximum queue length for facility $p \in H$ in terminal $q \in T$ during peak period n, measured in number of passengers;

MI: Maximum number of iterations in optimisation algorithms;

$m_{p,q}$: Demand-capacity ratio for facility $p \in H$ in terminal $q \in T$; see equation (8.4.1) on page 101;

$p_{i,t}$: Probability that the aircraft serving flight segment $i \in N$ is present at the airport at time step $t \in K$;

r: Predefined level of maximum overlap probability;

$s_{i,t}$: Binary coefficient indicating whether flight segment $i \in N$ is has a non-zero presence probability to be at the airport in time slot $t \in K$;

STA_l: The scheduled time of arrival of flight $l \in F$;

STD_l: The scheduled time of departure of flight $l \in F$;

T_1: Time in minutes for arriving and transfer passengers to walk from the gate to facilities (A1) and (T1), respectively;

T_2: Time in minutes of passengers to proceed from facilities (A1) to (A2);

T_3: Time in minutes between first and last passenger disembarking from aircraft;

T_4: Time in minutes between first and last passenger that use facilities (D1);

T_5: Time in minutes from passengers to proceed from facilities (D1) to facility (D2);

T_6: Time in between the last passenger to use facilities (D1) and the STD of flight $l \in F$;

$T_{i,p,q}$: Duration of use of facility $p \in H$ in terminal $q \in T$ by passengers of flight $i \in N_a \cup N_d$, equal to $t^e_{i,p,q} - t^s_{i,p,q}$;

$t^e_{i,p,q}$: End time for passengers of flight segment $i \in N_a \cup N_d$ to pass through facility $p \in H$ in terminal $q \in T$;

$t^s_{i,p,q}$: Start time for passengers of flight segment $i \in N_a \cup N_d$ to pass through facility $p \in H$ in terminal $q \in T$;

$T_{p,q,n}$: The length of duration of peak period n at facility $p \in H$ in terminal $q \in T$;

$t^e_{p,q,n}$: End time of peak demand period n at facility $p \in H$ in terminal $q \in T$;

$t^s_{p,q,n}$: Start time of peak demand period n at facility $p \in H$ in terminal $q \in T$;

$TD_{p,q,t}$: The total number passengers that use facility p in terminal q during time step t;

w_{al}: Scaling factor to ensure value scale of both elements of the objective function the FGAP model are well-balanced;

$W_{p,q,n}$: The maximum expected passenger waiting time at a facility $p \in H$ in terminal $q \in T$ during peak period n;

$W^{\max}_{p,q}$: The maximum expected passenger waiting time at a facility $p \in H$ in terminal $q \in T$;

W^T: Maximum waiting time threshold;

$\mathbf{x}$: Vector of decision variables of a linear programming problem;

$y^{pb}_{p,q,t}$: The parabolic peak approximation of peak n for facility $p \in H$ in terminal $q \in T$ of $y_{p,q,t}$;

$y^u_{p,q,t}$: Integer variable; indicates the passenger demand at facility $p \in H$ in terminal $q \in T$ from $t \in K$ until $t + \delta_t$ during iteration u of algorithm 2 on page 77;

Z: Value of the objective function of a linear programming problem;

Sets

$E^0_{j,t}$: Subset of N and is the set of flight segments assigned to gate j at time step t;

E^1_v: Subset of N and is the set of flight segments corresponding to unrealistic flight splitting assignment $v \in V$; see subsection A.4 on page 132 for a detailed explanation;

E^2_w: Subset of N and is the set of flight segments corresponding to violation $w \in W$; see subsection A.5 on page 134 for a detailed explanation;

F: The set of flights in the flight schedule;

G^1_i: Subset of M and is the set of gates flight segment $i \in N$ can be assigned to;

G^2_o: Subset of M and is the set of gates corresponding to pairing $o \in O$; see section 6.1 on page 79 for a detailed explanation;

G^3_q: Subset of M and is the set of gates whose hypothetical departing passenger stream cannot be handled by terminal $q \in T$; see section 6.2 on page 79 for detailed explanation on how this set is created;

H: The set of facilities considered at AMS;

K: The set of time steps within the planning horizon;

M: The set of gates available at the airport;

N: The set of flight segments that could be present at the airport during the planning horizon;

N_a: The set of flight segments where passengers disembark an aircraft; subset of N;

N_d: The set of flight segments where passengers board an aircraft; subset of N;

$S_{l,t}$: The set of flight splitting options of flight $l \in F$ at time step $t \in K$;

T:	The set of terminals at Amsterdam Airport Schiphol;
$U_{p,q}$:	The set of peak demand periods at facility $p \in H$ in terminal $q \in T$;
V:	The set of all combinations of functional segments and parking segments that should not be assigned to the same gate;
W:	The set of all combinations of flight segment that cause an overlap probability violation;

Part I

Scientific Article

Robust Flight-to-Gate Assignment with Airside and Landside Constraints

Jules L'Ortye, MSc student[a]

[a]*Faculty of Aerospace Engineering, Air Transport and Operations, Delft University of Technology*
Supervisors: dr. M. Mitici, dr. ir. D. Visser

Abstract

The Flight-to-Gate Assignment Problem (FGAP) covers the optimal assignment of flights, or rather the aircraft serving these flights, to the available aircraft stands. Existing FGAP models in literature do not consider airside and landside processes simultaneously. We propose a FGAP model with three specifications, where only airside constraints are active, both airside and landside constraint are active and passenger demand cannot exceed the fixed declared landside capacity, and both airside and landside constraint are active, and the landside passenger constraints are driven by the expected maximum passenger waiting time. The implementation of landside constraints results in a gate assignment at a increased cost, compared to gate assignment derived using inactive landside constraints. Imposing the constraint that passenger demand cannot exceed declared capacity creates a gate assignment at an increased cost compared to implementing a maximum passenger waiting time, but does offer a superior passenger experience since waiting times are non-existent.

Keywords: FGAP, Airside, Landside, Robust Optimisation, Linear Programming

1. Introduction

At large international hub airports, where hundreds of flights are handled daily, the process of assigning flights to gates is complex, involving airport resource constraints, airline preferences and quality of service requirements for passengers inside the terminals. This process becomes even more involved when taking into account the uncertainty in the arrival and departure flight times to and from the airport.

In the past years, several mathematical formulations have been proposed to solve the flight-to-gate assignment problem (FGAP). These approaches have as main input the strategic schedule of arrival and departure flight times at an airport, the type of aircraft associated with these flights and the set of airport gates. The resulting gate assignment is an optimal strategic solution. However, such gate assignments lack robustness as they are sensitive to changes in the arrival/departure flight times. In a real-life environment, flight arrival/departures are often subject to delays. In this case, the strategic gate

assignment solution can no longer be readily applied. Equally important, these approaches consider only airside related constraints and, at most, passenger-specific requirements, such as, for instance, minimal passenger walking distance to and from gates. However, the impact of the flight-to-gate assignment on the ability of the landside facilities (check-in, security, transfer, passport control) to provide a high quality of service inside the terminal, is not considered. For instance, a gate assignment can be obtained such that all airside constraints are satisfied and the walking distance for passengers is minimized. However, following this gate assignment, the flow of passengers at a landside facility may be such that the number of passengers requesting service from this facility increases significantly and service can no longer be sustained.

In this paper we propose a FGAP model that ensures a predefined level of robustness, while considering both landside and airside constraints. This model extends the robust FGAP model by Schaijk and Visser (2017), which considers airside constraints only. The landside constraints of our proposed robust FGAP model consider passenger demand at airport facilities and, in the case of high passenger demand, it reallocates departing passenger streams between terminals in the airport. We propose three distinct specifications of the robust FGAP model, where i) only airside constraints are active, ii) both airside and landside constraint are active, and passenger demand cannot exceed a fixed declared capacity at the airport facilities and iii) both airside and landside constraints are active, and the airport facility constraints are driven by the expected maximum passenger waiting time at airport facilities, rather than a fixed declared capacity. We apply these models in a case study for Amsterdam Airport Schiphol (AMS), and propose a flight-to-gate assignment using flight data for July 4, 2018.

The contributions of this paper are threefold: i) we propose a robust flight-to-gate assignment model that considers both airside and landside constraints, ii) we implement flight splitting options in the flight-to-gate assignment model, and iii) we describe a novel optimisation algorithm to implement a threshold for passenger waiting time at an airport.

The remainder of this article is structured as follows. Section 2 presents an overview of related literature. Section 3 describes the data employed for a case study of the flight-to-gate assignment problem. Section 4 describes the airport landside characteristics. Section 5 introduces the mathematical formulation of the flight-to-gate assignment problem with both airside and landside constraints. Section 6 introduces three specifications of the flight-to-gate assignment problem with: i) only airside constraints, ii) both airside and landside constraints and a fixed, declared capacity of the airport terminal, and iii) both airside and landside constraints and the landside constraints are driven by the maximum passenger waiting time in the terminal. Section 7 introduces Amsterdam Airport Schiphol airport-specific constraints for the flight-to gate assignment model. Section 8 presents the results of a case study of flight assignment at Amsterdam Airport Schiphol. In section 9 a sensitivity analysis is conducted. Finally, section 10 provides conclusions and gives recommendations for further research.

2. Prior work and contributions

Several researchers have focused on modeling the landside of an airport, focusing mainly on identifying the landside facilities and characterising the passenger streams inside airport terminals. Manataki and Zografos (2009) describe a high-level architecture of a hub airport. They consider an airport consisting

of an unrestricted, controlled, gates and arrivals controlled airport functional areas. Li et al. (2018) presents an insightful example of how a complex set of security facilities are distilled to a simple topology. Kusumaningtyas and Lodewijks (2013) describe the terminal topology at AMS. van Dijk and van der Sluis (2006) characterises the passenger arrival distribution as a triangular-shaped distribution. Solak et al. (2006) derive closed-form expressions for the expected maximum waiting time as a function of passenger demand and the declared capacity of airport facilities.

Yu et al. (2016) state that the mean of the buffer time and its standard deviation can be used a proxy for robustness of a gate assignment plan. The expected conflict duration among all flights at the gate is used to measure the robustness of a gate assignment plan (Yu et al., 2017). Additionally, Seker and Noyan (2012) propose three robustness measures based on the idle and buffer times: the expected variance of the idle times, the expected total semi-deviation, and the expected number of positive semi-deviations. Schaijk and Visser (2017) state that overlap probability is a proxy for robustness. The reader is referred to the work of Beyer and Sendhoff (2007) for a detailed reading on robust optimisation.

Yan and Chang (1997) and Yan and Huo (2001) propose a FGAP model which implements fixed buffer times. Diepen et al. (2012) describe a FGAP model where the gap times are used in the objective function. Seker and Noyan (2012) develop a FGAP model that incorporates robustness by analysing a large number of stochastic scenarios. Yu et al. (2016) introduce a FGAP model that aims to minimise the transfer passenger's walking distance in a quadratic model. Schaijk and Visser (2017) propose a FGAP model with a constraint that ensures the maximum overlap probability does not exceed a predefined level. Kim et al. (2013) develop three FGAP models that focus on different passenger experience metrics, namely: transfer time, aircraft taxi time and robustness of gate assignment. They describe that trade-offs between different objectives can increase the robustness of the gate assignment plan.

3. Case study data

The case studies presented in this paper are based on the scheduled arrival and departure flight times at AMS on July 4, 2018. Table 1 shows an example of the flight schedule considered. Arriving (Departing) aircraft at (from) AMS are assigned a unique flight number, which we refer to as FlightIDIn (FlightIDOut). Each arriving (departing) flight has a scheduled arrival time STA (scheduled departure time STD). We encode the size of an aircraft, ACSize, on a scale from 3 to 9, where 3 corresponds to a small aircraft (Fokker 100) and 9 corresponds to the largest passenger jets (Airbus A380-800). We also consider the type of customs associated with an arriving (departing) flight. Customs associated with arriving (departing) aircraft are referred to as CustomsIn (CustomsOut). CustomIn and CustomOut can be Schengen, which we encode by 1, EU Non-Schengen, which we encode by 2, or and Intercontinental customs, which we encode by 3. RegionIn (RegionOut) denotes the region the flight originates from (departs to). The parameter Airline indicates the IATA code of the airline that performs the flight. T_4 is the time in minutes between first and last passenger of a flight that use check-in facilities and T_6 is the time in minutes between the last passenger of flight to use check-in facilities and the STD of that flight.

The month of July accounted for 9.53% of the annual number of passengers at AMS in 2018 *(AMS Traffic Review 2018, 2019)*. We assume that the passenger load is spread evenly over this month, and therefore, each day in July, 2018, is considered a peak-day in terms of passenger demand. We consider

Table 1: Example of flights scheduled to arrive/depart at AMS on July 4, 2018, E=Europe, N= North-America.

FlightIDIn	FlightIDOut	STA	STD	ACSize	CustomsIn	CustomsOut	RegionIn	RegionOut	Airline	T_4	T_6
GA9231	GA9488	13:25	14:25	4	1	1	E	E	GIA	120	40
KL6060	KL6019	13:25	15:25	7	3	3	N	N	KLM	150	60
DL9505	DL9603	13:30	14:15	4	1	1	E	E	DAL	120	40
AF8306	AF8497	13:35	14:20	3	2	2	E	E	AFL	120	40
DL9272	DL9536	13:35	14:20	4	2	1	E	E	DAL	120	40

the flight schedule of July 4, 2018, as support for the flight-to-gate assignment problem in this paper. The flight schedule of July 4, 2018, at AMS contains 575 arrival and 549 departure movements; the difference is caused by flights with an arrival (departure) on July 3 (July 5), 2018. Flights within Europe account for 76.8% and 73.2% of arrival and departure movements, respectively. Wide-body aircraft, i.e., aircraft for which ACSize > 4, and narrow-body aircraft, i.e., the aircraft for which ACSize ≤ 4, serve 15.1% and 84.9% of the flights, respectively.

For the analysis of the AMS terminal we consider the entire set of gates at AMS. Table 2 gives an example of gates. GateID is the unique identifier of the gate. Size indicates the maximum aircraft size that the gate can accommodate. Customs indicates the customs level of the gate, encoded like CustomsIn and CustomsOut in Table 1. We also consider the type of the gate, which includes piers, platforms, aprons and towing trucks. The data set we consider consists of 132 piers, 135 platforms, 11 aprons and 63 towing trucks.

Table 2: Example of gates at AMS.

GateID	Size	Customs	Type
A34	8	3	Platform
D08	6	3	Pier
R72	8	3	Apron
THW	9	3	Towing truck

4. Airport landside characteristics

In this section we describe the main passenger streams and the airport landside facilities at AMS, which are considered in the flight-to gate assignment model with airside and landside constraints. In addition, we show the estimates of the hourly declared capacities of these facilities.

4.1. Airport terminal topology

Figure 1 shows a generic topology of a terminal at AMS. On the public side, the airport topology consists of the departure/arrival area. On the non-public side, the airport topology consists of the lounges/waiting area and the gates. Terminals at AMS are connected in the departure/arrival area without passenger movement restrictions. In the lounges/waiting area, terminals are connected with passenger movement restrictions between Schengen and Non-Schengen areas.

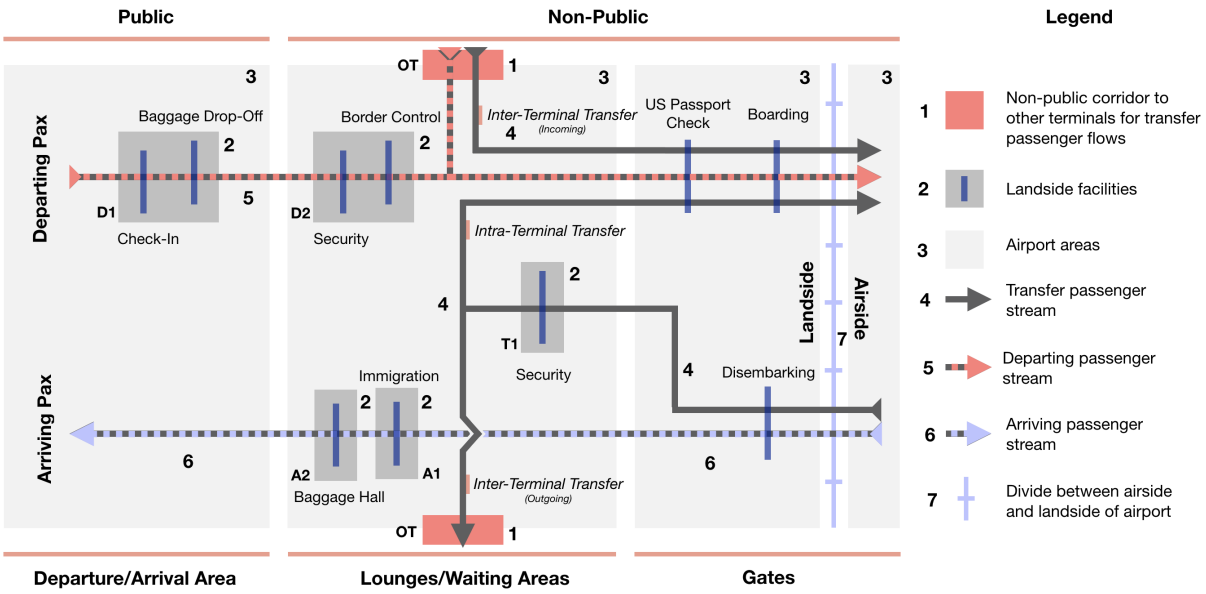

Figure 1: Generic topology of a terminal at AMS.

We consider three generic passenger streams at the airport: i) departing passenger stream, ii) arriving passenger stream and iii) transfer passenger stream. Passengers on arriving flights feed into arriving and transfer passenger streams. Passengers on departing flights are contained by the transfer and departing passenger streams. The stream of arriving passengers moves from the non-public area to the public area in the same terminal. The stream of departing passengers consists of two substreams with passengers that enter the non-public area from the public area in the same terminal and the non-public area from a different terminal. The transfer passenger stream consists of three substreams: incoming and outgoing inter-terminal transfer passenger streams and an intra-terminal transfer passenger stream. No data is available to determine the volumes of the inter-terminal transfer passenger streams versus the intra-terminal transfer passenger stream. Thus, all transfer passengers are assumed to be captured by the intra-terminal transfer passenger substream.

Table 3 shows the airport facilities considered in this paper, together with their associated passenger streams, as indicated in Figure 1. For departing passenger streams, the check-in and baggage drop-off facilities (D1) and the security facilities and border control (D2) are considered in the FGAP model. For arriving passenger streams, immigration (A1) and the baggage claim area (A2) are included in the FGAP model as distinct facilities. Finally, for transfer passenger streams security services (T1) are considered.

4.2. Hourly capacity of facilities in airport terminals

Table 4 indicates the estimated hourly declared capacity of facilities (A1) through (D2) in each terminal at AMS. The declared capacity is estimated using comparative data on declared terminal capacity at London Heathrow Airport (LHR) (Odoni, 2017) and expert opinion from AMS. Note that Terminal 1 and Terminal 4 only serve flights with a Schengen clearance level. As such, facilities (A1) and (T1) are not present in these terminals and, thus, their capacity is not given in Table 4.

Table 3: Overview of landside facilities. These facilities serve either arriving, transfer or departing passenger streams.

Indicator	Group Name	Pax Stream	Facilities Included
A1	Immigration	Arriving	Passenger immigration services
A2	Baggage Claim	Arriving	Baggage claim areas and lost & found
T1	Security	Transfer	Transfer security services
D1	Check-In	Departing	Check-in desk and bag drop facilities
D2	Security & Border Control	Departing	Security services and border control

Table 4: Overview of the declared capacity per hour of landside facilities at AMS.

Terminal	Declared Capacity [Pax/Hour]				
	A1	A2	T1	D1	D2
Terminal 1	N/A	3,420	N/A	1,690	3,040
Terminal 2	2,840	2,840	3,420	1,380	2,700
Terminal 3	2,500	2,500	1,080	1,230	2,220
Terminal 4	N/A	990	N/A	495	900

5. Flight-to-gate assignment model with airside and landside constraints

In this section we introduce a robust flight-to-gate assignment model with airside and landside constraints. First, we discuss the option of splitting a flight in segments associated with passengers disembarking, embarking the aircraft, the aircraft being towed or parked. Next, we describe the notion of presence probabilities of flight segments. Further, we introduce a passenger demand model within the terminal. Lastly, we describe the flight-to-gate assignment model with airside and landside constraints.

5.1. Flight splitting options

We assume that a flight with a schedule arrival time (STA) and a scheduled departure time (STD) at an airport can be split into flight segments in the period from arrival at the airport to departure from this airport. We consider 3 possible flight segments corresponding to: i) passengers disembarking and/or boarding an aircraft, ii) the aircraft being towed and, iii) the aircraft being parked. We define a functional flight segment as a flight segment where passenger disembark or board an aircraft. We consider a planning horizon of operations between 00:00 and 23:59 on the same calendar day. Below we characterise 1) flights without overnight stay, 2) flights with an overnight stay and a morning departure and 3) flights with an evening arrival and an overnight stay.

1. Flights without overnight-stay

The STA and STD of flights without an overnight-stay are both within the planning horizon. We define three different flight splitting options for a flight without an overnight-stay, which include: i) Flight is not split and is assigned to the one gate from its STA until its STD (see segment 1 in Figure 2); ii) Flight is split in 3 segments, including a functional flight segment, a towing segment and a second functional flight segment (see segments $2, 3, 4$ in Figure 2); iii) Flight is split in 5 segments, including a

functional flight segment, a towing segment, a parking segment, a second towing segment and a second functional flight segment (see segments $5, 6, 7, 8, 9$ in Figure 2);

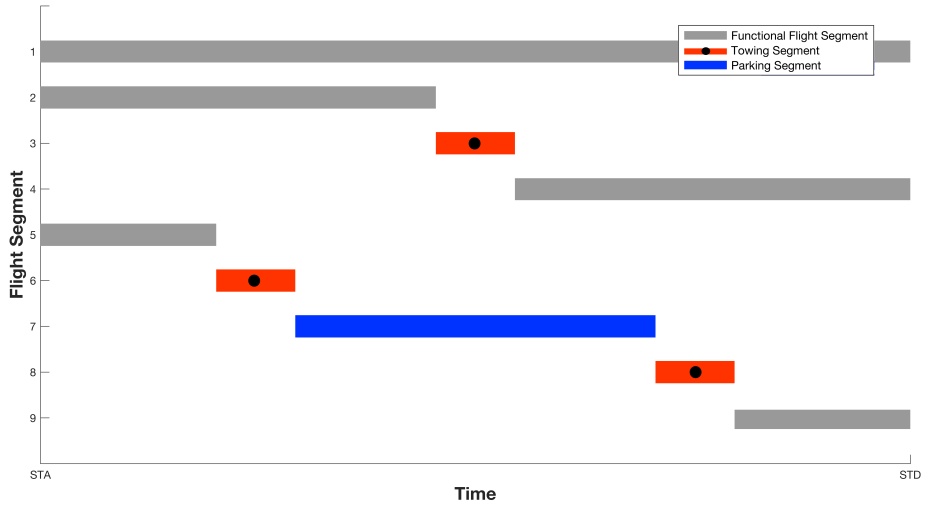

Figure 2: Splitting options for flights without overnight-stay.

We define the presence time of a flight to be equal to the time between the STA and STD of that flight. Flight splitting option i) can be applied irrespective of the presence time of a flight. Flight splitting option ii) can be applied if a flight has a minimum presence time of 130min (150min) for flights served by narrow-body (wide-body) aircraft. Flight segment 3 in Figure 2 has a fixed length of 10min, and flight segment 2 and 4 in Figure 2 are of equal length. Flight splitting option iii) can be applied if a flight has a minimum presence time of 170min (190min) for flights served by narrow-body (wide-body) aircraft. Flight segment 6 and 8 in Figure 2 have a fixed length of 10min, and flight segment 5 and 9 in Figure 2 have a fixed length of 55 and 65min for flights served by narrow-body aircraft and 75 and 85min for flights served by wide-body aircraft, respectively.

2. Flights with morning departure

The STA of a flight with a morning departure is outside of the planning horizon. Flight splitting options for a flight with a morning departure include: iv) Flight is not split and is assigned to one gate from 00:00 until its STD (see segment 1 in Figure 3a); v) Flight is split in 3 segments: a parking, a towing and a functional segment where passengers board the aircraft (see segments $2, 3, 4$ in Figure 3a).

Flight splitting option iv) can be applied irrespective of the presence time of a flight. Flight splitting option v) can be applied if a flight has a minimum presence time of 130min (150min) for flights served by narrow-body (wide-body aircraft). Flight segment 3 and 4 in Figure 3a have a fixed length of 10 and 65min (75min) for flights served by narrow-body (wide-body) aircraft.

3. Flights with evening arrival

The STD a flight with an evening arrival is outside the planning horizon. Flight splitting options for flights with an evening arrival include: vi) Flight is not split and is assigned to one gate from its STA until 23:59 (see segment 1 in Figure 3b); vii) Flight is split in 3 segments: a functional segment where passengers disembark, a towing and a parking segment (see segments $2, 3, 4$ in Figure 3b).

Flight splitting option vi) can be applied irrespective of the presence time of a flight. Flight splitting

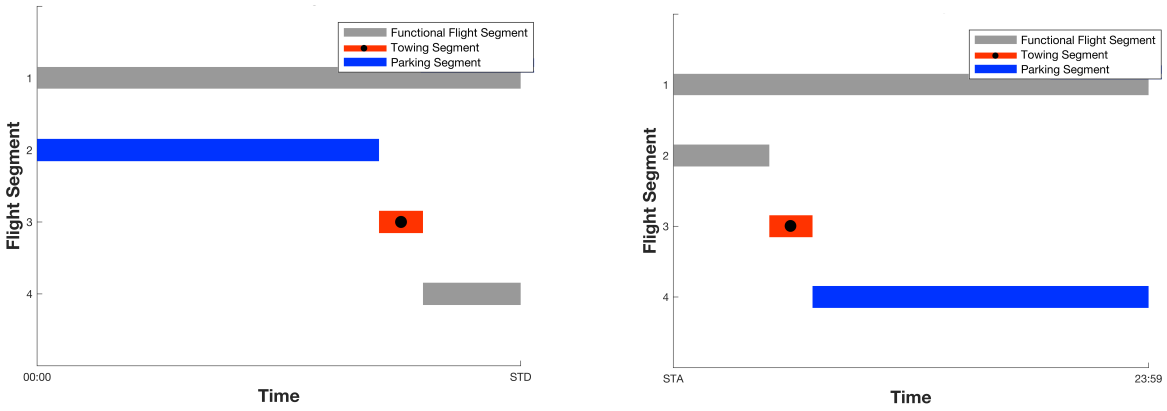

(a) Flights with overnight stay and morning departure.

(b) Flights with evening arrival and overnight stay.

Figure 3: Overnight-stay flight splitting options.

option vii) can be applied if a flight has a minimum presence time of 130min (150min) for flights served by narrow-body (wide-body) aircraft. Flight segment 3 and 4 in Figure 3b have a fixed length of 10 and 65min (75min) for flights served by narrow-body (wide-body) aircraft.

5.2. Presence probability of flight segments

In this section we determine the presence probability of flight segments, i.e., the probability that a flight segment is present at a particular time. First, let us introduce the following notation. Let F denote the set of all arriving and departing flights at the airport in a day, N denotes the set of all possible flight segments created by applying the flight splitting options (see Section 5.1, Flight splitting), and M denotes the set of gates at the airport. We consider the planning horizon to be discretised in time steps of 5min, with a total of K time steps for the entire planning horizon.

We define $p_{i,t}$ as the presence probability of flight segment $i \in N$ at time step $t \in K$, which is derived from the presence probability of flight $l \in F$ it belongs to, i.e.,:

$$p_{i,t} = fp_{l,t}, \quad i \in S_{l,t}, \quad t \in K, \tag{1}$$

where $fp_{l,t}$ is the presence probability of flight l from which flight segment i is derived and $S_{l,t} \subseteq N$ is the set that contains all possible flight segments of flight l at time step t.
Below we discuss how to determine the flight presence probability.

Flight presence probability

We determine the flight presence probability for a flight without an overnight stay as follows (Schaijk and Visser, 2017):

$$fp_{l,t} = fp_{l,t,arr} - |1 - fp_{l,t,dep}|, \quad l \in F, \quad t \in K, \tag{2}$$

where $fp_{l,t}$ denotes the flight presence of flight l at time step t, $fp_{l,t,arr}$ is the arrival flight presence probability of flight l at time step t and $fp_{l,t,dep}$ is the departure flight presence probability of flight l at time step t.

Figure 4 gives an example of $fp_{l,t,arr}$, $fp_{l,t,dep}$ and $fp_{l,t}$ for a flight l.

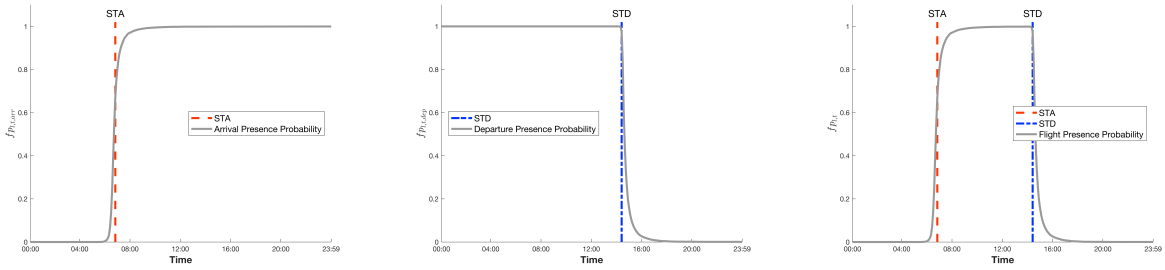

(a) $fp_{l,t,arr}$ (b) $fp_{l,t,dep}$ (c) $fp_{l,t}$

Figure 4: Example of $fp_{l,t,arr}$, $fp_{l,t,dep}$ and $fp_{l,t}$ for a flight l without an overnight stay, where $fp_{l,t}$ is constructed using eq. (5). This flight has a STA=06:50 and STD=14:25.

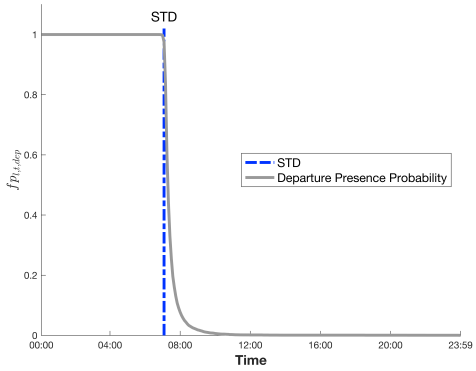

Figure 5: Example of $fp_{l,t,dep}$ for a flight l with a morning departure, where $fp_{l,t} = fp_{l,t,dep}$ (see also eq. (3)), STD=07:05.

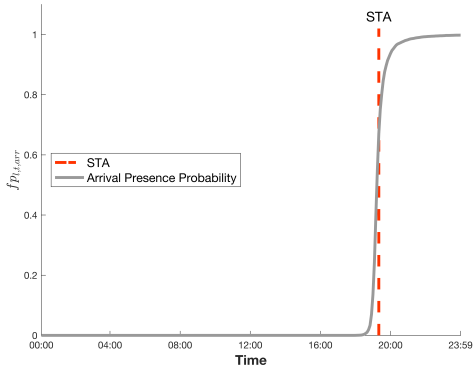

Figure 6: Example of $fp_{l,t,arr}$ for a flight l with a evening arrival, where $fp_{l,t} = fp_{l,t,arr}$ (see also eq. (4)), STA=19:20.

The flight presence probability for flights with a morning departure and evening arrival are computed using eq. (3) and (4), respectively,

$$fp_{l,t} = fp_{l,t,dep}, \quad l \in F, \quad t \in K, \qquad (3) \qquad\qquad fp_{l,t} = fp_{l,t,arr}, \quad l \in F, \quad t \in K. \qquad (4)$$

Figure 5 provides an example of $fp_{l,t,dep}$ and $fp_{l,t}$ for a flight l with a morning departure. Figure 6 gives an example of $fp_{l,t,arr}$ and $fp_{l,t}$ for a flight l with a evening arrival.

Arrival and departure flight presence probability per airline and region

The flight presence probability for an arriving (departing) leg of a flight $l \in F$ is determined using a linear model without intercept as follows:

$$fp_{l,t,u} = \beta_{a,u} fp_{a,t,u} + \beta_{r,u} fp_{r,t,u}, \quad l \in F, \quad t \in K, \quad u \in [arr, dep], \qquad (5)$$

where $fp_{a,t,arr}$ ($fp_{a,t,dep}$) is the arrival (departure) flight presence probability at time step t of the airline option $a \in A$ corresponding to flight l, and $fp_{r,t,arr}$ ($fp_{r,t,dep}$) corresponds to the arrival (departure) flight presence probability at time step t of the region option $r \in R$ corresponding to flight l.

We consider 18.663 arriving flight legs and 19.766 departing flight legs dated between July 1, 2018, and July 30, 2018, to estimate the variables $fp_{a,t,arr}$, $fp_{a,t,dep}$, $fp_{r,t,arr}$ and $fp_{r,t,dep}$ (see Schaijk and Visser (2017)).

The scaling coefficients in eq. (5), denoted by $\beta_{a,arr} = 0.4847$, $\beta_{a,dep} = 0.5836$, $\beta_{r,arr} = 0.5153$ and $\beta_{r,dep} = 0.4164$ are determined as follows:

$$\beta_{a,u} = \frac{\mathrm{var}_t(fp_{a,t,u})}{\mathrm{var}_t(fp_{a,t,u}) + \mathrm{var}_t(fp_{r,t,u})}, \quad a \in A, \quad u \in [arr, dep], \tag{6}$$

$$\beta_{r,u} = \frac{\mathrm{var}_t(fp_{r,t,u})}{\mathrm{var}_t(fp_{a,t,u}) + \mathrm{var}(fp_{r,t,dep})}, \quad r \in R, \quad u \in [arr, dep], \tag{7}$$

and their values reflect the variance of the variables $fp_{a,t,arr}$, $fp_{a,t,dep}$, $fp_{r,t,arr}$ and $fp_{r,t,dep}$, respectively.

5.3. Passenger demand model

We define N_a and N_d to be the set of flight segments where passengers disembark and board aircraft, respectively, $N_a \cup N_d \subseteq N$. We define H as the set of all facilities (A1) through (D2). Let T denote the set of terminals at the airport.

We define the total number of passengers that use facility p in terminal q during time step t as:

$$TD_{p,q,t} = \sum_{i \in N_a \cup N_d} D_{i,p,q,t} \cdot I_{i,p,q,t}, \quad p \in H, \quad q \in T, \quad t \in K, \tag{8}$$

where $D_{i,p,q,t}$ denotes the number of passengers of flight segment $i \in N_a \cup N_d$ that use facility $p \in H$ in terminal $q \in T$ during time step t and $I_{i,p,q,t}$ is an indicator function defined as follows:

$$I_{i,p,q,t} = \begin{cases} 1, & \text{if passenger streams of flight segment } i \text{ are handled by facility } p \text{ in terminal } q \\ & \text{during time step } t, \\ 0, & \text{otherwise.} \end{cases}$$

The integer variable $D_{i,p,q,t}$ is computed as follows:

$$D_{i,p,q,t} = \mathrm{round}\big(\rho_{i,p} \cdot \gamma_{i,p,q,t}\big), \quad i \in N_a \cup N_d, \quad p \in H, \quad q \in T, \quad t \in K, \tag{9}$$

where $\rho_{i,p}$ is the total number of passengers from flight segment i that will use facility p and $\gamma_{i,p,q,t}$ denotes the fraction of the total number of passengers from flight segment i that use facility p in terminal q during time step t.
Below we explain in detail how to determine $\rho_{i,p}$ and $\gamma_{i,p,q,t}$.

Passenger number from flight segment i that use airport facility p, denoted by $\rho_{i,p}$

For facilities (A1) and (A2), we determine $\rho_{i,p}$ as follows:

$$\rho_{i,p} = \begin{cases} \eta_i \cdot F_{LF} \cdot (1 - F_{TF}) & \text{if flight segment } i \in N_a \text{ and belongs to a SkyTeam flight,} \\ \eta_i \cdot F_{LF} & \text{if flight segment } i \in N_a \text{ and does not belong to a SkyTeam flight,} \\ 0 & \text{otherwise,} \end{cases} \tag{10}$$

where F_{TF} denotes the transfer rate for SkyTeam flights, $F_{TF} = 67\%$ *(AMS Traffic Review 2018, 2019)*, F_{LF} denotes the average load factor for a flight, $F_{LF} = 0.85$ *(AMS Traffic Review 2018, 2019)*, and η_i denotes the estimated number of seats on the aircraft serving flight segment i and we assume that only SkyTeam flights have transfer passengers.

For facilities (T1), we determine $\rho_{i,p}$ as follows:

$$\rho_{i,p} = \begin{cases} \eta_i \cdot F_{LF} \cdot F_{TF} & \text{if flight segment } i \in N_a \text{ and belongs to a SkyTeam flight,} \\ 0 & \text{otherwise.} \end{cases} \tag{11}$$

For facilities (D1), we determine $\rho_{i,p}$ as follows:

$$\rho_{i,p} = \begin{cases} \eta_i \cdot F_{LF} \cdot (1 - F_{TF}) \cdot F_{CI} & \text{if flight segment } i \in N_d \text{ and belongs to a SkyTeam flight,} \\ \eta_i \cdot F_{LF} \cdot F_{CI} & \text{if flight segment } i \in N_d \text{ and does not belong to a SkyTeam flight,} \\ 0 & \text{otherwise,} \end{cases} \tag{12}$$

where F_{CI} denotes the fraction of departing passengers that use either check-in facilities or bag-drop facilities, and we assume that $F_{CI} = 0.55$.

For facilities (D2), we determine $\rho_{i,p}$ as follows:

$$\rho_{i,p} = \begin{cases} \eta_i \cdot F_{LF} \cdot (1 - F_{TF}) & \text{if flight segment } i \in N_d \text{ and belongs to a SkyTeam flight,} \\ \eta_i \cdot F_{LF} & \text{if flight segment } i \in N_d \text{ and does not belong to a SkyTeam flight,} \\ 0 & \text{otherwise.} \end{cases} \tag{13}$$

Fraction of the total number of passengers from flight segment i that use facility p in terminal q during time step t, denoted by $\gamma_{i,p,q,t}$

Similar to Chun and Mak (1999), we assume that the distribution of the fraction of passengers from flight segment i using facility p in terminal q during time step t follows an elliptical distribution. The height of the elliptical distribution is given by $\gamma_{i,p,q,t}$. The support of this distribution is $[t^e_{i,p,q} - t^s_{i,p,q}]$, where $t^s_{i,p,q}$ and $t^e_{i,p,q}$ denote the start and end time for passengers arriving/departing with flight segment i to pass through facility p in terminal q. Facility-specific expressions for $t^s_{i,p,q}$ and $t^e_{i,p,q}$ are given in eq. (14) - (23) in Table 5.

The fraction of the total number of passengers from flight segment i that use facility p in terminal q during time step t, denoted by $\gamma_{i,p,q,t}$ is computed as follows:

$$\gamma_{i,p,q,t} = \frac{\lambda_{i,p,q,t}}{\sum_{t \in K} \lambda_{i,p,q,t}}, \quad i \in N_a \cup N_d, \quad p \in H, \quad q \in T, \tag{24}$$

where $\lambda_{i,p,q,t}$ is the elliptical function of the fraction of passengers boarding or disembarking flight segment i that use facility p in terminal q during time step t. We note that $\gamma_{i,p,q,t} \neq 0$ if $t^s_{i,p,q} \leq t \leq t^e_{i,p,q}$.

Here, $\lambda_{i,p,q,t}$ is:

$$\lambda_{i,p,q,t} = \begin{cases} \sqrt{1 - \left(\frac{t - (t^s_{i,p,q} + T_{i,p,q}/2)}{T_{i,p,q}/2}\right)^2} & \text{if} \quad t^s_{i,p,q} \leq t \leq t^e_{i,p,q}, \\ 0 & \text{otherwise,} \end{cases} \tag{25}$$

Table 5: Expressions of $t^s_{i,p,q}$ and $t^e_{i,p,q}$ for facilities (A1), (A2), (T1), (D1) and (D2), where $T_1 = 10$min is the time for arriving and transfer passengers to walk from the gate to facilities (A1) and (T1), respectively, $T_2 = 10$min is the time for passengers to proceed from facilities (A1) to facilities (A2), $T_3 = 45$min is the time between first and last passenger disembarking from aircraft, T_4 is the time between first and last passenger of flight segment $i \in N_d$ that use facilities (D1), $T_5 = 10$min is the time for the passengers to proceed from facilities (D1) to facilities (D2) and T_6 is the time between the last passenger of flight segment $i \in N_d$ to use facilities (D1) and the STD of flight segment $i \in N_d$. Values of T_4 and T_6 depend on characteristics of flight l that flight segment i belongs to and are derived from the flight schedule (see Table 1).

Facility	$t^s_{i,p,q}$		$t^e_{i,p,q}$	
A1	$\text{STA}_i + T_1$	(14)	$\text{STA}_i + T_1 + T_3$	(15)
A2	$\text{STA}_i + T_1 + T_2$	(16)	$\text{STA}_i + T_1 + T_2 + T_3$	(17)
T1	$\text{STA}_i + T_1$	(18)	$\text{STA}_i + T_1 + T_3$	(19)
D1	$\text{STD}_i - T_4 - T_6$	(20)	$\text{STD}_i - T_6$	(21)
D2	$\text{STD}_i - T_4 + T_5 - T_6$	(22)	$\text{STD}_i + T_5 - T_6$	(23)

.

where $T_{i,p,q} = t^e_{i,p,q} - t^s_{i,p,q}$.

An example of values of $\lambda_{i,p,q,t}$ and $\gamma_{i,p,q,t}$ are given in Figure 7a and 7b for facilities (A1) and Figure 7c and 7d for facilities (D2), respectively. By construction, $\max_t \lambda_{i,p,q,t} = 1$ and $\sum_{t \in K} \gamma_{i,p,q,t} = 1$ for $i \in N_a \cup N_d$, $p \in H$ and $q \in T$, and therefore, all arriving/departing passengers on flight i are accounted for. We note that the distribution of $\lambda_{i,p,q,t}$ and $\gamma_{i,p,q,t}$ has a larger support for facilities (D2) as compared to facilities (A1).

5.4. Mathematical model - flight-to-gate assignment with airside and landside constraints

In this section we describe the decision variables, objective function, constraints and optimisation algorithm of the flight-to-gate assignment model with airside and landside constraints.

Decision Variables

We assume that a flight segment $i \in N$ can be assigned only to a subset $G^1_i \subseteq M$ of gates. We consider the decision variables in eq. (26) - (28):

$$x_{i,j,t} = \begin{cases} 1 & \text{if flight segment } i \text{ is assigned to gate } j \text{ at timestep } t, \\ 0 & \text{otherwise,} \end{cases} \qquad i \in N, \quad j \in G^1_i, \quad t \in K. \tag{26}$$

$$z_{i,j,q} = \begin{cases} 1 & \text{if flight segment } i \text{ is assigned to gate } j \text{ and its} \\ & \text{departing passenger flow is assigned to terminal } q, \\ 0 & \text{otherwise,} \end{cases} \quad i \in N_d, \quad j \in G^1_i, \quad q \in T, \tag{27}$$

$$y_{p,q,t} = \sum_{i \in N_a \cup N_d} \sum_{j \in G^1_i} D_{i,p,q,t} z_{i,j,q}, \quad p \in H, \quad q \in T, \quad t \in K. \tag{28}$$

where $y_{p,q,t}$ denotes the number of passengers that use facility p in terminal q during time step t.

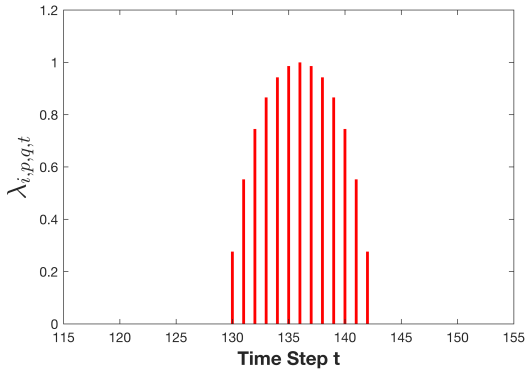

(a) Value of $\lambda_{i,p,q,t}$ of flight segment i at facilities (A1) in terminal q during time step t, with $t^s_{i,p,q} = 130$ and $t^e_{i,p,q} = 142$ and $\lambda_{i,p,q,t} \leq 1$.

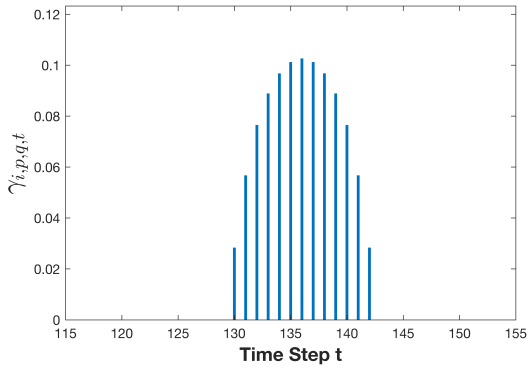

(b) Value of $\gamma_{i,p,q,t}$ of flight segment i at facilities (A1) in terminal q during time step t, with $t^s_{i,p,q} = 130$ and $t^e_{i,p,q} = 142$ and $\sum_t \gamma_{i,p,q,t} = 1$.

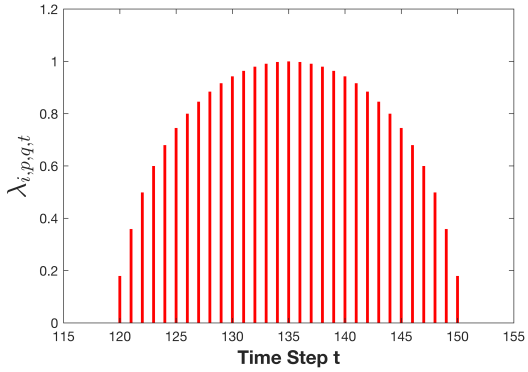

(c) Value of $\lambda_{i,p,q,t}$ of flight segment i at facilities (D2) in terminal q during time step t, with $t^s_{i,p,q} = 120$ and $t^e_{i,p,q} = 150$ and $\lambda_{i,p,q,t} \leq 1$.

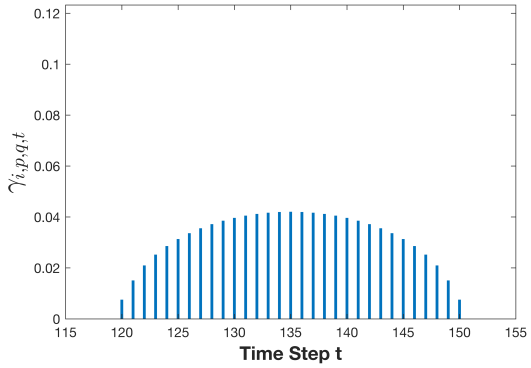

(d) Value of $\gamma_{i,p,q,t}$ of flight segment i at facilities (D2) in terminal q during time step t, with $t^s_{i,p,q} = 120$ and $t^e_{i,p,q} = 150$ and $\sum_t \gamma_{i,p,q,t} = 1$.

Figure 7: Example values of $\lambda_{i,p,q,t}$ and $\gamma_{i,p,q,t}$ of flight segment i at facilities (A1) and (D2) in terminal q over $t \in [115, 155]$.

Objective Function

We consider the following objective function:

$$\min_{x_{i,j,t}, z_{i,j,q}} Z = \sum_{i \in N} \sum_{j \in G_i^1} \sum_{t \in K} c^a_{i,j} x_{i,j,t} + w_{al} \sum_{i \in N_a \cup N_d} \sum_{j \in G_i^1} \sum_{q \in T} c^l_{i,j,q} z_{i,j,q}, \tag{29}$$

where $c^a_{i,j}$ and $c^l_{i,j,q}$ are time-invariant airside and landside cost coefficients, respectively. The objective function consists of two elements. The first element $\sum_{i \in N} \sum_{j \in G_i^1} \sum_{t \in K} c^a_{i,j} x_{i,j,t}$ expresses the cost of assigning flight segment $i \in N$ to gate $j \in G_i^1$ at time $t \in K$. The second element $\sum_{i \in N_a \cup N_d} \sum_{j \in G_i^1} \sum_{q \in T} c^l_{i,j,q} z_{i,j,q}$ expresses the cost of assigning flight segment $i \in N_a \cup N_d$ to gate $j \in G_i^1$ and its departing passenger stream to terminal $q \in T$.

The value of $c^a_{i,j}$ is based on size, customs and type requirements of flight $i \in N$ and gate $j \in G_i^1$, as

follows:

$$c^a_{i,j} = c^{\text{Customs}}_{i,j} + c^{\text{Size}}_{i,j} + c^{\text{Type}}_{i,j}. \tag{30}$$

where i) $c^{\text{Customs}}_{i,j}$ is the customs cost coefficients, ii) $c^{\text{Size}}_{i,j}$ is the size cost coefficients and iii) $c^{\text{Type}}_{i,j}$ denotes the type cost coefficient.

We discuss each airside cost coefficients below:

i) The cost of assigning flight segment i to gate j from a customs perspective is given by:

$$c^{\text{Customs}}_{i,j} = \begin{cases} 2^{1+\text{Customs}_j - \text{Customs}_i} - 1 & \text{if Customs}_j \geq \text{Customs}_i, \\ \infty & \text{otherwise,} \end{cases} \tag{31}$$

where Customs_i is the customs level of flight segment i and Customs_j is the customs level of gate j.

ii) The cost corresponding to assigning flight segment i to gate j from a size perspective is given by:

$$c^{\text{Size}}_{i,j} = \begin{cases} 2^{1+\text{Size}_j - \text{Size}_i} - 1 & \text{if Size}_j \geq \text{Size}_i, \\ \infty & \text{otherwise,} \end{cases} \tag{32}$$

where Size_i is the size of the aircraft serving flight segment i and Size_j is the size of gate j.

iii) The cost corresponding to assigning flight segment i to gate j from a size perspective is computed as a function of the type of flight segment i and the type of gate j, as shown in Table 6.

Table 6: Cost coefficients $c^{\text{Type}}_{i,j}$.

	Pier	Platform	Tow Truck	Apron
Functional flight segment	1	1000	∞	2000
Parking segment	100	10	∞	10
Towing segment	∞	∞	1	∞

The cost coefficients $c^l_{i,j,q}$ are constructed using eq. (33),

$$c^l_{i,j,q} = |q_j - q|\eta_i, \tag{33}$$

where q_j denotes the terminal that passenger streams to/from gate j are preferably allocated to and η_i denotes the number of seats in the aircraft serving flight segment i.

The weighting factor w_{al}=0.53 is used to scale the cost of the landside element accordingly; its value is computed using eq. (34),

$$E[c^a_{i,j}] = w_{al} \cdot E[c^l_{i,j,q}], \tag{34}$$

where the values of the cost coefficients $c^a_{i,j}$ and $c^l_{i,j,q}$ are based on the flight schedule of AMS on July 4, 2018 and the set of gates at AMS.

Constraints

Prior to discussing the constraints, additional notation is introduced. We define overlap probability at gate j during time step t to be the probability that two or more flight segments are assigned to a gate j during time step t. We make use of a scaling function $f(p_{i,t}, r)$ to ensure that addition of flight segment

presence probabilities $p_{i,t}$ is equal to 1 if the product of these flight presence probabilities equal to the maximum overlap probability r. We define $f(p_{i,t}, r)$ as follows Schaijk (2013):

$$f(p_{i,t}, r) = \frac{p_{i,t}}{r + p_{i,t}^2}. \tag{35}$$

An unrealistic flight splitting option is an assignment where a functional flight segment and a parking segment of a flight l are both assigned to gate j. We consider an example where a flight without an overnight stay is split using flight splitting option iii) (see subsection 5.1 1.). The flight is split in 5 segments, corresponding to segments 5 - 9 in Figure 2, indexed with i =131 - 135, which are a functional flight segment, a towing segment, a parking segment, a second towing segment and a second functional flight segment. We assume that during peak hours of operation all piers are running at full capacity and therefore flight segments 131, 133 and 135 of this flight are assigned to platform A34, and flight segments 132 and 134 of this flight are assigned to towing truck THW. Hence, this assignment of flight segments features a towing segment between a functional flight segment and parking segment, both of which are assigned to the same gate, and therefore, is unrealistic. We define $E_v^1 \subseteq N$ to be the set of flight segments in unrealistic flight splitting options $v \in V$. If we assume no other flight segments other than the flight segments in aforementioned example cause unrealistic flight splitting options, we have $V = [1, 2]$ with $E_1^1 = [131, 133]$ and $E_2^1 = [133, 135]$.

Additionally, we define:

$$s_{i,t} = \begin{cases} 1, & \text{if flight segment } i \text{ has a non-zero probability to be present at time } t, \\ 0, & \text{otherwise.} \end{cases}$$

We consider the following constraints:

$$\sum_{i \in N} f(p_{i,t}, r) p_{i,t} x_{i,j,t} \leq 1, \quad j \in M, \quad t \in K \tag{36}$$

$$s_{it} x_{i,j,t+1} - s_{i,t+1} x_{i,j,t} = 0, \quad i \in N, \quad j \in G_i^1, \quad t \in K \tag{37}$$

$$\sum_{i \in S_{l,t}} \sum_{j \in G_i^1} s_{i,t} x_{i,j,t} = 1, \quad l \in F, \quad t \in K, \tag{38}$$

$$\sum_{i \in E_v^1} x_{i,j,\tau} \leq 1, \quad j \in M, \quad v \in V \tag{39}$$

$$x_{i,j,t} = \sum_{q \in T} z_{i,j,q}, \quad i \in N_a, \quad j \in G_i^1, \quad t = STA_i \tag{40}$$

$$x_{i,j,t} = \sum_{q \in T} z_{i,j,q}, \quad i \in N_d, \quad j \in G_i^1, \quad t = STD_i \tag{41}$$

$$y_{p,q,t} = \sum_{i \in N_a \cup N_d} \sum_{j \in G_i^1} D_{i,p,q,t} z_{i,j,q}, \quad p \in H, \quad q \in T, \quad t \in K \tag{42}$$

$$y_{p,q,t} \leq b_{p,q,t}, \quad p \in H, \quad q \in T, \quad t \in K \tag{43}$$

Constraint (36) ensures that the overlap probability between flight segments scheduled at gate j at time t does not exceed a predefined level r (Schaijk and Visser, 2017). Constraint (37) ensures that a flight segment that is assigned to a particular gate at a particular time is not switched to a different

gate in a subsequent time step (Schaijk and Visser, 2017). Constraint (38) ensures that when a flight segment is present at the airport, it is assigned to one gate and only one. In addition, this constraint ensures that only one of the flight splitting options is selected. Constraint (38) extends constraint (3) in Schaijk and Visser (2017) to allow for flight splitting by summing over the set $S_{l,t}$. Constraint (39) ensures that all unrealistic flight splitting options are mitigated from the solution space, where τ is the first time step $t \in K$ flight segment i has a non-zero presence probability. Therefore, following the example presented above, constraint (39) ensures that flight segment 131 and 133 (133 and 135) cannot be assigned to the same gate. Constraints (40) and (41) indicate that for every flight segment $i \in N_a \cup N_d$ assigned to gate $j \in G_i^1$, departing passenger streams can only be directed to one terminal. If $x_{i,j,t}$ for $t = \{STA_i, STD_i\}$ is equal to 1, only one of the decision variables $z_{i,j,q}$ for $q \in T$ can take a value of 1. If $x_{i,j,t}$ for $t = \{STA_i, STD_i\}$ is equal to 0, $z_{i,j,q}$ for $q \in T$ are automatically set to 0. Constraint (42) indicates that the passenger demand imposed on facility $p \in H$ in terminal $q \in T$ at time $t \in K$ is a function of the decision variables $z_{i,j,q}$. Constraint (43) sets an upper bound to the value of $y_{p,q,t}$, denoted by the parameter $b_{p,q,t}$.

Optimisation algorithm - an iterative approach

We solve the FGAP model in eq. (29), (36) - (43) using an iterative solving algorithm to produce a valid solution.

Constraint (36) can be violated if three or more flight segments with a non-zero presence probability are assigned to gate j at time step t. We consider an example to clarify a possible violation of constraint (36). Assume three flight segments (i_x, i_y and i_z) are assigned to gate j at time step t, each with a presence probability $p_{i,t} = 0.2$ and the maximum allowed overlap probability $r = 0.1$. The scaled presence probability $f(p_{it}, r)p_{it}$ for each of these flight segments is equal to 0.2857. The sum of the scaled presence probability is less than 1, thus, these flight segments can be assigned to the same gate at the same time. However, the overlap probability of flight segments i_x, i_y and i_z at gate j at time t is 0.104, and therefore exceeds the maximum overlap probability $r = 0.1$, violating constraint (36).

To mitigate violations of constraint (36), we propose an iterative optimisation algorithm of the FGAP model in eq. (29), (36) - (43), which is as follows:

i) we solve FGAP model with airside and landside constraints in eq. (29), (36) - (43),

ii) we check for violations of the maximum overlap probability constraint (36),

iii) if a violation of constraint (36) occurs, we extend the FGAP model indicated by eq. (29), (36) - (43) with constraint (44),

$$\sum_{i \in E_w^2} x_{i,j,t} \leq 2, \quad j \in M, \quad t \in K, \quad w \in W \tag{44}$$

where E_w^2 denotes the set that contains the flight segments that each contribute to the violation $w \in W$ and the set W contains the violations of the maximum overlap probability constraint (36). This constraint ensures at most two flight segments that cause violation w of constraint (36) are assigned to the same gate,

iv) we solve FGAP model in eq. (29), (36) - (43), (44),

v) we repeats steps ii), iii) and iv) until no violations of constraint (36) occur or the maximum number of iterations is reached.

6. Specification of $b_{p,q,t}$ in passenger demand constraint (43)

The value of the parameter $b_{p,q,t}$ in constraint (43) can be set such that i) only airside constraints are active, ii) both airside and landside constraint are active, and passenger demand cannot exceed the declared landside capacity and iii) both airside and landside constraint are active, and the landside passenger constraints are driven by the expected maximum passenger waiting time, rather than a fixed upper bound. We discuss each of these 3 options below:

i) Active airside constraints and inactive landside constraints

We consider the model indicated by eq. (29), (36) - (43) and (44) and we set:

$$b_{p,q,t} = \infty. \tag{45}$$

Eq. (45) ensures only airside constraints are active since the decision variables related to the passenger demand, $y_{p,q,t}$, are not constrained in any way.

We refer to the model indicated by eq. (29), (36) - (43) and (44) with $b_{p,q,t} = \infty$ as the A-FGAP model.

ii) Active airside and landside constraints - passenger demand cannot exceed declared capacity

We consider the model indicated by eq. (29), (36) - (43) and eq. (44) and we set:

$$b_{p,q,t} = C_{p,q}, \quad t \in K, \tag{46}$$

where $C_{p,q}$ is the declared capacity of facility p in terminal q during a time step of 5min.

We assume fixed hourly declared capacity for each airport facility (see Table 4). We also assume that the number of passengers per hour is distributed uniformly over time. Thus, the value of $C_{p,q}$ is computed by dividing the hourly capacities in Table 4 with the factor 60/5, given that we consider time steps of 5min. Consider, as an example, facilities (D1) in Terminal 2. As shown in Table 4, this facility has a declared capacity of 1380 passengers/hour. The corresponding value of $C_{D1,2} = \frac{1380}{60/5} = 115$ passengers per 5min.

Eq. 46 ensures that for a given flight-to-gate assignment, passenger demand at any facility in the airport is at most the declared capacity of the facilities.

We refer to the model indicated by eq. (29), (36) - (43) and (44) with $b_{p,q,t} = C_{p,q}$ as the DC-FGAP model.

iii) Active airside and landside constraints - maximum passenger waiting time drives landside constraints

In this subsection, we first introduce the model for the expected passenger waiting time at airport facilities. Further, we will make use of this model to set the parameters $b_{p,q,t}$ in constraint (43), such that the expected maximum passenger waiting time does not exceed a user-defined threshold.

1. Expected maximum passenger waiting time model: We introduce a model to determine the expected maximum waiting time for a passenger at a facility in the airport. This model is applied to all facilities considered in this paper (see also Table 3).

We define a peak demand period $n \in U_{p,q}$ for facility p in terminal q as a period where the passenger demand per time step exceeds the average demand per time step, where $U_{p,q}$ is the set of peak periods at facility $p \in H$ in terminal $q \in T$. The expected maximum waiting time for facility p in terminal q during peak period n ($W_{p,q,n}$) is estimated to be (Solak et al., 2006):

$$W_{p,q,n} = \frac{E[L_{p,q,n}] + 1.65\sqrt{\text{Var}[L_{p,q,n}]}}{C_{p,q}}, \tag{47}$$

where $C_{p,q}$ is the declared capacity of facility p in terminal q during a time step with a length 5min, and $L_{p,q,n}$ is the queue length during peak period n at facility p in terminal q.

We assume that $L_{p,q,n}$ follows a Normal distribution with mean $E[L_{p,q,n}]$ and variance $\text{Var}[L_{p,q,n}]$. The scaling factor 1.65 in eq. (47) ensures we use the 95th percentile of the distribution of $L_{p,q,n}$ as a proxy for the maximum queue length during peak period n at facility p in terminal q.

To approximate $L_{p,q,n}$, Solak et al. (2006) propose to use a parabolic approximation of the passenger demand curve in a discrete time-system. The parabolic approximation of peak demand period n for facility p in terminal q, denoted by $y^{pb}_{p,q,t}$, is modelled as follows:

$$y^{pb}_{p,q,t} = \max_t(y_{p,q,t}) - a_{p,q,n}\Big(t - \frac{T_{p,q,n}}{2}\Big)^2, \tag{48}$$

where the scaling coefficient $a_{p,q,n} = 4(\max_t(y_{p,q,t}) - E_t[y_{p,q,t}])/T^2_{p,q,n}$ and $T_{p,q,n} = t^e_{p,q,n} - t^s_{p,q,n}$.

From Solak et al. (2006), the expected value of $L_{p,q,n}$ is computed as follows:,

$$E[L_{p,q,n}] \approx 0.95\sqrt[3]{C_{p,q}} + \frac{2(\max_t(y^{pb}_{p,q,t}) - C_{p,q})^{3/2} T_{p,q,n}}{3\sqrt{c_{p,q,n}\max_t(y^{pb}_{p,q,t})}} \tag{49}$$

where $c_{p,q,n} = 1 - E_t[y^{pb}_{p,q,t}]/\max_t(y^{pb}_{p,q,t})$. Also, the variance of $L_{p,q,n}$ is as follows (Solak et al., 2006):

$$\text{Var}[L_{p,q,n}] \approx -0.3{C_{p,q}}^{2/3} + 2\sqrt{c_{p,q,n}\max_t(y^{pb}_{p,q,t})(\max_t(y^{pb}_{p,q,t}) - C_{p,q})} - \frac{4(\max_t(y^{pb}_{p,q,t}) - C_{p,q})^{3/2}}{3\sqrt{c_{p,q,n}\max_t(y^{pb}_{p,q,t})}}. \tag{50}$$

2. Dynamically setting the value of $b_{p,q,t}$ in constraint (43) using $W_{p,q,t}$: We dynamically adjust the parameters $b_{p,q,t}$ in constraint (43) such that the expected maximum waiting time for passengers at the airport facilities considered does not exceed a user-defined threshold W^T. We achieve this as follows:

i) we set $b_{p,q,t} = \infty$ in constraint (43),

ii) we solve model indicated by eq. (29), (36) - (43) and eq. (44),

iii) we determine the expected maximum passenger waiting time $W_{p,q,n}$ associated with the flight-to-gate assignment obtained, for all $p \in H$, $q \in T$, and $n \in U_{p,q}$,

iv) we check if $W_{p,q,n} > W^T$ and if so, the value of $b_{p,q,t}$ is decreased as follows:

$$b_{p,q,t} = \max_{t \in [t^s_{p,q,n}, t^e_{p,q,n}]}(y_{p,q,t}) - \Delta_s, \quad t \in [t^s_{p,q,n}, t^e_{p,q,n}], \tag{51}$$

where $t^s_{p,q,n}$ and $t^e_{p,q,n}$ denote the start and end time of peak period n at facility p in terminal q, respectively, and Δ_s is a adjustment parameter. We select a value of $\Delta_s = 1$. This ensures that the optimality

of the final solution obtained for the FGAP model in eq. (29), (36) - (43) and eq. (44) is not compromised by setting a value of Δ_s too large.

v) We repeat steps ii), iii), iv) until $W_{p,q,n} \leq W^T$, for all $p \in H$, $q \in T$, and $n \in U_{p,q}$.

We refer to the model indicated by eq. (29), (36) - (43) and (44) where expected passenger waiting times drives landside constraints, as shown above, as the WT-FGAP model.

7. AMS-specific constraints

To reflect realistic operating conditions and restrictions at AMS, additional AMS-specific constraints are considered as follows.

Combined airside gate facilities

At AMS, the gates in the D-pier and H/M-pier are grouped in pairs. Gates in each pair have distinct landside facilities, but share airside facilities such as a jet bridge, etc. Thus, only one of the gates in each pair can be in use at any given time. Therefore, the models are extended with a constraint that enforces this rule as follows:

$$\sum_{j \in G_o^2} x_{i,j,t} \leq 1, \quad i \in N, \quad o \in O, \quad t \in K, \tag{52}$$

where the set O is the set of all gate pairs and G_o^2 denotes the gate indices of the gates in pair $o \in O$.

Terminal reallocation restrictions

Terminal reallocations of departing passenger streams are restricted in accordance with the topology of AMS as follows:

$$\sum_{i \in N} z_{i,j,q} = 0, \quad j \in G_q^3, \quad q \in T, \tag{53}$$

where G_q^3 denotes the set of gates whose departing passenger flows cannot be serviced by terminal $q \in T$, i.e., the set G_q^3 contains the gates whose departing passenger streams cannot be reallocated to terminal $q \in T$.

8. Results

This section presents the results of the flight-to-gate assignment models, taking into account AMS specific constraints. Results of the A-FGAP model are used a benchmark since this model considers airside constraints only. The DC-FGAP model ensures that the passenger demand at facility p in terminal q during time step t does not exceed the declared capacity $C_{p,q}$, where $C_{p,q}$ is derived using the hourly declared passenger capacities in Table 4. The WT-FGAP has an optimisation algorithm that dynamically adjusts the values of the parameters $b_{p,q,t}$ in constraint (43), such that the passenger waiting time does not exceed a user-defined threshold.

For computational reasons, a compression factor of 5 is applied to the the flight schedule on July, 4 2018 at AMS and set of gates at AMS, i.e., only every 5th flight and gate is included in the analysis.

All the models are solved using IBM CPLEX Optimization Studio (IBM, 2019) and a computer with a 2.3GHz Intel Core i5 processor and 16GB of DDR3 RAM.

8.1. Assignment of flight segments to gates

In this section we show the assignment of flights to gates taking into account: i) only airside constraints, ii) both airside and landside constraints with fixed landside facility capacities, and iii) both airside and landside constraints, without fixed facility capacities, and passenger waiting time constraints.

Figure 8 shows the assignment of flights to gates when considering only airside constraints (see Section 6 i)). The results show that functional and parking flight segments have a varying length, with a minimum duration of 45 and 90min, respectively. On average, a buffer time of 109.5min is allocated between flights. The minimum separation time between functional flight segments is 25min. One functional flight segment is assigned to a platform. All flight splitting options are used, except for flight splitting option v) (see Section 5.1, Flight splitting).

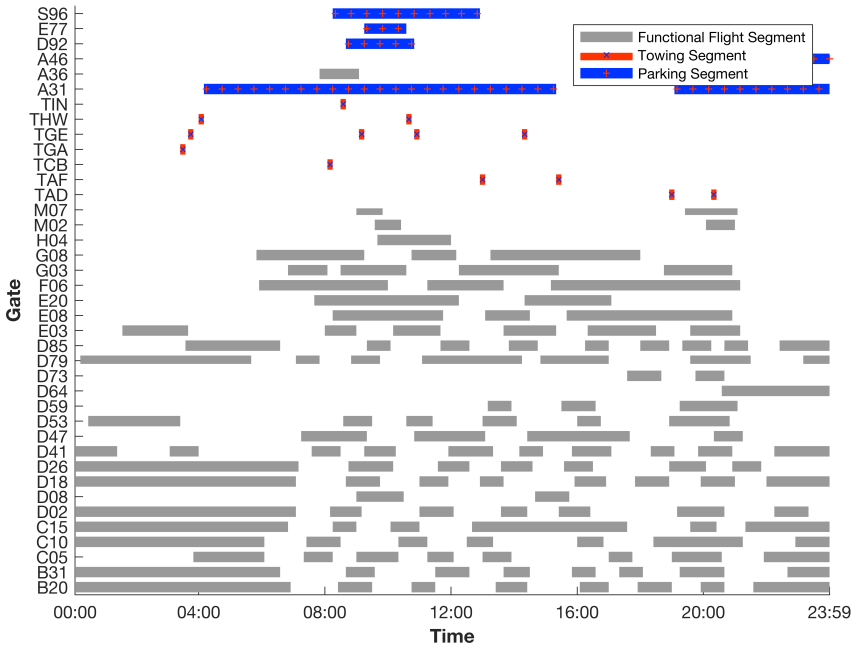

Figure 8: Assignment of flight segments to gates under the A-FGAP model, $r = 5\%$, 10 maximum number of iterations for the solving algorithm.

Figure 9 shows the assignment of flights to gates when considering both airside and landside constraints with fixed landside facility capacities (see Section 6 ii)). The results show that functional and parking flight segments have a varying length, with a minimum duration of 45 and 90min, respectively. The average buffer time is 104.9min, with a standard deviation of 9.5min. The minimum separation time between functional flight segments is 25min. Three functional flight segments are assigned to a platform. All flight splitting options are used, except for flight splitting option v) (see section 5.1, Flight splitting).

Figure 10 shows the assignment of flights to gates when considering both airside and landside constraints without fixed facility capacities, and passenger waiting time constraints (see Section 6 iii)). Functional and parking flight segments have a varying length, with a minimum duration of 45 and 90min, respectively. The average buffer time is 105.3min. The standard deviation of the buffer time has a value

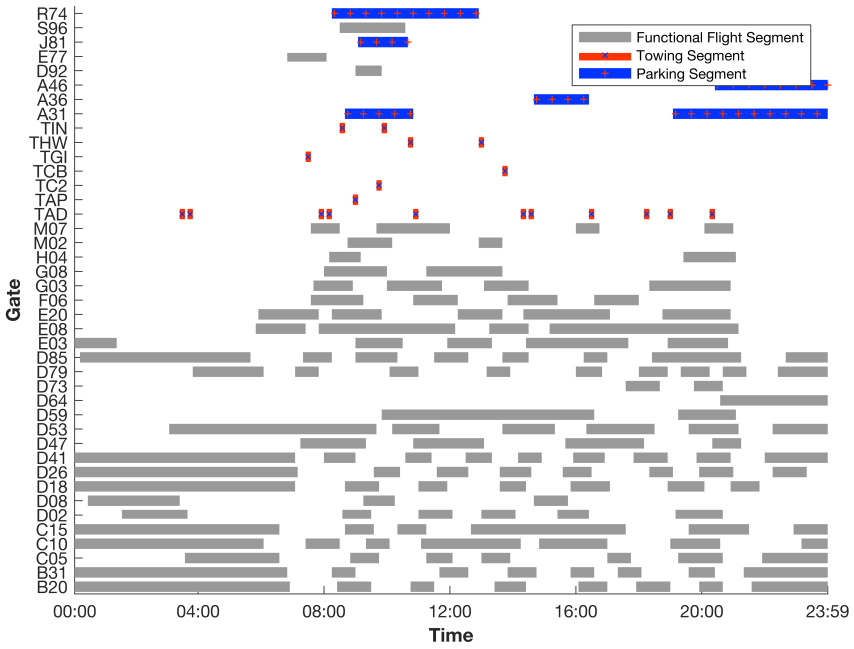

Figure 9: Gate assignment planning derived using the DC-FGAP model, $r = 5\%$ and a maximum number of 10 iterations of the solving algorithm.

of 9.3min and is marginally larger compared to the standard deviation found using the A-FGAP model. The minimum separation time between functional flight segments is equal to 25min. One functional flight segment is assigned to a platform. All flight splitting options are used, except for flight splitting option v) (see section 5.1, Flight splitting).

Figure 11a and 11b indicate the assignment of functional flight segments under the DC-FGAP and WT-FGAP models relative to the A-FGAP model, respectively. For example, Figure 11a shows that 13.7% and 14.5% of all functional flight segments are assigned to concourse C if the DC-FGAP model and the A-FGAP model are used, respectively. Reallocation of functional flight segments between concourses occurs when different FGAP models are used due to the equivalence in characteristics between gates in different concourses. For example, piers in concourses B, C and D59-87 have similar size and customs characteristics. A clear division between concourses that serve Schengen flights (B, C, D59-87, M) and concourses that serve Non-Schengen flights (A, D03-D57, E, F, G, H, S) is observed. The WT-FGAP model imposes passenger demand constraints that are less s as strict compared to the DC-FGAP model. Thus, less deviations from the solution of the A-FGAP model are needed when using the WT-FGAP model as compared to the DC-FGAP model.

8.2. Landside performance metrics

In this section we analyse the impact of the flight-to-gate assignment on the landside facilities by means of two metrics: the demand-capacity ratio and the expected maximum passenger waiting time.

We define the demand-capacity ratio for facility p in terminal q, denoted by $m_{p,q}$, to be ratio between the maximum passenger demand imposed on facility p in terminal q and the declared capacity $C_{p,q}$, as

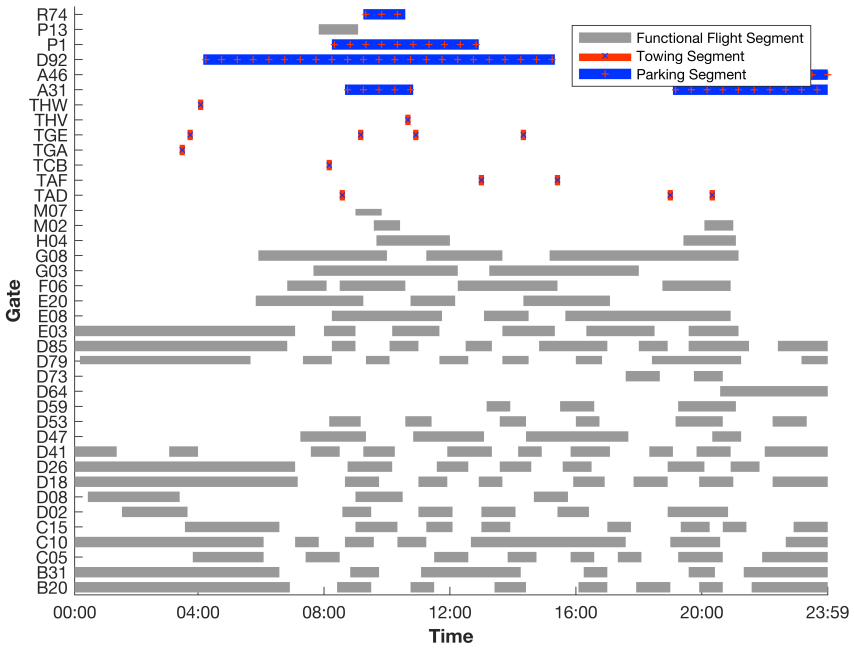

Figure 10: Gate assignment planning derived using the WT-FGAP, $r = 5\%$, $W^T = 25$min, and a maximum number of 10 iterations of the solving algorithm.

follows:

$$m_{p,q} = \max_t \frac{y_{p,q,t}}{C_{p,q}} \cdot 100\%, \quad p \in H, \quad q \in T. \tag{54}$$

Figures 12a and 12b provide an example of how this metric is computed for cases where $\max_t y_{p,q,t} < C_{p,q}$ and $\max_t y_{p,q,t} > C_{p,q}$, respectively.

We define the maximum expected passenger waiting time over all peak periods n at facility p in terminal q, denoted by $W^{\max}_{p,q}$, as follows:

$$W^{\max}_{p,q} = \max_n (W_{p,q,n}), \quad p \in H, \quad q \in T. \tag{55}$$

Figure 13a shows the demand-capacity ratios for all facilities and terminals at AMS under the A-FGAP model, which considers airside constraints only since values of $b_{p,q,t}$ are not bounded. Thus, $m_{p,q}$ can be larger than 100%, e.g., $m_{T1,3} = 250\%$ and all facilities in Terminal 2 and facilities (A2) in Terminal 4 have a $m_{p,q} > 100\%$. Facilities (D1) and (D2) have a value of $m_{p,q} < 30\%$. Figure 13b shows the expected maximum waiting times for all facilities and terminals at AMS under the A-FGAP model. For facilities (T1) in Terminal 3 and facilities (D1) in Terminal 2, $W^{\max}_{p,q} > W^T$. Due to a short duration of the peak demand periods at facilities (T1) in Terminal 2, the value of $m_{p,q} > 100\%$ but $W^{\max}_{p,q} < 1$min.

Figure 13c shows the demand-capacity ratios for all facilities and terminals at AMS under the DC-FGAP model, which imposes constraints such that $y_{p,q,t} \leq C_{p,q}$. Thus, $m_{p,q} \leq 100\%$ for all facilities and terminals. Facilities (A1) and (A2) in Terminal 3 and 4 and all facilities in Terminal 2 and 3 have a $m_{p,q}$ equal or close to 100%. As expected, Figure 13b shows that $W^{\max}_{p,q} < 1$min for all facilities and terminals.

Figure 13e shows the demand-capacity ratios for all facilities and terminals at AMS under the WT-FGAP model, which dynamically sets the values of the parameters $b_{p,q,t}$ such that all $W_{p,q,n} \leq W^T$.

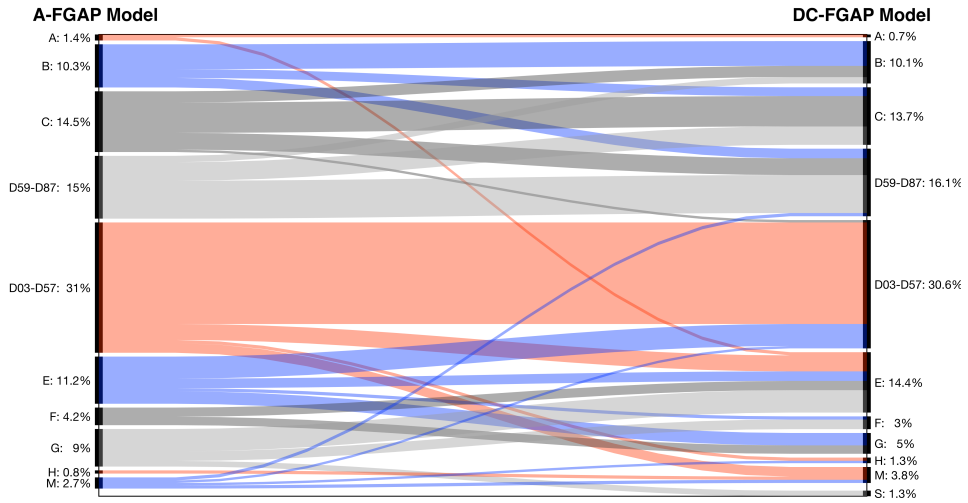

(a) DC-FGAP model vs. A-FGAP model.

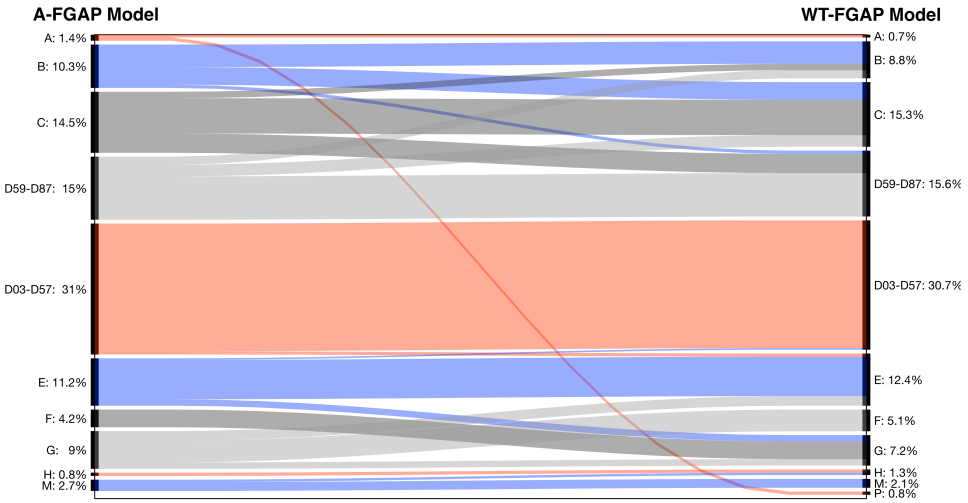

(b) WT-FGAP model vs. A-FGAP model.

Figure 11: Comparison of functional flight segment allocation to concourses at AMS of the the DC-FGAP model and WT-FGAP relative to the A-FGAP model, $r = 5\%$, $W^T = 25$min, and a maximum number of 10 iterations of the solving algorithm.

Facilities (A2) in Terminal 4, facilities (A1), (A2), (T1) in Terminal 3 and all facilities in Terminal 2 have $m_{p,q} > 100\%$. Figure 13f shows the expected maximum waiting times for all facilities and terminals at AMS under the WT-FGAP model. For facility (A2) in Terminal 3, facility (T1) in Terminal 3 and facilities (A1), (A2) and (D1) in Terminal 2, $W^{\max}_{p,q} > 5$min. All values of $W^{\max}_{p,q} < W^T$, as imposed by the WT-FGAP model.

Four iterations of the solving algorithm (see section 6 iii)) are needed to create a valid solution to the WT-FGAP model. Figures 14a - 14b and 14c - 14d show the passenger demand curves and non-infinity values of $b_{p,q,t}$ for facilities (A1) in Terminal 3 and facilities (D2) in Terminal 2 in iteration 1 and 4 of

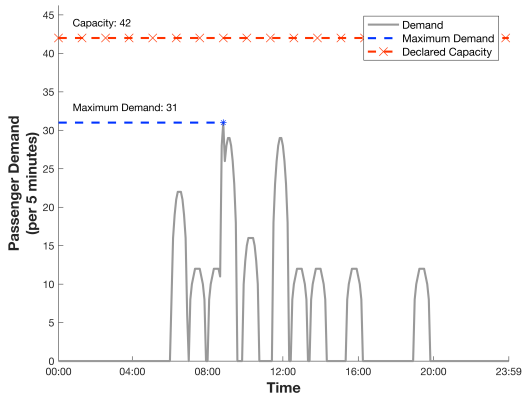

(a) Demand-capacity ratio at facilities (A1) in Terminal 3 where $\max_t y_{p,q,t} < C_{p,q}$; $m_{p,q} = 31/42 \cdot 100\% = 73.8\%$.

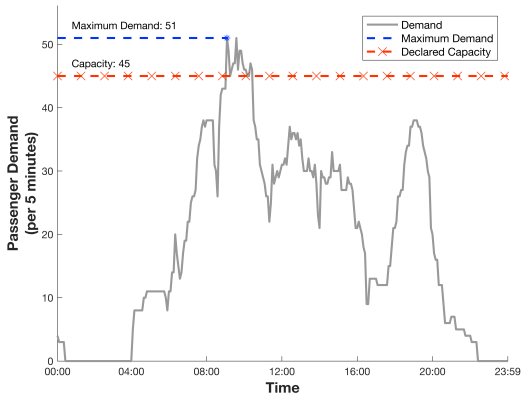

(b) Demand-capacity ratio at facilities (D2) in Terminal 2 where $\max_t y_{p,q,t} > C_{p,q}$; $m_{p,q} = 51/45 \cdot 100\% = 113.3\%$.

Figure 12: Examples of demand-capacity ratio $m_{p,q}$ calculated using the A-FGAP model, $r = 5\%$ and a maximum of 10 iterations for the solving algorithm.

the solving algorithm of the WT-FGAP model, respectively. All values of $b_{p,q,t} = \infty$ during iteration 1. In iteration 4 for these facilities, a subset of $b_{p,q,t}$ are given a finite value to ensure that $W^{\max}_{p,q} \leq W^T$. In general, $W^{\max}_{p,q} > W^T$ during the iterations of the optimisation algorithm for facilities (T1) in Terminal 3 and facilities (A1), (A2) and (D1) in Terminal 2. Therefore, values of $b_{p,q,t}$ in the WT-FGAP model have values other than infinity for facilities (T1) in Terminal 3 and facilities (A1), (A2) and (D1) in Terminal 2. Over all facilities, terminals and time steps, only 3.84% of the parameters $b_{p,q,t}$ in the WT-FGAP model need to have a finite value to ensure $W^{\max}_{p,q} \leq W^T$.

9. Sensitivity analysis

This section analyses the sensitivity of the objective function value of the FGAP models to the declared capacity $C_{p,q}$ and the maximum waiting time threshold W^T. The computation times of the AMS-specific FGAP models as a function of the data compression ratio are also described. All numbers presented in this section are based on the mean of $n = 5$ runs.

9.1. Declared capacity $C_{p,q}$

Figure 15a and 15b present the Pareto fronts of the objective function values of the FGAP models as a function of the declared capacity scaling factor $\alpha \in [0.7, 1.3]$, such that $C^{\text{scaled}}_{p,q} = \alpha \cdot C_{p,q}$. The solution to the A-FGAP model does not depend on the scaled declared capacity $C^{\text{scaled}}_{p,q}$, resulting in a horizontal Pareto front. The objective function value the WT-FGAP model decreases as the scaling factor α increases. However, these values deviate no more than 1% from the objective function value of the A-FGAP model. For scaling factors $\alpha < 0.95$, no feasible solutions are found for the DC-FGAP model. For scaling factors $\alpha \geq 0.95$, the objective function value of the DC-FGAP model decreases as the scaling factor α increases.

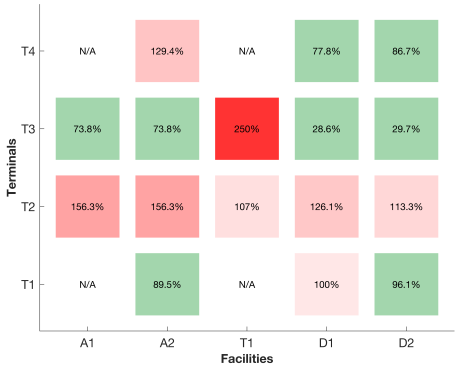

(a) A-FGAP: demand-capacity ratios $m_{p,q}$

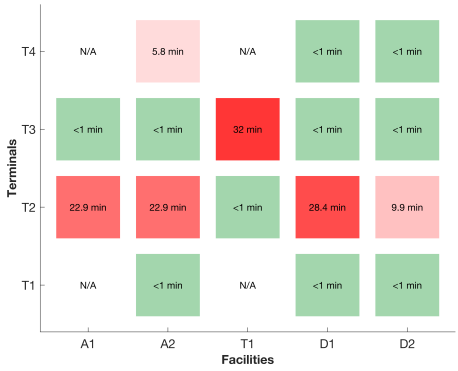

(b) A-FGAP: maximum waiting time $W_{p,q}^{\max}$.

(c) DC-FGAP: demand-capacity ratios $m_{p,q}$.

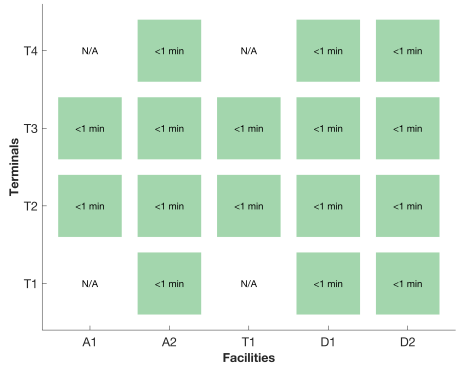

(d) DC-FGAP: maximum waiting time $W_{p,q}^{\max}$.

(e) WT-FGAP: demand-capacity ratio $m_{p,q}$.

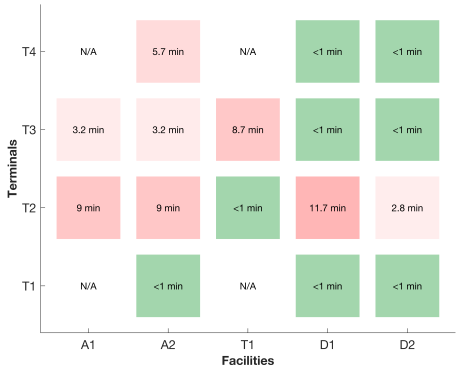

(f) WT-FGAP: maximum waiting time $W_{p,q}^{\max}$.

Figure 13: Overview of landside performance metrics for the AMS-Specific FGAP Models, $r = 5\%$, $W^T = 25$min, $\nu = 1.65$ and a maximum number of 10 iterations of the optimisation algorithm.

9.2. Waiting time threshold W^T

Figure 16 shows the Pareto fronts of objective function values as a function of the maximum waiting time threshold W^T. The Pareto front of the A-FGAP model and DC-FGAP model are horizontal lines because their objective function values do not depend on the value of W^T. The objective function value

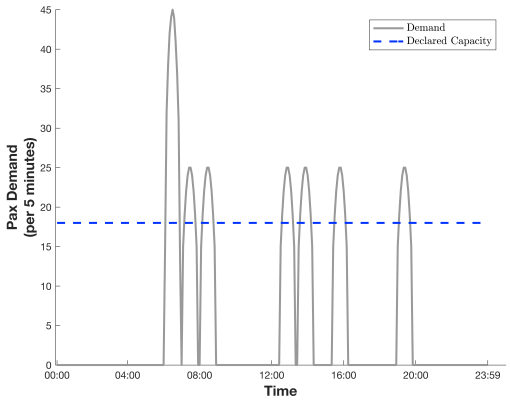

(a) Facilities (T1) in Terminal 3 in iteration 1.

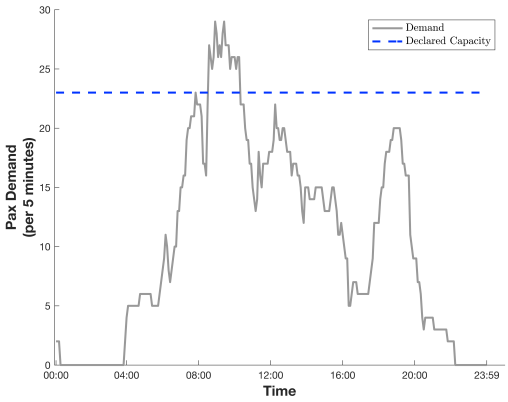

(b) Facilities (D1) in Terminal 2 in iteration 1.

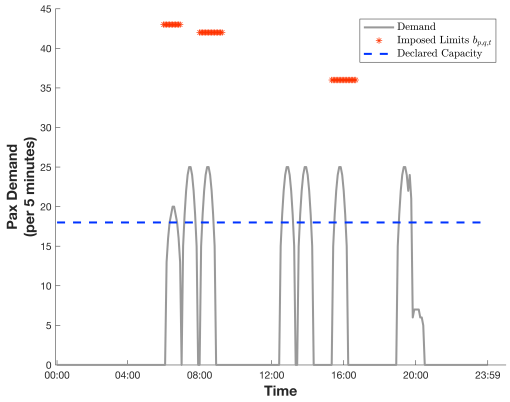

(c) Facilities (T1) in Terminal 3 in iteration 4.

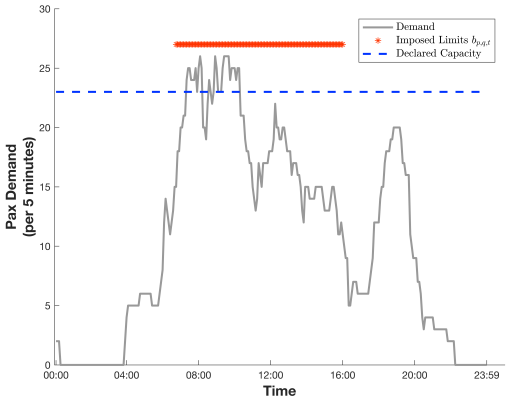

(d) Facilities (D1) in Terminal 2 in iteration 4.

Figure 14: Passenger demand for facilities (T1) in Terminal 3 and facilities (D1) in Terminal 2. In iteration 1 (Figure 14a - 14b), all values of $b_{p,q,t} = \infty$. In iteration 4 (Figure 14c - 14d), a subset of parameters $b_{p,q,t}$, whose value is set dynamically by the WT-FGAP model, has a value other than infinity such that all $W_{p,q,n} \leq W^T$. Results are obtained with $r = 5\%$, $W^T = 25$min, and a maximum number of 10 iterations of the solving algorithm.

of the WT-FGAP model decreases as the waiting time threshold W^T increases in value. If $W^T \to 0$, values of $b_{p,q,t}$ in constraint (43) approach $C_{p,q}$. If $W^T \to \inf$, values of $b_{p,q,t}$ are equal to infinity. Therefore, the objective function value of the WT-FGAP model is bounded; the lower bound ($W^T \to \inf$) and the upper bound ($W^T \to 0$) are the objective function values of the A-FGAP model and DC-FGAP model respectively.

9.3. Computation time

Table 7 indicates the build time and solving of the FGAP models as a function of the compression factor, based on the average of $n = 5$ runs. The A-FGAP, DC-FGAP and WT-FGAP models have the same mathematical model and, thus, their build times are equal. Build times increase exponentially as

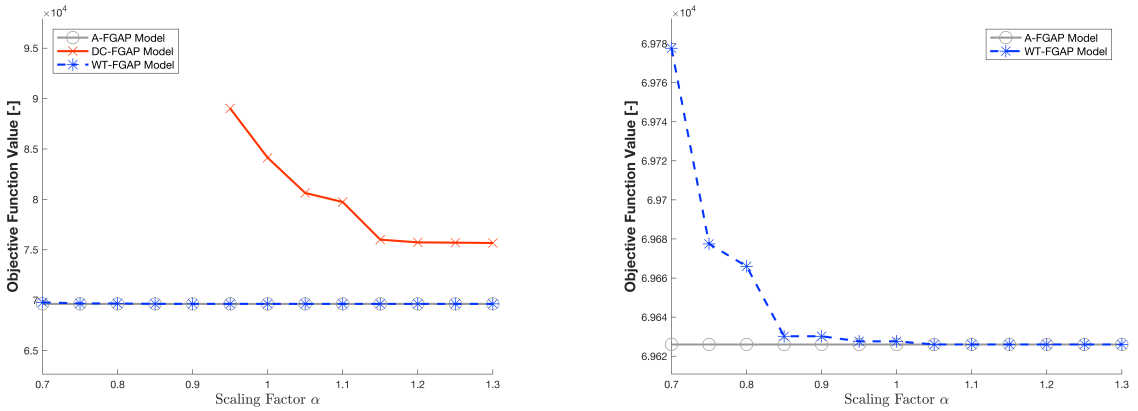

(a) Pareto front of scaling factor α.

(b) Close up of Pareto front of scaling factor α.

Figure 15: Pareto front of scaling factor α for capacity $C_{p,q}$ with $r = 5\%$, $W^T = 25$min, and a maximum number of 10 iterations of the solving algorithm, and based on $n = 5$ runs.

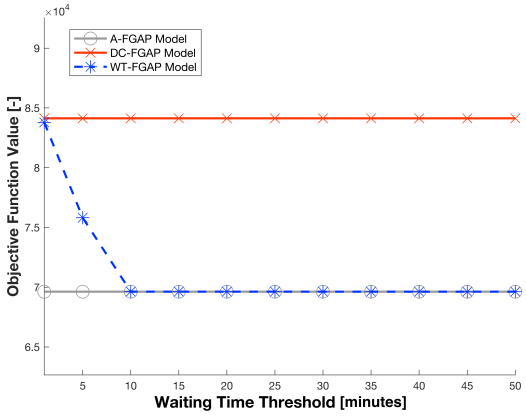

Figure 16: Pareto front of maximum waiting time threshold W^T with $r = 5\%$ and a maximum number of 10 iterations of the solving algorithm, and based on $n = 5$ runs.

the compression factor decreases. Solving times vary between the FGAP models considered. Solving times increase exponentially as the compression factor decreases.

10. Conclusions and recommendations

In existing literature, FGAP models do not consider airside and landside constraints simultaneously. Research on improving the robustness of the solution to the FGAP is ongoing. In this study, we proposed two FGAP models that consider airside and landside constraints simultaneously, alongside a benchmark model which considers airside processes only. The DC-FGAP model enforces upper bounds on passenger demand per time step at landside passenger facilities. The WT-FGAP model ensures a gate assignment plan is constructed such that the expected maximum waiting for passengers does not exceed a predefined threshold. We considered the flight schedule of July 4, 2018 as support for the flight-to-gate assignment problem in this paper.

Table 7: Overview of the average build time and solving time of the A-FGAP, DC-FGAP and WT-FGAP models, based on $n = 5$ runs.

	Compression Factor [-]					
	5	6	7	8	9	10
Build Time [s]						
· *A/DC/WT-FGAP*	1725.7	790.1	440.3	260.7	187.9	103.2
Solving Times [s]						
· *A-FGAP*	21.5	8.8	6.6	4.1	3.8	2.7
· *DC-FGAP*	37.5	17.6	9.5	6.4	5.2	4.0
· *WT-FGAP*	211.9	37.3	26.1	23.1	20.2	18.4

The A-FGAP model provides the most cost-efficient approach by at the expense of passenger comfort. The DC-FGAP model ensures a high level of passenger comfort by ensuring waiting times of less than one minute for airport passengers. However, this comes at an increased cost for the airport operator due to flight segment reallocation relative to the A-FGAP model. Finally, the WT-FGAP model provides an intermediate approach, where the expected maximum waiting time of passengers is ensured to be below a user-defined threshold with a 95% probability. The DC-FGAP model creates a gate assignment at an increased cost compared to the WT-FGAP model, but does offer a superior passenger experience since waiting times are non-existent.

Future work includes the implementation of flight-specific input, methods to decrease build and solving times, and probability modelling. Flight-specific input, including flight-specific presence probabilities, check-in rates, transfer-rates and load factor, allows for a more realistic representation of flights in the flight-to-gate assignment problem. A decrease in build and solving times allows for larger data sets to be analysed, possibly leading to an analysis of the flight-to-gate assignment problem covering all gates and flight in the planning horizon at AMS. As a result of flight splitting, presence probability curves of flight segments are non-continuous. Extending the analysis to produce continuous flight presence probabilities for flight segment will reduce the number of violations of the maximum overlap probability constraint.

Bibliography

O. Schaijk, H. Visser, Robust flight-to-gate assignment using flight presence probabilities, Transportation Planning and Technology 40 (8) (2017) 928–945.

I. Manataki, K. Zografos, A generic systems dynamics based tool for airport terminal performance analysis, Transportation Research Part C 17 (2009) 428–443.

Y. Li, X. Gao, Z. Xu, Z. Zhou, Network-based queuing model for simulating passenger throughput at an airport security checkpoint, Journal of Transport Management 66 (2018) 13–24.

I. Kusumaningtyas, G. Lodewijks, On the application of accelerating moving walkways to support passenger processes in Amsterdam Airport Schiphol, Transportation Planning and Technology 36 (7) (2013) 617–635.

N. van Dijk, E. van der Sluis, Check-in computation and optimization by simulation and IP in combination, European Journal of Operational Research 171 (2006) 1152–1168.

S. Solak, J. Clarke, E. Johnson, Airport terminal capacity planning using delay time approximations and multistage stochastic programming, georgia Institute of Technology, 2006.

C. Yu, D. Zhang, H. Lau, MIP-based heuristics for solving robust gate assignment problems, Computers and Industrial Engineering 93 (2016) 171–191.

C. Yu, D. Zhang, H. Lau, An adaptive large neighborhood search heuristic for solving a robust gate assignment problem, Expert Systems with Applications 84 (2017) 143–154.

M. Seker, N. Noyan, Stochastic optimization models for the airport gate assignment problem, Transport Research Part E: Logistics and Tranportation Research 48 (2) (2012) 438–559.

H. Beyer, B. Sendhoff, Robust optimization - A comprehensive survey, Computer methods in applied mechanics and engineering 196 (2007) 3190–3218.

S. Yan, C. Chang, A network model for gate assignment, Journal of Advanced Transportationq 32 (2) (1997) 176–189.

S. Yan, C. Huo, Optimization of multiple objective gate assignments, Transport Research Part A 35 (2001) 413–432.

G. Diepen, J. van den Akker, J. Hoogeveen, J. Smeltink, Finding a robust assignment of flights to gates at Amsterdam Airport Schiphol, Journal of Scheduling 15 (2012) 703–715.

S. Kim, E. Feron, J. Clarke, Airport gate scheduling for passengers, aircraft and operation, in: Europe Air Traffic Management Research and Development Seminar, 2013.

AMS Traffic Review 2018, Digital, Evert van de Beekstraat 202, 1118 CP Schiphol, Netherlands, 2019.

A. Odoni, Airport Demand Management, Lecture Notes AE4446: Delft University of Technology, 2017.

H. Chun, R. Mak, Intelligent resource simulation for an airport check-in counter allocation system, Transactions on Systems, Man and Cybernetics-Part: Applications and Reviews 29 (3) (1999) 325–335.

O. Schaijk, Finding robust solutions to the flight to gate assignment problem using flight presence probabilities, Master's thesis, Delft University of Technology, 2013.

IBM, IBM CPLEX Optimization Studio, URL `https://www.ibm.com/analytics/cplex-optimizer`, 2019.

Part II

Technical Report

Chapter 1

Introduction

The main purpose of gate scheduling is to find an assignment of flights, or rather the aircraft serving these flights, to the available gates (Dorndorf et al., 2007). This problem is known as the Flight-to-Gate Assignment Problem (FGAP). In this process, the start and end times for processing an aircraft at each of the available gates are determined. At large international airport, where hundreds of flights are handled daily, the process of gate scheduling is complex, involving airport resource constraints, airline preferences and quality of service requirements for passengers inside the terminals. This process becomes even more involved when taking into account the uncertainty in the arrival and departure flight times to and from the airport.

FGAP models proposed in literature often use the strategic schedule of arrival and departure flight times at an airport, the type of aircraft associated with these flights and the set of airport gates as input. The resulting gate assignment is an optimal strategic solution for the given input. However, such gate assignments lack robustness as they are sensitive to perturbations in the arrival/departure flight times. In a real-life environment, flight arrival/departures are often subject to delays. In this case, the strategic gate assignment solution can no longer be readily applied. Equally important, these approaches consider airside related constraints only and, at most, passenger-specific requirements, such as, for instance, minimal passenger walking distance to and from gates. However, the impact of the flight-to-gate assignment on the ability of the airport facilities (check-in, security, transfer, passport control) to provide a high quality of service inside the terminal, is not considered. For instance, a gate assignment can be obtained such that all airside constraints are satisfied and the walking distance for passengers is minimised. However, following this gate assignment, the flow of passengers at an airport facility may be such that the number of passengers requesting service from this facility increases significantly and service can no longer be sustained.

This report describes a FGAP model with airside and landside constraints where overlap probability is used as a proxy for robustness and this model extends the FGAP model developed by Schaijk & Visser (2017). Three distinct specifications of the FGAP model with airside and landside constraints are proposed: The A-FGAP model has active airside constraints and inactive landside constraints. The DC-FGAP model has active airside and landside constraints and enforces upper bounds on passenger demand per time step at landside passenger facilities. This upper bound is determined using the declared capacity. The WT-FGAP model has active airside and landside constraints and ensures a gate assignment plan is constructed such that the expected maximum waiting for passengers does not exceed a predefined threshold. A case study using the flight schedule of July 4, 2018, at Amsterdam Airport Schiphol (AMS) is used to determine the applicability

of the FGAP models.

The remainder of this report is structured as follows: Chapter 2 describes the problem statement and outlines the objective and research questions of this report. Chapter 3 provides a brief summary of literature on robust FGAP models and landside airport processes. Chapter 4 describes the techniques used to model landside airport processes. Chapter 5 provides an overview of the FGAP models included in this report. Chapter 6 extends these models to accurately model AMS and provides an overview of the model features. Chapter 7 elaborates on the tools used to construct the flight schedules and presents a summary of the data and model parameters. Chapter 8 presents the main results of the FGAP model introduced in this report. Chapter 9 describes the sensitivity analysis. Chapter 10 shows the results of the model verification procedure. Chapter 11 provides the main conclusion; recommendations to further explore the ongoing development of FGAP models are presented in chapter 12. Supporting theory and analysis are presented in appendix A. Appendix B describes supporting results. Appendix C outlines the project planning.

Chapter 2

Problem Statement

This chapter outlines the problem setting that is addressed in this thesis. Section 2.1 explains what the FGAP is and outlines its general characteristics. The second section presents limitations of current FGAP models and suggests how existing literature on this topic can be extended. Section 2.3 elaborates on the research structure of this thesis. In this section, the research objectives are identified and research questions are drafted to focus our efforts. A detailed overview of the planning of the project can be found in chapter C on page 149.

2.1 Flight to Gate Assignment Problem

The main purpose of gate scheduling is to find an assignment of flights, or rather the aircraft serving these flights, to the available aircraft stands. In this process, the start and completion times for processing an aircraft at each position are determined (Dorndorf et al., 2007). The FGAP is typically modelled using programming problem, which can assume a linear or a quadratic form. A programming problem can be decomposed in an objective and a set of constraints the solution has to comply with. Subsection 2.1.1 and 2.1.2 will describe the objective and constraints respectively.

2.1.1 Objectives

The model used to provide a solution to the FGAP can adhere to an extensive list of objectives. These objectives can either focus on passenger or airport preferences. Dorndorf et al. (2007) outlines the optimisation of the FGAP can be performed using different objective functions, which are indicated in the list below. In this non-exhaustive overview of objective functions, passenger-oriented (**PO**) and airport-oriented (**AO**) objectives are included. This list includes both linear and quadratic objectives.

- **PO:** Minimize the total walking distance for passengers;
- **AO:** Minimize the number of the un-gated (open) aircraft activities;
- **AO:** Minimize the deviation of the current schedule from a reference schedule in order to increase schedule attractiveness and passenger comfort;
- **AO:** Minimize the number of expensive aircraft towing procedures that otherwise decrease the available time for some ground operations on the ramp as well as in the terminal;

- **AO:** Maximize the adherence to preferences of certain aircraft for certain gates.

Multi-criteria objective functions can consider passenger or airport preferences simultaneously by including multiple factors in the determination of the decision variable coefficients. According to Dorndorf et al. (2007), multi-objective models provide a trade-off between objectives which are usually in conflict. Finding such a compromise between several goals may positively influence passenger satisfaction in addition to providing airlines and airport with cost-saving opportunities.

Schaijk & Visser (2017) use an objective function which aims to minimize cost, inspired by the work of Rhee (1992). The cost represents how desirable a flight-gate combination is and can be determined by modelling the cost of customs requirements, size constraints and type assignments. For each of these factors a matrix of coefficients for all flight-gate combinations is drafted. Each of these matrices are summed elements-wise to create the total cost matrix for the flight-gate combinations. The big M method is used to block infeasible options.

The objective function is a summation of the products of the coefficients and decision variables. The latter are modelled at time-variant variables, whereas the associated coefficients are assumed to be independent of time. Given that the objective function is expressed in total cost, the aim is to minimise the objective function.

Ding et al. (2004) propose a different way of incorporating multiple factors in the optimization procedure. They use two objective functions, pertaining to minimisation of the number of flights which are not assigned to any terminal gate and the minimisation of the passenger walking distance. This problem has primarily been solved using greedy methods as proposed by Xu & Bailey (2001).

2.1.2 Constraints

Constraints in a FGAP model ensures that the solution space only includes feasible options. Or in other words, a gate assignment plan must be suitable for airport services and facilities, whilst be physically feasible. As such, a well constructed schedule must satisfy the following set of strict rules and constraints, labelled **C1**-**C3** (Schaijk & Visser, 2017):

- **C1:** One gate can process only one aircraft at any given time;
- **C2:** Service requirements and space restrictions with respect to the adjacent gates must be fulfilled;
- **C3:** minimum ground time and minimum time between subsequent aircraft have to be assured.

Constraint **C1** ensures no two aircraft are assigned to the same gate at any given time. Neglecting this constraint would lead to assignments of flights to gates which simply are physically impossible. Constraint **C2** serves a similar purpose, as this constraint deals with operating conditions that are imposed by the gate assignment. Finally, constraint **C3** serves multiple purposes. In addition to ensuring that enough time is available to (dis-)embark passengers/cargo and perform necessary service tasks, an adequate separation between aircraft must be imposed to safeguard robustness of the gate assignment plan. The latter can be formulated as a fixed buffer time or other (stochastic) measures can be used to ensure robustness of the gate assignment schedule.

2.2 Limitations of Existing FGAP Models

Though extensive literature exists on solving the FGAP, there are several limitations that motivate the ongoing development of these models. This section lists those limitations and provides a brief overview of the ongoing research in these topics. Subsection 2.2.1 describes how existing FGAP models either incorporate landside or airside constraints, but do not incorporate these distinct sets of constraints simultaneously. Subsection 2.2.2 elaborates on the robustness of the solutions to the FGAP found in literature. It is imperative that the to-be developed model solutions builds upon the work of existing robust FGAP models.

2.2.1 Airside and Landside Constraints in FGAP Models

Passenger streams within the terminal can be separated into arriving, transfer and departing passenger streams. These streams are handled by a collection of airport facilities, transportation channels and holding areas. The gate assignment plan is a prime driver of how these streams are generated and therefore has a great impact on the level of utilisation of these landside facilities. For this reason, it is important to include both the landside and airside constraints in finding a solution for the FGAP. Existing FGAP models typically incorporate either landside or airside constraints, but do not incorporate these distinct sets of constraints simultaneously. For this reason, the implementation of landside constraints in addition to airside constraints is one of the two interest areas covered in this study.

Arriving, transfer and departing passenger streams each use a subset of the facilities in an airport. These facilities have a finite capacity. It is in the interest of the passenger and airport operators to ensure this capacity is not exceeded. Ensuring that this is not the case, will let passengers experience a higher level of service while airport operators are able to use the facilities in a more efficient manner. Given that these flows are stochastic in nature, it is important to ensure that the facilities are able to provide an adequate level of service once a particular gate assignment plan is implemented. In this process, it important to identify those facilities that act as a bottleneck for the passenger streams in the airport terminal.

Including the landside processes in the optimisation of the gate assignment planning will require the decision variables of the FGAP to be linked to the landside processes. Often these decision variables are binary variables indicating whether a flight is allocated to a gate at a certain time. The challenge herein is to establish the relationship between the gates flights are assigned to and the facilities that the passenger streams use in response to this gate assignment. Furthermore, one needs to model the demand that is imposed on these landside facilities resulting from the gate assignment plan. Restrictions in the model should ensure the gate assignment plan does not result in insufficient handling performance of the arriving, transfer and departing passenger streams.

2.2.2 Robustness

The second area within the domain of FGAP model this thesis addresses is the robustness of the solution to the FGAP. Models that are used to solve the FGAP typically fall short on one aspect in particular: optimal solutions are given with respect to the input data. The drawback lies in the fact that this input data may not reflect a real-world situation. A gate assignment plan that performs optimal under the scheduled flight plan, might not deliver optimal performance if deviations in the flight plan occur. Given that deviations from the planned flight schedule are inevitable and happen frequently, it is important to ensure the solution to the

FGAP is robust. For this reason, the implementation of robustness in finding a solution to the FGAP is the second area of interest covered in this study.

In their work, Schaijk & Visser (2017) provide an insightful example how robustness helps improve the gate assignment plan when deviations in the theoretical flight plan occur. Schaijk & Visser (2017) are able to use the ideas drafted by Andreatta et al. (2014) and create a model that generates a more robust gate assignment plan as compared to a gate assignment plan where a fixed buffer time is required. In their approach, flight presence probabilities are used to find a gate assignment plan that ensures the overlap probability between two flight scheduled at the same gate is less than a predefined percentage. The effectiveness of this approach is validated through a case study based on a limited volume of data. A real-life implementation of this model would require the use of more data to reflect actual operating conditions at the airport of focus. Nonetheless, the findings of their study can be used in the creation of the FGAP model covered by this study.

2.3 Research Structure

As described in section 2.2 on page 39, two areas of interest within the development of FGAP models are robustness and the implementation of both airside and landside processes in the model. The focus of this thesis will be placed on including these elements in the existing FGAP model by Schaijk & Visser (2017). This section describes the research structure, which is comprised of the research objectives and research (sub-)questions. In defining these elements, the methodology outlined by Verschuren & Doorewaard (2010) is closely followed.

2.3.1 Research Objective

Before the research objective can be defined, the type of the research project must be established. Verschuren & Doorewaard (2010) distinguishes between theory-oriented and practice-oriented research. This research falls within either of these categories, as the aim is to extend existing literature on the FGAP model in addition to applying the novel model to a case study. Within the domain of theory-oriented research, a focus is placed on theory development rather than the testing of existing theories. As for the practice-oriented side of our research, the focus is placed on design as a new model is developed which addresses the areas of interest stated in the previous section. In summary, our research has a focus on theory-development and design of a solution to a practical problem.

Given that the research objective is classified as theory-development combined with the design of a solution to a practical problem, the actual objective can be drafted. The objective of the research is to develop a FGAP model that includes both airside and landside constraints in addition to implementing an predefined level of robustness. Within this objective, two elements of importance can be identified. Most existing FGAP models in literature focus on either airside or landside constraints, whereas this research aims to extend those constraints to include both airside and landside constraints. In addition, the model should have an predefined level of robustness. A combination of these aspects will yield the novel FGAP model.

2.3.2 Research Questions

Using the objective defined in subsection 2.3.1, the core research question and associated sub-questions can be drafted. Combining the solutions to each of the sub-questions yields the solution to the core question of this research. The core question and sub-questions are listed in the following paragraphs.

2.3.2.1 Core Question

The core research question is directly linked to the objective of this research describes in subsection 2.3.1. Therefore, the core research question reads:

CQ: *How can a FGAP model be developed that incorporates airside and landside constraints in addition to an predefined level of robustness in the optimisation procedure?*

2.3.2.2 Sub-Questions

Subquestions **SQ-1** through **SQ-3** aim to provide the solutions to answer the core research questions. **SQ-1** focusses on feat of implementing airside and landside constraints simultaneously. **SQ-2** investigates how a predefined level of robustness can be implemented in the to-be developed FGAP model. Finally, **SQ-3** provides the framework which determines how the effectiveness of the new model solution can be determined.

SQ-1: *How can airside and landside constraints be implemented together in a FGAP model?*
- **SQ-1a:** *What decision variables can be used to model landside and airside processes?*
- **SQ-1b:** *Which landside constraints can be identified in the FGAP?*
- **SQ-1c:** *Which airside constraints can be identified in the FGAP?*
- **SQ-1d:** *What data is needed to power the proposed model?*

SQ2: *Which robust optimisation techniques can be applied to the FGAP?*
- **SQ-2a:** *Which robust optimisation techniques have previously been applied to the FGAP?*
- **SQ-2b:** *How can existing techniques be adjusted to be implemented in the novel FGAP model?*
- **SQ-2c:** *What is the desired level of robustness relative to performance?*

SQ3: *How can the novel FGAP model be tested on a simplified case study?*
- **SQ-3a:** *Which measures exist to measure the robustness of a gate assignment plan?*
- **SQ-3b:** *What is a relevant model for the flight to gate assignment problem that has a low complexity and computing time but is representative for the real problem?*

Chapter 3

Literature Review

This chapter presents the literature review related to FGAP models that include both landside and airside constraints in addition to implementing an predefined level of robustness. Section 3.1 outlines the literature in relation to landside processes. Section 3.2 discusses the implementation of robustness in existing FGAP models. Section 3.3 describes existing FGAP models.

3.1 Landside Processes

This section outlines the modelling of landside facilities at an airport. Subsection 3.1.1 provides an overview of airport functional areas and landside facilities. Subsection 3.1.2 outlines an existing passenger modelling technique by Manataki & Zografos (2009). Subsection 3.1.3 describes landside performance metrics.

3.1.1 Facilities

The first hierarchical level of the model architecture devised by Manataki & Zografos (2009) is comprised of airport functional areas. The following list gives an overview of the different functional areas that can be distinguished in an airport terminal. Functional area one through three serve departing passenger streams, whereas functional area four deals with arriving passenger streams. Depending on the airport architecture and origin and departure destinations, transfer passengers pass through all or a subset of these functional areas.

1. **Unrestricted Airport Functional Area:** includes all facilities in the landside of an airport up to and including the boarding pass or passport control facilities and after the arrival hall for arriving passengers. All airport users can access these facilities.

2. **Controlled Airport Functional Area:** includes all facilities in the area behind the boarding pass and passport control facilities and before gate areas. These facilities only serve departing passengers.

3. **Gates Airport Functional Area:** includes all facilities that exist around the gates. These facilities only serve departing passengers that have passed through security screening facilities that are a part of the Controlled Airport Functional Area.

4. **Arrivals Controlled Airport Functional Area:** includes all facilities arriving passengers pass through after accessing the terminal from the airside. These facilities guide them from the airside

to the arrivals' hall.

Every airport functional area is comprised of a network of modules. Each of these modules represents a service facility and a corresponding process. These facilities represent the second hierarchical level of the model architecture. Table 3.1 indicates the service facilities for each of the four airport functional areas. For the sake of brevity, only those facilities are considered that have a significant impact to the airport terminal performance and the level of service offered to passengers. As such, non-functional components such as restrooms, cleaning facilities and internet access points, etc., will not be considered to keep the scope of the study limited. Ancillary facilities include retail facilities as well as food and beverage facilities. Manataki & Zografos (2009) includes these service facilities in the model given that they can have an impact on passenger streams within the terminal.

Table 3.1: Overview of airport landside facilities. The landside area of an airport is divided in four functional areas, namely: Unrestricted Airport, Controlled Airport, Gates Airport and Arrivals' Controlled functional areas. This table is based on figure 2 by Manataki & Zografos (2009).

Unrestricted Airport Functional Area	Controlled Airport Functional Area	Gates Airport Functional Area	Arrivals' Controlled Airport Functional Area
Ticketing	Security Screening	Gate Lounges	Passport Control
Check-in	Waiting Lounges	Passport Control	Baggage Claim
Ancillary Facilities	Ancillary Facilities	Ancillary Facilities	Customs
Boarding Pass Control			Ancillary Facilities
Passport Control			
Arrival Hall			

Li et al. (2018) present an insightful example of how a complex set of security facilities are distilled to a simple topology. In this example, they show that it's not the detailed architecture what matters, but rather how facilities are grouped and connected to one another.

3.1.2 Passenger Modelling

The demand imposed on landside facilities can be calculated using the flight schedule, airport topology and related parameters as input. This is done using the methodology outlined in section 5.1 of Manataki & Zografos (2009); with an extension of this method it is possible to compute demand numbers at a facility-level, rather than a terminal-level. In summary, the following data must be available in addition to the flight schedule to compute passenger demand numbers:

1. The number of expected passengers per flight, which can be calculated using the number of aircraft seats or aircraft size and the flight load factor;
2. The passenger transfer rate per flight;
3. Passenger distribution patterns. These distributions describe at which rate passengers arrive prior to the scheduled time of departure and make their through the terminal post the scheduled time of arrival;
4. Topology of the airport, which enables to attribute passenger streams to different facilities.

In this context, facilities refers to a collection of facility units that handle the same passenger streams. For example, check-in facilities and security facilities in a particular terminal handle passenger streams corresponding to flights assigned to certain gates at the airport.

3.1.2.1 Number of Passengers

In order to compute the expected number of passengers per flight, three different parameters need to be known. The number of aircraft seats can be deduced from the aircraft type and operator. For example, a legacy carrier and and a low-cost carrier might operate the same type of aircraft, but a low-cost carrier will typically opt for a more high-density seating arrangement, resulting in more seats. A similar argument holds for the load factor. In general, legacy carriers achieve a lower passenger load factor as compared to low-cost carriers. In conclusion, the aircraft type, airline characteristics and the corresponding passenger load factor influence the expected number of passengers per flight.

3.1.2.2 Transfer Rates

Transfer rates denote the fraction of passengers on a flight that will connect to a different flight. In the context of most airports, this means that passenger do not enter the Unrestricted Airport Functional Area but rather stay within the remaining functional areas indicated by table 3.1. As such, these passengers will not use any facilities within the Unrestricted Airport Functional Area. In modelling the demand imposed on the landside facilities, it is of great importance to ensure the transfer passenger stream is modelled to adhere to this.

3.1.2.3 Pax Arrival Distributions

One of the key inputs used to determine the passenger demand imposed on landside facilities are the pax arrival distributions per flight. Since it is next to impossible to determine the exact pax arrival distribution for every flight, a generic pax arrival distribution for flights can be used. In their study, van Dijk & van der Sluis (2006) state that the pax arrival distribution can be modelled using a triangular shape. Here it is assumed that this distribution does not vary with the flight type. A more realistic yet feasible way to model pax arrival distributions may be to distinguish between different flight types. These flight types could include low-cost carrier flights and legacy-carrier flights. Chun & Mak (1999) takes a different approach and determines passenger arrival distributions for economy and first/business class passenger. In addition, these distributions are drafted for morning, afternoon and evening flights.

3.1.2.4 Topology

Kusumaningtyas & Lodewijks (2013) describe the topology of AMS in their study on the application of accelerating moving walkways to support passenger processes at AMS. At a high level, their description of the topology includes three different passengers streams. These include a departing, arriving, and transfer passenger streams. The subtopology can be divided in public and non-public areas. Additionally, another divide can be made between the departure/arrival hall, lounges/waiting areas and the gates. In addition to the streams within each terminal, an incoming stream from other terminals enters in the lounges/waiting areas. Similarly, an outgoing stream in the lounges/waiting areas is diverted to other terminals.

3.1.3 Landside Performance Metrics

In their study, van Dijk & van der Sluis (2006) describe how a steady state analysis to determine the behaviour of the check-in facilities under the imposed passenger streams is not justified. For this reason, indicators need to be found to determine the performance of the landside facilities as a function of the gate assignment planning. These metrics reflect to what extend the facilities are able to meet the demand that is imposed on them.

3.1.3.1 Passenger Demand Capacity

The first metric of landside capacity is the notion of passenger demand capacity. Facilities at AMS have a finite capacity which is expressed in the number of passengers per time unit that can b handled by airport facilities whilst no queues are forming. This capacity is dependent on the number of facilities available in the terminal, staffing restrictions, passenger demand characteristics and other factors. If the landside capacity is known, a gate assignment planning can be constructed such that the passenger demand imposed on the facilities at AMS does not exceed capacity. As a result, this will effectively eliminate queues from forming.

3.1.3.2 Maximum Expected Waiting Time

Solak et al. (2006) derive closed-form expressions that can be used to compute the expected maximum waiting time as a function of the passenger demand per time step and capacity of landside airport facilities. By approximating peaks in passenger demand using triangular, parabolic and elliptical approximations, an estimate of the maximum expected waiting can be made. Note that this methodology assumes waiting times for a Normal distribution.

3.2 Robustness

This section elaborates on the concept of robustness. Robustness of the gate assignment plan is defined as the capability of the schedule to absorb the minor disturbances and avoid long-running gate conflicts (Yu et al., 2016). Subsection 3.2.1 outlines the different measures that can be used to measure the robustness level of a gate assignment plan. Subsection 3.2.2 describes how robustness can be implemented in FGAP models.

3.2.1 Measures of Robustness

Yu et al. (2016) state that there are several ways to measure the robustness of a gate assignment plan. The mean of the buffer time and its standard deviation can be used a proxy for robustness of a gate assignment plan. The expected conflict duration among all flights at the gate is used to measure the robustness of a gate assignment plan (Yu et al., 2017). Additionally, Seker & Noyan (2012) propose three robustness measures based on the idle and buffer times: the expected variance of the idle times (EVI), the expected total semi-deviation (ETD), and the expected number of positive semi-deviations. Furthermore, the number of expected flight conflicts can be used as a proxy for robustness in the gate assignment plan.

3.2.2 Robustness in FGAP

Robustness of the gate assignment plan is defined as the capability of the schedule to absorb the minor disturbances and avoid long-running gate conflicts (Yu et al., 2016). The scope of FGAP models is limited to models consisting of an objective to be minimised or maximised, subject to a set of constraints, both of which are assumed to be linear. From a high-level perspective, two main strategies exist to implement robustness in FGAP models. Work by Diepen et al. (2012), Seker & Noyan (2012) and Yu et al. (2016) aim to create a robust gate assignment planning by making robustness part of the objective function. This is done by minimizing the gap cost, conflict cost and the number of conflicts, respectively. Other objective functions revolve around the minimisation of the buffer time with duration under a predefined value, and the minimisation of the gap between the maximum slack time and the minimum slack time to make the buffer evenly distributed. The second approach implements robustness by imposing additional constraints. Yan & Chang (1997) and Yan & Huo (2001) use models that impose a minimum fixed buffer between two consecutive assignment of flights at a gate. Work by Schaijk & Visser (2017) shows an FGAP model where the overlap probability of two flights assigned consecutively at a gate is set to not exceed a predefined threshold.

3.3 FGAP Models

This section introduces a variety of existing robust FGAP models. This section outlines the vastly different approaches to model the flight-to-gate assignment problem and derive a gate assignment plan from the model. Subsection 3.3.1 describes the scenario modelling technique developed by Seker & Noyan (2012). Subsection 3.3.2 elaborates on a FGAP model with a quadratic objective function and provides the methodology to transform this model to an equivalent linear model. Subsection 3.3.3 outlines the FGAP model by Schaijk & Visser (2017) which makes use of maximum overlap probability to increase robustness in the GAP. Finally, subsection 3.3.4 describes a FGAP model by Kim et al. (2013) that focusses on overall passenger experience through a trade-off between multiple objective functions.

3.3.1 Scenario Modelling

In their paper, Seker & Noyan (2012) indicate it is common to characterise the randomness in uncertain model parameters using a finite set of scenarios. The number of scenarios should reflect the number of random parameters, i.e., more random parameters require more scenarios to be included in the model to obtain a better representation of the randomness inherent to real-life applications. This also links to the main limitation of this method, as increasing the number of scenarios leads to computationally challenging models. The uncertain arrival and departure times are represented by random variables, with realisations corresponding to each scenario. The corresponding FGAP model generates a GAP which is feasible under the scheduled arrival and departure times and minimizes the number of flight conflicts that occur in each of the scenarios.

3.3.2 Transfer Walking Distance Modelling

Yu et al. (2016) introduce a FGAP model that aims to minimise the transfer passenger's walking distance. As a consequence, the objective in their model is of a quadratic form. They state that models with quadratic expressions in the objective are hard to solve even for small instances. In order to overcome this drawback,

they propose a linearisation method that removes the quadratic terms from the objective function. Though this subsection describes the model by Yu et al. (2016), the proposed linearisation method could possibly be applied to other FGAP models with a quadratic objective function.

3.3.3 Overlap Probability Modelling

Another example of a traditional FGAP model is indicated by equation (4.11) through (4.14) in the work of Schaijk & Visser (2017). Contrary to the basic FGAP model presented by Seker & Noyan (2012), time is directly modelled using decision variables which are time-dependent. Additionally, robustness is implemented in the gate assignment planning using flight overlap probabilities, rather than an extensive set of scenarios which are analysed by the model. This improves the computational intensity of the model without inducing further restrictions on the flexibility of the model. In their study, Schaijk & Visser (2017) state that robustness is often modelled using proxy variables like buffer times and gap cost functions. However, the overlap probability of two flights assigned consecutively to same gate is found to be a true measure of robustness. In this context, the overlap probability is defined as the chance that at a given time two aircraft are scheduled to be handled at the same gate. The traditional FGAP model is extended with a constraint that imposes an upper limit on the overlap probability.

3.3.4 Passenger Experience Modelling

In their paper, Kim et al. (2013) develop three FGAP models that focus on different passenger experience metrics, namely: transfer time, aircraft taxi time and robustness of gate assignment. All models share the same constraints but have different objective functions. These objective functions are non-linear. Kim et al. (2013) further propose to combine different objective functions using a weighting scheme. They state that trade-offs between different objectives can improve the efficiency of the passenger streams inside a terminal, in addition to increasing the robustness of the gate assignment plan.

Chapter 4

Airport Landside Characteristics

In modelling the performance of landside facilities, it is not the detailed architectural layout of the airport that matters. Rather, the topology of the airport and its terminals are of interest. The topology describes the way that individual entities are connected to each other, representing the terminals in an airport as a network (Manataki & Zografos, 2009). In the analysis of these systems, the topology provides a clear handle on how to model these systems. Section 4.1 describes airport topology of AMS. The topology of each of its terminals is described in section 4.2. The gate-terminal topology of AMS is outlined in section 4.3. The declared capacity of facilities at AMS is estimated in section 4.4.

4.1 Airport Topology AMS

A high-level, schematic overview of AMS is indicated in figure 4.1 on page 50. Three types of areas can be distinguished in this figure, namely the unrestricted airport functional areas, the (Non-)Schengen controlled airport functional areas and the gates functional areas. The unrestricted airport functional areas, the (Non-)Schengen controlled airport functional areas are separated using security and border control facilities.

AMS is comprised of four different terminals. Unlike many other airports, these terminals are interconnected on both the public and non-public side of each terminal. The terminals of AMS are located side-by-side in a half-moon shape, ranging from Terminal 1 to Terminal 4 in a counter-clockwise direction. Terminal 1 is allocated to gates that handle flights arriving from and departing to airports located in the Schengen area. Terminal 2 and 3 are allocated to gates that handle flights originating from and departing to destinations in the Non-Schengen area. Terminal 4 is a low-cost terminal which is able to handle flights in the Schengen area.

Terminal 4 is constructed as a separate entity and passengers cannot move to different terminals once they find themselves in a non-public area. In the controlled and gates functional areas, passengers can move between Terminal 1 and Terminal 2 through the filter indicated by the dashed orange line; between Terminal 2 and 3 passengers are allowed to move freely. Passengers are not allowed to move between Terminal 3 and 4 in the controlled and gates functional areas.

In total, AMS has seven piers - otherwise referred to as concourses - each which are connected to different terminals. Terminal 1 is directly connected to the B-pier, C-pier and the upper-level of the D-pier. Terminal 2 is connected to the lower level of the D-pier and the E-pier. Terminal 3 serves the F-pier, G-pier and the H-pier. Finally, Terminal 4 is connected to the M-pier.

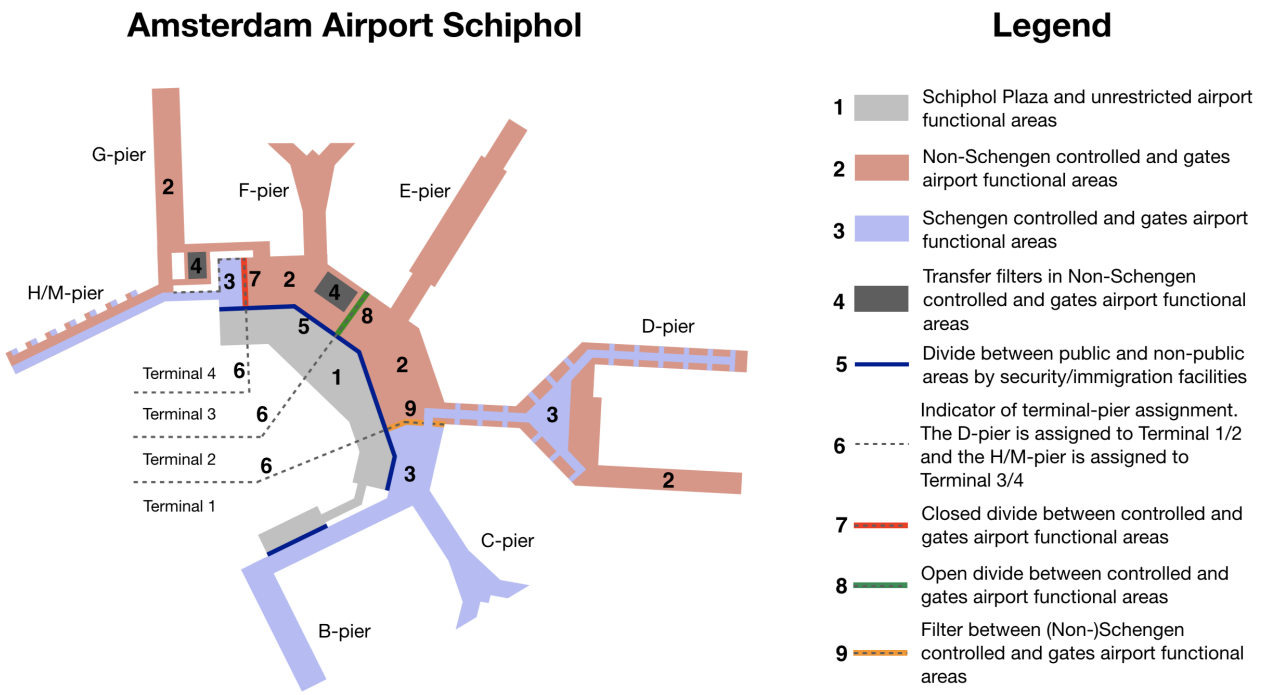

Figure 4.1: Airport topology of AMS. The airport consists of three terminals serving legacy carriers (Terminal 1 through 3) and a terminal serving low-cost carriers (Terminal 4). Terminal 1 and 4 handle flights within the Schengen area, whereas Terminal 2 and 3 handle flights to and from airports in the Non-Schengen area. In the controlled and gates functional areas, passengers can move between Terminal 1 and Terminal 2 through the inter-terminal filter; between Terminal 2 and 3 passengers are allowed to move freely. Passengers are not allowed to move between Terminal 3 and 4 in the controlled and gates functional areas. Gates in the D-pier and H/M-pier can be accessed with either a Schengen or a Non-Schengen customs clearing.

The D-pier is constructed such that the gates on the upper-level and lower-level of the pier use the same airside facilities, including the jet bridge. For this reason, only one of the gates that use the same airside facilities can be in use at any given time. Flights assigned to the D-pier with a Schengen classification are handled by the gates in the upper-level of the pier, whereas flights with a Non-Schengen classification are handled by the gates in the lower-level of the D-pier. A similar structure is used in the combined H/M-pier. This pier in total has 14 gates; consisting of gates H01 through H07 and M01 through M07. The H-gates handle Non-Schengen flights, and M-gates handle Schengen flights. Both these gates have distinctive landside facilities, yet share the same airside facilities. For this reason, only one of the gates in each pair can be in use at any given time.

4.2 Terminal Topology

This subsection present a terminal topology of terminals at AMS. It is assumed that each terminal has the same subtopology. The terminal topology can be divided in public and non-public areas. Additionally, another divide can be made between the departure/arrival hall, lounges/waiting areas and the gates. The terminal topology is indicated in figure 4.2 on page 51 and based on the work by Kusumaningtyas & Lodewijks (2013). This figure indicates the passenger flows, facilities and connections found to adjacent terminals for each terminal.

In figure 4.2, three major passenger streams can be distinguished, namely departing, arriving and transfer passenger streams. The stream of departing passengers is comprised of two substreams with passengers that enter the non-public area from the public area in the same terminal and the non-public area from a different terminal. The stream of arriving passengers moves from the non-public area to the public area in the same terminal. The transfer passenger streams is comprised of three substreams, which include incoming and outgoing inter-terminal transfer passenger streams and intra-terminal transfer passenger streams. To indicate the characteristics of these transfer substreams, an example is provided. Let the terminal topology indicated in figure 4.2 correspond to Terminal 2 at AMS. The incoming inter-terminal transfer passenger substream holds passengers who disembarked a flight in any terminal at AMS other than Terminal 2 and make their way to board their connecting flight in Terminal 2. The outgoing inter-terminal transfer passenger substream hold passengers who disembarked a flight in Terminal 2 and have a connecting flight in any other terminal at AMS besides Terminal 2. The intra-terminal transfer passenger substream holds passengers who disembarked a flight in Terminal 2 and will board their connecting flight in the same terminal. No data is available to determine the volumes of the inter-terminal transfer passenger streams versus the intra-terminal transfer passenger stream. Therefore, all transfer passengers are assumed to be captured by the intra-terminal transfer passenger substream.

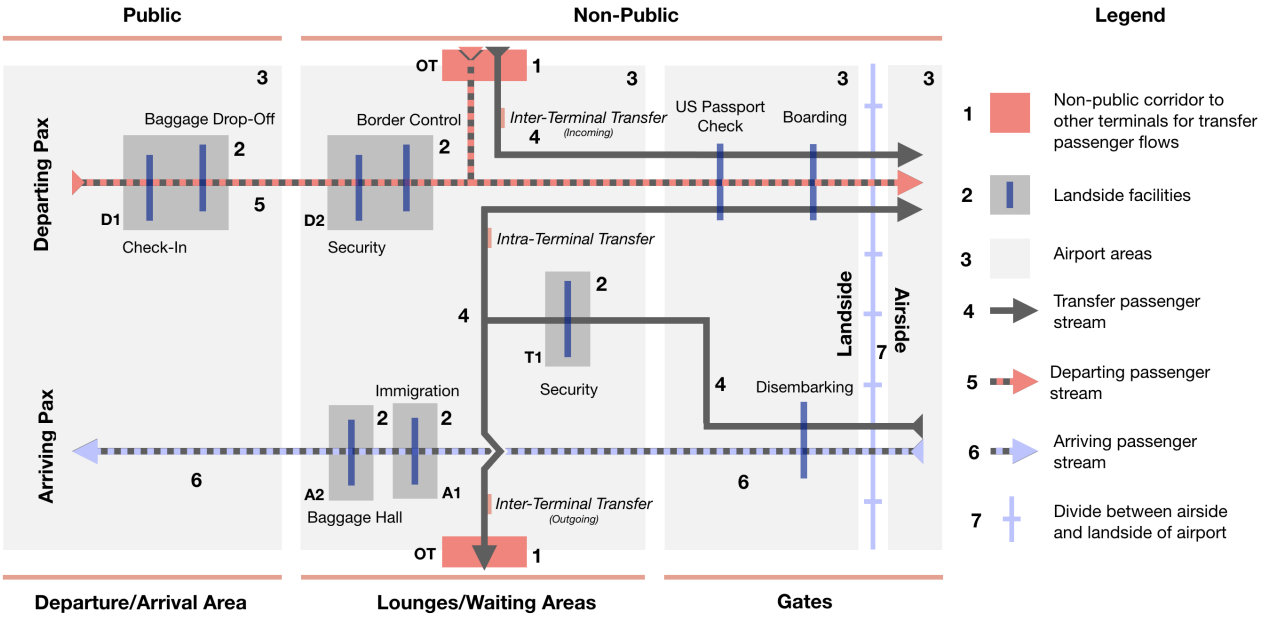

Figure 4.2: Generic terminal topology of AMS. Three passenger streams can be distinguished, namely departing, arriving and transfer passenger streams. All transfer passengers are assumed to be captured by the intra-terminal transfer passenger substream. For departing passenger streams, facilities (D1) and (D2) are included in the FGAP models. For transfer passenger streams, facilities (T1) are included. Facilities (A1) and (A2) are included in the FGAP models for arriving passenger streams.

The complete airport topology can be constructed by joining four of the sub-topologies indicated in figure 4.2 side-by-side. The red squares marked with OT indicate corridors between terminals in the non-public area which are used by ingoing and outgoing inter-terminal transfer passenger streams and departing passenger streams between non-public areas. Their permeability for passengers of each of these connections is described in figure 4.1 on page 50. The connection point between Terminal 1 and 2 is represented by the (Non-)Schengen filter and the connection point between Terminal 2 and 3 does not have any controlling measures. Though the

connection point between Terminal 3 and 4 theoretically exists, passengers are not allowed to move between these terminals in the gate and controlled airport functional areas.

The facilities shaded by the darker grey boxes in figure 4.2 are included in the FGAP models. These are the facilities present in the departure/arrival hall and the lounges/waiting areas. A tabular overview of the facilities is given in table 4.1. In the departure/arrival hall, the check-in and baggage drop-off facilities (D1) is considered in the model as one facility for departing passenger streams. For departing passenger streams, the security facilities and border control (D2) are modelled as one facility. For arriving passenger streams, immigration (A1) and the baggage claim area (A2) are included as distinct facilities. Finally, for transfer passenger streams security services (T1) are considered.

Table 4.1: Overview landside facilities that are included in the FGAP models. These facilities serve either arriving, transfer or departing passenger flows. Facilities D1 and D2 contain multiple facility streams However, these facilities are included in the model as one group to reduce overall model complexity. Facilities marked with the superscript [1] include both staffed and self-service versions of the facility.

Indicator	Group Name	Pax Stream	Facilities Included
A1	Immigration	Arriving	Passenger immigration services [1]
A2	Baggage Claim	Arriving	Baggage claim areas and lost & found
T1	Security	Transfer	Security services
D1	Check-In	Departing	Check-in desk [1] and bag drop facilities
D2	Security & Border Control	Departing	Security services and border control [1]

4.3 Gate-Terminal Topology

The gate-terminal topology indicates the preferred terminal to handle passenger streams to and from an aircraft assigned to a gate in one of AMS' concourses. The layout, as indicated by *Amsterdam Airport Terminal* (2018) and replicated in figure 4.1, suggests the following gates are tied to Terminals 1, 2, 3 and 4 at AMS:

- **Terminal 1:** concourses B and C and partly concourse D (gates D59 through D87)
- **Terminal 2:** concourse E and partly concourse D (gates D3 through D57)
- **Terminal 3:** concourses F, G and H
- **Terminal 4:** concourse M

Given that the terminals at AMS are interconnected, departing passengers can be handled at a terminal which does not match the preferred assignment as indicated by the list above. Note that several restrictions are in place. Terminal 4 acts as independent low-cost terminal and is therefore unable to handle flows of passengers outside of those going to and from the M-gates. Conversely, other terminals are not able to handle flows to and from concourse M. Flows preferably assigned to Terminal 1 have a Schengen clearance and therefore cannot be assigned to Terminal 2 and 3. A reversed argument also holds. Arriving passengers are assumed to exit the airport by using the facilities in the terminal corresponding to the gate-terminal assignment.

Platform and apron gates which are not included in this overview are assumed to be handled by Terminal 1 through 3. Passengers are shuttled between this terminal and the remote stands using airside passenger moving vehicles. The passenger load is assumed to be spread evenly over the three terminals.

4.4 Landside Declared Capacity AMS

The declared capacity indicates the number of passengers that can be handled at an airport facility per unit of time. To estimate the declared capacity of facilities at AMS, two sources of data are examined. Public data from London Heathrow (LHR) is used to estimate the landside capacity of AMS. Additionally, an expert opinion is used to estimate the landside capacity of AMS. A final estimate of the declared capacity of landside facilities at AMS is based on these two methods.

4.4.1 Comparison Study London Heathrow

An estimate of the declared capacity of AMS is made using data from public data from London Heathrow (LHR). This data describes the landside passenger capacity for Terminals 2 through 5 at LHR, collected from Odoni (2017). This data represent the maximum number of passengers that can disembark or board an aircraft per hour for each terminal at LHR. As a consequence, this number applies to the combined streams of O&D passengers and transfer passengers. Approximately 66.7% of the incoming and outgoing passengers is estimated to be an O&D passenger. In combination with the data from Odoni (2017), table 4.2 is constructed. This table indicates the landside capacity of each terminal at LHR expressed in the number of passengers that can be handled per hour.

Table 4.2: Overview of landside declared capacity of London Heathrow in 2016, which consists of four different terminals. Each of these terminals handles between 9.5 million and 31.9 million pax per annum, as indicated by the second column. The *O&D + Transfer Passengers* and *O&D Passengers* columns indicate the declared landside capacity with and without transfer passenger, respectively. The *Arriving Limit* and *Departure Limit* subcolumns indicate the theoretical upper limit on landside pax capacity per hour. Data in columns marked with the superscript [1] is obtained from *Heathrow Facts and Figures* (2018); data in columns marked with the superscript [2] is obtained from Odoni (2017).

Terminal	Annual Pax[1]	O&D + Transfer Passengers		O&D Passengers	
		Arrival Limit[2]	Departure Limit[2]	Arrival Limit	Departure Limit
Terminal 2	16.5 million	4,600	3,500	3.060	2,330
Terminal 3	17.7 million	4,000	3,500	2,660	2,330
Terminal 4	9.5 million	2,500	2,800	1,660	1,860
Terminal 5	31.9 million	5,650	5,000	3,760	3,330
Total	75.6 million	16,750	14,800	11,140	9,850

From the data in table 4.2, the average arrival and departure landside capacity per million annual passengers at LHR can be determined. For arriving passengers, an hourly landside capacity τ_{arr} of 147.3 passengers is computed per million annual passengers. Similarly, for departing passengers an hourly landside capacity τ_{dep} of 130.3 passengers is found per million annual passengers. These numbers are based on the overall annual demand and hourly capacity. Hence, these numbers do not reflect the differences between terminals and their efficiency in passenger handling.

The amount of passengers that use each of the terminals at AMS is not publicly available data. However, through analysis of available flight data it is known that terminals 1 through 4 handle 34.08%, 38.13%, 24.88% and 2.91% of the aircraft movements, respectively. The author recognises that aircraft carry a varying number of passengers and therefore the terminal movement percentages do not provide a perfect proxy for annual

passengers handled per annum by each terminal. According to *Traffic Review 2017* (2018), the total number of passenger at AMS in 2017 is equal to 68.4 million. Using the split calculated using the flight movements data, Terminal 1 through 4 are expected to handle 23.3 million, 26.1 million, 17.0 million and 2.0 million passenger per annum, respectively.

The landside capacity for AMS is determined by multiplying the hourly landside capacity for arriving (τ_{arr}) and departing (τ_{dep}) passengers per million annual passengers at LHR with the number of million passengers that use each terminal at AMS. Note that the numbers indicating the landside capacity for O&D passengers are used in this calculation. The results are indicated in table 4.3. In line with the annual number of passengers served, Terminal 2 has the highest landside capacity. The total capacity for O&D passengers is lower than the capacity at LHR, which is due to the fact that LHR serves more passengers annually.

Table 4.3: Overview of landside capacity per hour of AMS based on LHR data. For each of the terminals at AMS, the arriving and departing hourly O&D passenger capacity is computed by multiplying the per-million O&D passenger capacities derived from data from LHR with the millions of annual passengers that each of these terminals serve.

Terminal	Annual Pax	Arrival Limit	Departure Limit
Terminal 1	23.3 million	3,420	3,040
Terminal 2	26.1 million	3,840	3,400
Terminal 3	17.0 million	2,500	2,220
Terminal 4	2.0 million	290	260
Total	68.4 million	10,060	8,920

4.4.2 Expert Opinion AMS

A representative of Amsterdam Airport Schiphol, whose identity is known by the author, provided data to estimate the landside passenger capacity of AMS. This data includes the number of security lanes available per terminal at AMS and is used to estimate the capacity of facilities (T1) and (D2) in table 4.1 on page 52. Combined with the average processing time of passengers at these facilities, the hourly capacity is estimated. Here it is assumed that the average processing time at the bottleneck is equal to 20 seconds. Landside capacity of facilities (T1) and (D2) estimates are indicated in table 4.4.

Table 4.4: Overview of landside capacity of facilities (T1) and (D2) at AMS. Estimates of landside capacity are based on the number of facilities and the average processing time per passenger.

Terminal	Facility	Security Lanes	Capacity [hourly]
Terminal 1	D2	21	3,780
Terminal 2	D2	15	2,700
Terminal 2	T1	19	3420
Terminal 3	D2	14	2,520
Terminal 3	T1	6	1080
Terminal 4	D2	5	900
Total	D2	55	9,900
Total	T1	11	1,980

4.4.3 Synthesis Declared Capacity AMS

The data presented in tables 4.4 and 4.3 present a similar airport-wide landside passenger capacity. Nonetheless, their estimates vary within each terminal at AMS. The data in table 4.3 does not provide a capacity per facility; i.e. the capacity of the facilities (A1), (A2), (T1), (D1) and (D2) from table 4.1 on page 52 cannot readily be derived from these tables. This problem is solved by using these numbers as a proxy for the capacity of these facilities. Data from 4.4 can only be used to find the capacity of the facilities (D2) and (T1).

Data in table 4.3 is used to estimate the capacity of facilities (A1) through (D2) by assuming arrival and departure limits reflect the capacity of the facility groups that arriving and departing passengers use. As such, the arrival and departure limits reflect the capacity of the facilities that process arriving and departing passenger streams. For this reason, the facilities (D1) and (D2) have a capacity equal to the departure limit in each terminal. In a similar vein, the facilities (A1) and (A2) have a capacity equal to the arrival limit in each terminal. Given that not all departing passengers will use the facilities (D1), the capacity is set equal to the departure limit per terminal times the overall check-in rate $F_{CI} = 0.55$ (see table 7.4). No data is available on the capacity of the security facilities that serve transfer passenger flows. The overall transfer rate at AMS is 37%. It is therefore assumed that transfer facilities have 37% of the capacity of the arriving limits indicated in table 4.3.

To combine the capacity for all facilities derived from data in table 4.3 and facilities (D2) and (T1) derived from data in table 4.4, the minimum capacity is chosen. This marks a conservative effort in setting the capacity.

Table 4.5 indicates the estimated hourly declared capacity of facilities (A1) through (D2) in each terminal at AMS. The declared capacity is estimated using comparative data on declared terminal capacity at London Heathrow Airport (LHR) (Odoni, 2017) and expert opinion from AMS. Note that Terminal 1 and Terminal 4 only serve flights with a Schengen clearance level. As such, facilities (A1) and (T1) are not present in these terminals and, thus, their capacity is not given in table 4.5.

Table 4.5: Overview of declared landside capacity per hour for facilities (A1) through (D2) at AMS, which are based on data from table 4.3 and 4.4. In a conservative effort, the capacity reflects the minimum estimation as derived from these tables. Totals marked with the superscript [1] reflect the total capacity of the terminals where these facilities are present.

Terminal	Capacity Per Hour				
	A1	A2	T1	D1	D2
Terminal 1	N/A	3,420	N/A	1,690	3,040
Terminal 2	2,840	2,840	3,420	1,380	2,700
Terminal 3	2,500	2,500	1,080	1,230	2,220
Terminal 4	N/A	990	N/A	495	900
Total	5,340[1]	9,750	4,500[1]	4,450	8,860

Terminal 4 handles only 2.91% of all passengers at AMS. Using the capacity estimation method described in subsection 4.4.1, the hourly capacity of facilities in Terminal 4 is estimated to be below 300 passengers per hour. This number is unrealistically low and does not offer enough capacity to handle a single flight being assigned to a gate served by Terminal 4. For this reason, the capacity of facilities in Terminal 4 is derived from data in table 4.4. Herein it assumed that arrival capacity is 10% higher than the departure capacity.

Chapter 5

Theoretical FGAP Models

This chapter describes a flight-to-gate assignment model, associated with the A-FGAP, DC-FGAP and WT-FGAP models. Section 5.1 discusses the option of splitting a flight in segments associated with passengers disembarking, embarking the aircraft, the aircraft being towed or parked. Section 5.2 describes the notion of overlap probability. In section 5.3, the passenger demand model is introduced. The FGAP model with airside and landside constraints, which is based on the work by Schaijk & Visser (2017), is described in section 5.4. Section 5.5 provides the specifications of the passenger demand constraint in the A-FGAP, DC-FGAP and WT-FGAP models.

5.1 Flight Splitting

Given that flights can be scheduled to be present at the airport for a period longer than minimum turnaround time, it can be beneficial from a gate scheduling point of view to allow for flight splitting. This entails that flights can be divided in different flight segments, each of which are assigned to different gates. This allows for more flexibility and subsequently a more optimised gate assignment planning. A flight can be split in numerous flight segments, of which three categories exist. Functional flight segments are those where passengers board and/or disembark an aircraft. Towing movements are those where a flight is towed between two gates. Parking segments are those segments where a flight is parked at a gate without passengers boarding and/or disembark an aircraft. A planning horizon of operations between 00:00 and 23:59 on the same calendar day is considered.

5.1.1 Flights without an Overnight Stay

This subsection describes the flight splitting options for flights which do not include an overnight stay. The STA and STD of these flights are both within the planning horizon. In accordance with Schaijk (2013), three different flight splitting options are defined for a flight without an overnight stay. These are as follows:

- **Option 1:** Flight is not split and is assigned to the one gate from the STA until the STD; indicated by segment 1 in Figure 5.1;
- **Option 2:** Flight is split in three segments, including a functional flight segment, a towing segment and a functional flight segment; indicated by segment $2, 3, 4$ in Figure 5.1;

- **Option 3:** Flight is split in five segments, including a functional flight segment, a towing segment, a parking segment, a towing segment and a functional flight segment; indicated by segment $5, 6, 7, 8, 9$ in Figure 5.1;

The presence time of a flight is defined as the time between the STA and STD of that flight. Flight splitting option 1 can be applied irrespective of the presence time of a flight. Flight splitting option 2 can be applied if a flight has a minimum presence time of 130 and 150min for narrow-body and wide-body aircraft, respectively. Flight segment 3 in Figure 5.1 has a fixed length of 10min, and flight segment 2 and 4 in Figure 5.1 are of equal length. Flight splitting option 3 can be applied if a flight has a minimum presence time of 170min (190min) for narrow-body (wide-body) aircraft. Flight segment 6 and 8 in Figure 5.1 have a fixed length of 10min, and flight segment 5 and 9 in Figure 5.1 have a fixed length of 55 and 65min for narrow-body aircraft and 75 and 85min for wide-body aircraft, respectively.

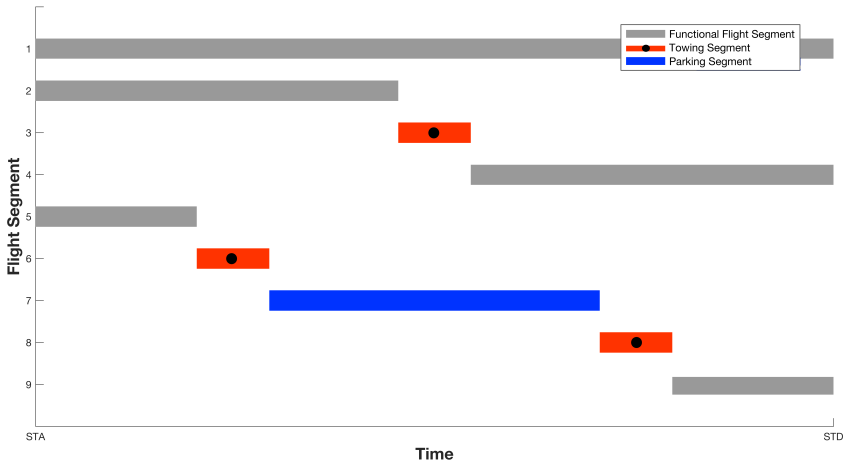

Figure 5.1: Overview of non-overnight-stay flight splitting options. Flight splitting option 1 contains flight segment 1. Flight splitting option 2 contains flight segments 2, 3 and 4. Finally, flight splitting option 3 contains flight segments 5 through 9.

5.1.2 Flights with an Overnight Stay

Flights with an overnight stay include those flights that have a STA or STD outside of the planning horizon. Two categories are distinguished: flights which depart after an overnight stay and flights which arrive and stay at the airport overnight.

5.1.2.1 Flights with a Morning Departure

Flights with a morning arrival have an STA on the calendar day prior to the calendar day that is being considered. Flight splitting options for morning overnight-stay flights include:

- **Option 4:** Flight is not split and is assigned to the one gate from 00:00 until the STD; indicated by segment 1 in figure 5.2a;

- **Option 5:** Flight is split in 3 segments: a parking, towing and boarding segment; indicated by segments $2, 3, 4$ in figure 5.2a.

Flight splitting option 4 can be applied irrespective of the presence time of a flight. Flight splitting option 5 can be applied if a flight has a minimum presence time of 130min (150min) for narrow-body (wide-body aircraft). Flight segment 3 and 4 in Figure 5.2a have a fixed length of 10 and 65min (75min) for narrow-body (wide-body) aircraft.

5.1.2.2 Flights with an Evening Errival

Flights with an evening arrival have an STD on the calender day after the calender day that is being considered. Flight splitting options for morning evening-stay flights include:

- **Option 6:** Flight is not split and is assigned to the one gate from the STA until 23:59; indicated by segment 1 in figure 5.2b;
- **Option 7:** Flight is split in three segments: a disembarking, towing and parking segment, indicated by segments $2, 3, 4$ in figure 5.2b.

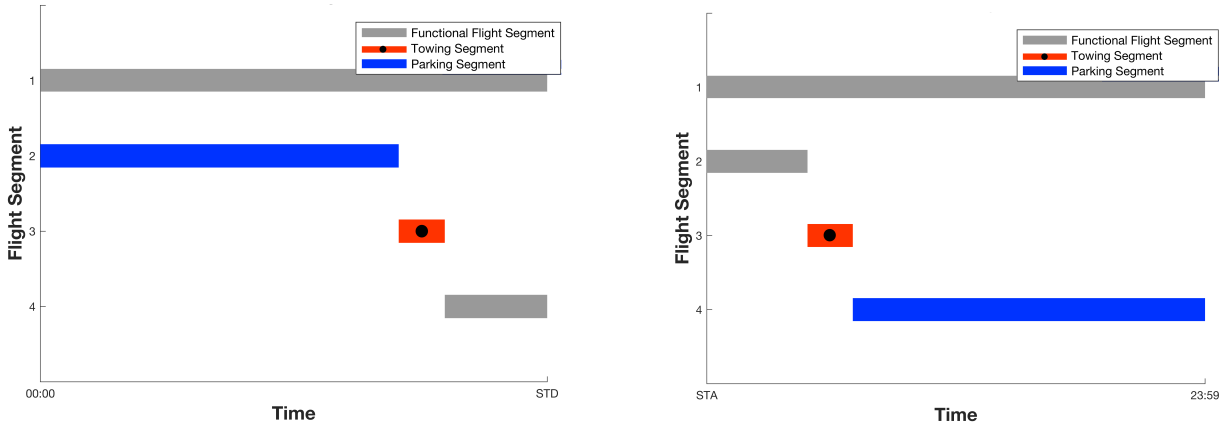

(a) Flight splitting options for flights with a morning departure.

(b) Flight splitting options for flights with an evening arrival.

Figure 5.2: Overview of splitting options for flights with an overnight stay. Figure 5.2a indicates the flight splitting options for flights which depart after an overnight stay. Flight splitting option 4 contains flight segment 1; option 5 contains flight segments 2 through 4. Figure 5.2b indicates the flight splitting options for flights which arrive and have an overnight stay after arrival. Flight splitting option 6 contains flight segment 1; option 7 contains flight segments 2 through 4.

Flight splitting option 6 can be applied irrespective of the presence time of a flight. Flight splitting option 7 can be applied if a flight has a minimum presence time of 130min (150min) for narrow-body (wide-body) aircraft. Flight segment 3 and 4 in Figure 5.2b have a fixed length of 10 and 65min (75min) for narrow-body (wide-body) aircraft.

5.2 Presence Probability

This section describes how to compute the presence probability of flight segments. Subsection 5.2.1 defines the presence probability of a flight segment. Subsection 5.2.2 outlines the construction of flight presence

probabilities. Subsection 5.2.3 describes the arrival and departure flight presence probability of airlines and regions included in this study.

5.2.1 Presence Probability of Flight Segments

First, notation is introduced. Let F denote the set of all arriving and departing flights at AMS in a day, N denotes the set of flight segments created by applying the flight splitting options and M denotes the set of available gates at the airport. A planning horizon is considered that is discretised in time steps of $\delta_t = 5\text{min}$, with a total of K time steps. The symbol $p_{i,t}$ denotes the presence probability of flight segment i at time step t, which is derived from the presence probability of flight $l \in F$ it belongs to, i.e.,:

$$p_{i,t} = fp_{l,t}, \quad i \in S_{l,t}, \quad t \in K, \tag{5.2.1}$$

where $fp_{l,t}$ is the presence probability of flight l from which flight segment i is derived and $S_{l,t} \subseteq N$ is the set that contains all possible flight segments of flight l at time step t.

Figure 5.3 on page 60 and figure 5.4 on page 61 indicate the presence probability $p_{i,t}$ of flight segment belonging to a flight without and with an overnight stay, respectively. The presence probability curve of the flight is cut to match the flight segments. Therefore, the flight presence probability curves of the flight segments are non-continuous.

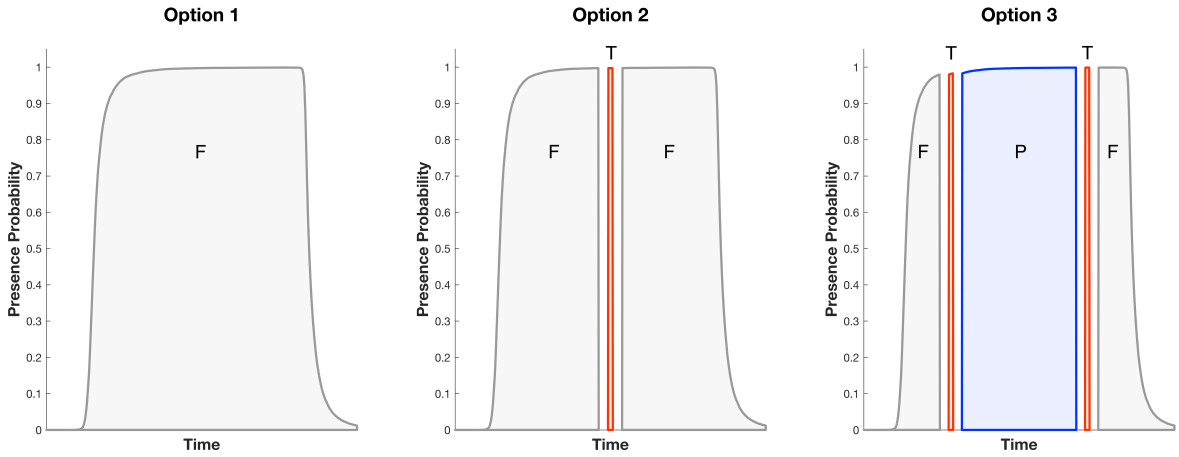

Figure 5.3: Presence probability curves for flight segments of a flight without an overnight stay. Functional flight, towing and parking segments are marked with a **F**, **T** and **P**, respectively. White space in-between these segments is included for aesthetic purposes only.

An example of the overlap probability between two flight segments is given in section A.1 on page 126. This example includes two flight segments derived from splitting flights without an overnight stay using option 1 in figure 5.3 on page 60.

5.2.2 Flight Presence Probability

The flight presence probability for a flight without an overnight stay is determined as follows (Schaijk & Visser, 2017):

$$fp_{l,t} = fp_{l,t,arr} - |1 - fp_{l,t,dep}|, \quad l \in F, \quad t \in K, \tag{5.2.2}$$

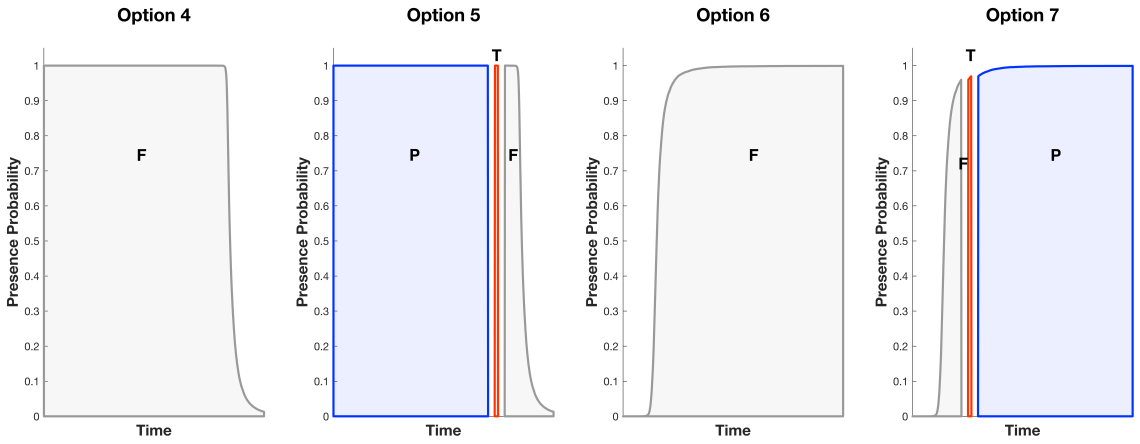

Figure 5.4: Presence probability curves for flight segments of a flight with an overnight stay. Options 4 and 5 correspond to a flight departing the airport after an overnight stay; option 6 and 7 arrives at the airport and has an overnight-stay afterwards. Functional flight, towing and parking segments are marked with a **F**, **T** and **P**, respectively. White space in-between these segments is included for aesthetic purposes only.

where $fp_{l,t}$ denotes the flight presence of flight l at time step t, $fp_{l,t,arr}$ is the arrival flight presence probability of flight l at time step t and $fp_{l,t,dep}$ is the departure flight presence probability of flight l at time step t.

Figure 5.5 gives an example of $fp_{l,t,arr}$, $fp_{l,t,dep}$ and $fp_{l,t}$ for a flight l.

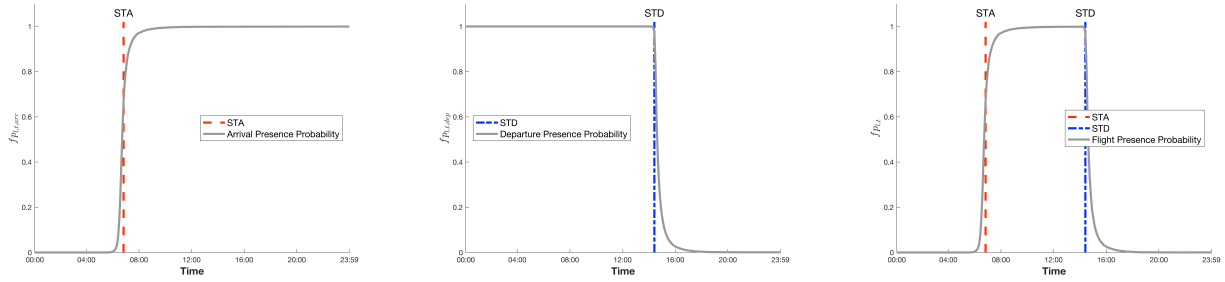

(a) $fp_{l,t,arr}$ **(b)** $fp_{l,t,dep}$ **(c)** $fp_{l,t}$

Figure 5.5: Example of $fp_{l,t,arr}$, $fp_{l,t,dep}$ and $fp_{l,t}$ for a flight l without an overnight stay, where $fp_{l,t}$ is constructed using equation (5.2.5). This flight has a STA and STD of 06:50 and 14:25, respectively.

The flight presence probability for flights with a morning departure and evening arrival are computed using equation (5.2.3) and (5.2.4),

$$fp_{l,t} = fp_{l,t,dep}, \quad l \in F, \quad t \in K, \qquad (5.2.3) \qquad fp_{l,t} = fp_{l,t,arr}, \quad l \in F, \quad t \in K. \qquad (5.2.4)$$

Figure 5.6 provides an example of $fp_{l,t,dep}$ and $fp_{l,t}$ for a flight l with a morning departure. Figure 5.7 gives an example of $fp_{l,t,arr}$ and $fp_{l,t}$ for a flight l with a evening arrival.

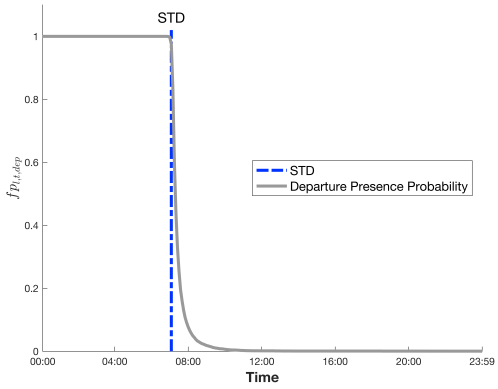

Figure 5.6: Example of $fp_{l,t,dep}$ for a flight l with a morning departure, where $fp_{l,t} = fp_{l,t,dep}$ (see also equation (5.2.3)). This flight has a STD of 07:05.

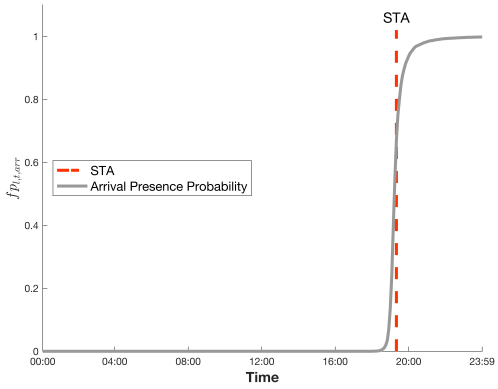

Figure 5.7: Example of $fp_{l,t,arr}$ for a flight l with a evening arrival, where $fp_{l,t} = fp_{l,t,arr}$ (see also equation (5.2.4)). This flight has a STA of 19:20.

5.2.3 Arrival and Departure Flight Presence Probability per Airline and Region

The flight presence probability for the arriving (departing) leg of a flight $l \in F$ is constructed using a linear model without intercept as follows:

$$fp_{l,t,u} = \beta_{a,u} fp_{a,t,u} + \beta_{r,u} fp_{r,t,u}, \quad l \in F, \quad t \in K, \quad u \in [arr, dep], \tag{5.2.5}$$

where $fp_{l,t,arr}$ ($fp_{l,t,dep}$) denotes the flight presence probability of the arriving (departing) leg of flight $l \in F$ at time step $t \in K$, $fp_{a,t,arr}$ ($fp_{a,t,dep}$) is the arrival (departure) flight presence probability at time step t of the airline option a corresponding to flight l, and $fp_{r,t,arr}$ ($fp_{r,t,dep}$) corresponds to the arrival (departure) flight presence probability at time step t of the region option r corresponding to flight l.

In total, 18.663 arriving flight legs and 19.766 departing flight legs dated between July 1, 2018, and July 30, 2018, are considered to estimate the variables $fp_{a,t,arr}$, $fp_{a,t,dep}$, $fp_{r,t,arr}$ and $fp_{r,t,dep}$ (see Schaijk & Visser (2017)).

The scaling coefficients in equation (5.2.5), denoted by $\beta_{a,arr} = 0.4847$, $\beta_{a,dep} = 0.5836$, $\beta_{r,arr} = 0.5153$ and $\beta_{r,dep} = 0.4164$ are set such that they reflect the variance of the variables $fp_{a,t,arr}$, $fp_{a,t,dep}$, $fp_{r,t,arr}$ and $fp_{r,t,dep}$, respectively. The values of the scaling coefficients are derived in detail in subsection 7.2.1 on page 84.

5.3 Landside Passenger Demand

This section discusses the landside passenger demand. Subsection 5.3.1 outlines the allocation of departing passenger streams to an airport terminal. Subsection 5.3.2 describes the landside passenger demand model.

5.3.1 Terminal Reallocation Options

Arriving and transfer passenger streams are handled by the terminal corresponding to the gate-terminal topology, outlined in subsection 4.3 on page 52. Departing passenger streams can be handled by a terminal which does not match the gate-terminal topology. This is illustrated in figure 5.8 on page 63. In both figures,

the arriving, transfer and departing passenger streams of flight segment $i \in N_d$ assigned to gate j are depicted. Assume this gate belongs to Terminal 2 according to the gate-terminal topology. Figure 5.8a indicates that all passenger streams are indeed handled by Terminal 2. Hence, no reallocation of the departing passenger stream is made. Sub-figure 5.8b shows that the departing passenger stream is reallocated to an adjacent terminal, namely Terminal 3. Among other reasons, this can help relieve congestion at facilities (D1) and (D2) in Terminal 2, given that Terminal 3 has the capacity to handle the departing passenger stream of flight segment i.

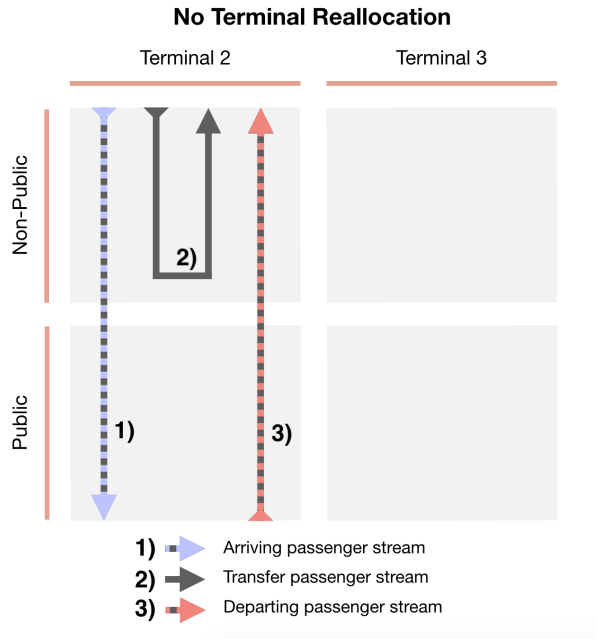

(a) No terminal reallocation of the departing passenger stream.

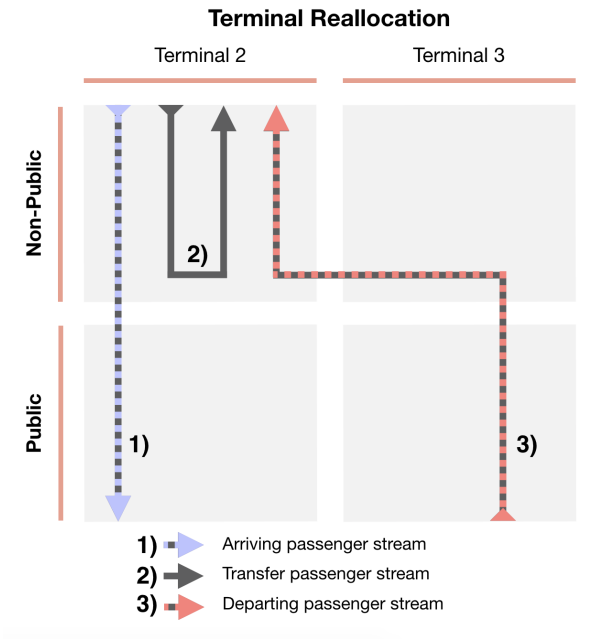

(b) Terminal reallocation of the departing passenger stream from Terminal 2 to Terminal 3.

Figure 5.8: Example of terminal reallocation options for departing passenger streams. In both figures, the arriving, transfer and departing passenger streams of flight segment i assigned to gate j are depicted. Here it is assumed that the gate j belongs to Terminal 2 according to the gate-terminal topology. Figure 5.8a indicates that all passenger streams are indeed handled by Terminal 2. Figure 5.8b shows that the departing passenger stream is reallocated to an adjacent terminal, namely Terminal 3.

Terminal reallocation options are incorporated in the FGAP model. Departing passenger streams caused by the assignment of the flight segment $i \in N_d$ to a gate j need not be handled by the preferred terminal according the gate-terminal topology. This yields an accurate representation of how departing passenger streams are handled by hub airports.

5.3.2 Passenger Demand Model

The sets N_a and N_d are defined as the set of flight segments where passengers disembark and board aircraft, respectively, $N_a \cup N_d \subseteq N$. Let H_a denote the set of facilities that serve passengers disembarking an aircraft, i.e. arriving and transfer passenger streams, and let H_d denote the set of facilities that serve passengers boarding an aircraft excluding the transfer passenger stream, i.e. departing passenger streams. The set of all

facilities is defined as $H = H_a \cup H_d$ and let T denote the set of terminals at AMS.

The total number passengers that use facility p in terminal q during time step t is defined as:

$$TD_{p,q,t} = \sum_{i \in N_a \cup N_d} D_{i,p,q,t} \cdot I_{i,p,q,t}, \quad p \in H, \quad q \in T, \quad t \in K, \tag{5.3.1}$$

where $D_{i,p,q,t}$ denotes the number of passengers of flight segment $i \in N_a \cup N_d$ that use facility $p \in H$ in terminal $q \in T$ during time step t and $1_{i,p,q,t}$ is defined as follows:

$$I_{i,p,q,t} = \begin{cases} 1, & \text{if passenger streams of flight segment } i \text{ are handled by facility } p \text{ in terminal } t \\ & \text{during time step } t, \\ 0, & \text{otherwise.} \end{cases}$$

The integer variable $D_{i,p,q,t}$ is computed as follows:

$$D_{i,p,q,t} = \text{round}(\rho_{i,p}\gamma_{i,p,q,t}), \quad i \in N_a \cup N_d, \quad p \in H, \quad q \in T, \quad t \in K, \tag{5.3.2}$$

where $\rho_{i,p}$ is the total number of passengers from flight segment i that will use facility p and $\gamma_{i,p,q,t}$ denote the fraction of the total number of passengers from flight segment i that use facility $p \in H$ in terminal $q \in T$ between time step t and $t + \delta_t$.

5.3.2.1 Passenger Number $\rho_{i,p}$

The expression for $\rho_{i,p}$ for facilities (A1) and (A2) is given in equation (5.3.3),

$$\rho_{i,p} = \begin{cases} \eta_i \cdot F_{LF} \cdot (1 - F_{TF}) & \text{if flight segment } i \in N_a \text{ and belongs to a SkyTeam flight,} \\ \eta_i \cdot F_{LF} & \text{if flight segment } i \in N_a \text{ and does not belong to a SkyTeam flight,} \\ 0 & \text{otherwise,} \end{cases} \tag{5.3.3}$$

where F_{TF} denotes the transfer rate for SkyTeam flights, $F_{TF} = 67\%$ (*Traffic Review 2018*, 2019), F_{LF} denotes the average load factor for a flight, $F_{LF} = 0.85$ (*Traffic Review 2018*, 2019), and η_i denotes the estimated number of seats on the aircraft serving flight segment i (see subsection 7.2.2).

The expression for $\rho_{i,p}$ for facilities (T1) is given in equation (5.3.4),

$$\rho_{i,p} = \begin{cases} \eta_i \cdot F_{LF} \cdot F_{TF} & \text{if flight segment } i \in N_a \text{ and belongs to a SkyTeam flight,} \\ 0 & \text{otherwise.} \end{cases} \tag{5.3.4}$$

The expression for $\rho_{i,p}$ for facilities (D1) is given in equation (5.3.5),

$$\rho_{i,p} = \begin{cases} \eta_i \cdot F_{LF} \cdot (1 - F_{TF}) \cdot F_{CI} & \text{if flight segment } i \in N_d \text{ and belongs to a SkyTeam flight,} \\ \eta_i \cdot F_{LF} \cdot F_{CI} & \text{if flight segment } i \in N_d \text{ and does not belong to a SkyTeam flight,} \\ 0 & \text{otherwise,} \end{cases} \tag{5.3.5}$$

where F_{CI} denotes the fraction of departing passengers that use either check-in facilities or bag-drop facilities, and it is assumed that $F_{CI} = 0.55$ (see subsection 7.2.2).

The expression for $\rho_{i,p}$ for facilities (D2) is given in equation (5.3.6),

$$\rho_{i,p} = \begin{cases} \eta_i \cdot F_{LF} \cdot (1 - F_{TF}) & \text{if flight segment } i \in N_d \text{ and belongs to a SkyTeam flight,} \\ \eta_i \cdot F_{LF} & \text{if flight segment } i \in N_d \text{ and does not belong to a SkyTeam flight,} \\ 0 & \text{otherwise.} \end{cases} \tag{5.3.6}$$

5.3.2.2 Passenger fractions $\gamma_{i,p,q,t}$

Similar to Chun & Mak (1999), it is assumed that the distribution of the fraction of passengers from flight segment i using facility p in terminal q during time step t follows an elliptical distribution. The height of the elliptical distribution is given by $\gamma_{i,p,q,t}$, and is the fraction of the total number of passengers from flight segment i that use facility p in terminal q between t and $t+\delta_t$. The support of this distribution is $[t^e_{i,p,q} - t^s_{i,p,q}]$, where $t^s_{i,p,q}$ and $t^e_{i,p,q}$ denote the start and end time for passengers arriving/departing with flight segment i to pass through facility p in terminal q.

Facility-specific expressions for $t^s_{i,p,q}$ and $t^e_{i,p,q}$ are given in table 5.1, where $T_1 = 10$min is the time for arriving and transfer passengers to walk from the gate to facilities (A1) and (T1), respectively, $T_2 = 10$min is the time for passengers to proceed from facilities (A1) to facilities (A2), $T_3 = 45$min is the time between first and last passenger disembarking from aircraft, $T_5 = 10$min is the time for the passengers to proceed from facilities (D1) to facilities (D2), T_4 is the time between first and last passenger of flight segment $i \in N_d$ that use facilities (D1) and T_6 is the time between the last passenger of flight segment $i \in N_d$ to use facilities (D1) and the STD of flight segment $i \in N_d$. Values of T_4 and T_6 depend on characteristics of flight segment i and are derived from the flight schedule (see table 7.1 on page 83).

Table 5.1: Expressions of $t^s_{i,p,q}$ and $t^e_{i,p,q}$ for facilities (A1), (A2), (T1), (D1) and (D2).

Facility	$t^s_{i,p,q}$	$t^e_{i,p,q}$
A1	$STA_i + T_1$	$STA_i + T_1 + T_3$
A2	$STA_i + T_1 + T_2$	$STA_i + T_1 + T_2 + T_3$
T1	$STA_i + T_1$	$STA_i + T_1 + T_3$
D1	$STD_i - T_4 - T_6$	$STD_i - T_6$
D2	$STD_i - T_4 + T_5 - T_6$	$STD_i + T_5 - T_6$

The fraction of the total number of passengers from flight segment i that use facility p in terminal q between t and $t + \delta_t$, denoted by $\gamma_{i,p,q,t}$ is computed using equation (5.3.7) as follows:

$$\gamma_{i,p,q,t} = \frac{\lambda_{i,p,q,t}}{\sum_{t \in K} \lambda_{i,p,q,t}}, \quad i \in N_a \cup N_d, \quad p \in H, \quad q \in T, \tag{5.3.7}$$

where $\lambda_{i,p,q,t}$ is the elliptical function of the fraction of passengers boarding or disembarking flight segment i that use facility p in terminal q between time step t and $t+\delta_t$. It is noted that $\gamma_{i,p,q,t} \neq 0$ if $t^s_{i,p,q} \leq t \leq t^e_{i,p,q}$.

The expression for $\lambda_{i,p,q,t}$ is given in equation (5.3.8),

$$\lambda_{i,p,q,t} = \begin{cases} \sqrt{1 - \left(\frac{t-(t^s_{i,p,q}+T_{i,p,q}/2)}{T_{i,p,q}/2}\right)^2} & \text{if} \quad t^s_{i,p,q} \leq t \leq t^e_{i,p,q}, \\ 0 & \text{otherwise,} \end{cases} \tag{5.3.8}$$

where $T_{i,p,q} = t^e_{i,p,q} - t^s_{i,p,q}$.

An example of values of $\lambda_{i,p,q,t}$ and $\gamma_{i,p,q,t}$ are given in Figure 5.9a and 5.9b for facilities (A1) and Figure 5.9c and 5.9d for facilities (D2), respectively. By construction, $\max_t \lambda_{i,p,q,t} = 1$ and $\sum_{t \in K} \gamma_{i,p,q,t} = 1$ for $i \in N_a \cup N_d$, $p \in H$ and $q \in T$, and therefore, all arriving/departing passengers on flight i are accounted for. The author notes that the distribution of $\lambda_{i,p,q,t}$ and $\gamma_{i,p,q,t}$ has a larger support for facilities (D2) as compared to facilities (A1).

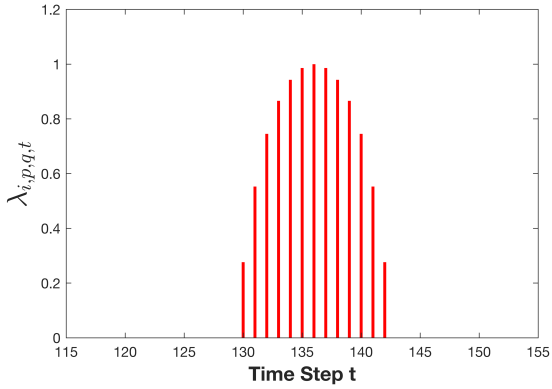

(a) Value of $\lambda_{i,p,q,t}$ of flight segment i at facilities (A1) in terminal q during time step t, with $t^s_{i,p,q} = 130$ and $t^e_{i,p,q} = 142$ and $\lambda_{i,p,q,t} \leq 1$.

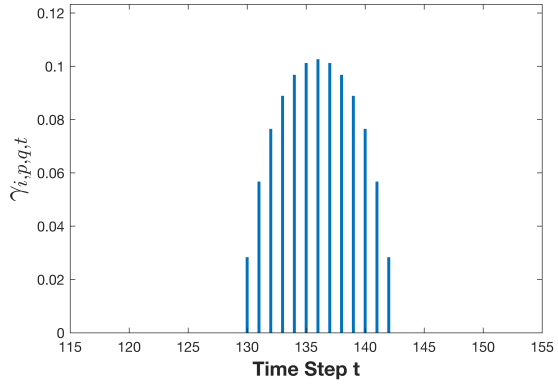

(b) Value of $\gamma_{i,p,q,t}$ of flight segment i at facilities (A1) in terminal q during time step t, with $t^s_{i,p,q} = 130$ and $t^e_{i,p,q} = 142$ and $\sum_t \gamma_{i,p,q,t} = 1$.

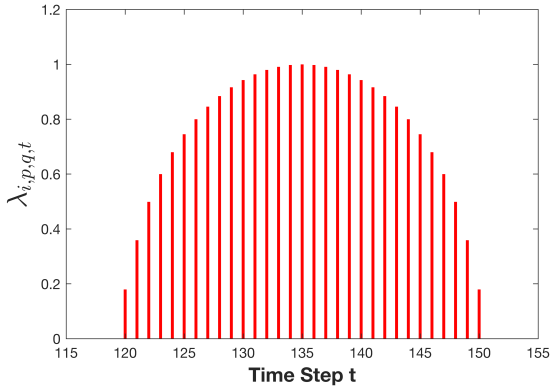

(c) Value of $\lambda_{i,p,q,t}$ of flight segment i at facilities (D2) in terminal q during time step t, with $t^s_{i,p,q} = 120$ and $t^e_{i,p,q} = 150$ and $\lambda_{i,p,q,t} \leq 1$.

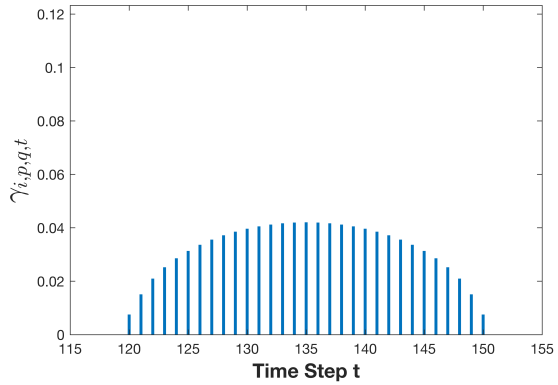

(d) Value of $\gamma_{i,p,q,t}$ of flight segment i at facilities (D2) in terminal q during time step t, with $t^s_{i,p,q} = 120$ and $t^e_{i,p,q} = 150$ and $\sum_t \gamma_{i,p,q,t} = 1$.

Figure 5.9: Example values of $\lambda_{i,p,q,t}$ and $\gamma_{i,p,q,t}$ of flight segment i at facilities (A1) and (D2) in terminal q over $t \in [115, 155]$.

5.4 FGAP Model with Airside and Landside Constraints

This subsection describes the mathematical model of the FGAP model with airside and landside constraints. Subsection 5.4.1 describes the decision variables of this model. The objective function is outlines in subsection 5.4.2. The constraints of the FGAP model are listed in subsection 5.4.3. Subsection 5.4.4 presents the optimisation algorithm of the FGAP model. Subsection 5.4.5 describes three techniques to lower the computational complexity of the FGAP model. For the interested reader, modelling techniques are summarised in section A.3 on page 129.

5.4.1 Decision Variables

The FGAP model has three distinct decision variables, denoted by $x_{i,j,t}$, $z_{i,j,q}$ and $y_{p,q,t}$. Assume that a flight segment $i \in N$ can be assigned only to a subset $G_i^1 \subseteq M$ of gates. The binary decision variables $x_{i,j,t}$ in equation (5.4.1) indicate whether flight segment $i \in N$ is assigned to gate $j \in G_i^1$ at time $t \in K$.

$$x_{i,j,t} = \begin{cases} 1 & \text{if flight segment } i \text{ is assigned to gate } j \text{ at timestep } t, \\ 0 & \text{otherwise,} \end{cases} \quad i \in N, \quad j \in G_i^1, \quad t \in K. \tag{5.4.1}$$

The decision variables $z_{i,j,q}$ in equation (5.4.2) are of the binary type and take a value of 1 if flight segment $i \in N_a \cup N_d$ is assigned to gate $j \in G_i^1$ and its departing passenger stream are handled by terminal $q \in T$ and takes a value of 0 otherwise (see subsection 5.3.1).

$$z_{i,j,q} = \begin{cases} 1 & \text{if flight segment } i \text{ is assigned to gate } j \text{ and its} \\ & \text{departing passenger flow is assigned to terminal } q, \\ 0 & \text{otherwise,} \end{cases} \quad i \in N_d, \quad j \in G_i^1, \quad q \in T. \tag{5.4.2}$$

The decision variables $y_{p,q,t}$ in equation (5.4.3) are of the general integer type and indicate the imposed passenger demand on facility $p \in H$ in terminal $q \in T$ and between t and $t + \delta_t$.

$$y_{p,q,t} = \sum_{i \in N_a \cup N_d} \sum_{j \in G_i^1} D_{i,p,q,t} z_{i,j,q}, \quad p \in H, \quad q \in T, \quad t \in K. \tag{5.4.3}$$

5.4.2 Objective Function

The objective function of the FGAP model with airside and landside constraints minimises the cost associated with the gate assignment plan from an airside and landside perspective and is indicated in equation (5.4.4),

$$\min_{x_{i,j,t}, z_{i,j,q}} Z = \sum_{i \in N} \sum_{j \in G_i^1} \sum_{t \in K} c_{i,j}^a x_{i,j,t} + w_{al} \sum_{i \in N_a \cup N_d} \sum_{j \in G_i^1} \sum_{q \in T} c_{i,j,q}^l z_{i,j,q}, \tag{5.4.4}$$

where $c_{i,j}^a$ and $c_{i,j,q}^l$ are time-invariant airside and landside cost coefficients, respectively. The objective function consists of two elements. The first element $\sum_{i \in N} \sum_{j \in G_i^1} \sum_{t \in K} c_{i,j}^a x_{i,j,t}$ expresses the cost of assigning flight segment $i \in N$ to gate $j \in G_i^1$ at time $t \in K$ and is equal to the objective function (equation (1)) of the

FGAP model by Schaijk & Visser (2017). The second element $\sum_{i \in N_a \cup N_d} \sum_{j \in G_i^1} \sum_{q \in T} c_{i,j,q}^l z_{i,j,q}$ expresses the cost of assigning flight segment $i \in N_a \cup N_d$ to gate $j \in G_i^1$ and its departing passenger stream to terminal $q \in T$.

5.4.2.1 Airside Cost Coefficients

The value of $c_{i,j}^a$ is based on size, customs and type requirements of flight $i \in N$ and gate $j \in G_i^1$, as follows:

$$c_{i,j}^a = c_{i,j}^{\text{Customs}} + c_{i,j}^{\text{Size}} + c_{i,j}^{\text{Type}}. \tag{5.4.5}$$

where i) $c_{i,j}^{\text{Customs}}$ is the customs cost coefficients, ii) $c_{i,j}^{\text{Size}}$ is the size cost coefficients and iii) $c_{i,j}^{\text{Type}}$ denotes the type cost coefficient.

5.4.2.1.1 Customs

The cost of assigning flight segment i to gate j from a customs perspective is given by:

$$c_{i,j}^{\text{Customs}} = \begin{cases} 2^{1+\text{Customs}_j - \text{Customs}_i} - 1 & \text{if Customs}_j \geq \text{Customs}_i, \\ \infty & \text{otherwise,} \end{cases} \tag{5.4.6}$$

where Customs_i is the customs level of flight segment i and Customs_j is the customs level of gate j.

5.4.2.1.2 Size

The cost corresponding to assigning flight segment i to gate j from a size perspective is given by:

$$c_{i,j}^{\text{Size}} = \begin{cases} 2^{1+\text{Size}_j - \text{Size}_i} - 1 & \text{if Size}_j \geq \text{Size}_i, \\ \infty & \text{otherwise,} \end{cases} \tag{5.4.7}$$

where Size_i is the size of the aircraft serving flight segment i and Size_j is the size of gate j.

5.4.2.1.3 Type

The cost corresponding to assigning flight segment i to gate j from a size perspective is computed as a function of the type of flight segment i and the type of gate j, as shown in Table 5.2.

Table 5.2: Cost coefficients $c_{i,j}^{\text{Type}}$.

	Pier	Platform	Tow Truck	Apron
Functional flight segment	1	1000	∞	2000
Parking segment	100	10	∞	10
Towing segment	∞	∞	1	∞

For functional flight segments, it is preferred that those segments are assigned to a pier gate, whereas platform and apron type gates provide less attractive assignments. This is reflected in the associated costs. Parking segments are ideally assigned to platform or aprons, and, at an increased cost, to piers. Towing flight segments can only be assigned to tow trucks.

5.4.2.2 Landside Cost Coefficients

The cost coefficients $c^l_{i,j,q}$ are constructed using equation (5.4.8),

$$c^l_{i,j,q} = |q_j - q|\eta_i, \tag{5.4.8}$$

where q_j denotes the terminal that passenger streams to and from gate j are preferably allocated to and η_i denotes the number of seats in the aircraft serving flight segment i.

The weighting factor w_{al}=0.53 is used to scale the cost of the landside element accordingly; its value is computed using equation (5.4.9),

$$E[c^a_{i,j}] = w_{al} \cdot E[c^l_{i,j,q}], \tag{5.4.9}$$

where the values of the cost coefficients $c^a_{i,j}$ and $c^l_{i,j,q}$ are based on the flight schedule of AMS on July 4, 2018 and the set of gates at AMS. A full derivation of the value of w_{al} is given in subsection 7.2.3 on page 88

The intuition behind this expression for $c^l_{i,j,q}$ is that it reflects the cost of assigning a flight segment $i \in N_a \cup N_d$ to a gate $j \in G^1_i$ and its departing passenger stream to terminal $q \in T$. If the assigned gate and terminal are satisfying the preferred assignment, indicated in subsection 4.3, the cost coefficient takes on a value of 0. If a flight segment is assigned to gate j and its departing passenger stream is not assigned to terminal q_j, the coefficient $c^l_{i,j,q}$ takes on a non-zero value. This value is equal to the absolute difference in terminal indicators q_j and q, expressed by $|q_j - q|$, multiplied with the number of seats in the aircraft serving flight segment i.

This reflects two important drivers of cost. The terminals of AMS are located side-by-side in a half-moon shape, ranging from Terminal 1 to Terminal 4 in a counter-clockwise direction. Moving a departing passenger stream across multiple terminals incurs a higher cost as compared to moving a departing passenger stream to an adjacent terminal. For example, moving the departing passenger stream from flight segment i from its preferred Terminal 1 to Terminal 3 should incur a higher cost than moving a flight segment from its preferred Terminal 1 to Terminal 2, given that the size of the flight does not change. This is reflected by $|q_j - q|$. In a similar vain, flight segments which operate larger aircraft result in larger streams of departing passengers that need to be diverted to a different terminal, reflected by the parameter η_i.

5.4.3 Constraints

Prior to introducing the constraints, additional notation is introduced. We define overlap probability at gate j during time step t to be the probability that two or more flight segments are assigned to a gate j during time step t. The scaling function $f(p_{i,t}, r)$ ensures that addition of flight segment presence probabilities $p_{i,t}$ is equal to 1 if the product of these flight presence probabilities equal to the maximum overlap probability r and is defined in equation (5.4.10),

$$f(p_{i,t}, r) = \frac{p_{i,t}}{r + p^2_{i,t}}. \tag{5.4.10}$$

A full derivation of $f(p_{i,t}, r)$ and a proof of implementation are given in section A.2 on page 127.

An unrealistic flight splitting option is an assignment where a functional flight segment and a parking segment of a flight l are both assigned to gate j. An example is considered where a flight without an overnight stay is split using flight splitting option iii) (see subsection 5.1.1). The flight is split in 5 segments, corresponding to segments 5 - 9 in Figure 5.1, indexed with i =131 - 135, which are a functional flight segment, a towing

segment, a parking segment, a second towing segment and a second functional flight segment. It is assumed that during peak hours of operation all piers are running at full capacity and therefore flight segments 131, 133 and 135 of this flight are assigned to platform A34, and flight segments 132 and 134 of this flight are assigned to towing truck THW. Hence, this assignment of flight segments features a towing segment between a functional flight segment and parking segment, both of which are assigned to the same gate, and therefore, is unrealistic. It is defined that $E_v^1 \subseteq N$ is the set of flight segments in unrealistic flight splitting options $v \in V$. If it is assumed that no other flight segments other than the flight segments in aforementioned example cause unrealistic flight splitting options, it is known that $V = [1, 2]$ with $E_1^1 = [131, 133]$ and $E_2^1 = [133, 135]$.

Further, it is defined that:

$$s_{i,t} = \begin{cases} 1, & \text{if flight segment } i \text{ has a non-zero probability to be present at time } t, \\ 0, & \text{otherwise.} \end{cases}$$

Constraint (5.4.11) ensures that the overlap probability between flight segments scheduled at gate j at time t does not exceed a predefined level r (Schaijk & Visser, 2017). Constraint (5.4.12) ensures that a flight segment that is assigned to a particular gate at a particular time is not switched to a different gate in a subsequent time step (Schaijk & Visser, 2017). Constraint (5.4.13) ensures that when a flight segment is present at the airport, it is assigned to one gate and only one. In addition, this constraint ensures that only one of the flight splitting options is selected. Constraint (5.4.13) extends constraint (3) in Schaijk & Visser (2017) to allow for flight splitting by summing over the set $S_{l,t}$. Constraint (5.4.14) ensures that all unrealistic flight splitting options are mitigated from the solution space, where τ is the first time step $t \in K$ flight segment i has a non-zero presence probability. Therefore, following the example presented above, constraint (5.4.14) ensures that flight segment 131 and 133 (133 and 135) cannot be assigned to the same gate. Constraints (5.4.15) and (5.4.16) indicate that for every flight segment $i \in N_a \cup N_d$ assigned to gate $j \in G_i^1$, departing passenger streams can only be directed to one terminal. If $x_{i,j,t}$ for $t = \{STA_i, STD_i\}$ is equal to 1, only one of the decision variables $z_{i,j,q}$ for $q \in T$ can take a value of 1. If $x_{i,j,t}$ for $t = \{STA_i, STD_i\}$ is equal to 0, $z_{i,j,q}$ for $q \in T$ are automatically set to 0. Constraint (5.4.17) indicates that the passenger demand imposed on facility $p \in H$ in terminal $q \in T$ at time $t \in K$ is a function of the decision variables $z_{i,j,q}$. Constraint (5.4.18) sets an upper bound to the value of $y_{p,q,t}$, denoted by the parameter $b_{p,q,t}$.

$$\sum_{i \in N} f(p_{i,t}, r) p_{i,t} x_{i,j,t} \leq 1, \quad j \in M, \quad t \in K \tag{5.4.11}$$

$$s_{it} x_{i,j,t+1} - s_{i,t+1} x_{i,j,t} = 0, \quad i \in N, \quad j \in G_i^1, \quad t \in K \tag{5.4.12}$$

$$\sum_{i \in S_{l,t}} \sum_{j \in G_i^1} s_{i,t} x_{i,j,t} = 1, \quad l \in F, \quad t \in K, \tag{5.4.13}$$

$$\sum_{i \in E_v^1} x_{i,j,\tau} \leq 1, \quad j \in M, \quad v \in V \tag{5.4.14}$$

$$x_{i,j,t} = \sum_{q \in T} z_{i,j,q}, \quad i \in N_a, \quad j \in G_i^1, \quad t = STA_i \tag{5.4.15}$$

$$x_{i,j,t} = \sum_{q \in T} z_{i,j,q}, \quad i \in N_d, \quad j \in G_i^1, \quad t = STD_i \tag{5.4.16}$$

$$y_{p,q,t} = \sum_{i \in N_a \cup N_d} \sum_{j \in G_i^1} D_{i,p,q,t} z_{i,j,q}, \quad p \in H, \quad q \in T, \quad t \in K \tag{5.4.17}$$

$$y_{p,q,t} \leq b_{p,q,t}, \quad p \in H, \quad q \in T, \quad t \in K \tag{5.4.18}$$

Constraint (5.4.11) and (5.4.12) are the same as constraint (5) and (4) included in the FGAP model by Schaijk & Visser (2017), respectively. Constraint (5.4.13) extends constraint (3) in Schaijk & Visser (2017) to allow for flight splitting by summing over the set $S_{l,t}$. Constraints (5.4.14) - (5.4.18) are not included in a similar form in the FGAP model by Schaijk & Visser (2017). Constraint (5.4.14) is elaborated on in more detail in section A.4 on page 132.

5.4.4 Optimisation algorithm

The FGAP model in equation (5.4.4), (5.4.11) - (5.4.18) using an iterative solving algorithm to produce a valid solution. Figure 5.10 on page 71 indicates the general structure of the optimisation algorithm of the FGAP model.

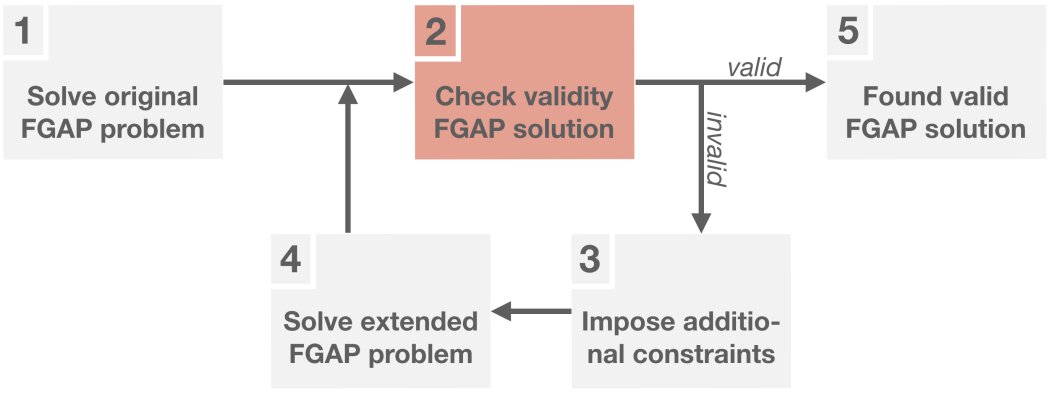

Figure 5.10: Graphical representation of FGAP model optimisation algorithm. The FGAP model is solved (1) and its solution is checked for validity (2). If the solution is not valid, additional constraint are added to the FGAP model (3). This model is solved (4) and its solution is once again checked for validity. This process is repeated until a valid solution (5) is found or the maximum number of iterations is reached.

Constraint (5.4.11) can be violated if three or more flight segments with a non-zero presence probability are assigned to gate j at time step t. An example is considered to clarify a possible violation of constraint (5.4.11). Assume three flight segments (i_x, i_y and i_z) are assigned to gate j at time step t, each with a presence probability $p_{i,t} = 0.2$ and the maximum allowed overlap probability $r = 0.1$. The scaled presence probability $f(p_{it}, r)p_{it}$ for each of these flight segments is equal to 0.2857. The sum of the scaled presence probability is less than 1, thus, these flight segments can be assigned to the same gate at the same time. However, the overlap probability of flight segments i_x, i_y and i_z at gate j at time t is 0.104, and therefore exceeds the maximum overlap probability $r = 0.1$, violating constraint (5.4.11).

To mitigate violations of constraint (5.4.11), an iterative optimisation algorithm is proposed of the FGAP model in equation (5.4.4), (5.4.11) - (5.4.18). This algorithm follows the structure indicated in figure 5.10 and is as follows:

i) The FGAP model with airside and landside constraints in equation (5.4.4), (5.4.11) - (5.4.18) is solved;

ii) A check for violations of the maximum overlap probability constraint (5.4.11) is performed, by computing the overlap probability at gate j during time step t, denoted by $OP_{j,t}$;

iii) If a violation of constraint (5.4.11) occurs, the FGAP model indicated by equation (5.4.4), (5.4.11) - (5.4.18) is extended with constraint (5.4.19),

$$\sum_{i \in E_w^2} x_{i,j,t} \leq 2, \quad j \in M, \quad t \in K, \quad w \in W \tag{5.4.19}$$

where E_w^2 denotes the set that contains the flight segments that each contribute to the violation $w \in W$ and the set W contains the violations of the maximum overlap probability constraint (5.4.11). This constraint ensures at most two flight segments that cause violation w of constraint (5.4.11) are assigned to the same gate;

iv) The FGAP model in equation (5.4.4), (5.4.11) - (5.4.18), (5.4.19) is solved;

v) Steps ii), iii) and iv) are repeated until no violations of constraint (5.4.11) occur or the maximum number of iterations is reached.

Algorithm 1 on page 72 indicates the optimisation algorithm that is used to find a valid solution to the FGAP model in more detail.

Algorithm 1: Optimisation algorithm to find a valid solution to the FGAP model indicated by equation (5.4.4), (5.4.11) - (5.4.18).

Result: Valid solution to FGAP model indicated by equation (5.4.4), (5.4.11) - (5.4.18)

```
Set flag: maximum overlap probability constraint flag (F_V = 0) ;
Set loop variables: loop counter i = 1 and maximum number of iterations MI = 10 ;
while (F_V = 1 or i = 1) and i ≤ MI do
    Solve FGAP model indicated by equation (5.4.4), (5.4.11) - (5.4.18);
    Set I_V = 1 if OP_{j,t} > r for j ∈ M, t ∈ K, else I_V = 0;
    if I_V = 1 then
        forall w ∈ W do
            Add constraint (5.4.19) on page 72 to the FGAP model;
        end
        Set maximum overlap probability flag F_V = 1;
    else
        Set maximum overlap probability flag F_V = 0;
    end
    Increment loop counter: i = i + 1
end
```

5.4.5 Computational Complexity

Three techniques are used to lower the computational complexity of the FGAP model, which include data compression, Big-M blocking and matrix construction. Data compression indicates every nth flight and every nth gate is included in the problem scope. This decreases the problem size by a factor $1/n^2$. Big-M blocking

removes infeasible flight assignment options from the problem space. Using the FGAP model and the flight schedule on July 4, 2018, this results in a reduction of the problem size of 64.2%. Finally, smart matrix construction using group allocation is used to decrease the complexity of constructing the computational model in Matlab. These techniques are described in more detail in section A.6 on page 136.

5.5 Specification of $b_{p,q,t}$ in passenger demand constraint (5.4.18)

The value of the parameter $b_{p,q,t}$ in constraint (5.4.18) can be set such that i) only airside constraints are active, ii) both airside and landside constraint are active, and passenger demand cannot exceed the fixed declared landside capacity and iii) both airside and landside constraint are active, and the landside passenger constraints are driven by the expected maximum passenger waiting time, rather than a fixed upper bound. Each of these options are discussed in the following subsections.

5.5.1 A-FGAP Model

This subsection introduces the A-FGAP model, which has active airside constraints and inactive landside constraints. The model indicated by equation (5.4.4), (5.4.11) - (5.4.18) and (5.4.19) is considered, where:

$$b_{p,q,t} = \infty. \tag{5.5.1}$$

Equation (5.5.1) ensures only airside constraints are active since the decision variables related to the passenger demand, $y_{p,q,t}$, are not constrained in any way.

The model indicated by equation (5.4.4), (5.4.11) - (5.4.18) and (5.4.19) with $b_{p,q,t} = \infty$ is referred to as the A-FGAP model.

5.5.2 DC-FGAP Model

This subsection introduces the DC-FGAP model, which has active airside and landside constraints and passenger demand cannot exceed the declared capacity. The model indicated by equation (5.4.4), (5.4.11) - (5.4.18) and equation (5.4.19) is considered, where:

$$b_{p,q,t} = C_{p,q}, \quad t \in K, \tag{5.5.2}$$

where $C_{p,q}$ is the declared capacity of facility p in terminal q during a time step of length $\delta_t = 5$min.

A fixed hourly declared capacity is assumed for each airport facility (see Table 4.5). It is also assumed that the number of passengers per hour is distributed uniformly over time. Thus, the value of $C_{p,q}$ is computed by dividing the hourly capacities in table 4.5 with the factor 60/5, given that time steps of $\delta_t = 5$min are considered. Consider, as an example, facilities (D1) in Terminal 2. As shown in table 4.5, this facility has a declared capacity of 1380 passengers/hour. The corresponding value of $C_{D1,2} = \frac{1380}{60/5} = 115$ passengers per 5min.

Equation (5.5.2) ensures that for a given flight-to-gate assignment, passenger demand any facility in the airport is at most the declared capacity of the facilities.

The model indicated by equation (5.4.4), (5.4.11) - (5.4.18) and (5.4.19) with $b_{p,q,t} = C_{p,q}$ is referred to as the DC-FGAP model.

5.5.3 WT-FGAP Model

This subsection introduces the WT-FGAP model, which has active airside and landside constraints and the landside passenger constraints are driven by the expected maximum passenger waiting time. First, the model for the expected passenger waiting time is introduced. Subsequently, this model is used to set the parameters $b_{p,q,t}$ in constraint (5.4.18), such that the expected maximum passenger waiting time does not exceed a user-defined threshold.

5.5.3.1 Expected maximum passenger waiting time model

In this subsection, a model to determine the expected maximum waiting time for a passenger at a facility in the airport is described. This model is applied to all facilities considered in this report (see also Table 4.1).

A peak demand period $n \in U_{p,q}$ for facility p in terminal q is defined as a period where the passenger demand per time step exceeds the average demand per time step, where $U_{p,q}$ is the set of peak periods at facility p in terminal q. The expected maximum waiting time for facility p in terminal q during peak period n ($W_{p,q,n}$) is estimated to be (Solak et al., 2006):

$$W_{p,q,n} = \frac{E[L_{p,q,n}] + 1.65\sqrt{\text{Var}[L_{p,q,n}]}}{C_{p,q}}, \tag{5.5.3}$$

where $C_{p,q}$ is the declared capacity of facility p in terminal q during a time step of length $\delta_t = 5$min, and $L_{p,q,n}$ is the queue length during peak period n at facility p in terminal q.

It is assumed that $L_{p,q,n}$ follows a normal distribution with mean $E[L_{p,q,n}]$ and variance $\text{Var}[L_{p,q,n}]$. The scaling factor 1.65 in equation (5.5.3) ensures the 95th percentile of the distribution of $L_{p,q,n}$ is used as a proxy for the maximum queue length during peak period n at facility p in terminal q.

To approximate $L_{p,q,n}$, Solak et al. (2006) propose to use a parabolic approximation of the passenger demand curve in a discrete time-system. The parabolic approximation of peak demand period n for facility p in terminal q, denoted by $y^{pb}_{p,q,t}$, is modelled as follows:

$$y^{pb}_{p,q,t} = \max_t(y_{p,q,t}) - a_{p,q,n}(t - \frac{T_{p,q,n}}{2})^2, \tag{5.5.4}$$

where the scaling coefficient $a_{p,q,n} = 4(\max_t(y_{p,q,t}) - E_t[y_{p,q,t}])/T^2_{p,q,n}$ and $T_{p,q,n} = t^e_{p,q,n} - t^s_{p,q,n}$.

From Solak et al. (2006), the expected value of $L_{p,q,n}$ is computed as follows:,

$$E[L_{p,q,n}] \approx 0.95\sqrt[3]{C_{p,q}} + \frac{2(\max_t(y^{pb}_{p,q,t}) - C_{p,q})^{3/2} T_{p,q,n}}{3\sqrt{c_{p,q,n}\max_t(y^{pb}_{p,q,t})}} \tag{5.5.5}$$

where $c_{p,q,n} = 1 - E_t[y^{pb}_{p,q,t}]/\max_t(y^{pb}_{p,q,t})$. Also, the variance of $L_{p,q,n}$ is as follows (Solak et al., 2006):

$$\text{Var}[L_{p,q,n}] \approx -0.3{C_{p,q}}^{2/3} + 2\sqrt{c_{p,q,n}\max_t(y^{pb}_{p,q,t})(\max_t(y^{pb}_{p,q,t}) - C_{p,q})} - \frac{4(\max_t(y^{pb}_{p,q,t}) - C_{p,q})^{3/2}}{3\sqrt{c_{p,q,n}\max_t(y^{pb}_{p,q,t})}}. \tag{5.5.6}$$

Figure 5.11 shows a passenger demand curve for facility p in terminal q, based on fictitious data. For this example, the average demand $E_t[y_{p,q,t}]$ is assumed to be equal to 30 passengers per 5 minutes. In total, 7 peak periods exist where the passenger demand $y_{p,q,t} > E_t[y_{p,q,t}]$ The declared capacity $C_{p,q}$ is set to be equal to 40 passengers per 5 minutes. It is only for peak 1 and peak 7 that the demand curve exceeds the declared

capacity. Applying the parabolic peak demand approximation by Solak et al. (2006), these peak 1 and peak 7 have an expected maximum waiting time equal to 21.2 and 18.7 minutes, respectively. Given that the peak demand for peak 2 through 6 is below the declared capacity, the expected maximum waiting time is less than 1 minute for these peaks.

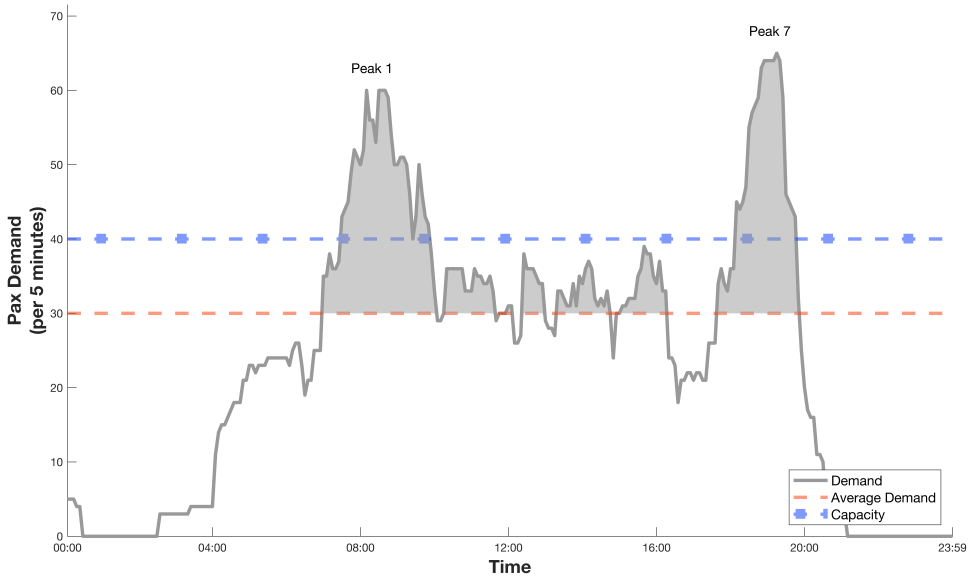

Figure 5.11: Example of expected maximum waiting time with fictitious demand curve for facility p in terminal q. An average incoming demand ($E_t[y_{p,q,t}]$) of 30 passengers per 5 minutes and declared capacity $C_{p,q}$ of 40 passengers per 5 minutes are assumed. For peak 1 and 7, the actual demand exceeds the declared capacity and therefore the expected maximum waiting at a 95% level is equal to 21.2 and 18.7 minutes, respectively. These numbers are based on the maximum expected waiting time computed using the parabolic peak demand approximation and equation (5.5.3).

5.5.3.2 Dynamically setting the value of $b_{p,q,t}$ in constraint (5.4.18) using $W_{p,q,t}$

Constraint (5.4.18) is dynamically adjusted such that the expected maximum waiting time for passengers at the airport facilities considered does not exceed a user-defined threshold W^T. This is achieved as follows:

i) The parameters $b_{p,q,t}$ in constraint (5.4.18) are set as follows $b_{p,q,t} = \infty$;

ii) The model indicated by equation (5.4.4), (5.4.11) - (5.4.18) and equation (5.4.19) is solved;

iii) The expected maximum passenger waiting time $W_{p,q,n}$ associated with the flight-to-gate assignment obtained, is determined for all $p \in H$, $q \in T$, and $t \in K$;

iv) It is determined if $W_{p,q,n} > W^T$ and if so, the value of $b_{p,q,t}$ is decreased as follows:

$$b_{p,q,t} = \max_{t \in [t^s_{p,q,n}, t^e_{p,q,n}]}(y_{p,q,t}) - \Delta_s, \quad t \in [t^s_{p,q,n}, t^e_{p,q,n}], \tag{5.5.7}$$

where $t^s_{p,q,n}$ and $t^e_{p,q,n}$ denote the start and end time of peak period n at facility p in terminal q, respectively, and Δ_s is a adjustment parameter. A value of $\Delta_s = 1$ is selected to ensure that the optimality of the final

solution obtained for model in equation (5.4.4), (5.4.11) - (5.4.18) and equation (5.4.19) is not compromised by setting a value of Δ_s too large;

v) Steps ii), iii), iv) are repeated until $W_{p,q,n} \leq W^T$, for all $p \in H$, $q \in T$, and $n \in U_{p,q}$.

The model indicated by equation (5.4.4), (5.4.11) - (5.4.18) and (5.4.19) where expected passenger waiting times drives landside constraints, as shown above, is referred to as the WT-FGAP model.

Algorithm 2 on page 77 shows the optimisation algorithm of the WT-FGAP model, which merges the optimisation algorithm described in this subsection and the optimisation algorithm described in algorithm 1 on page 72.

Algorithm 2: Optimisation algorithm to find a valid solution to the WT-FGAP model indicated by equation (5.4.4), (5.4.11) - (5.4.18), (5.5.7)

Result: Valid solution to WT-FGAP model, indicated by equation (5.4.4), (5.4.11) - (5.4.18), (5.5.7)

```
Set flags: maximum overlap probability constraint flag (F_V = 0) and maximum waiting time threshold
  flag (F_WT = 0) ;
Set loop variables: loop counter i = 1 and maximum number of iterations MI = 10 ;
while (F_V = 1 or F_WT = 1 or i = 1) and i ≤ MI do
    Solve WT-FGAP model;
    Identify peak demand periods n for facilities p ∈ H and terminals q ∈ T;
    Set I_WT = 1 if W_{p,q,n} > W^T for p ∈ H, q ∈ T, n ∈ U_{p,q}, else I_WT = 0;
    Set I_V = 1 if OP_{j,t} > r for j ∈ M, t ∈ K, else I_V = 0;
    if I_WT = 1 then
        forall p ∈ H do
            forall q ∈ T do
                forall n ∈ U_{p,q} do
                    if W_{p,q,n} ≥ W^T then
                        Determine start time t^s_{p,q,n} and end time t^e_{p,q,n} of peak demand period n at
                          facility p in terminal q;
                        Set b_{p,q,t} using equation (5.5.7) ;
                    end
                end
            end
        end
        Set maximum waiting time flag F_WT = 1;
    else
        Set maximum waiting time flag F_WT = 0;
    end
    if I_V = 1 then
        forall w ∈ W do
            Add constraints in equation (5.4.19) on page 72 to the WT-FGAP model;
        end
        Set maximum overlap probability flag F_V = 1;
    else
        Set maximum overlap probability flag F_V = 0;
    end
    Increment loop counter: i = i + 1
end
```

Chapter 6

AMS-Specific FGAP Models

The FGAP models described in chapter 5 do not reflect realistic operating conditions and restrictions of AMS. For this reason, additional constraints are formulated and added to the A-FGAP, DC-FGAP and WT-FGAP models. Constraints for combined gate airside facilities and terminal reallocation restrictions are described in section 6.1 and 6.2, respectively.

6.1 Combined Gate Airside Facilities

Gates in the D-pier and H/M-pier are grouped in pairs (see section 4.1 on page 49). Gates in each pair have distinct landside facilities, but share airside facilities such as a jet bridge, etc. For this reason, only one of the gates in each pair can be in use at any given time.The FGAP models are extended with a constraint that enforces this rule. The mathematical notation of this constraint is presented in equation (6.1.1),

$$\sum_{j \in G_o^2} x_{i,j,t} \leq 1, \quad i \in N, \quad o \in O, \quad t \in K, \tag{6.1.1}$$

where the set O is the set of all gate pairs. The set O is indexed by o, and G_o^2 denotes the gate indices of the gates in pair $o \in O$.

As an example, assume that six of the gates in the set M belong to a total of three gate pairs. These are, for example, (D08, D64), (D12, D66) and (M02, H02). Following this example, the set G_o^2 can contain the indices j corresponding to gates (D08, D64), (D12, D66) or (H02, M02).

6.2 Terminal Allocation Restrictions

A subset of possible terminal reallocations of departing passenger streams are not feasible due to the separation of different terminals within AMS (see section 4.1 on page 49). For example, passengers cannot move between Terminal 4 and Terminal 3 in the controlled and gates airport functional area. This is because Terminal 4 acts as a separate entity within the airport. As a consequence, additional constraints need to be imposed on the decision variable $z_{i,j,q}$ to ensure the solution space only includes feasible options. Infeasible terminal reallocations of departing passenger streams are removed from the solution space using the constraint in equation (6.2.1),

$$\sum_{i \in N} z_{i,j,q} = 0, \quad j \in G_q^3, \quad q \in T, \tag{6.2.1}$$

where G_q^3 denote the set of gates whose departing passenger flows terminal $q \in T$ cannot service. In order words, the set G_q^3 contains the gates whose departing passenger streams cannot be reallocated to terminal $q \in T$.

Chapter 7

Data Analysis

This chapter presents the analysis and summary statistics of the input for the FGAP models. Section 7.1 provides summary statistics of the arriving and departing flight lists, flight schedules and the empirical flight presence probabilities. Section 7.2 describes how the model parameters included in the AMS-specific FGAP models are derived. Section A.7 on page 138 describes how flight lists and flight schedules are constructed using the Schiphol Flight API.

7.1 Data Sample

This section summarises the data sources used in this study. Subsection 7.1.1 provides insight in the lists of arriving and departing flights. Subsection 7.1.2 describes the flight schedule used as support for the analysis of the flight-to-gate assignment problem. Subsection 7.1.3 summarises the gates that are included in the data set. Subsection 7.1.4 elaborates on the empirical flight presence probability curves.

7.1.1 Flight Lists

The lists of arriving and departing flights are comprised of data adhering to the schemas introduced in table A.2 and A.3, respectively. These lists hold flight data at AMS dated between July 1, 2018 and July 30, 2018. The lists are comprised of 18,663 arriving flight legs and 19,766 departing flight legs. The relatively large difference between these numbers can be explained by the different levels of performance of the data collection script for arriving and departing flights. The data collection tool exhibits unstable behaviour for arriving flights on the 3rd, 19th and 24th of July, 2018. For departing flights, unstable behaviour occurs on the 6th, 7th, 19th and 30th of July 2018. As a consequence, the arriving and departing flight lists for each of the corresponding dates are deemed to be incomplete.

Figures 7.1a and 7.1c on page 82 indicate the number of arriving flights per airline and region, respectively. Figures 7.1b and 7.1d on page 82 show the number of flights per day per airline and region, respectively. Only airlines which have an average of over 25 flight legs arriving or departing per calender day are included in figures reffig:dist11 and 7.1b. Given that the vast majority of flight legs has an origin or destination in Europe, this region is plotted separately in figures 7.1c and 7.1d.

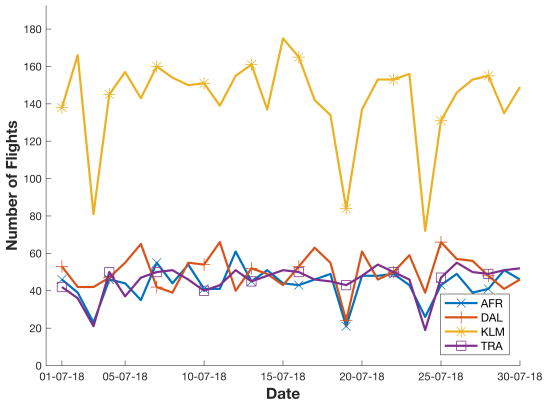

(a) Number of arriving flight legs per day per airline. Four airlines which on average have over 25 arrivals per day are included in this figure.

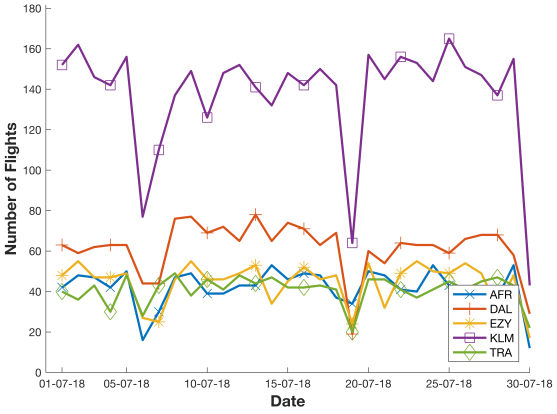

(b) Number of departing flight legs per day per airline. Five airlines which on average have over 25 arrivals per day are included in this figure.

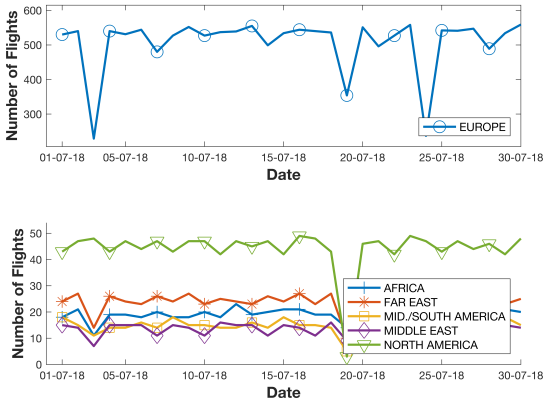

(c) Number of arriving flight legs per day per region.

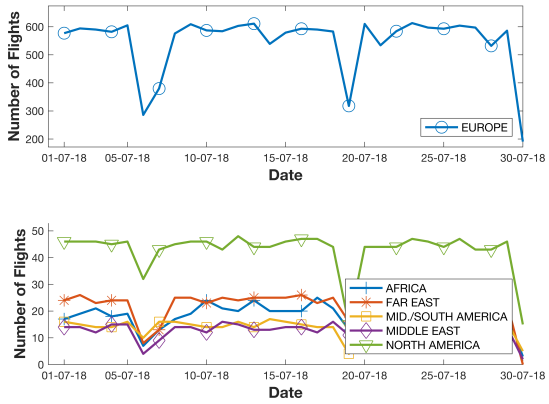

(d) Number of departing flight legs per day per region.

Figure 7.1: Overview of number of flight legs per airline and region. The data collection script exhibits unstable behaviour for arriving flights on the 3rd, 19th and 24th of July, 2018. For departing flights, unstable behaviour occurs on the 6th, 7th, 19th and 30th of July, 2018. Given that the number of flights departing to a European destination greatly out numbers the other regions, Europe is plotted separately.

7.1.2 Flight Schedules

Table 7.1 shows an example of the flight schedule with variables that are used as input for the FGAP models. Arriving (Departing) aircraft at (from) AMS are assigned a unique flight number, which is referred to as FlightIDIn (FlightIDOut). Each arriving (departing) flight has a STA (STD). The size of an aircraft, ACSize, is encoded on a scale from 3 to 9, where 3 corresponds to a small aircraft (Fokker 100) and 9 corresponds to the largest passenger jets (Airbus A380-800). The type of customs associated with an arriving (departing) flight is also included. Customs associated with arriving aircraft are referred to as CustomsIn, while customs associated with departing aircraft are referred to as CustomsOut. Both CustomIn and CustomOut can be Schengen, which is encoded by 1, EU Non-Schengen, which is encoded by 2, or and Intercontinental customs, which is encoded by 3. RegionIn (RegionOut) denotes the region the flight originates from (departs to). Airline

indicates the IATA code of the airline that performs the flight. T_4 is the time in minutes between first and last passenger of a flight that use check-in facilities and T_6 is the time in minutes between the last passenger of flight to use check-in facilities and the STD of that flight.

Table 7.1: Example of flights scheduled to arrive/depart at AMS on July 4, 2018. Only those variables that are used by the FGAP models are included in this example.

FlightIDIn	FlightIDOut	STA	STD	ACSize	CustomsIn	CustomsOut	RegionIn	RegionOut	Airline	T_4	T_6
GA9231	GA9488	13:25	14:25	4	1	1	Europe	Europe	GIA	120	40
KL6060	KL6019	13:25	15:25	7	3	3	North-America	North-America	KLM	150	60
DL9505	DL9603	13:30	14:15	4	1	1	Europe	Europe	DAL	120	40
AF8306	AF8497	13:35	14:20	3	2	2	Europe	Europe	AFL	120	40
DL9272	DL9536	13:35	14:20	4	2	1	Europe	Europe	DAL	120	40

The month of July accounted for 9.53% of the annual number of passengers at AMS in 2018 (*Traffic Review 2018*, 2019). Therefore, each day in July, 2018 is considered a peak-day in terms of passenger demand. Flight schedules are constructed for calender days between July 1, 2018 and July 30, 2018 that have complete lists of arriving and departing flight legs. As such, flight schedules can be constructed for all dates between July 1, 2018 and July 30, 2018, with the exception of the 3rd, 6th, 7th, 19th, 24th and 30th of July 2018. Between all available flight schedules, the amount of flight movements varies between 623 and 705 per calender day.

The flight schedule of July 4, 2018 is considered as support for the flight-to-gate assignment problem in this paper. The flight schedule of July 4, 2018 at AMS contains 575 arrival and 549 departure movements; the difference is caused by flights with an arrival and departure on different calendar days. Flights within Europe account for 76.8% and 73.2% of arrival and departure movements, respectively. Wide-body aircraft, i.e., aircraft for which ACSize > 4, and narrow-body aircraft, i.e., the aircraft for which ACSize ≤ 4, serve 15.1% and 84.9% of the flights, respectively.

7.1.3 Gates

Four types of gates exists, namely piers, platforms, aprons and towing trucks. Piers typically include one or more jet bridges and allow passengers and crew to board and disembark the aircraft without setting foot on the tarmac. Platforms are allocated spaces on the tarmac where passengers and crew can board and disembark through moveable staircases. Aprons are allocated spaces in the tarmac that typically facilitate parking movements of aircraft and are therefore located further away from the terminal than platform gates. In rare cases, aprons can support boarding and disembarking processes. If a flight is split in different flight segments, a tow truck is needed to transport the aircraft from one gate to another.

Table 7.2 gives an example of gates. GateID is the unique identifier of the gate. The metric Size indicates the maximum aircraft size that the gate can accommodate. The metric Customs indicates the customs level of the gate. Type indicates whether the gate is a pier, platform, apron or towing truck.

Piers can handle aircraft with a maximum size of 3 through 9. Additionally, customs levels vary between Schengen, NonSchengen European Union and Intercontinental. In total, 132 piers are included in the data set. Platforms can handle aircraft with a maximum size of 4 through 9 and customs levels vary between Non-Schengen European Union and Intercontinental. In total, AMS has 132 platform gates. A total of 11 aprons are present at AMS, all of which with a size of 8 and Intercontinental customs levels. Independent of the gate assignment prior and post the towing movements, towing trucks are able to handle any aircraft at

Table 7.2: Example of gates at AMS.

GateID	Size	Customs	Type
A34	8	3	Platform
D08	6	3	Pier
R72	8	3	Apron
THW	9	3	Towing truck

any customs level and any size.

7.1.4 Empirical Presence Curves Airlines/Regions

The variables $fp_{a,t,arr}$, $fp_{a,t,dep}$, $fp_{r,t,arr}$ and $fp_{r,t,dep}$ correspond to flight arrival/departure presence probabilities of the airline a or region r corresponding to flight l. The methodology to construct these variables is described in detail bij Schaijk (2013). To construct these presence probabilities, atleast 200 data points of each combination of a/r and arr/dep are needed. Thus, a minimum of 200 deviations from STA or STD are needed to construct a arrival or departure presence curve belonging to a airline or region option. Using the complete data set, this leads to arriving and departing empirical presence curves for 20 airlines and 7 regions. The arriving and departing empirical presence curves for the 20 airlines and 7 regions are indicated in figure 7.2 on page 85. Given that arrival times generally cannot be influenced by the airport, the arrival presence curves represent a wide sigmoid function. On the other hand, an aircraft seldom departs before the STD. As such, the departing presence curves are equal to 1 almost entirely up to the STD. Furthermore, it is observed that large differences in presence probabilities between airlines exist for both the arrival and departure presence curves. The same argument holds for the arrival and departure presence curves per region.

7.2 FGAP Model Parameters

This section provides an overview of the model parameters that are included in the FGAP models. Subsection 7.2.1 describes the derivation of the scaling parameters in equation (5.2.5). Subsection 7.2.2 elaborates on the input parameters of the passenger demand model, introduced in subsection 5.3.2. Subsection 7.2.3 describes how the value of the scaling factor w_{al} in equation (5.4.4) is determined.

7.2.1 Scaling Coefficients Flight Presence Probability Model

This subsection describes how the scaling parameters in equation (5.2.5) on page 62 are derived. These scaling parameters include the parameters $\beta_{a,arr}$, $\beta_{a,dep}$, $\beta_{r,arr}$ and $\beta_{r,dep}$. Intuitively, one could argue that a larger variance between the curves within a category signals a better explanatory power of the category as a whole. Conversely, if the curves of the options within a category have a low variance, the category might not be suitable to explain the differences in flight presence probabilities belonging to different options within a category. This thought gives rise to the idea of using the variance of the flight presence probability as a proxy for the values of the scaling coefficients in the linear models indicated in equation (5.2.5). As such, the value of $\beta_{a,arr}$, $\beta_{a,dep}$, $\beta_{r,arr}$ and $\beta_{r,dep}$ is estimated by equation (7.2.1) through (7.2.4),

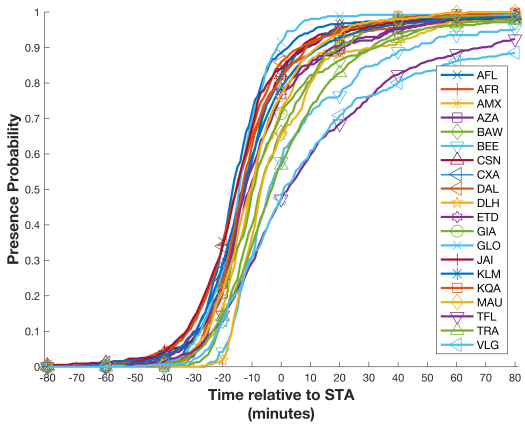

(a) Presence probabilities of arriving flights per airlines $fp_{a,t,arr}$. In total, 20 airlines a have enough data to construct presence probabilities.

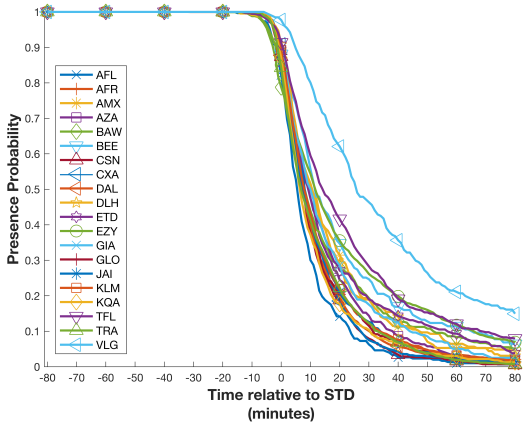

(b) Presence probabilities of departing flight legs per airlines $fp_{a,t,dep}$. In total, 20 airlines a have enough data to construct presence probabilities.

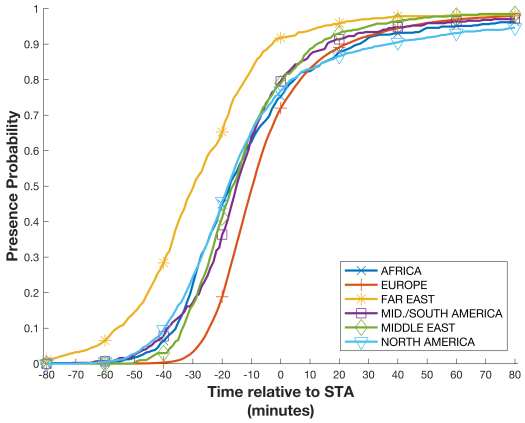

(c) Presence probabilities of arriving flight legs per region $fp_{r,t,arr}$. All regions r in the data sample have enough data to construct presence probabilities.

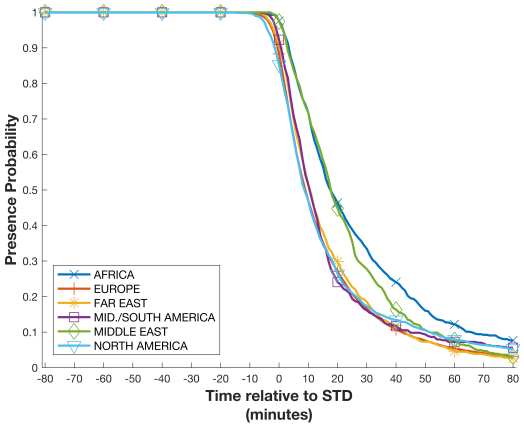

(d) Presence probabilities of departing flight leg per region $fp_{r,t,dep}$. All regions r in the data sample have enough data to construct presence probabilities.

Figure 7.2: Overview of flight presence probabilities for arriving/departing flight legs per airline and region option. Plots are based on arriving and departing flight lists at AMS dated between July 1, 2018 and July 30, 2018.

$$\beta_{a,arr} = \frac{\text{var}_t(fp_{a,t,arr})}{\text{var}_t(fp_{a,t,arr}) + \text{var}_t(fp_{r,t,arr})}, \quad (7.2.1) \qquad \beta_{a,dep} = \frac{\text{var}_t(fp_{a,t,dep})}{\text{var}_t(fp_{a,t,dep}) + \text{var}(fp_{r,t,dep})}, \quad (7.2.2)$$

$$\beta_{r,arr} = \frac{\text{var}_t(fp_{r,t,arr})}{\text{var}_t(fp_{a,t,arr}) + \text{var}_t(fp_{r,t,arr})}, \quad (7.2.3) \qquad \beta_{r,dep} = \frac{\text{var}_t(fp_{r,t,dep})}{\text{var}_t(fp_{a,t,dep}) + \text{var}_t(fp_{r,t,dep})}. \quad (7.2.4)$$

For arriving flights, $\beta_{a,arr}$ and $\beta_{r,arr}$ are computed to have a value of 0.4847 and 0.5153. respectively. For departing flights, values of 0.5836 and 0.4164 are found for $\beta_{a,dep}$ and $\beta_{r,dep}$, respectively.

7.2.2 Demand Model Parameters

The passenger demand model, described in subsection 5.3.2 on page 63, uses input parameters derived from the flight schedule and other sources of information. This subsection describes the derivation of these input parameters.

Sizes for commercial airliners range from 3 till 9, where 3 and 9 correspond to a smaller single-aisle aircraft (Fokker 70) and the largest passenger jets (Airbus A380-800) and are denoted by ACSize in table 7.1 on page 83. The model parameter η_i indicates the number of seats in the aircraft serving flight segment i. Table 7.3 provides a mapping between the value of ACSize and η_i for flight segment i. Estimates of the number of seats are based on the average number of seats in a regular seating arrangement found within the included aircraft types.

Table 7.3: Mapping between the value of ACSize and η_i for flight segment i. The number of seats reflects the average number of seats in a regular seating arrangement found within the included aircraft types. Note that the list of example aircraft types is not exhaustive but reflects aircraft types present at AMS on July 4, 2018.

ACSize	Seats (η_i)	Example Aircraft Types				
3	100	Fokker 70	Fokker 100	Embraer 190	Boeing 733	Boeing 735
4	160	Airbus A318	Airbus A320	Embraer 195	Boeing 736	Boeing 738
5	220	Boeing 752				
6	250	Boeing 753	Boeing 763			
7	280	Airbus A332	Airbus A333	Airbus A343	Boeing 764	Boeing 788
8	350	Boeing 744	Boeing 772	Boeing 773	Boeing 789	Airbus A359
9	530	Airbus A388				

Values of T_4 and T_6 depend on characteristics of flight segment $i \in N_d$. Figure 7.3 indicates these empirical cumulative density functions (CDFs) for both T_4 and T_6. The check-in interval T_4 ranges between 80 and 200 minutes. The most common value is 140 minutes and its mean is 133 minutes. The departure interval T_6 varies between 40 and 80 minutes with a mean of 45 minutes. Its most common value is 40 minutes.

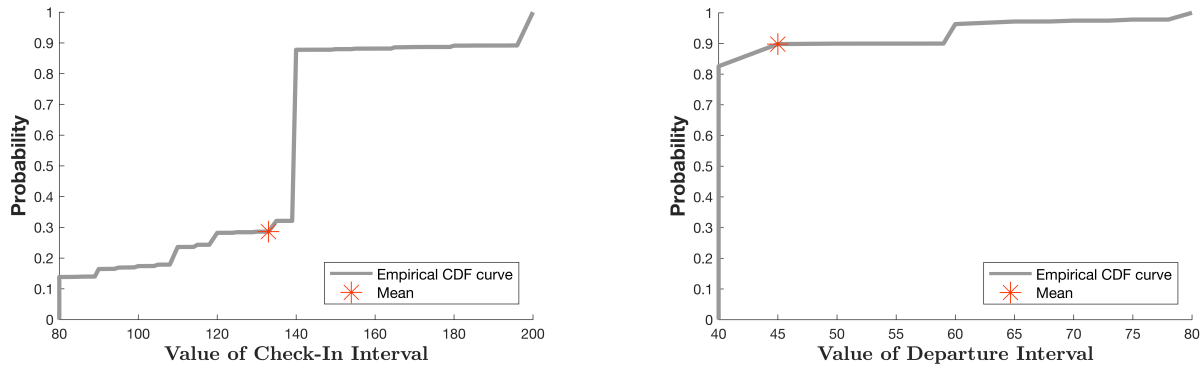

(a) Empirical CDF of check-in interval T_4.

(b) Empirical CDF of departure interval T_6.

Figure 7.3: Empirical CDF of T_4 and T_6, denoting the check-in interval and departure interval, respectively. The check-in interval T_4 ranges between 80 and 200 minutes. The most common value is 140 minutes and its mean is 133 minutes. The departure interval T_6 varies between 40 and 80 minutes. Its mean is 45 minutes and its most common value is 40 minutes. Plots are based on arriving and departing flight lists at AMS dated between July 1, 2018 and July 30, 2018.

To establish the value of the parameter F_{CI}, the passenger profiles at AMS are examined. Table 7.4 shows the profiles of five different passenger types, each with their own distinct characteristics. These include passengers who travel for business, leisure, congress or study and visiting acquaintances, in addition to a group of passengers which travel for another reason than the reasons mentioned here. Per profile, table 7.4 indicates the percentage of annual passengers at AMS these profiles account for, the corresponding number of passengers, average check-in rate and a description with other important features of the profile. The overall check-in rate F_{CI} is computed as a weighted average of the check-in rates of the individual profiles, which is calculated to be equal to 55%.

Table 7.4: Overview of passenger profiles at AMS, which include passengers which travel for business, attending a congress or other study-relayed reasons, leisure and visiting acquaintances. Passengers with reasons to travel other than the ones mentioned beforehand are grouped in a fifth profile. Types, percentages and quantity are based on *Traffic Review 2017* (2018), check-in rates and travel frequencies are based on an estimate by the author. By computing the weighted average of the check-in rates per profile, an overall check-in rate of 55% is found.

Type	Percentage	Quantity	Check-In Rate	Travel Frequency
Business	29%	19.8 million	20%	Frequent travellers
Congress & Study	3%	2.1 million	30%	Occasional travellers
Leisure	47%	32.2 million	70%	Infrequent travellers
Visiting Acquaintances	20%	13.7 million	70%	Occasional travellers
Other	2%	1.4 million	50%	Occasional travellers

The value of the transfer rate F_{TF} is derived from public data indicated by *Traffic Review 2017* (2018). The overall transfer rate at AMS is equal to 37%. However, it is assumed that only airlines which are a member of the SkyTeam Alliance carry transfer passengers. All members of the SkyTeam Alliance as of November 1, 2018, are indicated in table 7.5. Using the flight schedule of July 4th, 2018, with a compression factor 5, SkyTeam flights have a transfer rate of $F_{TF} = 67\%$ to ensure the overall transfer rate is equal to 37%.

Table 7.5: Overview SkyTeam member airlines. This overview is made on November 1, 2018, and is subject to change over time. Using the flight schedule of July 4th, 2018, with a compression factor 5, SkyTeam flights have a transfer rate of 67% to ensure the overall transfer rate is equal to 37%.

IATA	Airline	IATA	Airline
AFL	Aeroflot	DAL	Delta Airlines
ARG	Aerolineas Argentinas	GIA	Garuda Airlines
AMX	AeroMexico	KQA	Kenya Airways
AEA	Air Europa	KLM	KLM
AFR	Air France	KAL	Korean Air
AZA	Alitalia	MEA	Middle East Airlines
CAL	China Airlines	SVA	Saudia
CES	China Eastern Airlines	ROT	Tarom
CSN	China Southern Airlines	HVN	Vietnam Airlines
CSA	Czech Airlines	CXA	XiamenAir

7.2.3 Scaling Parameter Objective Function

The objective function of the FGAP models, indicated by equation (5.4.4) on page 67, is comprised of two elements. The first element $\sum_{i\in N}\sum_{j\in G_i^1}\sum_{t\in K} c^a_{i,j}x_{i,j,t}$ expresses the cost of assigning flight segment $i \in N$ to gate $j \in G_i^1$ at time $t \in K$ and is equal to the objective function (equation (1)) of the FGAP model by Schaijk & Visser (2017). The second element $\sum_{i\in N_a\cup N_d}\sum_{j\in G_i^1}\sum_{q\in T} c^l_{i,j,q}z_{i,j,q}$ expresses the cost of assigning flight segment $i \in N_a \cup N_d$ to gate $j \in G_i^1$ and its departing passenger stream to terminal $q \in T$. The weighting factor w_{al} is used to scale the cost of the landside element accordingly

Figure 7.4 on page 88 shows the empirical CDFs of the cost coefficients $c^a_{i,j}$ and $c^l_{i,j,q}$. These cost coefficients are constructed using the flight schedule from July 4, 2018, a maximum overlap probability r=5% and a compression factor of 5. As figure 7.4 shows, the maximum value differs greatly between the two cost coefficients. In addition, the empirical CDFs are non-continuous, which is caused by the fact that the cost coefficients are constructed using a discrete, finite set of cost coefficient values. Because the cost coefficients $c^a_{i,j}$ are constructed using a more intricate set of rules, this CDF is somewhat less non-continuous as compared to the CDF of $c^l_{i,j,q}$. The cost coefficients $c^a_{i,j}$ and $c^l_{i,j,q}$ have a mean of 80 and 150, respectively.

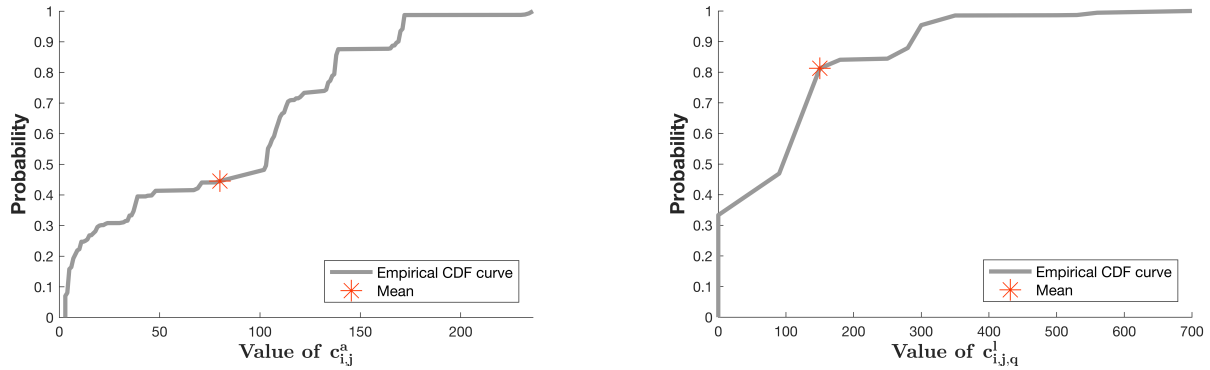

(a) Empirical CDF of cost coefficients $c^a_{i,j}$.

(b) Empirical CDF of cost coefficients $c^l_{i,j,q}$.

Figure 7.4: Empirical CDF of cost coefficients $c^a_{i,j}$ and $c^l_{i,j,q}$. These cost coefficients are constructed using the flight schedule from July 4, 2018, a maximum overlap probability r=5% and a compression factor of 5. Both graphs show a distinct pattern cost coefficients are non-continuous. Given that the cost coefficients $c^a_{i,j}$ are constructed using a more complicated set of rules, a larger variation in values exist as compared to the cost coefficients $c^l_{i,j,q}$, which are constructed from a smaller set of possible values. However, the magnitude of $c^l_{i,j,q}$ is significantly larger as compared to $c^a_{i,j}$.

To determine the value of w_{al}, it assumed that its value is chosen such that the mean of $c^a_{i,j}$ is equal to the mean of $w_{al}c^l_{i,j,q}$. The value of $w_{al} = 0.53$ is set using equation (7.2.5),

$$E[c^a_{i,j}] = w_{al}\cdot E[c^l_{i,j,q}], \tag{7.2.5}$$

where the values of the cost coefficients $c^a_{i,j}$ and $c^l_{i,j,q}$ are based on the flight schedule of AMS on July 4, 2018 and the set of gates at AMS.

Chapter 8

Results

This section presents the results of the flight-to-gate assignment models, taking into account AMS-specific constraints (6.1.1) - (6.2.1). Unless stated otherwise, the results in this chapter are obtained using the parameter set indicated in table 8.1. A planning horizon of operations between 00:00 and 23:59 on the same calendar day is considered. The results of the A-FGAP model are presented in section 8.1. Results of the DC-FGAP model are presented in section 8.2. Section 8.3 presents the results of the WT-FGAP model. Section 8.4 provides a comparison of the FGAP models.

Table 8.1: Overview of parameter values used to obtain results of the A-FGAP, DC-FGAP and WT-FGAP models. Unless stated otherwise, the results in this chapter are obtained using these parameter values.

Parameter	Value
Date of flight schedule AMS	July 4, 2018
Data compression factor	5
Length time step δ_t	5 minutes
Maximum overlap probability r	5%
Waiting time threshold W^T	25 minutes
Maximum number of iterations MI	10

8.1 Results A-FGAP Model

The results of the A-FGAP model, indicated by equations (5.4.4), (5.4.11) - (5.4.18), (5.4.19), (5.5.1), (6.1.1) and (6.2.1), are discussed in this section. A single iteration of algorithm 1 on page 72 is sufficient to ensure the solution to the A-FGAP model is valid. The airside results are described in subsection 8.1.1. Subsection 8.1.2 outlines the landside results.

8.1.1 Airside Results A-FGAP Model

This subsection describes the airside results of the A-FGAP model. Summary statistics of the gate assignment plan are presented first, followed by an overview of the maximum overlap probability per pier.

8.1.1.1 Gate Assignment Plan A-FGAP Model

Figure 8.1 on page 90 shows the gate assignment planning created using the A-FGAP model. Functional and parking flight segments have a varying length, with a minimum duration of 45 and 90min, respectively. On average, a buffer time of 109.5min is allocated between flights. The buffer time has a standard deviation of 9.1min. Given that the A-FGAP model does not implement a fixed minimum buffer time, flights can be assigned to the same gate shortly after each other as long as the maximum overlap probability constraint in equation (5.4.11) is not violated. The minimum separation time for this gate assignment plan is equal to 25min.

In figure 8.1, only those gates are included to which atleast one flight segment is allocated during the planning horizon. The complete set of gates M includes a total of 69 gates, of which 39 gates are assigned at least one flight segment. All 26 piers have atleast one flight segment allocated to them. Pier D08 and D64 share the same landside facilities, and therefore constraints in equation (6.1.1) are implemented that ensure only of these gates is in use at any given time. Over 85% of flight segments in the set N are functional flight segments, which are preferably assigned to piers. As such, platforms and aprons are assigned less flight segments as compared to piers. Of the 27 platforms included in the set of gates, only 6 are assigned at least one flight segment during the planning horizon. Though 2 aprons are included in the set of gates, no flights are assigned to aprons during the planning horizon. In total, 7 of 14 available towing trucks are included in the gate assignment plan.

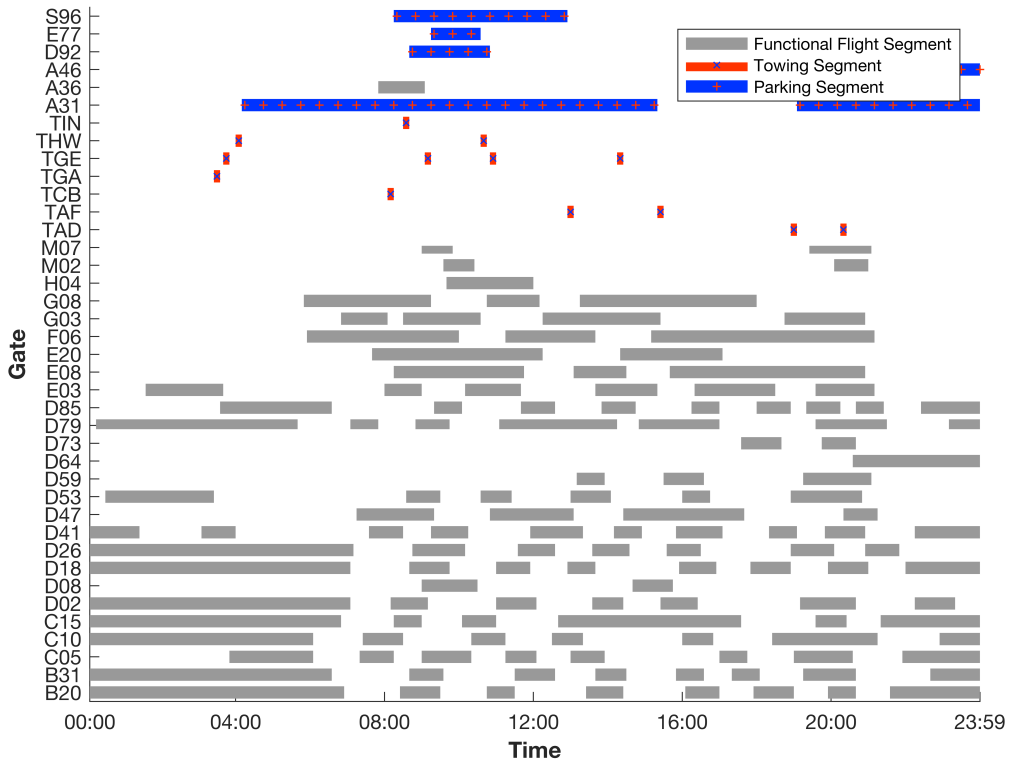

Figure 8.1: Gate assignment plan of the A-FGAP model. Results are obtained using the flight schedule of July 4, 2018, a compression factor of 5, $r = 5\%$, $\delta_t = 5$min and $MI = 10$.

Due to the short presence time of flights at the airport or sub-optimality of more complex flight splitting

options, the majority of flights is not split. As such, most flights consist of one functional flight segment, i.e. flight splitting option 1 (see subsection 5.1.1). Flights with a morning departure, often with a presence time in excess of 5 hours, are not split due to the abundance of piers available between 00:00 until 07:00. Overall, all flight splitting options are used, with the exception of the splitting option 5 (see subsection 5.1.2).

Due to limited gate capacity, flight segments cannot always be assigned to a gate that ensure the lowest cost is achieved. The cost coefficients $c^a_{i,j}$ are invariant with time and depend on customs requirements, size constraints and type assignments. The latter factor drives a preferred assignment of functional flight segments to piers. Due to crowding at the piers, not all functional flight segments can be assigned to a pier. The aircraft with tail number PKGIK has a STA and STD of 07:50 and 12:05, respectively. This flight is split into five different segments, as indicated by flight splitting option 3 (see subsection 5.1.1). The arrival functional flight segment is assigned to platform A36, which is able to handle flight segments with a maximum size of 8 and an Intercontinental customs clearing. Several piers are not assigned a flight segment during the time slot the arrival functional flight segment of the aircraft with tail number PKGIK is scheduled to be present at the airport. However, these gates are not able to suffice the size requirement of this aircraft. Therefore, this segment is assigned to a platform.

8.1.1.2 Maximum Overlap Probability A-FGAP Model

Figure 8.2 shows the maximum overlap probability for all piers. At piers D08, D64, H04, M02 and M07 all flight segments have non-overlapping flight presence probability curves, resulting in a maximum overlap probability of 0. All other gates have flight segment presence probability curves which overlap, resulting in non-zero maximum overlap probabilities. Omitting the aforementioned piers from the analysis, the maximum overlap probability per pier varies between 0.64% and 4.94%. Hence, the maximum overlap probability of $r = 5\%$ is not exceeded. Section B.1 on page 144 describes the overlap probability for piers B31, D18, D85 and E03 in more detail.

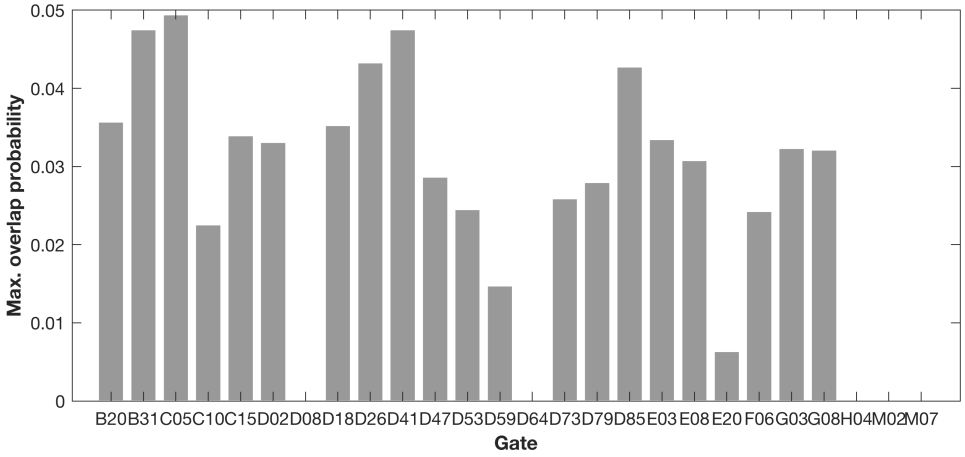

Figure 8.2: Maximum overlap probability for all piers that are assigned at least one flight segment. Omitting the piers where the overlap probability is 0% throughout the planning horizon, the maximum overlap probability varies between 0.64% and 4.94%. Hence, the maximum overlap probability of $r = 5\%$ is not exceeded. Results are obtained using the flight schedule of July 4, 2018, a compression factor of 5, $r = 5\%$, $\delta_t = 5$min and $MI = 10$.

8.1.2 Landside Results A-FGAP Model

Figure 8.3 shows the passengers demand imposed on facilities (A1), (T1), (D1) and (D2) per terminal at AMS derived using the A-FGAP model. The demand curves imposed on the facilities (A2) are horizontally shifted curves as compared the plot in in figure 8.3a and therefore are omitted from this report. The dashed lines in figure 8.3a through 8.3d indicate the declared capacity $C_{p,q}$. Facilities (A1) and (T1) in Terminals 1 and 4 do not have a declared capacity because these facilities are non-existent. This reflects that Terminal 1 and 4 serve passenger streams with a Schengen customs clearance. The A-FGAP model does not impose landside constraints and, therefore, the passenger demand can exceed the declared capacity. All facilities in Terminal 2, facilities (T1) in Terminal 3 and facilities (A2) in Terminal 4 experience a passenger demand which exceeds the declared capacity.

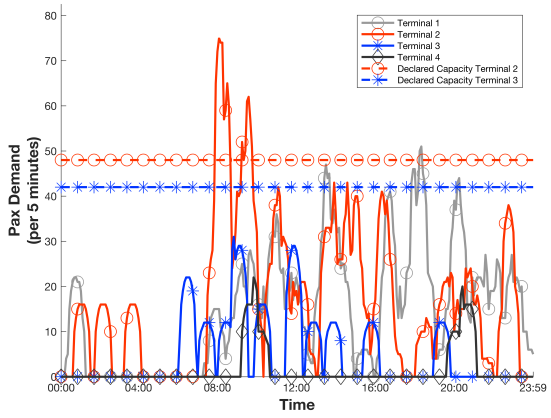

(a) Number of passengers passing through arrival immigration (A1) per terminal per time step t.

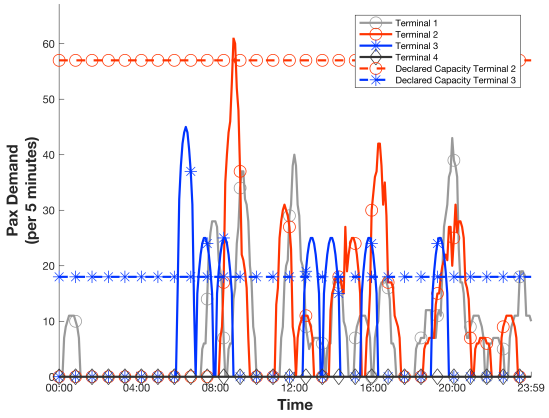

(b) Number of transfer passengers passing through transfer security (T1) per terminal per time step t.

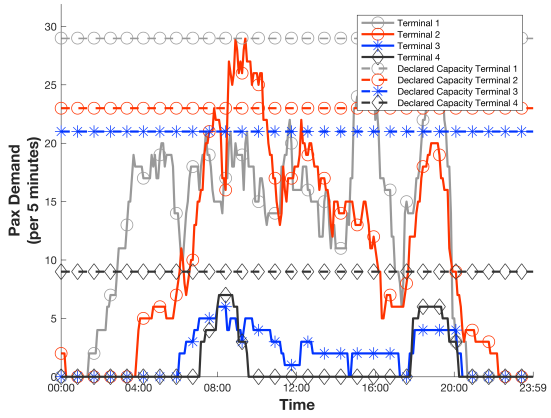

(c) Number of departing passengers using check-in facilities (D1) per terminal per time step t.

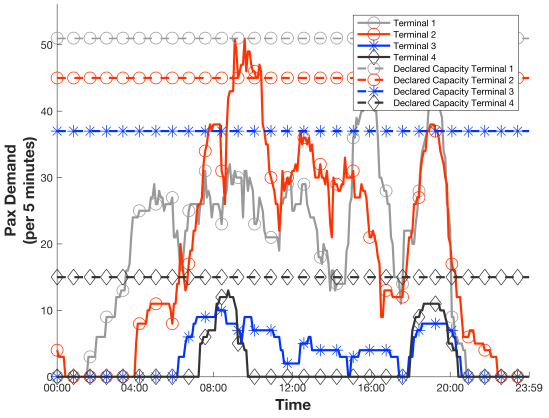

(d) Number of departing passengers passing through security/border control (D2) per terminal per time step t.

Figure 8.3: Overview of passenger demand on landside facilities, derived using the A-FGAP model. No landside constraints are imposed by the A-FGAP model; passenger demand can exceed the declared capacity. Results are obtained using the flight schedule of July 4, 2018, a compression factor of 5, $r = 5\%$, $\delta_t = 5$min and $MI = 10$.

Passenger demand curves for facilities (A1) and (T1), in figures 8.3a and 8.3a, respectively, are erratic as short peaks of high demand can be observed alongside periods with no passenger demand. Passenger demand curves for facilities (D1) and (D2), in figures 8.3c and 8.3d, respectively, are more continuous and intermediate periods without passenger demand are uncommon. This difference is caused by the passenger processing intervals T_3 and T_4, with T_4 typically being equal to 3-4x T_3. Hence, the width of the interval in which arriving passengers for each flight make their way through the terminal is up to 75% smaller than the width of the interval in which departing passengers for a flight move through the terminal. Therefore, streams of arriving passenger often follow a more erratic pattern as compared to departing passenger streams.

Subsection 7.1.2 on page 82 indicates that Terminal 1 through 4 handle 34.08%, 38.13%, 24.88% and 2.91%, respectively of the aircraft movements. Using the results from figure 8.3, Terminals 1 through 4 are computed to handle 43.1%, 44.9%, 8,9% and 3.1% of the total passengers at AMS on July 4, 2018. The passenger split between terminals introduced in subsection 4.4.1 on page 53 implied that Terminal 3 handles 24.88% of all passengers. The discrepancy between the calculated split and estimated split is explained by the implementation of the compression factor, causing concourses F, G and H to be under-represented in the data sample.

8.2 Results DC-FGAP Model

The results of the DC-FGAP model, indicated by equations (5.4.4), (5.4.11) - (5.4.18), (5.4.19), (5.5.2), (6.1.1) and (6.2.1), are discussed in this section. A single iteration of algorithm 1 on page 72 is sufficient to ensure the solution to the DC-FGAP model is valid. The airside results are described in subsection 8.2.1. Subsection 8.2.2 outlines the landside results.

8.2.1 Airside Results DC-FGAP Model

This subsection describes the gate assignment planning found using the DC-FGAP model. Summary statistics and insights in the gate assignment plan are presented first, followed by a brief description of the maximum overlap probability per pier.

8.2.1.1 Gate Assignment Plan DC-FGAP Model

Figure 8.4 on page 94 shows the gate assignment planning derived using the DC-FGAP model. Functional and parking flight segments have a varying length, with a minimum duration of 45 and 90min, respectively. The average buffer time, equal to 104.9min, is slightly smaller as compared to the average buffer time of the gate assignment plan derived using the A-FGAP model. The standard deviation of the buffer time has a value of 9.5min and is marginally larger compared to the standard deviation found using the A-FGAP model. The minimum separation time is equal to 25min.

Figure 8.4 only includes those gates which are assigned atleast one flight segment during the planning horizon. As was the case with the solution to the A-FGAP model, all piers are assigned atleast one flight segment during the planning horizon. In addition, 7 out of 27 available platforms are in use and 1 out of 2 aprons are assigned flight segments. In total, 7 towing trucks are included in the gate assignment planning. Given that towing segments only occur when flights are split into multiple flight segments, the

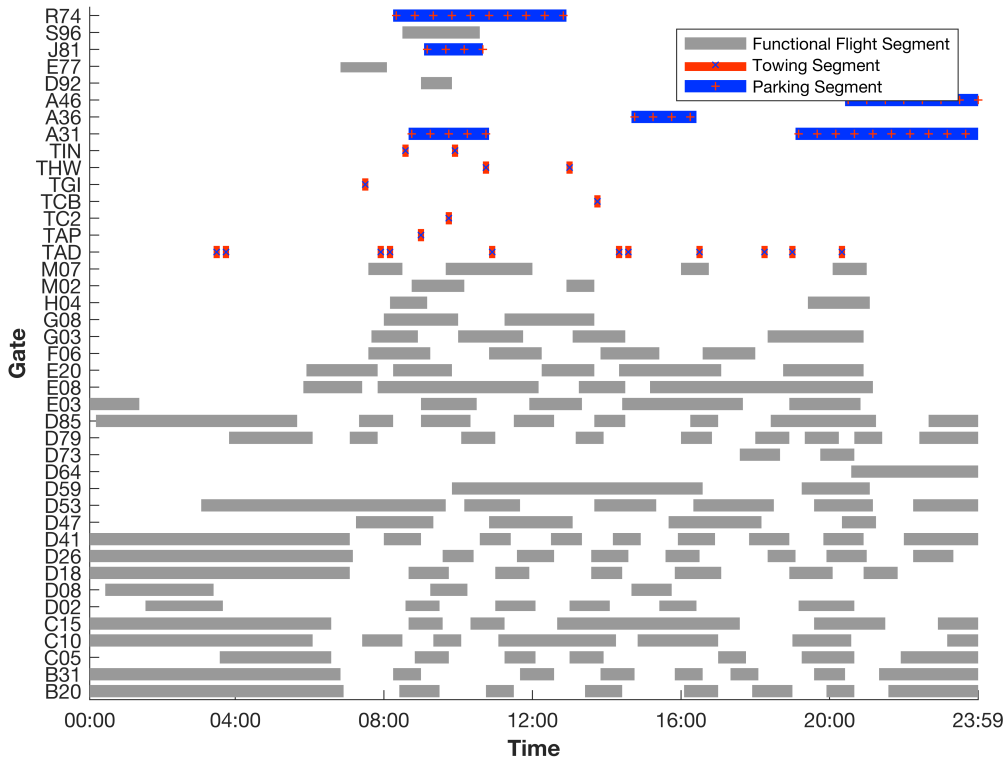

Figure 8.4: Gate assignment plan of the DC-FGAP model. Results are obtained using the flight schedule of July 4, 2018, a compression factor of 5, $r = 5\%$, $\delta_t = 5$min, $MI = 10$ and the declared capacity $C_{p,q}$.

presence probability of these segments is non-continuous. This is exemplified by figures 5.3 and 5.4 on page 61. Therefore, the towing movements are assigned to towing trucks with little to no buffer time in between.

The gate assignment plan created using the DC-FGAP model has three functional flight segments which are assigned to a platform. This increase in platform assignments relative to the A-FGAP model is caused by passenger demand constraint (5.4.18) on page 71. Due to limited landside capacity for preferred assignments, flight segments are moved to platforms such that demand constraint (5.4.18) is met. Given that landside constraints are inactive in the A-FGAP model, the gate assignment plan depicted in figure 8.1 and 8.4 differ.

8.2.1.2 Overlap Probability DC-FGAP Model

Figure 8.5 shows the maximum overlap probability for all piers to which atleast one flight segment is assigned to during the planning horizon. At piers D08, D59, D64, H04, M02 and M07 all flight segments have non-overlapping flight segment presence probability curves, resulting in a maximum overlap probability of 0%. All other gates have flight segment presence probability curves which overlap, resulting in non-zero maximum overlap probabilities. Omitting the aforementioned piers from the analysis, the maximum overlap probability varies between 1.54% and 4.94%. Hence, the maximum overlap probability of $r = 5\%$ is not exceeded.

Red lines in figure 8.5 denote the maximum overlap probability per gate derived using the A-FGAP model. On average, the maximum overlap probability per pier is 0.28% higher when comparing the GAP of the DC-FGAP model to the GAP of the A-FGAP model. This is to be expected, as the average separation time between each flight segment is reduced from 109.5min to 104.9min.

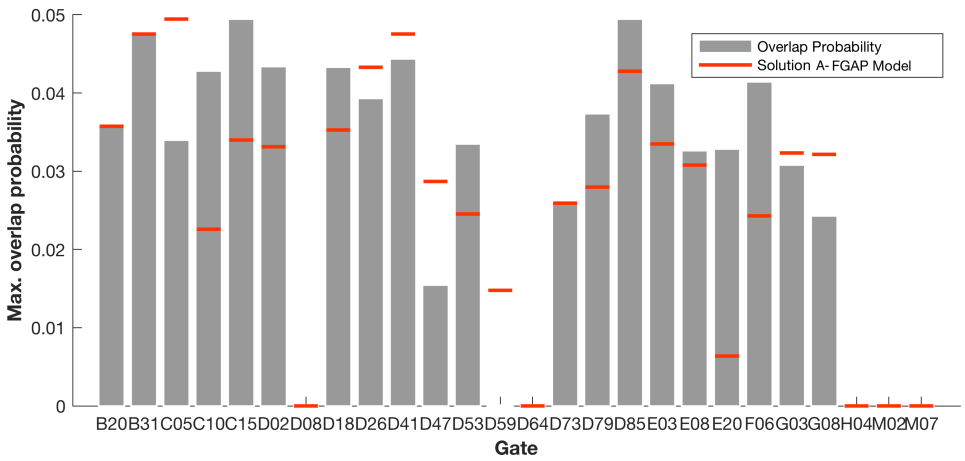

Figure 8.5: Maximum overlap probability for all piers that are assigned at least one flight segment. Omitting the piers where the overlap probability is 0% throughout the planning horizon, the maximum overlap probability varies between 0.64% and 4.94%. Hence, the maximum overlap probability of $r = 5\%$ is not exceeded. Results are obtained using the flight schedule of July 4, 2018, a compression factor of 5, $r = 5\%$, $\delta_t = 5$min, $MI = 10$ and the declared capacity $C_{p,q}$.

8.2.2 Landside Results DC-FGAP Model

Figure 8.6 on page 96 shows the passenger demand imposed on facilities (A1), (T1), (D1) and (D2) derived using the DC-FGAP model. As imposed by the DC-FGAP model, passenger demand per time step cannot exceed the declared capacity. Facilities (D1) in Terminal 1 and facilities (A1), (A2) and (T1) in Terminal 2 experience a passenger demand equal to the declared capacity. Hence, constraint (5.4.18) is binding for these facilities and terminal during atleast one time step. Passenger demand for facilities (A1) and (T1) is erratic, whereas passenger demand for facilities (D1) and (D2) is more continuous. The difference in values of the parameters T_3 and T_4 is the reason for this phenomenon (see subsection 8.1.2).

8.3 Results WT-FGAP Model

The results of the A-FGAP model, indicated by equations (5.4.4), (5.4.11) - (5.4.18), (5.4.19), (5.5.7), (6.1.1) and (6.2.1), are discussed in this section. Four iterations of algorithm 2 on page 77 are needed to create a valid solution to the WT-FGAP model; a detailed description of the results of the optimisation algorithm is given in section B.2 on page 146. The airside results are described in subsection 8.3.1. Subsection 8.3.2 outlines the landside results.

8.3.1 Airside Results WT-FGAP Model

This subsection describes the airside results of the WT-FGAP model. Summary statistics and insights in the GAP are presented first, followed by a brief description of the maximum overlap probability per pier.

8.3.1.1 Gate Assignment Plan WT-FGAP Model

Figure 8.7 on page 97 indicates the gate assignment plan derived using the WT-FGAP model. Functional and parking flight segments have a varying length, with a minimum duration of 45 and 90min, respectively. The

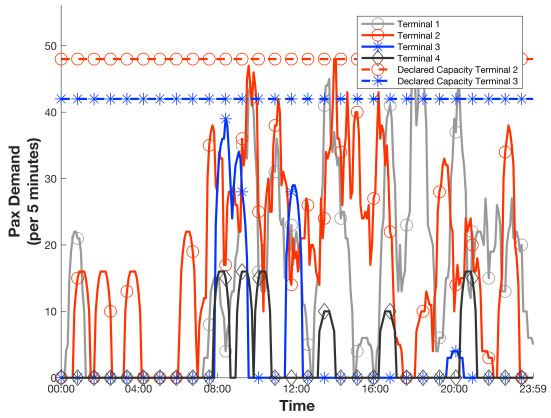

(a) Number of passengers passing through arrival immigration (A1) per terminal per time step t.

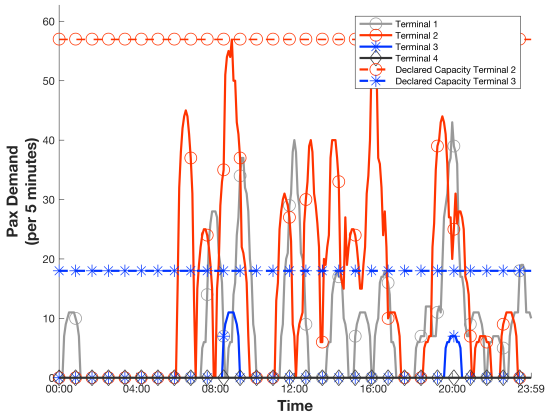

(b) Number of transfer passengers passing through transfer security (T1) per terminal per time step t.

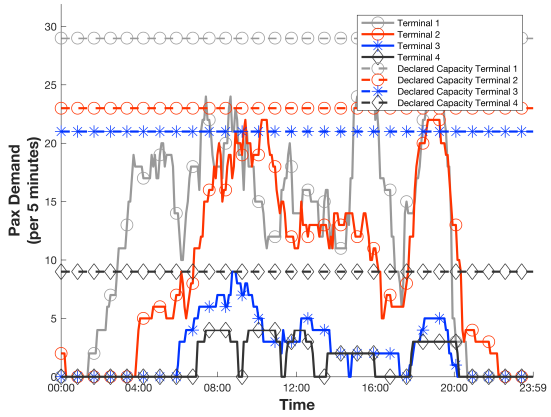

(c) Number of departing passengers using check-in facilities (D1) per terminal per time step t.

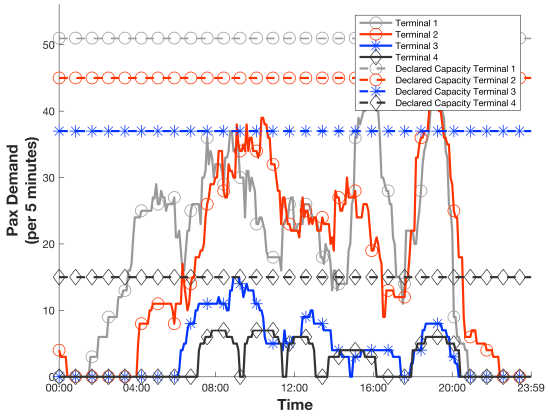

(d) Number of departing passengers passing through security/border control (D2) per terminal per time step t.

Figure 8.6: Overview of passenger demand on landside facilities, modelled using the DC-FGAP model. Passenger demand per time step t for each facility p in terminal q in figure 8.6 cannot exceed the corresponding declared capacity $C_{p,q}$. Results are obtained using the flight schedule of July 4, 2018, a compression factor of 5, $r = 5\%$, $\delta_t = 5$min, $MI = 10$ and the declared capacity $C_{p,q}$.

average buffer time is equal to 105.3min and therefore is slightly smaller as compared to the average buffer time of the gate assignment plan derived using the A-FGAP model. The standard deviation of the buffer time has a value of 9.3min and is marginally larger compared to the standard deviation found using the A-FGAP model. The minimum separation time is equal to 25min.

Figure 8.7 includes the gates to which atleast one flight segment is assigned during the planning horizon. Similar to the gate assignment plan derived using the A-FGAP model and the DC-FGAP model, all piers are assigned atleast one flight segment. In addition, 5 out of 27 available platforms are in use and 1 out of 2 aprons are assigned flight segments. In total, 7 towing trucks are included in the gate assignment planning. Similar to the A-FGAP model, one functional flight segment is assigned to a platform gate. This flight segment

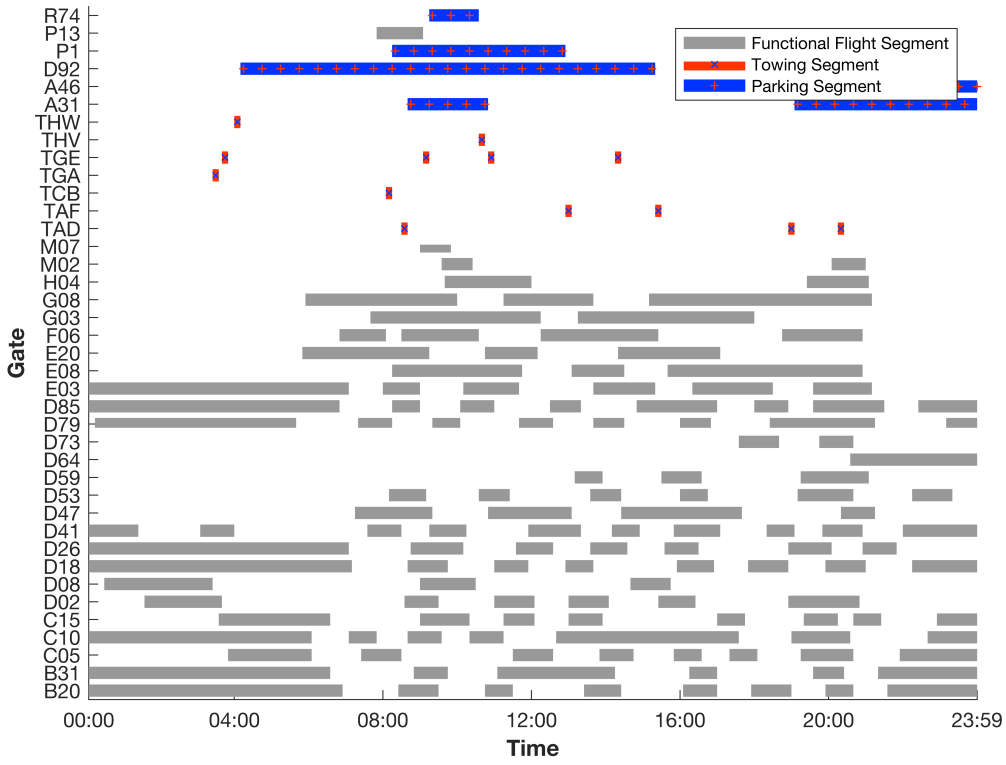

Figure 8.7: Gate assignment plan of the WT-FGAP model. Results are obtained using the flight schedule of July 4, 2018, a compression factor of 5, $r = 5\%$, $\delta_t = 5$min, $MI = 10$, $W^T = 25$min and the declared capacity $C_{p,q}$.

is covered by an aircraft with tail number PKGIK. Due to size requirements, the flight segment cannot be assigned to one of the available gates in the D-pier (see subsection 8.1.1.1 on page 90).

8.3.1.2 Maximum Overlap Probability WT-FGAP Model

Figure 8.8 shows the maximum overlap probability for all piers to which atleast one flight segment is assigned to. At piers D08, D64, H04, M02 and M07, all flight segments have non-overlapping flight segment presence probability curves, resulting in a maximum overlap probability of 0%. All other gates have flight segment presence probability curves which overlap, resulting in non-zero maximum overlap probabilities. Omitting the aforementioned piers from the analysis, the maximum overlap probability varies between 1.44% and 4.94%. Hence, the maximum overlap probability of $r = 5\%$ is not exceeded.

Red lines in figure 8.8 denote the maximum overlap probability per gate derived using the A-FGAP model. On average, the maximum overlap probability per pier is 0.17% higher when comparing the GAP of the WT-FGAP model to the GAP of the A-FGAP model. This is to be expected, as the average separation time between each flight segment is reduced from 109.5min to 105.3min.

8.3.2 Landside Results WT-FGAP Model

Figure 8.9 on page 99 depicts the passenger demand curves imposed on facilities (A1), (T1), (D1) and (D2). The WT-FGAP model ensures the expected maximum passenger waiting time is below a predefined threshold;

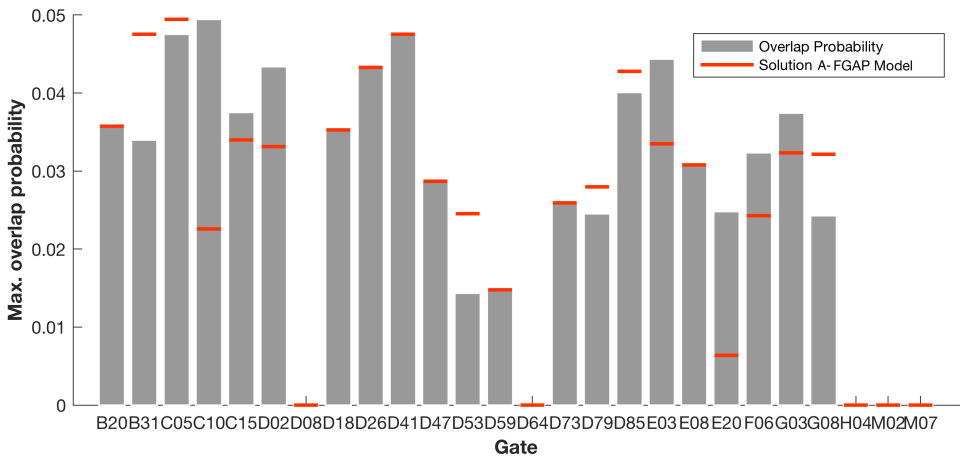

Figure 8.8: Maximum overlap probability for all piers that are assigned at least one flight segment. Omitting the piers where the overlap probability is 0% throughout the planning horizon, the maximum overlap probability varies between 0.64% and 4.94%. Hence, the maximum overlap probability of $r = 5\%$ is not exceeded. Results are obtained using the flight schedule of July 4, 2018, a compression factor of 5, $r = 5\%$, $\delta_t = 5$min, $MI = 10$, $W^T = 25$min and the declared capacity $C_{p,q}$.

hence passenger demand can exceed the declared capacity. Passenger demand in all facilities in Terminal 2, facilities (A1), (A2) and (T1) in Terminal 3 and facilities (A2) in Terminal 4 exceeds the declared capacity during atleast one time step. Passenger demand for facilities (A1) and (T1) is erratic, whereas passenger demand for facilities (D1) and (D2) is more continuous. The difference in values of the parameters T_3 and T_4 is the reason for this phenomenon (see subsection 8.1.2).

Four iterations of the solving algorithm (see subsection 5.5.3.2) are needed to create a valid solution to the WT-FGAP model. Figures 8.10a - 8.10b and 8.10c - 8.10d show the passenger demand curves and non-infinity values of $b_{p,q,t}$ for facilities (A1) in Terminal 3 and facilities (D2) in Terminal 2 in iteration 1 and 4 of the solving algorithm of the WT-FGAP model, respectively. All values of $b_{p,q,t} = \infty$ during iteration 1. In iteration 4 for these facilities, the values of $b_{p,q,t}$ are dropped to ensure that $W^{\max}_{p,q} \leq W^T$. In general, $W^{\max}_{p,q} > W^T$ during the iterations of the optimisation algorithm for facilities (T1) in Terminal 3 and facilities (A1), (A2) and (D1) in Terminal 2. Therefore, values of $b_{p,q,t}$ in the WT-FGAP model have values other than infinity for facilities (T1) in Terminal 3 and facilities (A1), (A2) and (D1) in Terminal 2. Over all facilities, terminals and time steps, only 3.84% of the parameters $b_{p,q,t}$ in the WT-FGAP model need a value other than infinity to ensure $W^{\max}_{p,q} \leq W^T$.

8.4 Model Comparison

This section provides a comparison between the results of the A-FGAP model, DC-FGAP model and WT-FGAP model. Subsection 8.4.1 compares the objective function values of the models. Subsection 8.4.2 describes the differences in functional flight segment allocation between the FGAP models. Subsection 8.4.3 describes the landside performance metrics of the FGAP models.

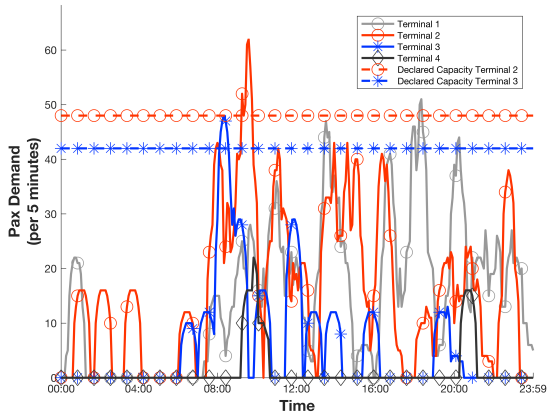

(a) Number of passengers passing through arrival immigration (A1) per terminal per time step t.

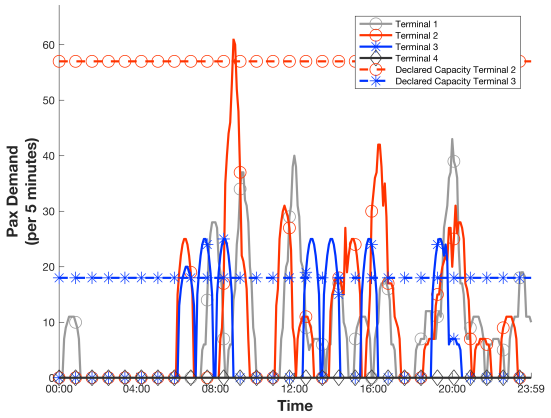

(b) Number of transfer passengers passing through transfer security (T1) per terminal per time step t.

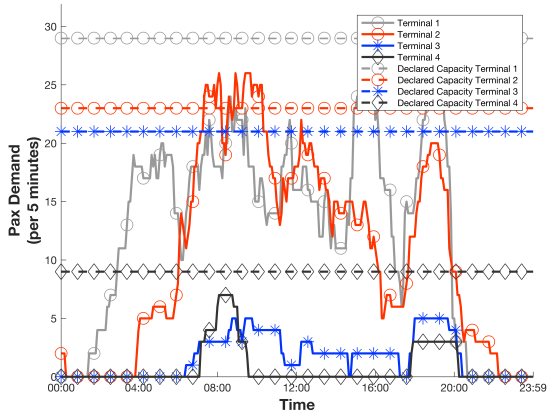

(c) Number of departing passengers using check-in facilities (D1) per terminal per time step t.

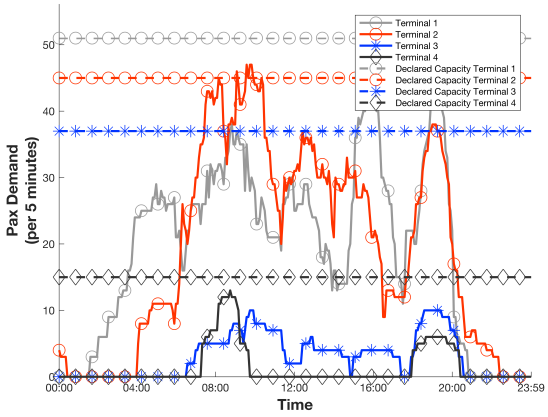

(d) Number of departing passengers passing through security/border control (D2) per terminal per time step t.

Figure 8.9: Overview of passenger demand on landside facilities, modelled using the WT-FGAP model. The passenger demand $y_{p,q,t}$ can exceed the declared capacity $C_{p,q}$, as long as the maximum waiting time threshold W^T is not exceeded. Results are obtained using the flight schedule of July 4, 2018, a compression factor of 5, $r = 5\%$, $\delta_t = 5$min, $MI = 10$, $W^T = 25$min and the declared capacity $C_{p,q}$.

8.4.1 Objective Function Value

Table 8.2 on page 101 indicates the values of the objective functions of the FGAP models, based on the mean of $n = 5$ runs. The objective function value of the A-FGAP model has the lowest value, followed extremely closely by the objective function value of the WT-FGAP model. The DC-FGAP model has a significantly higher value of the objective function. This value is 20.83% higher as the objective function value of the WT-FGAP model. This can be explained by the relatively small amount of differences between the GAP of the A-FGAP model and the WT-FGAP model. However, large differences between the GAP of the A-FGAP model and the DC-FGAP model exist. These differences are elaborated on in more detail in subsection 8.4.2

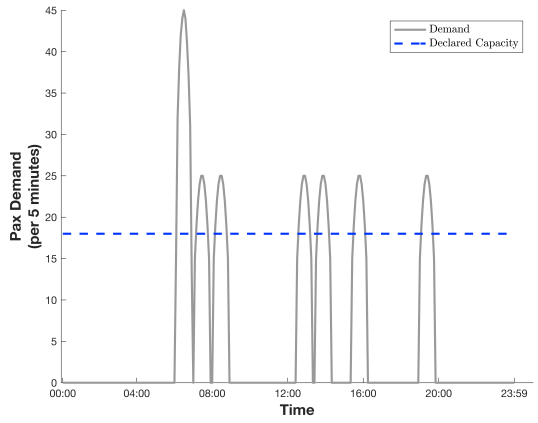

(a) Facilities (T1) in Terminal 3 in iteration 1.

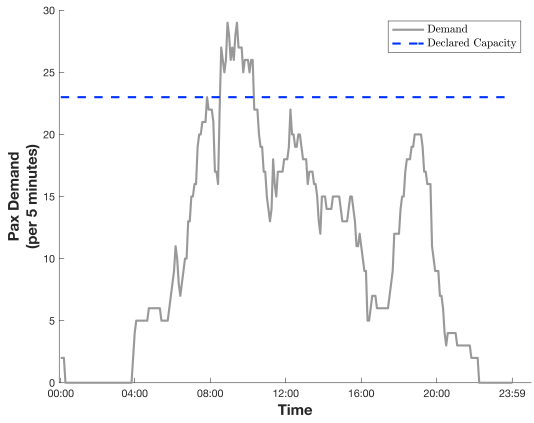

(b) Facilities (D1) in Terminal 2 in iteration 1.

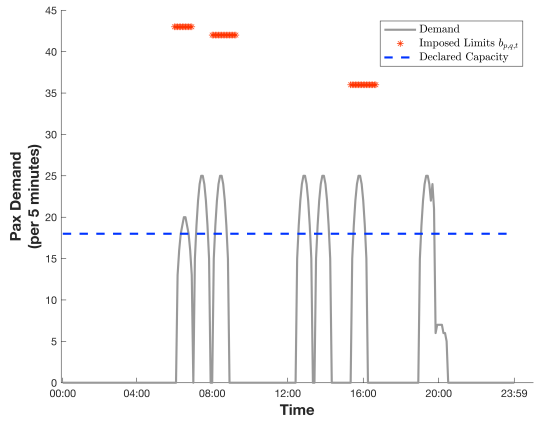

(c) Facilities (T1) in Terminal 3 in iteration 4.

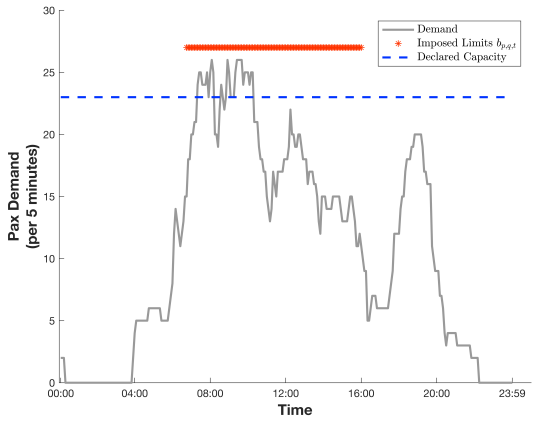

(d) Facilities (D1) in Terminal 2 in iteration 4.

Figure 8.10: Passenger demand for facilities (T1) in Terminal 3 and facilities (D1) in Terminal 2. In iteration 1 (Figure 8.10a - 8.10b), all values of $b_{p,q,t} = \infty$. In iteration 4 (Figure 8.10c - 8.10d), $b_{p,q,t}$, whose value is set dynamically by the WT-FGAP model, has values other than infinity such that all $W_{p,q,n} \leq W^T$. Results are obtained with $r = 5\%$, $W^T = 25$min, and a maximum number of 10 iterations of the solving algorithm.

on page 100.

8.4.2 Functional Flight Segment Allocation

Figure 8.11a on page 102 indicates the assignment of functional flight segments per concourse of the DC-FGAP model relative to the A-FGAP model. For example, 13.7% of all functional flight segments are assigned to concourse C if the DC-FGAP model is used, whereas 14.5% of all functional flight segments are assigned to concourse C if the A-FGAP model is used. Reallocation of flight segments between the A-FGAP model and DC-FGAP model in commonplace because of the equivalence in gate characteristics between gates within different concourses. For example, piers in concourses B, C and D59-87 have similar size and customs characteristics. Therefore, the assignment of functional flight segments is interchangeable between these concourses. However,

Table 8.2: Overview of objective function values of the A-FGAP, DC-FGAP and WT-FGAP model. Results are obtained using the flight schedule of July 4, 2018, a compression factor of 5, $r = 5\%$, $\delta_t = 5$min, $MI = 10$, $W^T = 25$min and the declared capacity $C_{p,q}$, based on the mean of $n = 5$ runs.

Model	Objective Function Value [-]
A-FGAP Model	69,626.3
DC-FGAP Model	84,130.5
WT-FGAP Model	69,628.1

a clear divide between concourses that serve Schengen flights (B, C, D59-87, M) and concourses that serve Non-Schengen flights (A, D03-D57, E, F, G, H, S) can be observed. In other words, flight segments are reallocated inside these groups, but not between these groups.

Figure 8.11b on page 102 indicates the assignment of functional flight segments per concourse of the WT-FGAP model relative to the A-FGAP model. As an example, 12.4% of all functional flight segments are assigned to concourse E if the DC-FGAP model is used, whereas 11.2% of all functional flight segments are assigned to concourse E if the A-FGAP model is used. A clear divide between concourses that serve Schengen flights and Non-Schengen flights is observed. However, a lower number of flight segment reallocation occur in Figure 8.11b relative to figure 8.11a. The WT-FGAP model imposes passenger demand constraints that are less tight as compared to the DC-FGAP model. Therefore, less deviations from the solution to the A-FGAP model are needed when using the WT-FGAP model as compared to the DC-FGAP model.

8.4.3 Landside Performance Metrics

Two metrics are used to determine the landside performance of the FGAP models. Subsection 8.4.3.1 describes the metric of demand-capacity ratios. Subsection 8.4.3.2 outlines the metric of the maximum expected passenger waiting time.

8.4.3.1 Demand-Capacity Ratio

The demand-capacity ratio for a facility p in terminal q is defined as the maximum passenger demand imposed on facility p in terminal q as a ratio of the corresponding declared capacity $C_{p,q}$. This is formalised by the expression in equation (8.4.1),

$$m_{p,q} = \max_t \frac{y_{p,q,t}}{C_{p,q}} \cdot 100\%, \quad p \in H, \quad q \in T. \tag{8.4.1}$$

Figures 8.12a and 8.12b provide an example of how this metric is computed for cases where $\max_t y_{p,q,t} < C_{p,q}$ and $\max_t y_{p,q,t} > C_{p,q}$, respectively. Data in figures 8.12a and 8.12b is derived from the A-FGAP model and corresponds to facilities (A1) in Terminal 3 and facilities (D2) in Terminal 2, respectively.

8.4.3.1.1 Demand-Capacity Ratio A-FGAP Model

Figure 8.13a on page 105 shows the demand-capacity ratios for all facilities and terminals at AMS under the A-FGAP model, which does not impose constraints on landside passenger demand. Thus, $m_{p,q}$ may be larger than 100%, e.g., $m_{T1,3} = 250\%$ and all facilities in Terminal 2 and facilities (A2) in Terminal 4 have a $m_{p,q} > 100\%$. Facilities (D1) and (D2) have a value of $m_{p,q} < 30\%$.

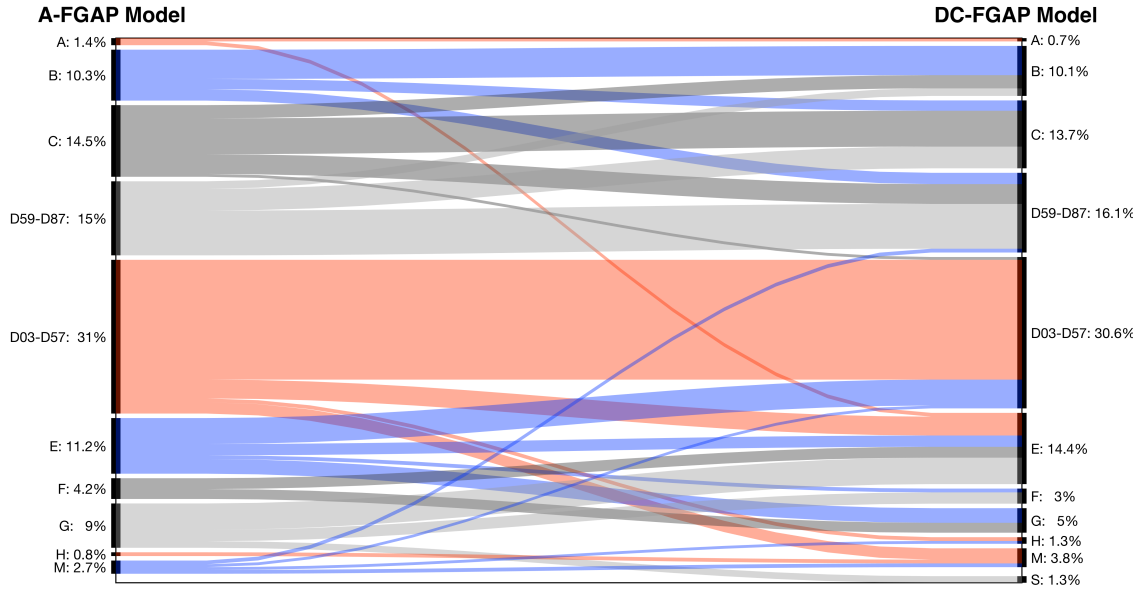

(a) Functional flight segment allocation to concourses at AMS of the DC-FGAP model versus the A-FGAP model.

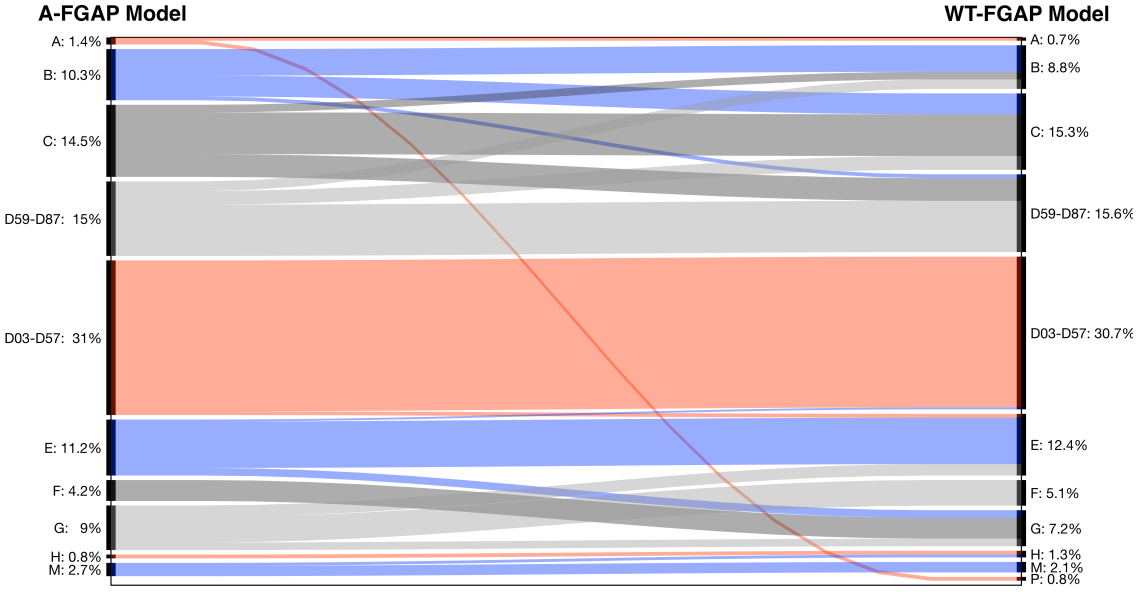

(b) Functional flight segment allocation to concourses at AMS of the WT-FGAP model versus the A-FGAP model.

Figure 8.11: Comparison of functional flight segment allocation to concourses at AMS of the the DC-FGAP model and WT-FGAP relative to the A-FGAP model. Results are obtained using the flight schedule of July 4, 2018, a compression factor of 5, $r = 5\%$, $\delta_t = 5\text{min}$, $MI = 10$, $W^T = 25\text{min}$ and the declared capacity $C_{p,q}$.

8.4.3.1.2 Demand-Capacity Ratio DC-FGAP Model

Figure 8.13c shows the demand-capacity ratios for all facilities and terminals at AMS under the DC-FGAP model, which imposes constraints such that $y_{p,q,t} \leq C_{p,q}$. Thus, $m_{p,q} \leq 100\%$ for all facilities and terminals.

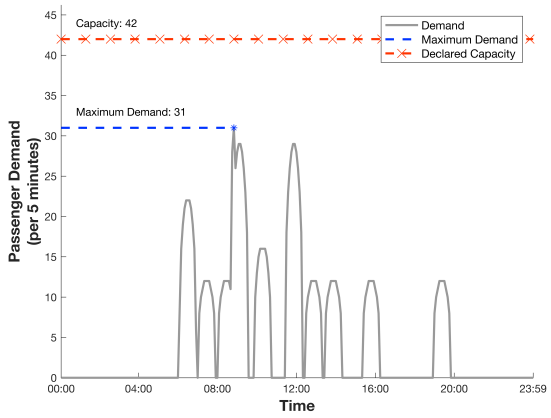

(a) Demand-capacity ratio at facilities (A1) in Terminal 3 where $\max_t y_{p,q,t} < C_{p,q}$; $m_{p,q} = 31/42 \cdot 100\% = 73.8\%$.

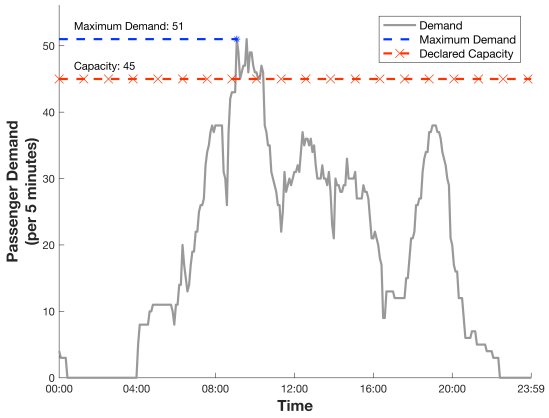

(b) Demand-capacity ratio at facilities (D2) in Terminal 2 where $\max_t y_{p,q,t} > C_{p,q}$; $m_{p,q} = 51/45 \cdot 100\% = 113.3\%$.

Figure 8.12: Demand-capacity ratio $m_{p,q}$ calculated using the A-FGAP model. Results are obtained using the flight schedule of July 4, 2018, a compression factor of 5, $r = 5\%$, $\delta_t = 5$min, $MI = 10$, and the declared capacity $C_{p,q}$.

Facilities (A1) and (A2) in Terminal 3 and 4 and all facilities in Terminal 2 and 3 have a $m_{p,q}$ equal or close to 100%.

8.4.3.1.3 Demand-Capacity Ratio WT-FGAP Model

Figure 8.13e on page 105 shows the demand-capacity ratios for all facilities and terminals at AMS under the WT-FGAP model, which dynamically sets the values of the parameters $b_{p,q,t}$ such that all $W^{\max}_{p,q} \leq W^T$. Facilities (A2) in Terminal 4, facilities (A1), (A2), (T1) in Terminal 3 and all facilities in Terminal 2 have $m_{p,q} > 100\%$.

8.4.3.1.4 Comparison Demand-Capacity Ratio FGAP Models

Values of $m_{p,q}$ show the most extreme values for the A-FGAP model, since this model does not impose constraints on landside passenger demand. The DC-FGAP enforces $m_{p,q} < 100\%$ by construction of constrain (5.4.18). The WT-FGAP dynamically set the values of $b_{p,q,t}$ to ensure the expected maximum waiting does not exceed a predefined threshold. Therefore, values of $m_{p,q}$ derived using the WT-FGAP model attain values between the values of $m_{p,q}$ derived using the A-FGAP model and DC-FGAP model.

8.4.3.2 Expected Maximum Waiting Time

The maximum expected waiting time over all peak periods n at facility p in terminal q is computed using equation (8.4.2),

$$W^{\max}_{p,q} = \max_{n \in U_{p,q}} (W_{p,q,n}), \quad p \in H, \quad q \in T. \tag{8.4.2}$$

8.4.3.2.1 Expected Maximum Waiting Time A-FGAP Model

Figure 8.13b on page 105 shows the expected maximum waiting times for all facilities and terminals at AMS under the A-FGAP model. For facilities (T1) in Terminal 3 and facilities (D1) in Terminal 2, $W_{p,q}^{\max} > W^T$. Due to a short duration of the peak demand periods at facilities (T1) in Terminal 2, the value of $m_{p,q} > 100\%$ but $W_{p,q}^{\max} < 1\text{min}$.

8.4.3.2.2 Expected Maximum Waiting Time DC-FGAP Model

Figure 8.13d on page 105 indicates the expected maximum waiting per facility and terminal for the solution to the DC-FGAP model. As expected, this figure shows that $W_{p,q}^{\max} < 1\text{min}$ for all facilities and terminals.

8.4.3.2.3 Expected Maximum Waiting Time WT-FGAP Model

Figure 8.13f shows the expected maximum waiting times for all facilities and terminals at AMS under the WT-FGAP model. For facility (A2) in Terminal 3, facility (T1) in Terminal 3 and facilities (A1), (A2) and (D1) in Terminal 2, $W_{p,q}^{\max} > 5\text{min}$. All values of $W_{p,q}^{\max} < W^T$, as imposed by the WT-FGAP model.

8.4.3.2.4 Comparison Expected Maximum Waiting Time FGAP Models

Figure 8.13b shows that for the A-FGAP model, $W_{p,q}^{\max} > W^T$ for facilities (D1) in Terminal 2 and facilities (T1) in Terminal 3. The DC-FGAP imposes the constraint that $y_{p,q,t} < C_{p,q}$ and therefore all values of $W_{p,q}^{\max} < 1\text{min}$. Using the WT-FGAP model, values of $W_{p,q}^{\max} \leq W^T$ for all facilities and terminals. In general, expected maximum waiting times derived using the WT-FGAP model attain values between the expected maximum waiting times derived using the A-FGAP model and DC-FGAP model.

(a) A-FGAP model: demand-capacity ratios $m_{p,q}$

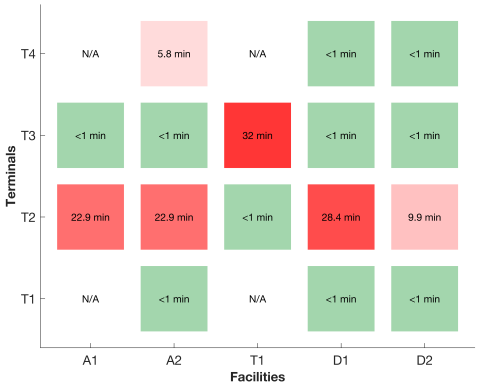

(b) A-FGAP model: max. waiting time $W_{p,q}^{\max}$.

(c) DC-FGAP model: demand-capacity ratios $m_{p,q}$.

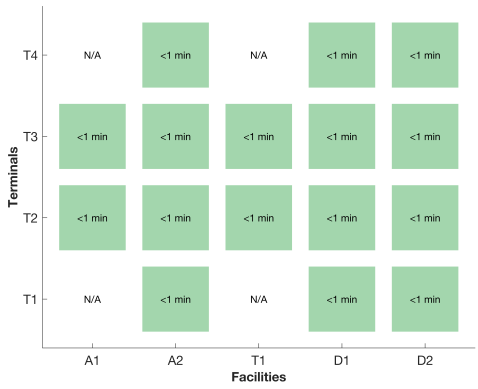

(d) DC-FGAP model: max. waiting time $W_{p,q}^{\max}$.

(e) WT-FGAP model: demand-capacity ratios $m_{p,q}$.

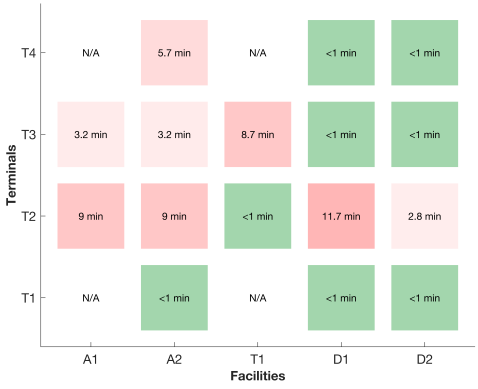

(f) WT-FGAP model: max. waiting time $W_{p,q}^{\max}$.

Figure 8.13: Overview of landside performance metrics for the FGAP Models, obtained using the parameter set in table 8.1. Red squares indicate values of $m_{p,q}$ larger or equal to 100% or expected maximum waiting times in excess of 1 minute. Results are obtained using the flight schedule of July 4, 2018, a compression factor of 5, $r = 5\%$, $\delta_t = 5$min, $MI = 10$, $W^T = 25$min and the declared capacity $C_{p,q}$.

Chapter 9

Sensitivity Analysis

The results presented in chapter 8 are dependent on the value of the input parameters listed in table 8.1 on page 89. Section 9.1 investigates the sensitivity of the objective function value of the FGAP models to changes in the declared capacity $C_{p,q}$. Section 9.2 examines the influence of the maximum waiting time threshold W^T on the objective function value of the FGAP models. Section 9.3 outlines the effect of changing the compression factor on the computation time of the FGAP models. All numbers presented in this chapter are based on the mean of $n = 5$ runs.

9.1 Declared Capacity

Figure 9.1a on page 108 presents the Pareto fronts of the objective function values of the FGAP models as a function of the declared capacity scaling factor $\alpha \in [0.7, 1.3]$, such that $C_{p,q}^{\text{scaled}} = \alpha \cdot C_{p,q}$. A close up of the Pareto fronts of the A-FGAP model and WT-FGAP model is given in figure 9.1b on page 108. The solution to the A-FGAP model does not depend on the scaled declared capacity $C_{p,q}^{\text{scaled}}$, resulting in a horizontal Pareto front, with a value equal to the value indicated in table 8.2 on page 101. The objective function value of the WT-FGAP model decreases as the scaling factor α increases. However, these values deviate no more than 1% from the objective function value of the A-FGAP model. For scaling factors $\alpha < 0.95$, no feasible solutions are found for the DC-FGAP model. For scaling factors $\alpha \geq 0.95$, the objective function value of the DC-FGAP model decreases as the scaling factor α increases.

9.2 Waiting Time Threshold

Figure 9.2 shows the Pareto fronts of objective function values as a function of the maximum waiting time threshold W^T. The value of the threshold W^T. is varied between 1 minute and 50 minutes, with a step length of 5 minutes. The Pareto front of the A-FGAP model and DC-FGAP model are horizontal lines with values matching the values indicated in table 8.2 on page 101, because their objective function values do not depend on the value of W^T. The objective function value of the WT-FGAP model decreases as the waiting time threshold W^T increases in value. If $W^T \to 0$, values of $b_{p,q,t}$ in constraint (5.4.18) approach $C_{p,q}$. If $W^T \to \inf$, values of $b_{p,q,t}$ are equal to infinity. Therefore, the objective function value of the WT-FGAP model is bounded; the lower bound ($W^T \to \inf$) and the upper bound ($W^T \to 0$) are the objective function values of the A-FGAP

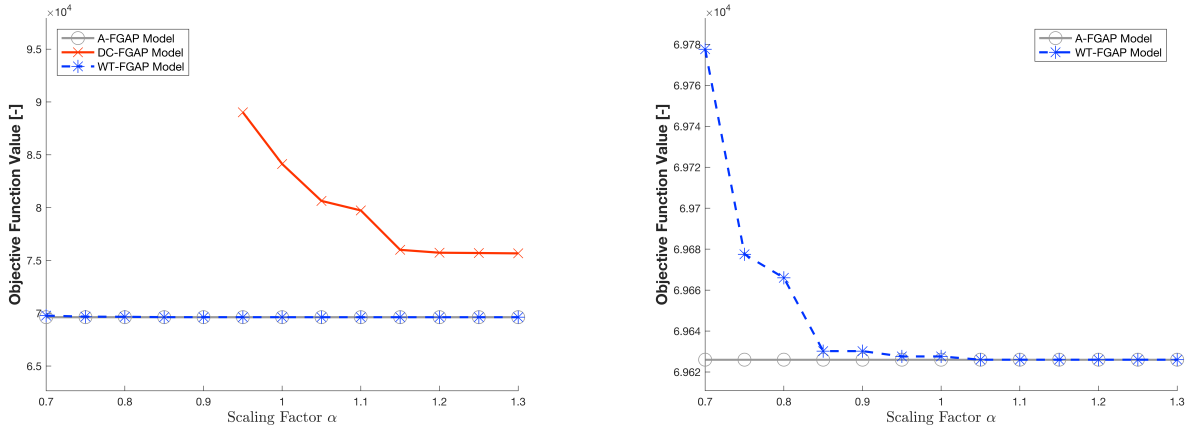

(a) Pareto front for scaling factor α.

(b) Close up of Pareto front for scaling factor α.

Figure 9.1: Pareto front of the objective function value of the FGAP models as a function of α. The solution to the A-FGAP model does not depend on the declared capacity $C_{p,q}$. Results are obtained using the flight schedule of July 4, 2018, a compression factor of 5, $r = 5\%$, $\delta_t = 5$min, $MI = 10$, $W^T = 25$min, and based on $n = 5$ runs.

model and DC-FGAP model, respectively.

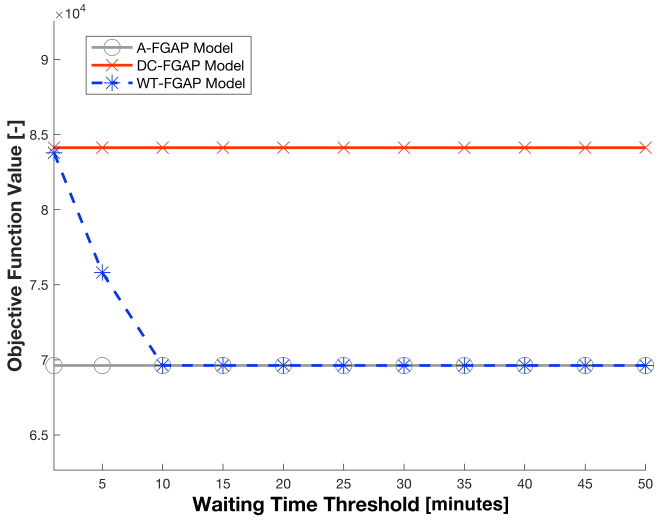

Figure 9.2: Pareto front of the objective function value of the FGAP models as a function of maximum waiting time threshold W^T. Results are obtained using the flight schedule of July 4, 2018, a compression factor of 5, $r = 5\%$, $\delta_t = 5$min, $MI = 10$, and the declared capacity $C_{p,q}$, and based on $n = 5$ runs.

9.3 Computation time

Table 9.1 indicates the build time and solving of the FGAP models as a function of the compression factor, based on the average of $n = 5$ runs. The A-FGAP, DC-FGAP and WT-FGAP models have the same mathematical model and, thus, their build times are equal. Build times increase exponentially as the compression factor decreases. Solving times vary between the FGAP models considered. Solving times increase

exponentially as the compression factor decreases.

Table 9.1: Overview of the average build time and solving time of the A-FGAP, DC-FGAP and WT-FGAP models, based on $n = 5$ runs.

	Compression Factor [-]					
	5	6	7	8	9	10
Build Time [s]						
· *A/DC/WT-FGAP*	1725.7	790.1	440.3	260.7	187.9	103.2
Solving Times [s]						
· *A-FGAP*	21.5	8.8	6.6	4.1	3.8	2.7
· *DC-FGAP*	37.5	17.6	9.5	6.4	5.2	4.0
· *WT-FGAP*	211.9	37.3	26.1	23.1	20.2	18.4

Chapter 10

Verification & Validation

This chapter presents the verification and validation of the FGAP models. Unless stated otherwise, the results in this chapter are obtained using the parameter values indicated in table 8.1 on page 89. Section 10.1 describes the verification of the FGAP models. The validation of the FGAP models is described in section 10.2.

10.1 Verification

This section provides the verification results of the A-FGAP, DC-FGAP, and WT-FGAP model. Subsection 10.1.1 describes the verification of the airside characteristics of the FGAP models. Subsection 10.1.2 compares the airside characteristics of the models presented in this report to the results presented by Schaijk & Visser (2017). Subsection 10.1.3 elaborates on the verification of the landside characteristics of the FGAP models.

10.1.1 Verification Airside Characteristics

The airside characteristics used to verify the FGAP models include size, customs and type requirements. These characteristics are included in the A-FGAP, DC-FGAP and WT-FGAP models. Analytical verifiable case studies are presented to verify the implementation of these characteristics in the FGAP models. These cases include one flight segment, and a fixed number of gates. Within these gates, one gate corresponds to the preferred assignment of the flight segment. By showing that the A-FGAP model produces the expected results, the model can be assumed to correctly incorporate the airside characteristics included in the verification study. The results presented in this subsection pertain to the A-FGAP, DC-FGAP and WT-FGAP models.

10.1.1.1 Size Assignment

The size of a flight segment is based on the information derived from the flight schedule. Sizes for commercial airliners range from 3 till 9, where 3 and 9 correspond to a smaller single-aisle aircraft (Fokker 100) and the largest passenger jets (Airbus A380-800). The size handle capacity of gates is described in more detail in subsection 7.1.3 on page 83 and varies between 3 and 9. The cost of assigning a flight segment to a gate from a size perspective is expressed in equation (5.4.7) on page 68. This equation states that this cost is a function of the difference between the size handle capacity of the gate and the size of a flight segment, given that the size handle capacity is equal or larger than the size of the flight. If the size of the flight segment is larger than the size handle capacity of the gate, the assignment in infeasible.

In the case study, one functional flight segment is considered. This flight segment, performed by an aircraft with tail number PHEXC, has a size of 3. Gates B20, C15 and D64 are included with a corresponding maximum size handle capacity of 3, 4 and 6, respectively. All other characteristics of the gates are the same, and therefore do not influence the decision of the model to which gate the functional flight segment is assigned. As shown by figure 10.1 on page 112, the model correctly assigns the functional flight segment to gate B20, given that this incurs the least amount of cost from a size perspective. In other words, assigning the functional flight segment to gates C15 or D64 yields a higher cost related to size, and therefore is suboptimal.

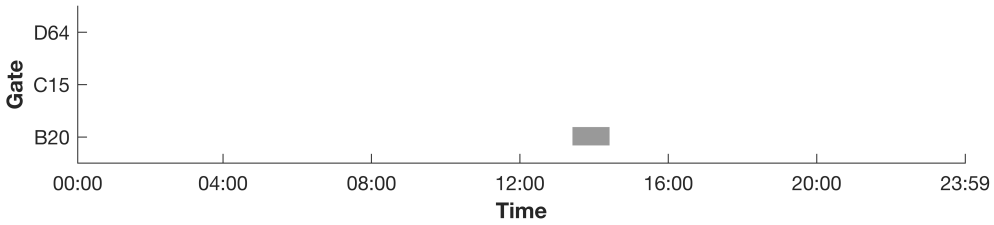

Figure 10.1: Verification of airside size characteristic FGAP models. One functional flight segment is considered. This flight segment, performed by an aircraft with tail number PHEXC, has a size of 3. Gates B20, C15 and D64 are included with a corresponding maximum size handle capacity of 3, 4 and 6, respectively. The model correctly assigns the functional flight segment to gate B20, given that this minimises the cost of assigning this flight segment to a gate with respect to the size criterion.

10.1.1.2 Customs Assignment

The customs requirement of a flight segment is based on the information derived from the flight schedule. Three different types of customs requirements are distinguished, namely Schengen, Non-Schengen European Union and Intercontinental customs. In order to quantify these types, these are given a custom level of 1, 2 and 3, respectively. The customs level of gates is derived from an existing data set, described in more detail in subsection 7.1.3 on page 83. The cost of assigning a flight segment to a gate from a customs perspective is expressed in equation (5.4.6) on page 68. This equation states that this cost is a function of the difference between the customs level of the gate and the customs requirement of the flight. Herein, it is assumed that gates with a lower customs level than the flight segment cannot serve this flight.

In the case study, one functional flight segment is considered. This flight segment, performed by an aircraft with tail number YUAPC, has an Intercontinental customs level. Gates B31 and D41 are included with a corresponding customs level of Schengen and Intercontinental, respectively. All other characteristics of the gates are the same, and therefore do not influence the decision of the model to which gate the functional flight segment is assigned. As shown by figure 10.2 on page 113, the model correctly assigns the functional flight segment to gate D41. The functional flight segment cannot be assigned to gate B31 since this gate has a Schengen customs level.

10.1.1.3 Type Assignment

The type requirement of a flight segment is based on the flight splitting options, which are discussed in more detail in subsection 5.1 on page 57. The cost of assigning a flight segment to a gate from a type perspective is expressed in table 5.2 on page 68. Towing movements can only be assigned to towing trucks. Parking segments can be assigned to platforms, aprons, and, at a very high cost to piers. Functional flight segments

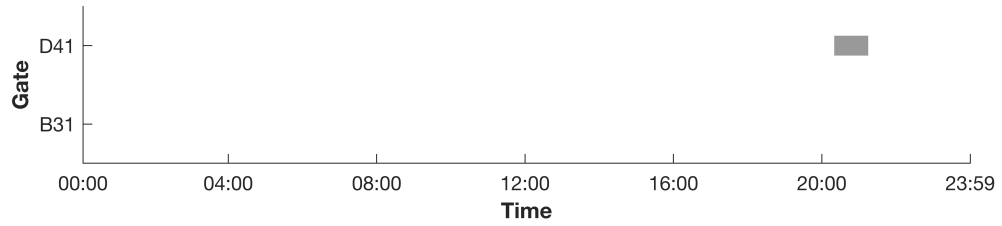

Figure 10.2: Verification of airside size characteristic FGAP models. One functional flight segment is considered. This flight segment, performed by an aircraft with tail number YUAPC, has an Intercontinental customs level. Gates B31 and D41 are included with a corresponding customs level of Schengen and Intercontinental, respectively. The model correctly assigns the functional flight segment to gate D41, given that the functional flight segment cannot be assigned to gate B31.

can be assigned to piers, and at a higher cost to platforms and aprons. This ensures that the gate assignment plan derived using one of the proposed FGAP models adheres to airport operators' assignment preferences.

In this case study, one functional flight segment is considered, performed by an aircraft with tail number PHHXJ. A number of assignment options are included, namely gate D41, towing truck THW and platform A31. The size characteristics vary among these assignment options. However, in this assignment the type characteristic is driving because of the larger magnitude of cost relative to the size characteristic. Therefore the influence of size can be neglected in this analysis. As shown by figure 10.3 on page 113, the model correctly assigns the functional flight segment to gate D41, given that this incurs the least amount of cost from an type assignment perspective. The functional flight segment cannot be assigned to towing truck THW and assigning the flight segment to platform A31 would incur a high cost.

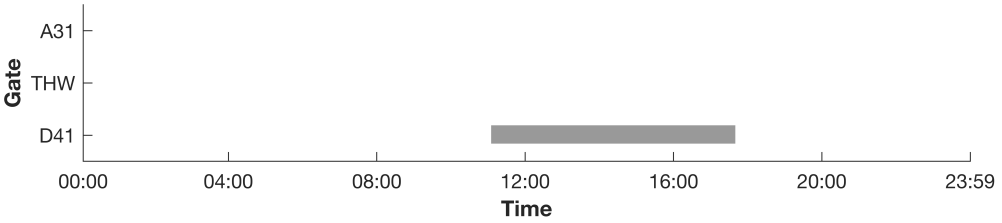

Figure 10.3: Verification of airside type characteristic FGAP models. One functional flight segment is considered, performed by an aircraft with tail number PHHXJ. A number of assignment options are included, namely gate D41, towing truck THW and platform A31. The model correctly assigns the functional flight segment to gate D41, given that this incurs the least amount of cost from an type assignment perspective.

10.1.2 Comparison Schaijk & Visser (2017)

In their study, Schaijk & Visser (2017) examine the applicability of their robust FGAP model with a case study using the flight schedule of AMS at April 11, 2013. Flights with an overnight stay are not included in this flight schedule. A total of 22 piers, mostly in the B, C and D-pier, are considered, and platforms, aprons and towing trucks are omitted from their analysis. In addition, their model does implement flight splitting options. They provide results for a maximum overlap probability $r = 7, 10, 15\%$.

The models introduced in this paper implement flight splitting options. In addition, the flight schedule at AMS on July 4, 2018, is used and flights with an overnight stay are included. A representative selection of piers, platforms, aprons and towing trucks is included in the analysis, based on a compression factor of 5.

Results in this report are obtained using a maximum overlap probability of $r = 5\%$.

The differences in the set-up between the case studies of Schaijk & Visser (2017) and this report block any direct comparison of the results. However, gates that are considered in both studies are shown to have similar occupation patterns, i.e. up to 7 flights/flight segments with a short turn-around time are assigned to a gates in the B, C and D-pier between 07:00 and 21:00. Therefore, it can be assumed that the results presented in this paper are in line with the results presented by Schaijk & Visser (2017).

10.1.3 Verification Landside Characteristics

This subsection presents the verification of the landside characteristics of the FGAP models. Analytical verifiable case studies are presented to verify the implementation of these characteristics in the FGAP models. By showing that the DC-FGAP model produces the expected results, the model can be assumed to correctly incorporate the landside characteristics included in the verification study. The results presented in this subsection pertain to the A-FGAP, DC-FGAP and WT-FGAP models.

10.1.3.1 Passenger Demand

The gate-terminal topology is outlined in section 4.3 on page 52 and indicates the preferred assignment of passenger streams to a terminal as a function of the gate. In this case study, it assumed that landside terminal capacity is unbounded. In other words, all parameter values $b_{p,q,t}$ are set to infinity. The case study encompasses a functional flight segment that is assigned to gate B20. In accordance to the gate-terminal topology, the departing, transfer and arriving passenger streams should be handled by Terminal 1. Figure 10.4 on page 115 shows that this indeed the case for facilities (A1), (T1), (D1) and (D2). Therefore, the passenger demand modelling feature of the A-FGAP, DC-FGAP, WT-FGAP models is verified.

10.1.3.2 Terminal Reallocation Options

The binary decision variables $z_{i,j,q}$ indicate whether flight segment $i \in N_a \cup N_d$ is assigned to gate $j \in G_i^1$ and its departing passenger streams are handled by terminal $q \in T$. To verify the implementation of this feature in the FGAP models, the case study presented in subsection 10.1.3.1 is extended. The upper bounds of passenger demand per time step, denoted by $b_{p,q,t}$, are set equal to 0 for facilities D1 and D2 in Terminal 1 and all time steps $t \in K$. As such, departing passenger streams should be redirected to a different terminal given Terminal 1 is not able to handle these streams. Figure 10.5 shows that this indeed happens. Arriving and transfer passenger streams are handled by facilities (A1) and (T1) in Terminal 1, respectively. However, departing passenger streams are handled by facilities (D1) and (D2) in Terminal 2. Though this comes at an increased cost, this solution is feasible and in this case, optimal.

10.2 Validation

This section describes the validation of the A-FGAP, DC-FGAP and WT-FGAP models, which is based on estimates of the annual passenger counts of these models. To estimate these numbers, the number of passengers in the arriving, departing and transfer passenger streams are summed. Applying corrections pertaining to transfer passenger streams, the compression factor and seasonality, the number of annual passengers at AMS can be estimated. These corrections are based on the fact that transfer passengers make both an arrival and

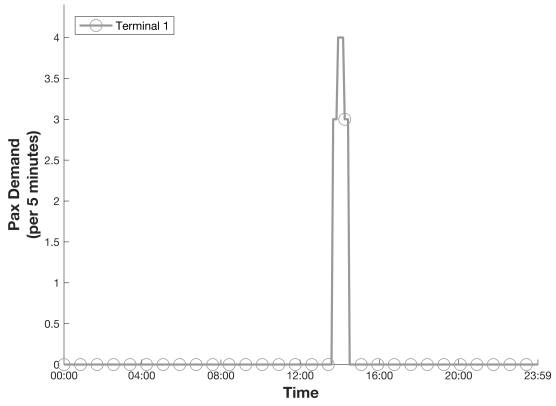

(a) Number of passengers passing through arrival immigration (A1) in Terminal 1 per time step t.

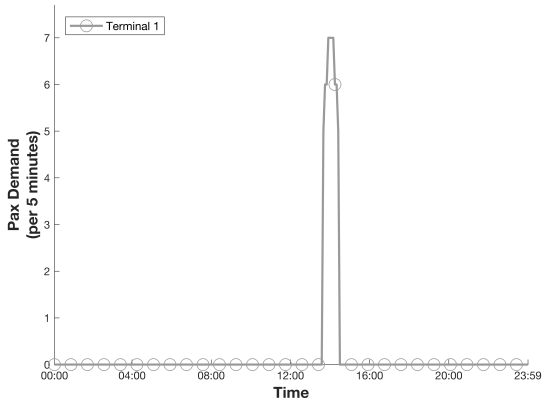

(b) Number of transfer passengers passing through transfer security (T1) in Terminal 1 per time step t.

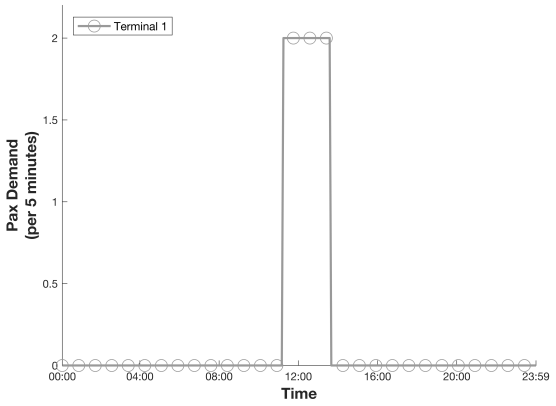

(c) Number of departing passengers using check-in facilities (D1) in Terminal 1 per time step t.

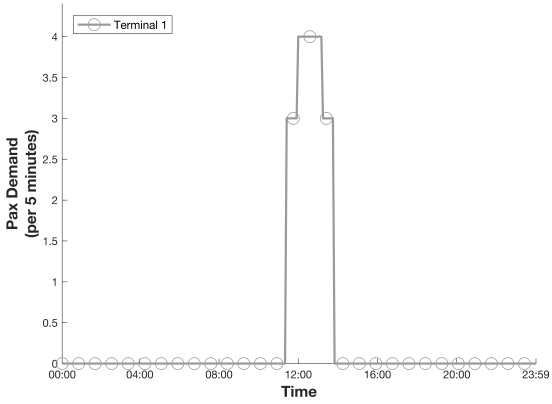

(d) Number of departing passengers passing through security/border control (D2) in Terminal 1 per time step t.

Figure 10.4: Verification of passenger demand modelling in FGAP models. A functional flight segment is assigned to B20. As such, all passenger streams are handled by Terminal 1 in accordance with the gate-terminal topology presented in subsection 4.3 on page 52.

a departure, a compression factor of 5 is used and the total number of passengers in July at AMS accounted for 9.53% of the annual number of passengers in 2018 (*Traffic Review 2018*, 2019). The equation to estimate the annual number of passengers at AMS AP is indicated by equation (10.2.1),

$$AP = \left(\sum_{q \in T} \sum_{t \in K} (y_{A2,q,t} + 2 \cdot y_{T1,q,t} + y_{D2,q,t}) \right) \cdot 31 \cdot \frac{1}{0.0953} \cdot 5. \tag{10.2.1}$$

Using results from the A-FGAP, DC-FGAP and WT-FGAP models, an annual number of passengers of 69.1 million is calculated for all of the models. According to *Traffic Review 2018* (2019), 71 million passengers were handled by AMS in 2018.

Two reasons are identified why the estimate of annual passengers at AMS in 2018 is below the value given by *Traffic Review 2018* (2019). During the construction of the flight lists, a process described in subsection

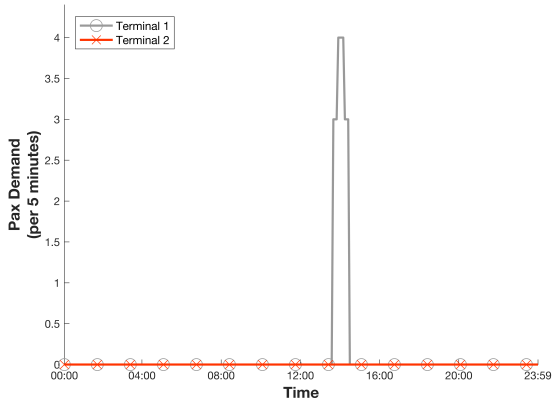

(a) Number of passengers passing through arrival immigration (A1) in Terminal 1 per time step t.

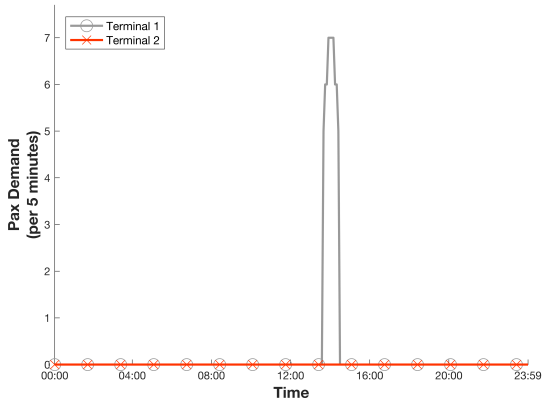

(b) Number of transfer passengers passing through transfer security (T1) in Terminal 1 per time step t.

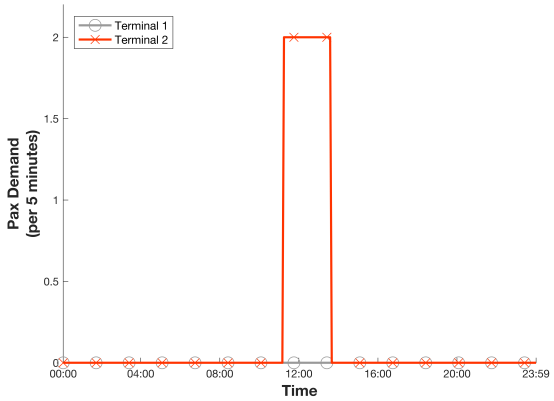

(c) Number of departing passengers using check-in facilities (D1) in Terminal 1 and 2 per time step t.

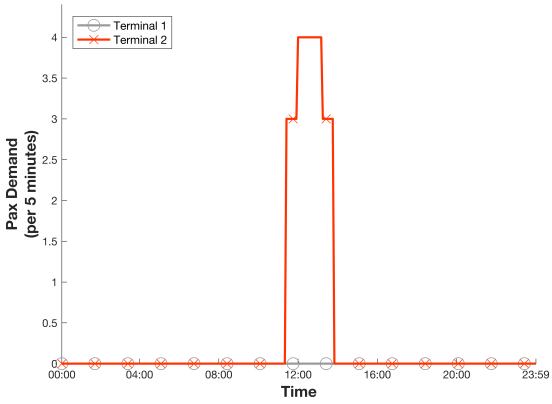

(d) Number of departing passengers passing through security/border control (D2) in Terminal 1 and 2 per time step t.

Figure 10.5: Verification of terminal reallocation modelling in the FGAP models. The upper bounds of passenger demand per time step, denoted by $b_{p,q,t}$, are set equal to 0 for facilities (D1) and (D2) in Terminal 1 and all time steps $t \in K$. As such, departing passenger streams are handled by facilities (D1) and (D2) in Terminal 2.

A.7.1, incomplete data snippets are filtered out. As a consequence, certain flight data cannot be processed, causing certain flights not to be included in the arriving or departing flight lists. In addition, subsection A.7.2.1 explained that in order for the daily flight schedules to be constructed, lists of alternating arrivals and departures per aircraft registration are created. In order to ensure these lists are indeed alternating, certain arrivals or departures are removed from the data sample. As indicated in subsection A.7.2.1 on page 140, this resulted in the removal of the 0.64% of the flight movements.

Chapter 11

Conclusion

The flight-to-gate assignment problem aims to find an optimal assignment of flights, or rather the aircraft serving these flights, to the available aircraft stands. This problem is known as the Flight-to-Gate Assignment Problem (FGAP). Existing models in literature do not consider airside and landside processes simultaneously. Research on improving the robustness of the solution to the FGAP is still ongoing. This research aims to include both airside and landside constraints in model to solve the FGAP, using a robust optimisation technique. The objective of this research therefore is to develop a FGAP model with landside and airside constraints in addition to implementing an predefined level of robustness.

This report describes a FGAP model with airside and landside constraints where overlap probability is used as a proxy for robustness. Three distinct specifications of the FGAP model with airside and landside constraints are proposed: The A-FGAP model has active airside constraints and inactive landside constraints. The DC-FGAP model has active airside and landside constraints and enforces upper bounds on passenger demand per time step at landside passenger facilities. The WT-FGAP model has active airside and landside constraints and ensures a gate assignment plan is constructed such that the expected maximum waiting for passengers does not exceed a predefined threshold. The A-FGAP model creates a gate assignment at the lowest cost, but does not consider passenger experience. The DC-FGAP model creates a gate assignment at an increased cost compared to the WT-FGAP model, but does offer a superior passenger experience since waiting times are non-existent.

A case study of Amsterdam Airport Schiphol using the flight schedule of July 4, 2018 as support for the flight-to-gate assignment problem is presented. The A-FGAP model provides the most cost-efficient approach as compared to the DC-FGAP and WT-FGAP models, but at the expense of passenger comfort. The DC-FGAP model ensures a high level of passenger comfort by ensuring waiting times of less than one minute airport passengers. However, this comes at an increased cost for the airport operator due to flight segment reallocation. Finally, the WT-FGAP model provides an intermediate approach, where the expected maximum waiting time of passengers is ensured to be below user-defined threshold with a 95% probability. The DC-FGAP model creates a gate assignment at an increased cost compared to the WT-FGAP model, but does offer a superior passenger experience since waiting times are non-existent.

Chapter 12

Recommendations

This chapter presents the recommendations for further research in the field of robust FGAP models implementing airside and landside constraints. Despite that the DC-FGAP and WT-FGAP models meet the objectives set in chapter 2 on page 37, several shortcomings can be identified. These shortcomings are grouped in two categories: data collection and modelling approach, which are discussed in sections 12.1 and 12.2, respectively.

12.1 Data Collection

Data is gathered through a variety of data sources, including the Schiphol Flight API and static databases. This approachs resolves some of the key shortcomings of the study by Schaijk & Visser (2017). However, the addition of more, rich data can improve the model quality by allowing for flight-specific modelling techniques.

- **Flight presence probabilities:** The flight presence probability curves for each flight $l \in F$ are constructed using flight presence probability curves from an airline option a and region r (see equation (5.2.5)). Though this modelling approach allows for the modelling of different characteristics of flights, this concept could be extended further. Specific flight presence probabilities can be created if a large enough number of data points for that flight is collected. This can be done by gathering data from a period which spans multiple months, rather than a single month.

- **Time parameters:** The parameters T_1, T_2, T_3 and T_5 in table 5.1 are assumed to be constant over all flights. Passenger profiles vary between flights, and therefore the values of these parameters can vary significantly between different flights.

- **Declared capacity AMS:** A key input to the DC-FGAP and WT-FGAP models are the estimates of declared capacity at AMS indicated by table 4.5 on page 55. Public data from LHR and an expert opinion are used to create these estimates. Unfortunately, none of these sources provide a complete estimate of the declared capacity for each facility p in terminal q. As such, proprietary data of AMS is needed to validate the numbers in table 4.5.

12.2 Modelling Approach

This study extends the study by Schaijk & Visser (2017) and addresses key methodological issues that stem from their approach. However, several shortcomings pertaining to the methodology presented in this report are identified.

- **Flight presence probabilities:** A flight presence probability curve is a continuous curve which converges to zero for extreme deviations of the STA and STD. However, when flight splitting is introduced, presence probability curves from individual flight segments are no longer continuous. This is illustrated in figures 5.3 and 5.4. As a consequence, flight segments with non-continuous flight presence probability curves can be assigned to the same gate with little to no buffer time in between. Further modelling improvements can be made by making the flight presence probability curves continuous for individual flight segments. This increases the robustness of the solution derived using the FGAP model models described in chapter 5.
- **Flight-specific modelling:** Together with flight-specific input, the models can be adapted such flight-specific parameters inputs are supported. This would entail that key characteristics are derived from the information in the flight schedule and parameter inputs are selected accordingly.
- **Maximum waiting times:** One of the key components of the WT-FGAP model is the approximation of maximum waiting time, as described by Solak et al. (2006). Through a parabolic approximation, the expected maximum waiting time is computed for a peak period. However, the approximations can be replaced by analytical methods to provide a more accurate measure of expected maximum waiting time.
- **Time-variant declared capacity:** In the DC-FGAP model, the value of the model parameters $b_{p,q,t}$ is assumed to be invariant with time and set using the declared capacity indicated in table 4.5 on page 55. In reality, declared capacity can vary over time because of staffing restrictions, economic incentives or maintenance downtime. It is therefore advisable to model the parameters $b_{p,q,t}$ in the DC-FGAP model in a time-variant manner to best reflect the operating conditions and constraints at AMS.

References

Amsterdam airport terminal. (2018, October). Retrieved October 28, 2018, from https://www.amsterdam-airport.com/terminal.php

Andreatta, G., Capanna, L., Giovanni, L. D., Righi, L., & Monaci, M. (2014). Efficiency and robustness in a support platform for intelligent airport ground handling. *Journal of Intelligent Transportation Systems*, *18*, 121-130.

Bazaraa, M., Sherali, H., & Shetty, C. (2006). *Nonlinear programming: Theory and algorithms* (3rd ed.). Hoboken, NJ: Wiley-Interscience.

Birgin, E., Bueno, L., & Martinez, J. (2016). Sequential equality-constrained optimization for nonlinear programming. *Computational Optimization and Applications*, *65*(3), 699-721.

Chun, H., & Mak, R. (1999). Intelligent resource simulation for an airport check-in counter allocation system. *Transactions on Systems, Man and Cybernetics-Part: Applications and Reviews*, *29*(3), 325-335.

Diepen, G., van den Akker, J., Hoogeveen, J., & Smeltink, J. (2012). Finding a robust assignment of flights to gates at amsterdam airport schiphol. *Journal of Scheduling*, *15*, 703-715.

Ding, H., Lim, A., Rodrigues, B., & Zhu, Y. (2004). New heuristics for the over-constrained airport gate assignment problem. *Computers and Operations Research*, *32*, 1867-1868.

Dong, L., Yu, B., & Zhao, G. (2016). A spline smoothing homotopy method for nonconvex nonlinear programming. *Optimization*, *65*(4), 729-749.

Dorndorf, U., Drexl, A., Nikulin, Y., & Pesch, E. (2007). Flight gate scheduling: State-of-the-art and recent developments. *Omega*, *35*, 326-334.

Heathrow facts and figures. (2018, January). Retrieved November 6, 2018, from https://www.heathrow.com/company/company-news-and-information/company-information/facts-and-figures

Hillier, F., & Lieberman, G. (2009). *Introduction to operations research* (9th ed.). McGraw-Hill.

Huang, Q., Zhu, Z., & Wang, X. (2013). A predictor-corrector algorithm combined conjugate gradient with homotopy interior point for general nonlinear programming. *Applied Mathematics and Computation*, *219*(9), 4379-4386.

Kim, S., Feron, E., & Clarke, J. (2013). Airport gate scheduling for passengers, aircraft and operation. In *Europe air traffic management research and development seminar.*

Kusumaningtyas, I., & Lodewijks, G. (2013). On the application of accelerating moving walkways to support passenger processes in amsterdam airport schiphol. *Transportation Planning and Technology*, *36*(7), 617-635.

Li, Y., Gao, X., Xu, Z., & Zhou, Z. (2018). Network-based queuing model for simulating passenger throughput at an airport security checkpoint. *Journal of Transport Management*, *66*, 13-24.

Manataki, I., & Zografos, K. (2009). A generic systems dynamics based tool for airport terminal performance analysis. *Transportation Research Part C*, *17*, 428-443.

Narciso, M., & Piera, M. (2015). Robust gate assignment procedures from an airport management perspective. *Omega*, *50*, 82-95.

Odoni, A. (2017, 03). *Airport demand management.* Lecture Notes AE4446: Delft University of Technology.

Rhee, C. (1992, July). A linear programming solution to gate assignment. *Report LR-698*.

Schaijk, O. (2013). *Finding robust solutions to the flight to gate assignment problem using flight presence probabilities* (Unpublished master's thesis). Delft University of Technology.

Schaijk, O., & Visser, H. (2017). Robust flight-to-gate assignment using flight presence probabilities. *Transportation Planning and Technology*, *40*(8), 928-945.

Seker, M., & Noyan, N. (2012). Stochastic optimization models for the airport gate assignment problem. *Transport Research Part E: Logistics and Tranportation Research*, *48*(2), 438-559.

Solak, S., Clarke, J., & Johnson, E. (2006). *Airport terminal capacity planning using delay time approximations and multistage stochastic programming.* (Georgia Institute of Technology)

Traffic review 2017. (2018). Digital. Evert van de Beekstraat 202, 1118 CP Schiphol, Netherlands.

Traffic review 2018. (2019). Digital. Evert van de Beekstraat 202, 1118 CP Schiphol, Netherlands.

van Dijk, N., & van der Sluis, E. (2006). Check-in computation and optimization by simulation and ip in combination. *European Journal of Operational Research*, *171*, 1152-1168.

Verschuren, P., & Doorewaard, J. (2010). *Designing a research project* (2nd ed.). Eleven International Publishing.

Xu, J., & Bailey, G. (2001). The airport gate assignment problem: mathematical model and a tabu search algorithm. *Proceedings of the 34th Annual Hawaii International Conference on Systems Sciences, IEEE*, 3032.

Yan, S., & Chang, C. (1997). A network model for gate assignment. *Journal of Advanced Transportationq*, *32*(2), 176-189.

Yan, S., & Huo, C. (2001). Optimization of multiple objective gate assignments. *Transport Research Part A*, *35*, 413-432.

Yu, C., Zhang, D., & Lau, H. (2016). Mip-based heuristics for solving robust gate assignment problems. *Computers and Industrial Engineering*, *93*, 171-191.

Yu, C., Zhang, D., & Lau, H. (2017). An adaptive large neighborhood search heuristic for solving a robust gate assignment problem. *Expert Systems with Applications*, *84*, 143-154.

Appendix A

Supporting Theory & Analysis

A.1 Overlap Probability Example

Table A.1 indicates flight data for four flight segments. All flight segments in this section are derived from splitting flights without an overnight stay using option 1 in figure 5.3 on page 60. Flight segments X1 and X2 have the same arrival and departure time, but belong to different airline option a and origin/destination region option r. The same holds for flight segments Y1 and Y2. The names of the airlines and regions have been encoded using integers for confidentiality reasons.

Table A.1: Example of overlap probability flight segments. Flight segments denoted by either X or Y have the same arrival and departure time, but correspond to different airline options a and arrival/departure region options r.

	Time		Airline		Region	
	In	Out	In	Out	In	Out
Flight segment X1	12:00	14:00	1	1	3	3
Flight segment Y1	14:20	16:00	8	8	4	4
Flight segment X2	12:00	14:00	2	2	4	4
Flight segment Y2	14:20	16:00	5	5	7	7

Figure A.1a on page 126 shows the presence probabilities of flight segment X1 and Y1 and their overlap probability. In a similar vein, figure A.1b on page 126 shows the presence probabilities of flight segments X2 and Y2 and their overlap probability. Despite that the arrival and departure time for the X/Y flight segments are the same, stark differences in the presence probabilities can be seen. Flight segments X2 and Y2 have 'wider' flight presence probability, resulting in a significantly higher maximum overlap probability as compared to flight segments X1 and Y1. This shows that even though flight arrival and departure times are similar, flight characteristics have a large impact on the overlap probability of two flight segments.

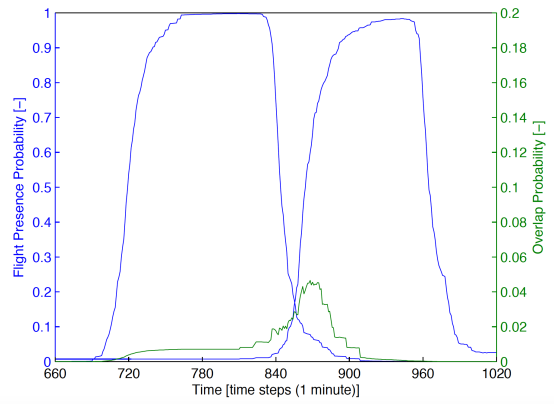

(a) Presence probabilities and overlap probability of flight segments X1 and Y1

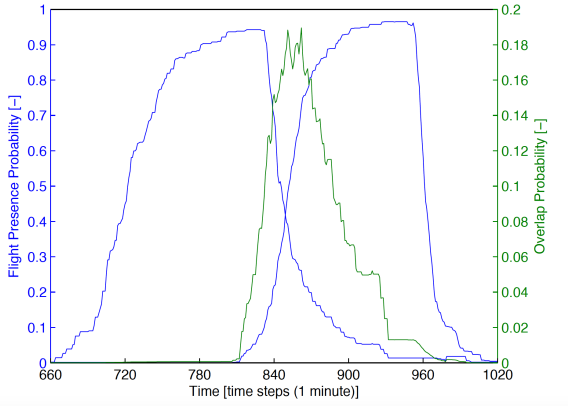

(b) Presence probabilities and overlap probability of flight segments X2 and Y2.

Figure A.1: The presence probabilities and the overlap probability of the flight segments X1 and Y1, and X2 and Y2. Flight segments X1 and X2 have the same arrival and departure time, and the same holds for flight segments Y1 and Y2. Given that these flights have different characteristics, the presence probabilities of these flight segments are different between both examples, resulting in different maximum overlap probabilities.

A.2 Presence Probability Scaling Function

The following section will elaborate on the derivation of the scaling $f(p_{it}, r)$ and provide a proof of its implementation. Subsection A.2.1 shows the derivation of the scaling function $f(p_{it}, r)$. Subsection A.2.2 provides a proof of implementation.

A.2.1 Derivation

Let r denote the maximum allowed overlap probability and p_{it} denotes the flight presence probability (at the apron) of flight i in time slot t. The maximum allowed presence probability of a flight assigned to the same gate in time slot t , denoted by $p_{i,t}^{\max}$, can be computed following Schaijk (2013):

$$p_{i,t}^{\max} = \frac{r}{p_{it}}. \tag{A.2.1}$$

To incorporate the maximum overlap probability in the FGAP model, the presence probabilities of flight segment i at time step t, $p_{i,t}$, is scaled accordingly. Let us define the following expressions:

$$p_{i,t}^{\text{scaled}} = f \cdot p_{i,t}, \tag{A.2.2}$$

$$p_{i,t}^{\text{max,scaled}} = f \cdot p_{i,t}^{\max}, \tag{A.2.3}$$

where f represents the to-be developed scaling function. This scaling function should be designed such that the following condition is met:

$$p_{i,t}^{\text{scaled}} + p_{i,t}^{\text{max,scaled}} = 1. \tag{A.2.4}$$

Substituting equations A.1.2 and A.1.3 in equation A.2.4 yields the following expression:

$$f \cdot p_{i,t} + f \cdot p_{i,t}^{\max} = 1. \tag{A.2.5}$$

As a final step, substituting equation A.2.1 in this expression and solving for f yields the following expression:

$$f = f(p_{i,t}, r) = \frac{p_{i,t}}{r + p_{i,t}^2} \tag{A.2.6}$$

A.2.2 Proof of Implementation

This subsection aims to proof that if the presence probabilities of two flights i_x and i_y at timestep t are equal to r when multiplied, the constraint $\sum_{i \in N} f(p_{it}, r) p_{it} x_{ijt} \leq 1$ holds. Let this condition be described by the following expression:

$$p_{i_x,t} p_{i_y,t} = r \Leftrightarrow p_{i_x,t} = \frac{r}{p_{i_y,t}}. \tag{A.2.7}$$

The proof that this equation holds, assuming that all $x_{i,j,t}$ is 0 for all $i \notin \{i_x, i_y\}$, is indicated below:

$$\sum_{i \in N} f(p_{i,t}, r) p_{i,t} x_{i,j,t} = \frac{p_{i_x,t}}{r + p_{i_x,t}^2} p_{i_x,t} \cdot 1 + \frac{p_{i_y,t}}{r + p_{i_y,t}^2} p_{i_y,t} \cdot 1 \tag{A.2.8}$$

$$= \frac{p_{i_x,t}}{\frac{r}{p_{i_x,t}} + p_{i_x,t}} + \frac{p_{i_y,t}}{\frac{r}{p_{i_y,t}} + p_{i_y,t}} \tag{A.2.9}$$

$$= \frac{p_{i_x,t}}{\frac{r}{p_{i_x,t}} + p_{i_x,t}} + \frac{\frac{r}{p_{i_y,t}}}{\frac{r}{\frac{r}{p_{i_y,t}}} + \frac{r}{p_{i_y,t}}} \tag{A.2.10}$$

$$= \frac{p_{i_x,t}}{\frac{r}{p_{i_x,t}} + p_{i_x,t}} + \frac{\frac{r}{p_{i_y,t}}}{p_{i_x,t} + \frac{r}{p_{i_x,t}}} \tag{A.2.11}$$

$$= \frac{\frac{r}{p_{i_x,t}} + p_{i_x,t}}{\frac{r}{p_{i_x,t}} + p_{i_x,t}} \tag{A.2.12}$$

$$= 1. \tag{A.2.13}$$

A.3 Modelling Techniques

The FGAP is most commonly modelled using (non-)linear programming formulations. This chapter provides the reader with a brief overview of the basics of the latter techniques, and shows its potential to model the FGAP. The first section will elaborate on the basics of linear programming. Subsequent sections will elaborate on integer linear programming and integer non-linear programming. For a detailed reading on this matter, the reader is referred to Hillier & Lieberman (2009).

A.3.1 Basics of Linear Programming

Linear programming is a mathematical model that can be used to model a problem that is comprised of a linear objective and linear constraints; a function of decision variables. Certain symbols are commonly used to denote the various components of a linear programming model. These symbols are listed below, along with their interpretation for the general problem of allocating resources to activities (Hillier & Lieberman, 2009).

Z: value of overall measure of performance;
x_j: level of activity j (for $j = 1, 2, ..., n$);
c_j: increase in Z that would result from each unit increase in level of activity j;
b_i: amount of resource i that is available for allocation to activities (for $i = 1, 2, ..., m$);
a_{ij}: amount of resource i consumed by each unit of activity j.

The model describes the problem of making decisions about the levels of activities. These are denoted by the decision variables (x_j, for $j = 1, 2, ..., n$). The collections of input constants c_j, b_i, a_{ij} are denoted as the problem parameters. All symbols can be rewritten in matrix form, by setting:

$$\begin{aligned} \mathbf{x} &= (x_1, x_2, ..., x_n)^T; \\ \mathbf{c} &= (c_1, c_2, ..., c_n)^T; \\ \mathbf{b} &= (b_1, b_2, ..., b_m)^T; \end{aligned} \qquad A = \begin{bmatrix} a_{11} & a_{12} & \dots & a_{1n} \\ a_{21} & a_{22} & \dots & a_{2n} \\ \vdots & \vdots & \ddots & \vdots \\ a_{m1} & a_{m2} & \dots & a_{mn} \end{bmatrix}$$

In common terminology, the standard form of a linear programming model consists of an objective function, set of constraints and non-negativity constraints. The function being minimized, $Z = \mathbf{c}^T\mathbf{x}$, is called the objective function (equation A.3.1a). Restrictions on the decision variables are imposed using constraints. In general, two types of constraints are considered: equality constraints (equation A.3.1b) and non-equality constraints (equation A.3.1c). Equality constraints are of the form $A_{eq}\mathbf{x} = \mathbf{b}_{eq}$, whereas inequality constraints assume the form of $A_{ineq}\mathbf{x} \leq \mathbf{b}_{ineq}$. Finally, the non-negativity constraints (equation A.3.1d) ensure that the decision variables cannot assume negative values; this is formulated by the constraint $\mathbf{x} \geq 0$. In conclusion, the standard form of a linear programming model can be expressed by equation A.3.1a through A.3.1d.

$$\min_{x} \quad Z = \mathbf{f}\mathbf{x} \tag{A.3.1a}$$

$$\text{s.t.} \quad A_{eq}\mathbf{x} = \mathbf{b}_{eq}, \tag{A.3.1b}$$

$$A_{ineq}\mathbf{x} \leq \mathbf{b}_{ineq}, \tag{A.3.1c}$$

$$\mathbf{x} \geq 0. \tag{A.3.1d}$$

For a problem the modelled as a linear programming problem, the problem has to suffice four different characteristics. If these characteristics are met, the problem can be modelled using the techniques explained in this section.

1. **Proportionality:** The contribution of each activity to the value of the objective function Z is proportional to the level of the activity x_j, as represented by the $c_j x_j$ term in the objective function. In a similar vein, the contribution of each activity to the left-hand side of each functional constraint is proportional to the level of the activity x_j, as represented by the $a_{ij} x_j$ term in the constraint.

2. **Additivity:** Every function in a linear programming model (whether the objective function or the function on the left-hand side of a functional constraint) is the sum of the individual contributions of the respective activities.

3. **Divisibility:** Decision variables in a linear programming problem are allowed to have any values, including non-integer values, that satisfy the functional and non-negativity constraints. Thus, these variables are not restricted to just integer values.

4. **Certainty:** The value assigned to each parameter of a linear programming model is assumed to be known constant.

Several methods exist to solve a linear programming problem. One of these methods is the Simplex method, which can be deemed to be the most intuitive and understandable method. For an elaborate reading on the Simplex method and other LP solving methods, the reader is advised to consult chapter 4 of Hillier & Lieberman (2009).

A.3.2 Integer Linear Programming

Though the linear programming model form allows for flexibility in modelling a wide variety of problems, the latter model is often not used to model the FGAP. In many practical applications, the decision variables only make sense if they have integer values. For example, it is often necessary to assign people, machines or vehicles to activities in integer values. However, another area of application may be of even greater importance, namely, a problem consisting of interrelated yes-or-no decisions. These statements give us the motivation to elaborate on the field of integer linear programming.

Recall that the divisibility assumption of linear programming model states that decision variables in a linear programming problem are allowed to have any values, including non-integer values, that satisfy the functional and non-negativity constraints. Most FGAP models have decision variables which either assume decision variables can assume a non-negative integer value or a binary value (i.e. 0 or 1), which are referred to as Integer Linear Programming (IP) problems and Binary Integer Linear Programming (BIP) problems, respectively. If only some of the decision variables are required to have integer values - therefore the divisibility assumption holds for the remaining decision variables - the problem is referred as a Mixed Integer Linear Programming (MIP) problem.

A.3.3 Non-Linear Programming

A key assumption of linear programming is, as the name would suggest, that all its function (objective function and constraints functions) are linear. Although this assumption holds for many different applications, it frequently does not hold. In the context of the FGAP, quadratic objectives can be introduced by modelling the variance of idle times, the number of positive semi-deviations or the transfer passenger walking distance, just to name a few.

According to Hillier & Lieberman (2009), the general form of a non-linear programming model is described by equation A.3.2b through A.3.2c, where $f(\mathbf{x})$ and $g_i(\mathbf{x})$ are given (non-)linear functions of the n decision variables.

$$\max_{x} \quad Z = f(\mathbf{x}) \tag{A.3.2a}$$

$$\text{s.t.} \quad g_i(\mathbf{x}) \leq b_i, \quad i = 1, 2, ..., m \tag{A.3.2b}$$

$$\mathbf{x} \geq 0 \tag{A.3.2c}$$

Because of the many types of of non-linear programming problem formulations and solving algorithms, the review on non-linear programming is purposely kept rather brief. The reader is referred to the works of Bazaraa et al. (2006) for a more elaborate reading on non-linear programming. Additionally, Huang et al. (2013), Dong et al. (2016) and Birgin et al. (2016) describe novel techniques which can be used to solve non-linear programming problems.

A.4 Mitigation Unrealistic Flight Splitting Options

Though the implementation of flight splitting options for both non-overnight-stay flights and overnight-stay flights yields a more realistic solution to the flight-to-gate assignment problem, one shortcoming is addressed. Under certain circumstances, it is optimal to split a flight and assign the functional flight segment(s) and parking segment to the same gate. This happens when towing cost plus parking cost are lower per time step as compared to the actual assignment of a functional flight segment to a particular gate.

Figure A.2 on page 132 shows an example of a gate assignment plan showing the assignment of functional flight segments, towing segments and parking segments to the available gates over the planning horizon. At gate P12, a non-overnight-stay flight is split using option 3, i.e. two functional segments, two towing segments and a parking segment. The functional segments and parking segment are assigned to the same gate. Hence, the towing movements do not serve any purpose. Therefore, this assignment is not realistic and should be mitigated from the solution space of the A-FGAP model.

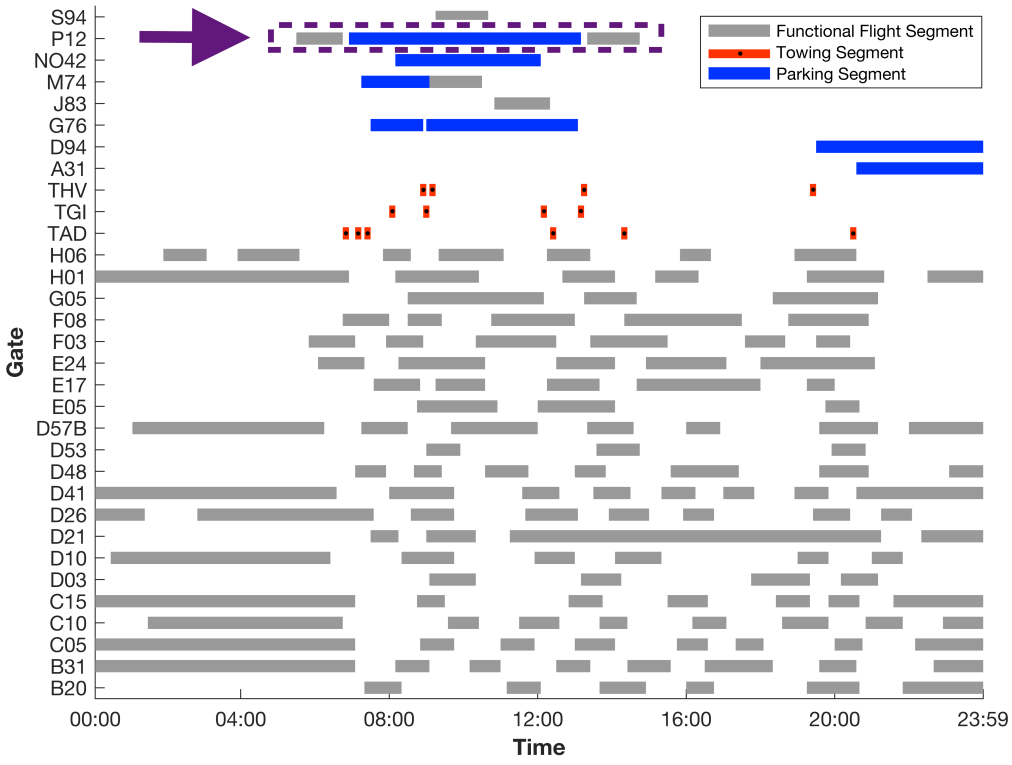

Figure A.2: Gate assignment without mitigation of unrealistic flight splitting options, obtained using the A-FGAP model without constraint (5.4.14). As indicated by the arrow and dashed purple box, an unrealistic flight splitting option occurs at gate P12. This entails a non-overnight-stay flight, which is split according the flight splitting option 3 containing segments 5, 6, 7, 8, 9 in figure 5.1. The functional flight segments (5, 9) and parking segment (7) are assigned to the same gate, and therefore is an unrealistic flight splitting option. Results are obtained using the flight schedule of July 4, 2018, a compression factor of 5, $r = 5\%$, $\delta_t = 5$min and $MI = 10$.

To prevent unrealistic flight splitting options as shown in figure A.2, a constraint to prevent this needs to be implemented in the FGAP model. Intuitively, functional and parking flight segments belonging to the same flight should not be assigned to the same gate.

Let V denote the set of all combinations of functional segments and parking segments that should not be assigned to the same gate. In this context, E_v^1 corresponds to the set of indices of flight segments in $v \in V$. Let us once again consider the unrealistic flight splitting option indicated by the purple, dashed square in figure A.2. Assume the index i of these flight segments are 121, 123 and 125. The towing movements in between these segments have the index 122 and 124. As such, the set V contains two combinations v, and for each of these combinations E_v^1 is equal to $\{121, 123\}$ and $\{123, 125\}$.

The mathematical formulation of the constraint that functional and parking flight segments belonging to the same flight should not be assigned to the same gate is shown in equation A.4.1,

$$\sum_{i \in E_v^1} x_{i,j,t} \leq 1, \quad j \in M, \quad v \in V, \tag{A.4.1}$$

where t_i is the first time step flight segment i is scheduled be to present.

The intuition behind this constraint is that only one of the flight segments in E_v^1 can be assigned to a gate $j \in M$ at time $t \in K$.

A.5 Maximum Overlap Probability Constraint Violation

Figure A.3 on page 134 indicates the assignment of flight segments at gate D21 at AMS. Just before the 16:00 time stamp, the probability mass in the upper and lower tail of the blue curves are non-zero while the curve in red still indicates a significant presence probability. Therefore, three flight segments have a non-zero presence probability at that particular time. The overlap probability of these flight segments does not exceed $r = 0.05$ and therefore the assignment to gate D21 is valid, even though strictly speaking, the constraint does not cover this occurrence.

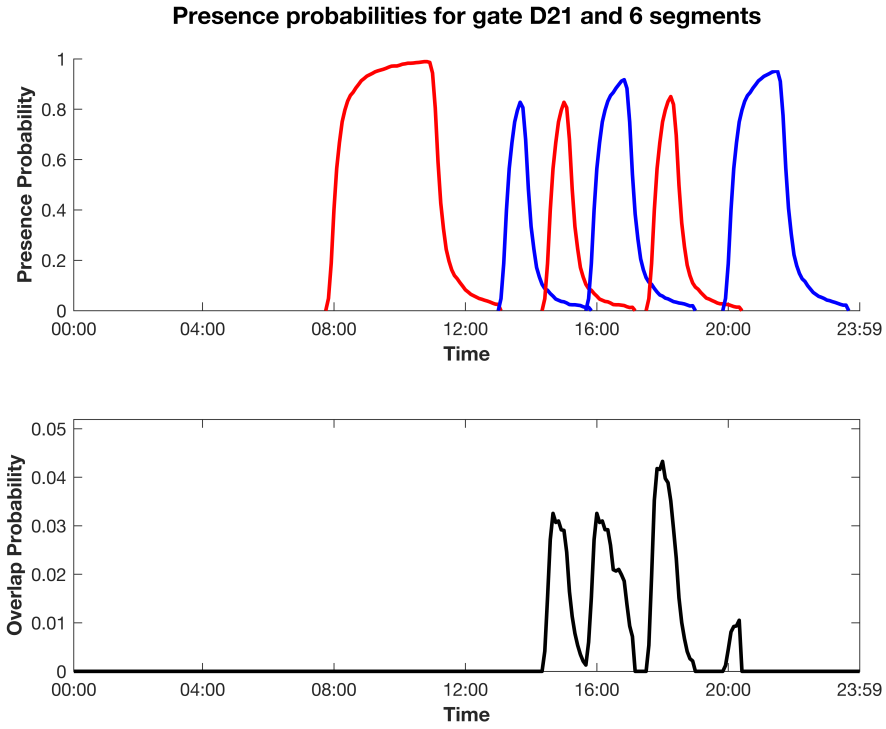

Figure A.3: Example of triple overlap of non-zero flight segment presence probabilities at gate D21 at AMS. Just before 16:00, the probability mass in the upper and lower tail of the blue curves are non-zero while the curve in red still indicates a significant presence probability. As such, at that point in time the presence probabilities of three flights assigned to that gate is non-zero. Data represents the flight schedule from July 4th, 2018, with a data compression factor of 10.

The FGAP model as described by Schaijk & Visser (2017) includes flight splitting options. In the context of overlap probability, it is important to know that the presence probabilities of segments of a split flight can be non-continuous. This can be seen in figure A.4 on page 135. The blue curve between the 13:00 and 14:00 time stamp presents the first segment of a flight that post disembarking of passengers is towed to a different location. As such, the presence probability abruptly drops to zero in a non-continuous fashion. This gives rise to scenarios where triple presence probability overlaps can occur more easily.

In this figure, the flight segments that border the aforementioned flight segment each have overlap of their presence probability masses with the presence probability of this aforementioned segment. Near the 14:00 time stamp, all three flights have a non-zero probability mass. The maximum overlap is computed to be 0.646, violating the maximum overlap probability constraint.

The mathematical model that is introduced in subsection 5.4 on page 67 and data of July 4, 2018, is

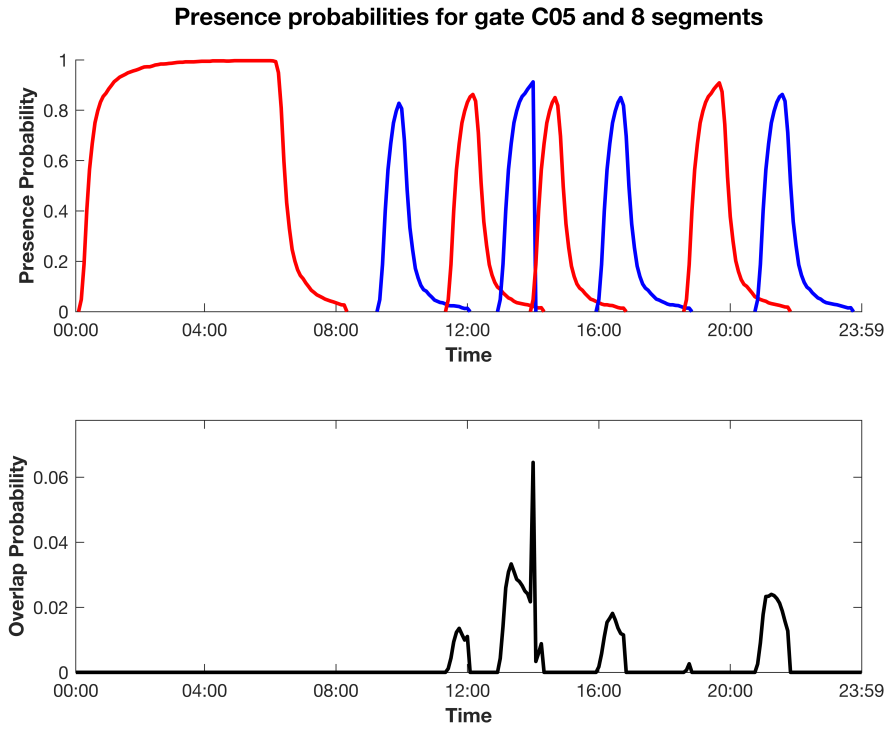

Figure A.4: Example of triple overlap of non-zero flight segment presence probabilities at gate C05 at AMS which violates the maximum overlap probability constraint. At the 14:00 time stamp, the upper and lower tails of the red curves are non-zero, while the blue curve has a presence probability close to 1. As such, at that point in time the presence probabilities of three flights assigned to that gate is non-zero. Data represents the flight schedule from July 4, 2018, with a data compression factor of 10.

used to compute for each pier the amount of flights that are assigned to this gate with a non-zero presence probability. Zero assignments at a time t means no flight segment is assigned to this pier with a non-zero presence probability. One assignment indicates that exactly one flight segment is assigned to the pier at time t with a non-zero presence probability. Having zero or one assignment happens 40.58% and 47.90% of all times. Having two or three assignment happens 11.51% and 0.02% of times. Four or more assignments at any given time do not happen.

A.6 Computational Complexity FGAP Models

This section presents three techniques to lower the computational complexity of the A-FGAP, DC-FGAP and WT-FGAP models. These include data compression, Big-M blocking and matrix construction.

A.6.1 Compression

A daily flight schedule at AMS can contain upwards of 650 arrival and departure pairs. In addition, over 300 piers, aprons, platform and towing trucks are available. If time is modelled with discrete time steps with a length of 5 minutes, the A-FGAP model will have in excess of 56 million decision variables. Though including the complete problem space in our model would yield the most trustworthy results, practicality takes preference. For this reason, a compression factor is introduced. This compression factor indicates the fraction of flights and gates that are included in the problem space. For example, if the compression factor is equal to 5, every 5th flight and every 5th gate is included in the problem scope. With a compression factor of 5, the problem scope size is reduced to 4% of the original problem; the number of initial decision variables is reduced to 2.2 million.

A.6.2 Big-M Blocking

The computational complexity of a FGAP model is a function of the number of decision variables. The number of decision variables are influenced by the number of flight segments, gates and time steps included in the model. Reducing the number of flight segments and gates by 20% each, results in a problem size of only 64% of the original problem size. It stands to reason that reducing the number of decision variables without altering the features of the model can be very beneficial to reduce the computational complexity.

The objective function of the FGAP models in equation (5.4.4) is a linear function where each binary decision variable $x_{i,j,t}$ is assigned a cost coefficient. If an assignment of flight segment i to gate j is deemed to be infeasible, gate j will not be included in the set G_i^1 as cost of such an assignment are assumed to be infinite. This method is known as the Big-M method. Given that these decision variables do not add the size of the solution space but do increase the size of the problem space, it makes sense to remove these decision variables from the problem space.

An example of a linear programming problem was shown in equations A.3.1a through A.3.1d on page 130. In this notation, the equality and inequality constraint matrices A_{eq} and A_{ineq} are included. To remove obsolete decision variables from the problem space, the decision variables and associated columns in the constraints matrices A_{eq} and A_{ineq} are dropped from the model. This is graphically illustrated in figure A.5 on page 137. All decision variables which are blocked through the Big-M method from taking on a value of 1 are indicated in the dark red boxes. The corresponding columns in the constraints matrices are indicated in the lighter red columns. Both these decision variables and their corresponding columns can be deleted from the linear programming problem without altering its solution space and optimal solution.

In order to quantify the effectiveness of the Big-M blocking technique, a case study using the A-FGAP model has been conducted. Dependent on the selected day, data compression factor and objective function settings, between 50% and 65% of the binary decision variables are blocked from attaining the value 1 through the Big-M method. As such, this reduces the problem size with an equal percentage. Using the A-FGAP model, the flight schedule of July 4, 2018 and a compression factor of 5, the time needed to create the input for

Figure A.5: Graphical representation of a linear programming problem indicating the intuition behind the column reduction of the linear programming model. Binary decision variables which are blocked from attaining the value 1 through the Big-M method are indicated by the darker red boxes in the f-vector. As such, the columns of the matrices A_{eq} and A_{ineq} corresponding these binary decision variables can be removed. This greatly reduces the problem size.

the CPLEX model is reduced by 53%. Run times are 484 seconds and 1031 seconds for the reduced problem and original problem respectively.

A.6.3 Matrix Construction

Matlab is used to create the linear programming problem on which the A-FGAP model is based. To streamline the construction of the matrices A_{eq} and A_{ineq}, two modelling techniques are used. These include sparse matrix representation and joint allocation of coefficients in the matrices A_{eq} and A_{ineq}.

If a matrix only has a small percentage of non-zero elements, sparse matrix representation greatly reduces the memory required to store large errors. Given that only information is stored about the non-zero elements in the matrix, the computational burden is greatly reduced. For example, an identity matrix with dimensions of 10,000-by-10,000 requires little under 800 megabytes of storage. If this matrix were to converted to a sparse matrix, only 0.25 megabytes are needed to store this matrix. Though the matrices A_{eq} and A_{ineq} typically have a higher number of non-zero elements than an identity matrix with a similar number of elements, sparse matrix representation provides a significant decrease in computational complexity.

In addition to sparse matrix representation, joint allocation of coefficients is used to make the construction of the matrices A_{eq} and A_{ineq} less computationally expensive. By determining patterns in the coefficients, smaller blocks of A_{eq} and A_{ineq} which are joined after each of the smaller blocks is constructed.

A.7 Data Collection and Processing

The Schiphol Flight API allows users to query a rich data set of arriving and departing flights at AMS. This section describes how flights lists and flight schedules from AMS are created using this API. Subsection A.7.1 describes how lists of arriving and departing flights are constructed. Subsection A.7.2 outlines how daily flight schedules are created from the arriving and departing flight lists.

A.7.1 Flight Lists

Flight lists are constructed for arriving and departing flights. By connecting to the Schiphol Flight API, data is queried. This data is processed in a series of Python functions in a vertical hierarchy, which include getData, getFlightsDay and getFlightListFromAPI. The function getData queries the API and produces a list of maximum 20 flights. These lists are concatenated in the function getFlightsDay which constructs a flight list for a complete day. The function getFlightListFromAPI gathers these daily flight lists and combines them into one flight list for the corresponding date range. The following subsections elaborate on each of these functions, starting at the lowest level of the hierarchy.

A.7.1.0.1 getData

The function getData serves as the core function and connects directly to the Schiphol Flight API. The aim of this function is to create a two-dimensional list that contains information about either arriving or departing flights, subject to input parameters. The function contains several error checking methods that ensure incomplete or faulty data from the API is handled appropriately. The functionalities of the function can be split in to two sections, namely querying the data from the API and structuring the queried data in a two-dimensional list.

The function getData dynamically builds the query that is used to retrieve data from the API. This query includes the following parameters alongside configuration parameters: scheduled flight date, flight direction and page number. The scheduled flight date indicates the date at which flights should be present at the airport. The flight direction sets whether information of arriving or departing flights should be queried. The page parameter is linked to a time period during the scheduled flight date. Per page, a maximum of 20 flights can be queried. This limit is set by the API. The queried data is presented in JSON format, and can easily be handled using standard Python libraries. A filter ensures that only commercial passenger flights are processed.

The variables included in the list of arriving flights are indicated in table A.2 on page 139. With the exception of the TimeDiff variable, all variables can be directly retrieved from the queried data from the Schiphol Flight API. The variables included in the list of departing flights are tabulated in table A.3 on page 139. With the exception of the TimeDiff, CheckinInterval (T_4) and the DepartureInterval (T_6) variables, all variables can be directly retrieved from the queried data from the Schiphol Flight API.

A.7.1.0.2 getFlightsDay

The function getFlightsDay iterates over all pages included in the scheduled flight date. For each page, the output of the function getData is appended to the daily flight list. Given that the Schiphol Flight API support a maximum hit rate of 200 hits per minute, a pause statement ensures that the actual hit rate lies below this

Table A.2: Overview variables arriving flight list. With the exception of the TimeDiff variable, all variables can be directly retrieved from the queried data from the Schiphol Flight API.

Variable	Type	Description
Rego	String	Registration number of the aircraft that performed flight
FlightNumber	String	Main flight number that was allocated to flight
STA	Integer	Scheduled time of arrival in [*hhmm*] form
ATA	Integer	Actual time of arrival in [*hhmm*] form
AC Type	String	Type of the aircraft
Origin	String	Origin of the flight in three-letter ICAO code
Airline	String	Three-letter IATA identifier of airline of flight
Gate	String	Gate identifier at AMS
Terminal	Integer	Terminal number passenger streams are assigned to
Codeshares	List	List of codeshares of the flight
TimeDiff	Integer	Difference between STA and ATA in minutes
BaggageClaim	String	Indicator of the baggage carousel number

Table A.3: Overview variables departing flight list. With the exception of the TimeDiff, CheckinInterval (T_4) and the DepartureInterval (T_6) variables, all variables can be directly retrieved from the queried data from the Schiphol Flight API.

Variable	Type	Description
Rego	String	Registration number of the aircraft that performed flight
FlightNumber	String	Main flight number that was allocated to flight
STD	Integer	Scheduled time of departure in [*hhmm*] form
ATD	Integer	Actual time of departure in [*hhmm*] form
AC Type	String	Type of the aircraft
Destination	String	Destination of the flight in three-letter ICAO code
Airline	String	Three-letter IATA identifier of airline of flight
Gate	String	Gate identifier at AMS
Terminal	Integer	Terminal number passenger streams are assigned to
Codeshares	List	List of codeshares of the flight
TimeDiff	Integer	Difference between STD and ATD in minutes
CheckinInterval (T_4)	Integer	Length of check-in interval in minutes
DepartureInterval (T_6)	Integer	Length of interval between closing check-in desks and STD in minutes

maximum by approximately 10%. By ensuring the hit rate limitations are met at the minute-level, hit rate limits at an hourly and daily scale are also automatically satisfied.

In addition, built-in check handle edge-cases and process them correctly. One of the more interesting features of the API is that flights are not necessarily unique. For example, the same physical flight can be included in the code more than once. This is caused by code shares. The function createUniqueFlightList ensures that code shares are filtered and only one instance of the flight is included in the data. Flight characteristics are based on the aircraft registration of the aircraft. For example, an aircraft owned by KLM

but indicated multiple times in the flight list due to code shares will be filtered to an extend that only the KLM flight will remain present in the data set.

A.7.1.0.3 getFlightListFromAPI

The function getFlightListFromAPI combines the daily flight lists created for all dates in the set date range. In addition, this function creates in the input which is used in getData to structure the query for the Schiphol Flight API. Finally, this function perform additional checks to ensure the maximum hit rate stipulated by the API is not exceeded.

A.7.2 Flight Schedules

Table A.4 indicates all the variables that are included in the daily flight schedules. In this table, the columns NOS, MOS and EOS indicate if the variable included in the flight schedule for flights without an overnight stay, flights with a morning departure and flights with an evening arrival, respectively. All variables that are derived from data in the arriving and departing flight lists are marked with 'FL' in the Origin column. The collection of these variables is referred to as the primary flight schedule. Subsection A.7.2.1 explains how the primary flight schedule is created. Variables that have markers 'AX' and 'RX' are generated using other external sources of information, which are described in subsection A.7.2.2.

A.7.2.1 Construct Primary Flight Schedules

The primary flight schedule is constructed by combining all flight schedules for each individual aircraft registration.

From the arriving and departing flight lists, the unique aircraft registrations (ACReg) are gathered that are present at AMS during the calender day that is being considered. Per aircraft registration, all arriving and departing flight legs are sorted based on their STA and STD. If the data set is complete, the sorted list consists of alternating arriving and departing flights. Due to a number of complexities, this is not always the case. For example, flights are missing, cancelled or the queried data proves to be incomplete. In total, 0.64% of all data is removed to create a consistent alternating list of arrivals and departures for all aircraft registrations.

The cleaned sorted lists per aircraft registration can be sliced in pairs of an arriving and a departing flight leg. Each pair will make up one entry in the flight schedule which follows the schema introduced in table A.4. If the sorted list does not start with an arriving flight, the first flight, i.e. a departing flight, will be paired up with an overnight stay of the aircraft at the airport. Similarly, if the sorted list ends with an arriving flight, the arriving flight will be paired with an overnight stay at the airport.

As an example, fictional data indicated in table A.5 is used to draft an example of these occurrences. In this table, three aircraft are considered and their movements, either arriving (0) or departing (1), are indicated along their STA and STD, respectively. The first aircraft (PHHXB) has two arrivals and one departure. Aircraft two (PHXRD) has two arrivals and two departures. Finally, aircraft three (PHIKJ) has one arrival and two departures during the day. Figure A.6 shows the flight presence indicator for the three aircraft in table A.5. The first aircraft (PHHXB) has two arrivals and one departure and thus has an overnight stay at the end of the planning horizon. Aircraft two (PHXRD) has two arrivals and two departures and therefore

Table A.4: Overview variables in flight schedule. The Origin column indicates where the data is sourced; FL indicates the data is gathered from the arriving and departing flight lists and the markers 'AX' and 'RX' indicate the data is collected from external data sources. The columns NOS, MOS and EOS indicate if the variable included in the flight schedule for flights without an overnight stay, flights with a morning departure and flights with an evening arrival, respectively.

Variable	Origin	Type	NOS	MOS	EOS	Description
Date	FL	Integer	✓	✓	✓	Index of day in the set date range
ACReg	FL	String	✓	✓	✓	Rego of the aircraft performing flights
IDIn	FL	String	✓		✓	Flight number of arriving flight leg
IDOut	FL	String	✓	✓		Flight number of departing flight leg
STAnum	FL	Integer	✓		✓	STA of arriving flight leg in [*hhmm*] format
STDnum	FL	Integer	✓	✓		STD of departing flight leg in [*hhmm*] format
STA	FL	DateTime	✓		✓	STA of arriving flight leg in DateTime format
STD	FL	DateTime	✓	✓		STD of departing flight leg in DateTime format
ATA	FL	DateTime	✓		✓	ATA of arriving flight leg in DateTime format
ATD	FL	DateTime	✓	✓		ATD of departing flight leg in DateTime format
ACType	FL	String	✓	✓	✓	Aircraft type corresponding to the ACReg
Origin	FL	String	✓		✓	Origin of arriving flight leg
Destination	FL	String	✓	✓		Destination of departing flight leg
Operator	FL	String	✓	✓	✓	Main airline that performs the flights
GateGroupIn	FL	String	✓		✓	Assigned gate group for arriving flight leg
GateGroupOut	FL	String	✓	✓		Assigned gate group for departing flight leg
GateIn	FL	String	✓		✓	Assigned gate for arriving flight leg
GateOut	FL	String	✓	✓		Assigned gate group for departing flight leg
TerminalIn	FL	Integer	✓		✓	Terminal that handles arriving passengers
TerminalOut	FL	Integer	✓	✓		Terminal that handles departing passengers
BaggageBelt	FL	String	✓		✓	Assigned baggage belt for arriving flight leg
CheckInInterval (T_4)	FL	Integer	✓	✓		Length of check-in interval for departing flight leg
DepartureInterval (T_6)	FL	Integer	✓	✓		Time between closing check-in and STD
ArrDepInterval	FL	Integer	✓			Time span between STA and STD
ACSize	AX	Integer	✓	✓	✓	Size of the aircraft, ranging from 3 till 9
RegionIn	RX	String	✓		✓	Region of origin
RegionOut	RX	String	✓	✓		Region of destination
CustomsIn	RX	String	✓		✓	Custom requirements for arriving flight leg
CustomsOut	RX	String	✓	✓		Custom requirements for departing flight leg

does not have any overnight stays. Aircraft three (PHIKJ) has one arrival and two departures during the day and therefore has an overnight stay at the beginning of the planning horizon.

A.7.2.2 Enrich Primary Flight Schedules

As indicated in table A.4 in the column Origin, variables with the marker 'AX' and 'RX' are collected from data sources other than the Schiphol Flight API. In this context, 'AX' corresponds to an Excel file that contains an exhaustive list of aircraft types and size characteristics. The 'RX' marker indicates an Excel file that links airport to regions and customs requirements.

The variable ACSize indicates the AC size and is gathered by matching the variable ACType already present in the flight schedule with the same entry in the 'AX' Excel file. As such, the size of the aircraft

Table A.5: Fictional data arrival/departure data for three different aircraft. The type column indicates whether a movement is an arrival (0) or a departure (1) The first aircraft (PHIKJ) has two arrivals and one departure. Aircraft two (PHXRD) has two arrivals and two departures. Finally, aircraft three (PHHXB) has one arrival and two departures during the day.

PHIKJ		
Type	STA	STD
0	6:40	
1		9:10
0	20:00	

PHXRD		
Type	STA	STD
0	7:30	
1		10:25
0	17:55	
1		21:40

PHHXB		
Type	STA	STD
1		6:40
0	15:50	
1		28:20

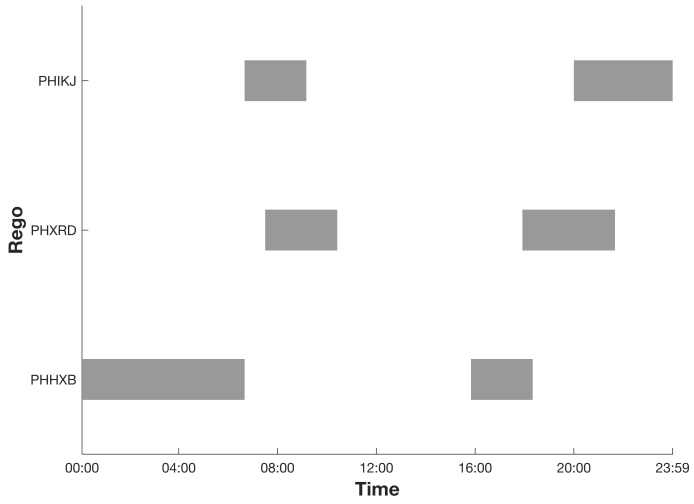

Figure A.6: Example of flights with and without an overnight stay. The first aircraft (PHHXB) has two arrivals and one departure and an overnight stay at the end of the planning horizon. Aircraft two (PHXRD) has two arrivals and two departures and therefore and does not include an overnight stay. Finally, aircraft three (PHIKJ) has one arrival, two departures during the day and a overnight stay at the start of the planning horizon.

can be added to each entry in the primary flight schedule. The region of the origin and associated customs requirements of am arriving flight can be found by matching the origin airport code in the primary flight schedule and the 'RX' Excel file. In a similar vein, the region of the destination and associated customs requirements of a departing flight are found.

Appendix B

Supporting Results

B.1 Flight Presence Probability Curves A-FGAP Model

Figure B.1 shows the flight presence probability curves for the flight segments assigned to piers B31, D18, D85 and E03. These piers are chosen such that the reader is presented with a cross-section of the different piers. Pier B31 and D85 both have a Schengen clearance, whereas piers D18 and E03 are able to serve flights with a Non-Schengen or Intercontinental clearance. Whereas piers B31, D18 and D85 are able to serve flights segment with a maximum size of 4, pier E03 can handle aircraft of size 8. The maximum overlap probability for these gates varies between 3.35% and 4.75%. Piers B31, D18 and D85 include flight segments belonging to overnight-stay flights. A simultaneous non-zero presence probability for three flights at a certain time step occurs at pier D85. However, the recalculated overlap probability does not exceed $r = 5\%$ and therefore the gate assignment planning does not violate the maximum overlap probability constraint 5.4.11 on page 70.

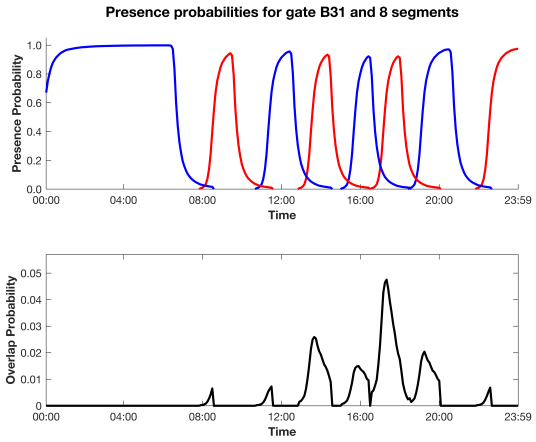

(a) Presence probability curves of flight segments assigned to gate B31. In total, 8 segments are assigned to this gate with a maximum overlap probability of 4.75%.

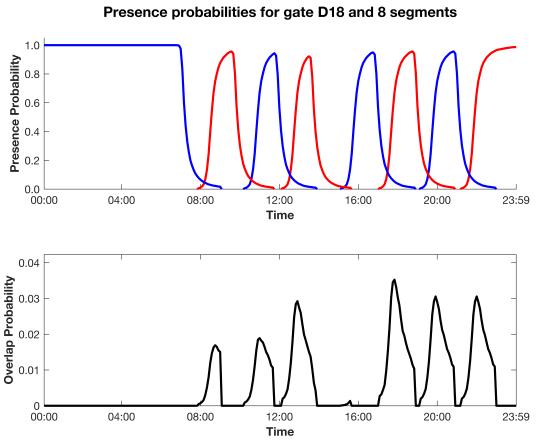

(b) Presence probability curves of flight segments assigned to gate D18. In total, 8 segments are assigned to this gate with a maximum overlap probability of 3.53%.

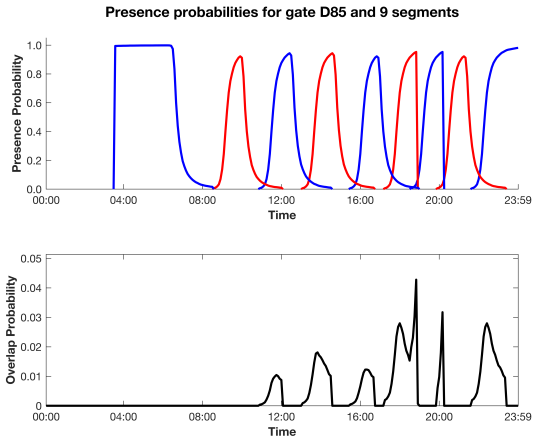

(c) Presence probability curves of flight segments assigned to gate D85. In total, 9 segments are assigned to this gate with a maximum overlap probability of 4.28%.

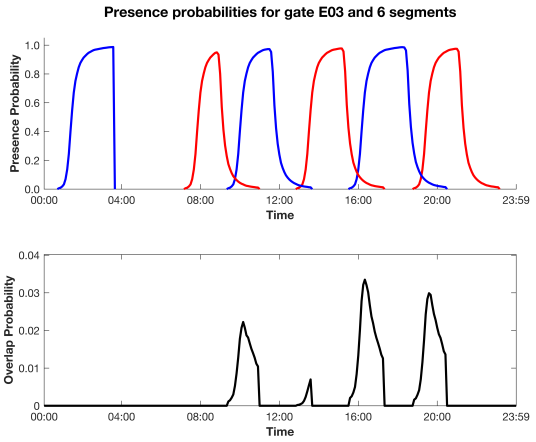

(d) Presence probability curves of flight segments assigned to gate E03. In total, 6 segments are assigned to this gate with a maximum overlap probability of 3.35%.

Figure B.1: Flight segments assigned to gates B31, D18, D79 and E03. These gates are among those with the largest number of flight segments assigned to them during the planning horizon. Nonetheless, the maximum overlap probability at each of these gates varies between 2.58% and 4.53%.

B.2 Optimisation Algorithm WT-FGAP Model

A solution to the WT-FGAP can be invalid if the maximum overlap probability criterion is violated due to non-zero presence probabilities of three or more flights at the same gate and time step. In addition, a solution can be invalid if threshold for the maximum waiting time is exceeded. If either of these violations is detected, another iteration to find a valid solution will follow. A total of four iterations of algorithm 2 on page 77 are needed before a valid solution to the WT-FGAP model is found. During each of these iterations, one or more violations of the waiting time criterion are found. No violations of the maximum overlap probability criterion are found in any of the iteration cycles.

To get a better grasp on the optimisation algorithm, the metric $h^u_{p,q}$ is introduced, expressed by equation B.2.1. In this equation, u denotes the index of each iteration cycle of the optimisation algorithm. This metric computes the number of passengers handled in iteration cycle u as a percentage of the the number of passengers handled in iteration cycle 1 for facility $p \in H$ in terminal $q \in T$. Let $y^u_{p,q,t}$ denote the passenger demand at facility $p \in H$ in terminal $q \in T$ during time step $t \in K$ in iteration cycle u.

$$h^u_{p,q} = \frac{\sum_{t \in K} y^u_{p,q,t}}{\sum_{t \in K} y^1_{p,q,t}} \times 100\%, \quad p \in H, \quad q \in T \tag{B.2.1}$$

Figure B.2 indicates a graphical overview of the metric $h^u_{p,q}$ of each iteration step. As such, all numbers in figure B.2a indicate a value of 100%. Blue squares indicate the facilities where certain values of $b_{p,q,t}$ are set to a non-infinity value to remove demand peaks that cause a waiting time violation from the solution space.

As can be seen from figure B.2 on page 147, waiting time violations occur in Terminal 2 and 3. In Terminal 2, these occur at facilities A1, A2 and D1. Passenger demand constraints pertaining to facility D1 are tightened during iteration 1, whereas passenger demand constraints pertaining to facilities A1 and A2 are tightened during iteration 3. In Terminal 3 waiting time violations occur at facility T1. In this facility, passenger demand constraints are tightened during two iterations, i.e. during iteration 1 and 2. The darker the shade of blue, the larger the number of parameters $b_{p,q,t}$ that has been given a non-infinity value.

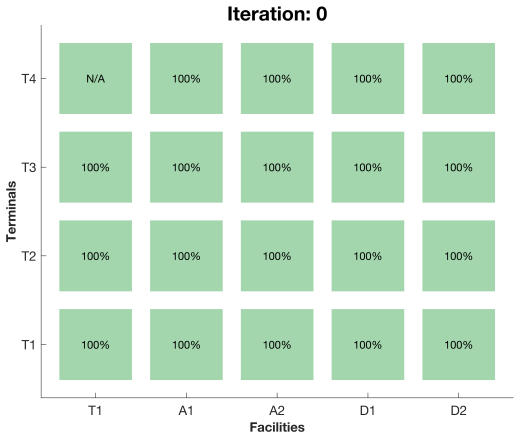

(a) First iteration step of algorithm 2

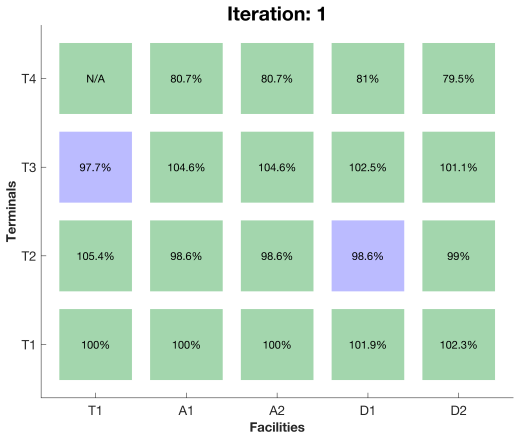

(b) Second iteration step of algorithm 2

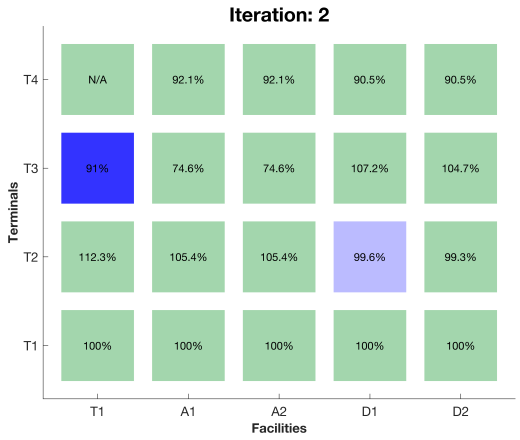

(c) Third iteration step of algorithm 2

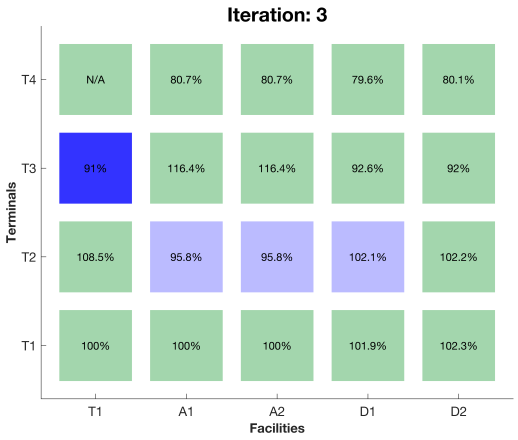

(d) Fourth iteration step of algorithm 2

Figure B.2: Overview of solving algorithm cycles employed by the WT-FGAP model. Percentages indicated the metric $h^u_{p,q}$, which is the number of passengers handled in iteration cycle u as a percentage of the the number of passengers handled in iteration cycle 1 for facility $p \in H$ in terminal $q \in T$. Blue squares indicate the number parameters $b_{p,q,t}$ that have a non-infinity value.

Appendix C

Project Planning

In order to complete the thesis in a timely fashion, it is important to have a concrete plan. The Gantt chart in figure C.1 on page 151 indicates the proposed planning. The thesis was started in March 2018 and is expected to be finished in April 2019, concluded by the thesis defense. Key intermediate milestones include the kick-off meeting, the mid-term review and the greenlight meeting. The final thesis will be handed in between the greenlight meeting and the thesis defense, as marked by the dashed vertical line without a label.

The elements in this planning and a short description of these elements are indicated in the following list:

- **Literature Review:** Document that aims to summarize existing literature on FGAP models, implementation of robustness in these models and airside and landside constraints. In addition, this document should outline the structure of research and set an appropriate objective and associated research questions.
- **Examine Codebase:** Work through the existing code base developed by Schaijk & Visser (2017) and ensure a proper understanding of its working is established.
- **Data Analysis:** Provide insight in available data and summarise the data using key metrics.
- **Connect Flight API:** Enrich existing data with landside information attained through the Schiphol Flight API.
- **Initial Model Development:** Develop functioning FGAP model which incorporates both airside and landside constraints and a pre-specified level of robustness. Run simple unit tests to ensure basic functionalities.
- **Reporting:** Write thesis report. Among other elements, this report will contain the methodology, summary of used data, results of verification and validation steps and results of the case studies. This report should be able to be read as a stand-alone document.
- **Verification & Validation:** Verify and validate the results of the to-be developed FGAP model. Verification is done by using artificial data, whereas validation aims to assess the outcome of the model when using real-life data.
- **Develop Case Studies:** Use the model to create a solution to the FGAP of a specified airport. Given the availability of the data, this airport will be Amsterdam Airport Schiphol (AAS).

- **Prepare Defense:** Create all the materials needed for the defense and ensure proper arrangements are set.
- **Defense:** Conduct the defense.

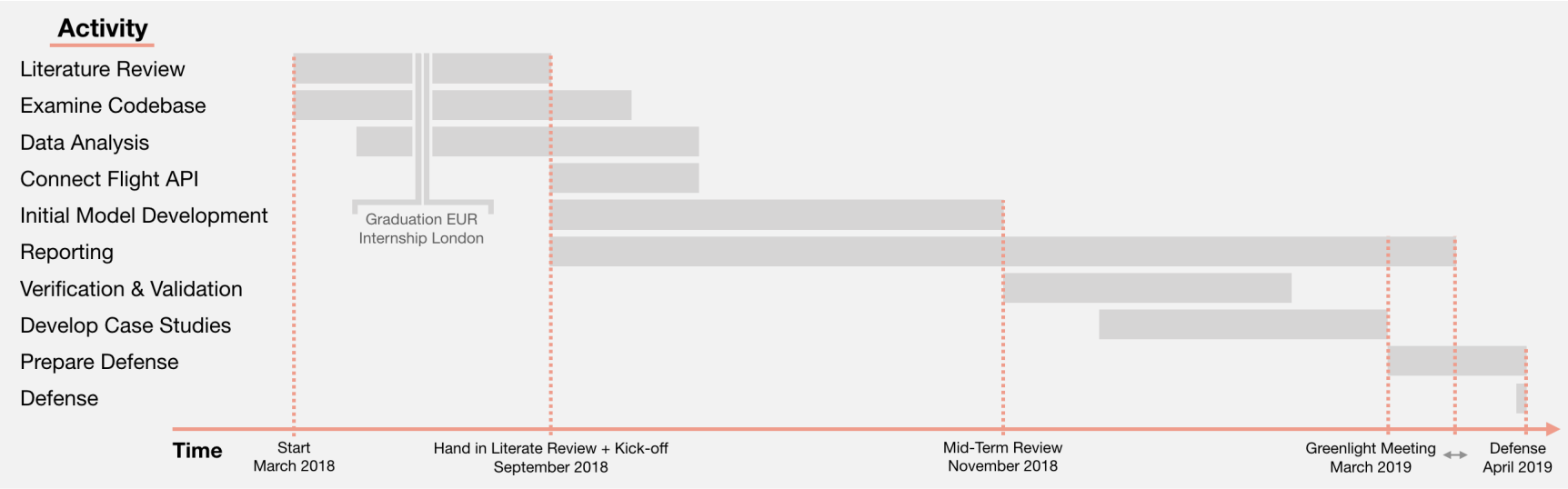

Figure C.1: Gantt Chart for thesis project. The thesis was started in March 2018 and is expected to be finished in April 2019, concluded by the thesis defense. Key intermediate milestones include the kick-off meeting, the mid-term review and the greenlight meeting. The final thesis will be handed in between the greenlight meeting and the thesis defense, as marked by the dashed vertical line without a label.